J. Puriwat et al. / Catalysis Communications 12 (2010) 80-85

$$CH_2 = CH - CH_2 - CH_3 \xrightarrow{-H^+} CH_2 - CH - CH - CH_3 \xrightarrow{+H^+} CH_3 - CH = CH - CH_3$$
1-butene Carbanion intermediate 2-butene

Scheme 1. Mechanism for 1-butene isomerization to 2-butene.

BET surface area 42 m²/g. The MgO crystalline phase (average crystallite size 6.8 nm and surface area 180 m²/g) was obtained by calcination of the Mg(OH)₂ at 400 °C. Increasing calcination temperature from 400 to 800 °C resulted in the sintering of MgO and as a consequence, the BET surface area decrease to 59 m²/g. As revealed by CO₂-TPD results, the Mg(OH)₂ phase contained only medium strength basic sites while the MgO phase exhibited both weak and strong basic strengths. The activity of the catalyst increased in the order of MgO400>MgO600≈uncalcined sample>MgO200>MgO800 with more than 99% selectivity to 2-butene. The isomerization activity mainly proceeded on the strong basic sites of MgO while the medium basic sites from hydroxyl groups were the responsible active sites for the Mg(OH)₂ phase. The weak basic sites in MgO catalysts did not participate much in the reaction. The strong basic sites of MgO were correlated well with the presence of oxygen atoms in the lattice of crystalline MgO.

Acknowledgments

The financial supports from the Thailand Research Fund (TRF) and the Office of the Commission on Higher Education are gratefully acknowledged. The authors would like to thank the SCG Chemicals Co., Ltd., Thailand for the scholarship for Jiraporn Puriwat and the provision of facilities.

References

- M.-L. Bailly, C. Chizallet, G. Costentin, J.-M. Krafft, H. Lauron-Pernot, M. Che, J. Catal. 235 (2005) 413–422.
- [2] K. Tanabe, W.F. Holderich, Appl. Catal. A 181 (1999) 399-434.
- [3] J. Li, R.J. Davis, J. Phys. Chem. B 109 (2005) 7141–7148.
- [4] Y. Ono, T. Baba, Catal. Today 38 (1997) 321–337.
- [5] C. Chizallet, G. Costentin, H. Lauron-Pernot, J.M. Krafft, P. Bazin, J. Saussey, F. Delbecq, P. Sautet, M. Che, Oil and Gas Sci. Tech.-Rev. IFP 61 (2006) 479–488.

- [6] M.A. Aramendía, J.A. Benítez, V. Borau, C. Jiménez, J.M. Marinas, J.R. Ruiz, F. Urbano, Langmuir 15 (1999) 1192–1197.
- [7] G. Zhang, H. Hattori, K. Tanabe, Appl. Catal. 36 (1988) 189-197.
- 8] J. Schwank, S. Galvagno, G. Parravano, J. Catal. 63 (1980) 415-424.
- [9] J.M. Driessen, E.K. Poels, J.P. Hindermann, V. Ponec, J. Catal. 82 (1983) 26–34.
- 10] S. Huang, S. Liu, W. Xin, J. Bai, S. Xie, Q. Wang, L. Xu, J. Mol. Catal. A 226 (2005) 61–68.
- [11] J.C. Mol, J. Mol. Catal. A 213 (2004) 39-45.
- [12] M.J. Baird, J.H. Lunsford, J. Catal. 26 (1972) 440–450.
- [13] T. Matsuda, M. Sugimoto, React. Kinet. Catal. Lett. 44 (1991) 69-73.
- [14] T. Matsuda, J. Tanabe, N. Hayashi, Y. Sasaki, H. Miura, K. Sugiyama, Bull. Chem. Soc. Japan 55 (1982) 990–994.
- [15] K.J. Klabunde, H. Matsuhashi, J. Am. Chem. Soc. 109 (2002) 1111-1114.
- 16] M.A. Aramendia, J.A. Betez, V. Borau, C. Jimnez, J.M. Marinas, J.R. Ruiz, F. Urbano, J. Solid State Chem. 144 (1999) 25–29.
- [17] M.A. Aramendia, J.A. Bentez, V. Borau, C. Jimnez, J.M. Marinas, J.R. Ruiz, F.J. Urbano, Colloids Surf., A 168 (2000) 27–33.
- [18] M.A. Aramendia, V. Borau, C. Jimnez, J.M. Marinas, J.R. Ruiz, F.J. Urbano, Appl. Catal. A 244 (2003) 207–215.
- [19] X.-F. Wu, G.-S. Hu, B.-B. Wang, Y.-F. Yang, J. Crystal Growth 310 (2008) 457–461.
- [20] I.F. Mironyuk, V.M. Gun'ko, M.O. Povazhnyak, V.I. Zarko, V.M. Chelyadin, R. Leboda, J. Skubiszewska-Zieba, W. Janusz, Appl. Surf. Sci. 252 (2006) 4071–4082.
- [21] W. Jiang, X. Hua, Q. Han, X. Yang, L. Lu, X. Wang, Powder Tech. 191 (2009) 227–230.
- 22] J.-P. Hsu, A. Nacu, Colloids Surf., A 262 (2005) 220–231.
- 23] D. An, X. Ding, Z. Wang, Y. Liu, Colloids Surf., A 356 (2010) 28–31.
- [24] A. Kumar, J. Kumar, J. Phys. Chem. Solids 69 (2008) 2764–2772.
- [25] C. Chizallet, G. Costentin, H. Lauron-Pernot, J.M. Krafft, P. Bazin, J. Saussey, F. Delbecq, P. Saufet, M. Che, Oil and Gas Sci. Tech. 61 (2006) 479–488.
- [26] G. Busca, V. Lorenzelli, Mater. Chem. 7 (1982) 89.
- [27] G.A.H. Mekhemer, S.A. Halawy, M.A. Mohamed, M.I. Zaki, J. Phys. Chem. B 108 (2004) 13379.
- [28] K. Teramura, T. Tanaka, H. Ishikawa, Y. Kohno, T. Funabiki, J. Phys. Chem. B 108 (2004) 346–354
- [29] V.K. D'iez, C.R. Apestegu'ia, J.I. Di Cosimo, Catal. Today 63 (2000) 53-62.
- [30] M.J. Larsen, Y. Ma, H. Qian, H. Toftlund, P.B. Lund, E.M. Skou, Solid State Ionics 181 (2009) 201–205.
- [31] E. Giamello, A. Ferrero, S. Coluccia, A. Zecchina, J. Phys. Chem. 95 (1991) 9385–9391.
- [32] H. Matsuhashi, M. Oikawa, K. Arata, Langmuir 16 (2000) 8201-8205.
- [33] J. Li, W.-L. Dai, K. Fan, J. Phys. Chem. C 112 (2008) 17657-17663.
- [34] M. Foster, M. Furse, D. Passno, Surf. Sci. 502-503 (2002) 102-108.



Contents lists available at ScienceDirect

Catalysis Communications

journal homepage: www.elsevier.com/locate/catcom



The effect of phosphorous precursor on the CO oxidation activity of P-modified TiO₂ supported Ag catalysts

Nattaya Comsup, Joongjai Panpranot, Piyasan Praserthdam*

Center of Excellence on Catalysis and Catalytic Reaction Engineering, Department of Chemical Engineering, Faculty of Engineering, Chulalongkorn University, Bangkok 10330, Thailand

ARTICLE INFO

Article history:
Received 20 April 2010
Received in revised form 18 June 2010
Accepted 23 June 2010
Available online 1 July 2010

Keywords:
P-modified TiO₂
CO oxidation
Ag/TiO₂
Phosphorous precursor

ABSTRACT

Nanocrystalline TiO_2 and P-modified TiO_2 with P/Ti atomic ratio 0.01 were prepared by the solvothermal method and employed as the supports for Ag/TiO_2 catalysts for CO oxidation reaction. The incorporation of phosphorus into the TiO_2 lattice in the form of Ti-O-P resulted in an increase of both surface area and metal dispersion. The P-modified TiO_2 supported Ag catalysts using phosphorus precursor in the form of oxide promoted the weak adsorbed oxygen species and resulted in catalytic activity improvement in CO oxidation. However, the use of phosphorous precursor in the form of phosphate such as H_3PO_4 , $(NH_4)_2HPO_4$, $(C_2H_5)_3PO_4$ could result in the strongly adsorbed oxygen species and/or the bidentate of phosphate species blocking the active sites instead.

© 2010 Elsevier B.V. All rights reserved.

1. Introduction

Titanium dioxide (TiO_2) is a reducible metal oxide that has been widely used as a support for noble metal catalysts in CO oxidation because it exhibits a stronger interaction with group VIII noble metals than other metal oxides [1–6]. The strong metal–support interaction has been shown to play an important role in increasing the metal dispersion, which leads to enhancing the catalytic activity for CO oxidation. Additionally, the promoting effect of the reducible support may result from the creation of second active sites at the metal–support interface [7].

The addition of trace element to TiO₂ support is a simple way to modify its physicochemical properties such as crystallite size, crystal defects, surface area, thermal stability, and the interaction between metal and support. Support modification has been shown to result in an improved CO oxidation activity in many catalyst systems. For examples, Yu et al. [8] reported that doping of La in TiO₂ during the solgel synthesis induced the creation of the second active site on the surface of Au/TiO₂ which promoted the fast CO oxidation. Peza-Ledesma et al. [9] reported that the use of SBA-15 modified with 10 wt. % of TiO₂ as support materials led to a high dispersion of supported gold catalysts which promoted the catalytic activity toward CO oxidation. Similarly, Hernandez et al. [10] found that the well dispersion of gold catalyst on the cerium-modified silica support provided the formation of small gold particle and the coverage of

Despite a number of studies reporting the support modification effect in CO oxidation activity, the modification of support with a nonmetallic modifier has received little attention as compared to the metallic ones. Most of the non-metallic modifier reported in the literature was in the form of anionic species such as nitrate ion [11,12], sulfate ion [13,14], and phosphate ion [15]. Both positive and negative effects of the non-metallic modifier on CO oxidation activities have been found. The negative effect of sulfate ion was reported by Ruth et al. [13] in which the Au/TiO2 catalyst was deactivated by the blocking of SO2 at the interface between an Au particle and the TiO₂ support. Kim and Woo [14] reported that SO₂ treatment increased the adsorption strength between Au and CO which suppressed the migration of absorbed CO on the Au particles to Au–TiO₂ interface to form CO₂, resulting in a decrease of CO oxidation activity. On the other hand, modification with phosphate ion showed a positive effect on CO oxidation activity. Incorporation of phosphate ion in TiO2 support could prevent sintering of Au particles at high temperature treatment, as a consequence higher CO oxidation activity was obtained [12,15]. However, an over-loading of phosphate ions may block the active sites instead.

In the present study, the effect of phosphorus precursors on the P-modified TiO_2 supported Ag catalysts has been extensively investigated. The catalysts were characterized by N_2 physisorption, X-ray diffraction (XRD), transmission electron microscopy (TEM), X-ray photoelectron spectroscopy (XPS), Fourier transformed infrared spectroscopy (FT-IR), temperature programmed desorption of oxygen (O_2 -TPD), and pulse chemisorption. The catalyst activities were evaluated in the CO oxidation in a fixed-bed reactor.

cerium on the silica support promoted the effectiveness of oxygen mobility, which led to higher catalytic activity in CO oxidation.

^{*} Corresponding author. Tel.: +66 2218 6883; fax: +66 2218 6766. E-mail address: piyasan.p@chula.ac.th (P. Praserthdam).

2. Experimental

2.1. Preparation of TiO₂ and P-modified TiO₂

The TiO₂ nanoparticles were prepared by the solvothermal method according the procedure described in our previous work in Ref [16]. Typically, about 25 g of Titanium (IV) n-butoxide (TNB) was mixed with 100 cm³ of 1,4-butanediol in a test tube. The mixed solution in the test tube was placed in a 300 cm³ autoclave. An addition of 30 cm³ of 1,4-butanediol was added to the gap between the test tube and the autoclave wall. After purging with nitrogen into the autoclave reactor, the system was heated to 320 °C at a rate of 2.5 °C/min and held at that temperature for 4 h. The P-modified TiO₂ supports were prepared by addition of a certain amount of phosphorus precursor into the mixed solution of TNB and 1,4-butanediol before setting up in the autoclave. Four phosphorus precursors used in this study were H₃PO₄, (NH₄)₂HPO₄, (C₂H₅)₃PO₄, and P₂O₅. After the autoclave was naturally cooled to room temperature, the resulting powder was repeatedly washed with methanol and dried in air for 12 h. As determined by the inductively coupled plasma optical emission spectroscopy (Agilent Optima 2100 DV ICP-OES), the mean value of P/Ti molar ratio for all the P-modified TiO₂ samples was $0.01 \pm 6\%$.

2.2. Preparation of Ag/TiO₂ catalysts

The TiO_2 supported Ag catalysts were prepared by the incipient wetness impregnation method. An aqueous solution of 1.98~M of $AgNO_3$ equal to the pore volume of the TiO_2 support, i.e. $0.7~cm^3g^{-1}$ STP, was added drop-wise to the support during intensive mixing to give a metal content of 10~at.% with respect to the atomic weight of the TiO_2 support. After impregnation, the catalysts were dried at room temperature for 6~h and then at $110~^{\circ}C$ overnight in an oven. The dried catalysts were calcined in air at $450~^{\circ}C$ for 3~h. The series of catalysts are denoted by their atomic percentages of silver loading, the phosphorus content in the TiO_2 supports, and type of phosphorus precursor. For example, $10\%Ag/TiO_2-H_3PO_4$ is referred to the catalyst containing 10~at.% Ag on the P-modified TiO_2 support prepared from H_3PO_4 precursor. The actual amount of Ag loading determined by the ICP-AES was $6.7\pm6\%$.

2.3. Catalyst characterization

The XRD measurements were performed using the SIEMENS D5000 diffractometer with Cu $\rm K_{\alpha}$ radiation. The average crystallite size and phase composition of P-modified TiO $_2$ were determined by the Scherrer equation. The XRD patterns were scanned at a rate of 2.4° min $^{-1}$ in the range of $2\theta=20$ –80°. The BET specific surface area of the samples was measured by $\rm N_2$ adsorption at 77 K using a Micromeritics ASAP 2020 instrument. The FT-IR spectra were recorded at room temperature on a Nicolet 6700 spectrometer using a KBr pellet for sample preparation, in the range of 400–4000 cm $^{-1}$ with 4 cm $^{-1}$ resolution. The particle sizes of Ag/TiO $_2$ catalysts were investigated by transmission electron microscopy (TEM) with a Philips CM100 microscope. The chemical states of the elements were measured by XPS technique using an Amicus photoelectron spectrometer with Mg $\rm K_{\alpha}$ X-ray source at current of 20 mA and 10 keV, resolution of 0.1 ev/step, and pass energy of 75 eV. The binding energy was calibrated by the C 1s peak at 285.0 eV.

The amount of metal active sites for Ag/TiO₂ catalysts were determined using N₂O pulse chemisorption according to the method previously reported by our group [17]. About 100 mg of the catalyst sample was first reduced in hydrogen (50 cm³/min) at 200 °C for 1. Then the catalyst was cooled down to 150 °C in He stream and a certain amount of N₂O was injected into the He stream in front of the catalyst bed. The N₂O was analyzed by TCD gas chromatography using a packed Porapak N column. The metal active site of the Ag/TiO₂ catalyst was calculated assuming a simplified reaction stoichiometry of Ag:O = 2.

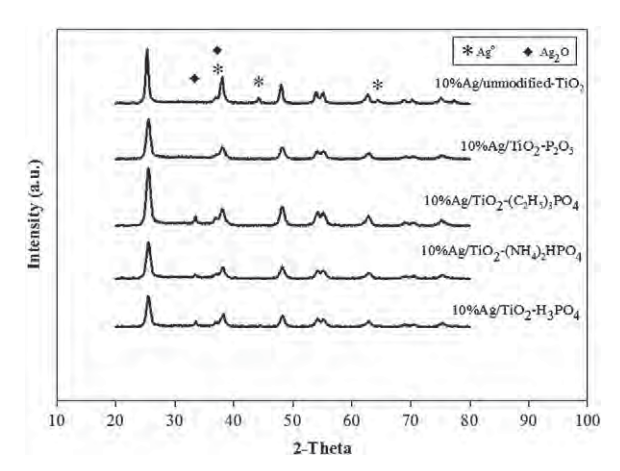


Fig. 1. XRD patterns of 10 at.% Ag catalysts supported on TiO₂ and P-modified TiO₂ with different phosphorus precursors

The O_2 -TPD profiles were performed in order to study the characteristics of oxygen adsorption and desorption on the catalyst surface. Approximately, 0.1 g of the catalyst was reduced in hydrogen flow (50 cm³/min) at 200 °C for 1 h. Subsequently the sample was cooled down to room temperature in He stream (30 cm³/min) and held at that temperature in oxygen stream (30 cm³/min) for 1 h to adsorb oxygen on the catalyst surface. Then the gas flow was switched to He gas flow (30 cm³/min) for 1 h in order to remove the physically adsorbed oxygen on the catalyst surface. The temperature was ramped with a heating rate of 10 °C/min to 600 °C. The oxygen desorption signal was detected by the thermal conductivity detector (TCD) during programmed heating.

2.4. Reaction study

The activity of the catalyst samples in CO oxidation was carried out in a fixed-bed glass tube microreactor (i.d. 5 mm) with 100 mg of catalyst packed at the center of the reactor between two quartz wool plugs. The catalyst bed temperature was measured by inserting a thermocouple into the reactor below the catalyst bed. The reactant feed gas consisted of 1% CO, 2% O₂ and He as balance, with a total flow rate of $100 \text{ cm}^3/\text{min}$ (GHSV $\approx 30,600 \text{ h}^{-1}$). Prior to the start of the reaction, the catalyst was first reduced in-situ in flowing H2 at 200 °C for 1 h with a flow rate of 50 cm³/min. Following the *in-situ* reduction of the catalyst, the reactant gas mixture was switched into the reactor. The temperature of the furnace was increased from room temperature to the desired temperature and held at that temperature for 20 min. The concentration of CO in the exit stream from the reactor was analyzed on line by gas chromatography with a Shimadzu GC-8ATP gas chromatograph provided with a thermal conductivity detector (TCD) and a Porapak Q column with He as the carrier gas. The conversion of CO was defined as the percentage of the CO in feed

Table 1Physical properties and amount of active sites of 10 at.% Ag catalyst supported on TiO₂ and P-modified TiO₂ with different phosphorus precursors.

Catalyst	TiO ₂ crystalli	te size (nm)	BET	Active site
	Before Ag loading	After Ag loading	surface (m ² /g)	(×10 ²⁰ atom- Ag/g-cat.)
10%Ag/unmodified-TiO ₂	15.2	16.2	52	1.27
10%Ag/TiO ₂ -H ₃ PO ₄	10.8	11.2	75	3.57
10%Ag/TiO ₂ -(NH ₄) ₂ HPO ₄	10.0	10.0	76	3.76
10% Ag/TiO ₂ - $(C_2H_5)_3$ PO ₄	9.8	10.1	74	3.64
10%Ag/TiO ₂ -P ₂ O ₅	9.5	10.4	75	3.89

stream that was converted to analyzed product. The temperature at which the conversion of CO equals 50% (defined as light-off temperature) is used for evaluation of the catalyst performance.

3. Results and discussion

3.1. Effect of P doping on the physicochemical properties of Ag/TiO $_2$ catalysts

The XRD patterns of the unmodified TiO_2 and P-modified TiO_2 supported Ag catalysts prepared with different precursors of phosphorus modifier are shown in Fig. 1. The major peak of pure anatase (101) phase TiO_2 was observed at 2θ around 25° for all the catalyst samples. Doping of TiO_2 with P led to broadening of the XRD peaks as well as a slight shift of the XRD reflections towards higher angles. According to the Bragg's law, an increase of 2θ values indicated a decrease of the distance between crystal planes, which is in close relationship with the lattice parameters. For the 10%Ag/unmodified- TiO_2 , diffraction peaks corresponding to metallic Ag appeared at $2\theta = 38.1^\circ$, 44.4° , and 64.5°

and the peaks at 32.8° and 38° were assigned to Ag₂O [18,19]. The intensities of the XRD characteristic peaks of metallic Ag (44.4° and 64.5°) for the P-modified TiO₂ samples became weak, whereas the peaks of Ag₂O (32.8°) became strong except those of 10%Ag/TiO₂–P₂O₅ in which the peaks corresponding to any Ag species were not clearly seen. The low intensity of Ag metallic peaks for the P-modified TiO₂ may be ascribed to the smaller Ag particles and/or the oxidation of some of the metallic Ag to Ag₂O.

Table 1 summarizes the crystallite size of the unmodified and the P-modified TiO₂ supported Ag catalysts, which was calculated from the Scherrer equation. The crystallite sizes of all the P-modified TiO₂ were found to be smaller than the unmodified one, and as a consequence the BET surface areas increased. The existence of phosphorus in the TiO₂ framework may inhibit the growth of anatase TiO₂ crystals [20]. There was little impact of phosphorous precursor on the crystallite size and BET surface area of P-modified TiO₂. All the P-modified TiO₂ had an average crystallite size of ~10 nm and BET surface area of 75 m²/g. The XRD results were found to be in good agreement with those observed from the TEM micrographs (Fig. 2). The average crystallite sizes of

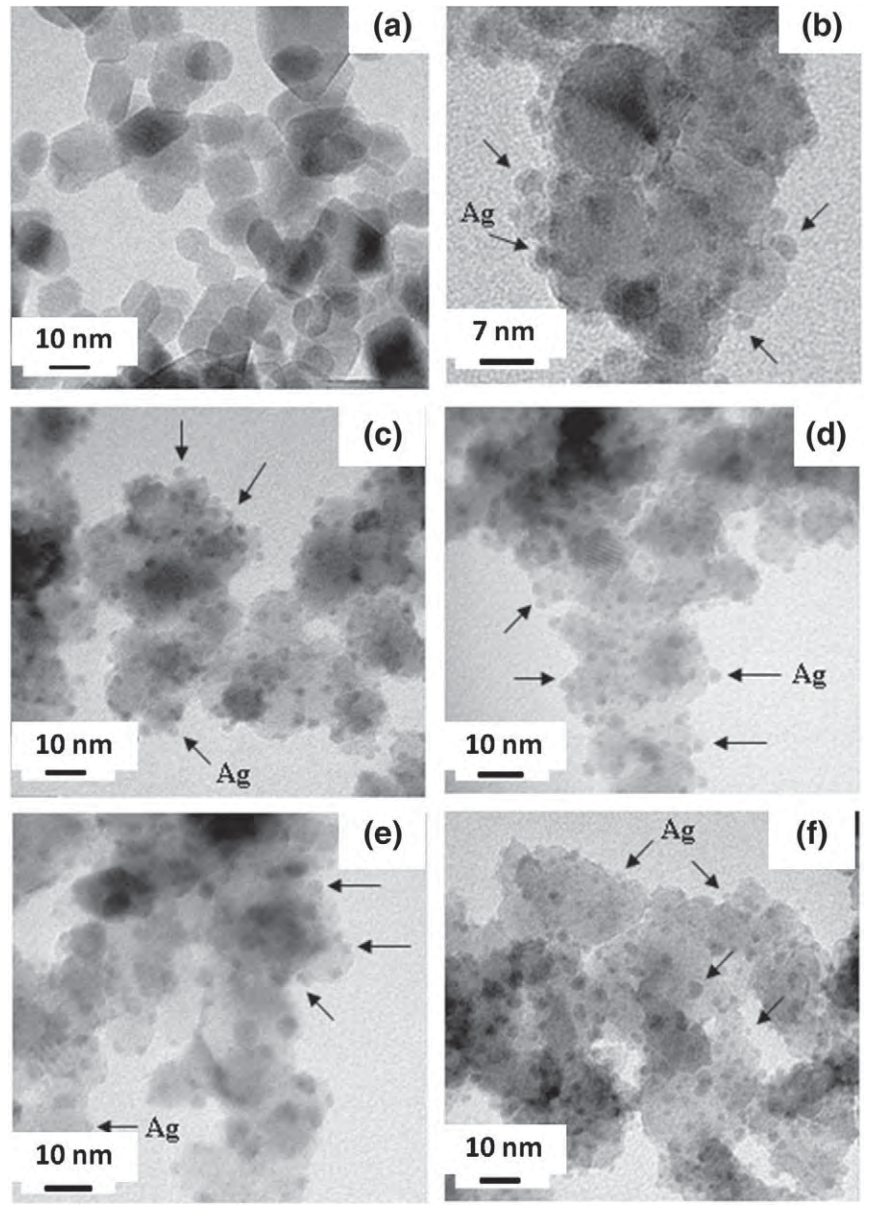
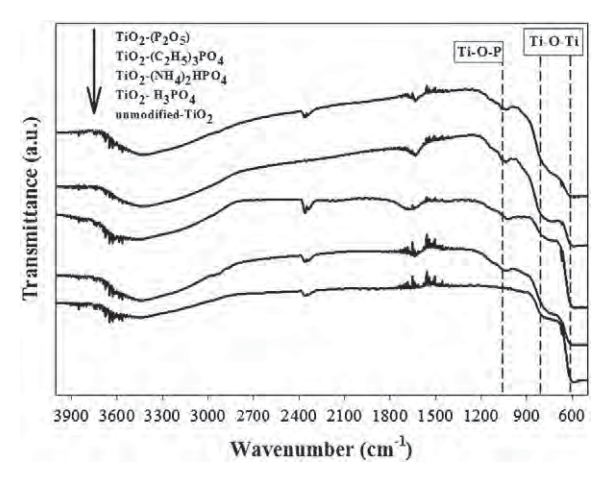


Fig. 2. The TEM micrographs of unmodified TiO₂ (a), 10%Ag/unmodified-TiO₂ (b), 10%Ag/TiO₂-HPO₄ (c), 10%Ag/TiO₂-(NH₄)₂HPO₄ (d), 10%Ag/TiO₂-(C₂H₅)₃PO₄ (e), 10%Ag/TiO₂-P₂O₅ (f) catalysts.

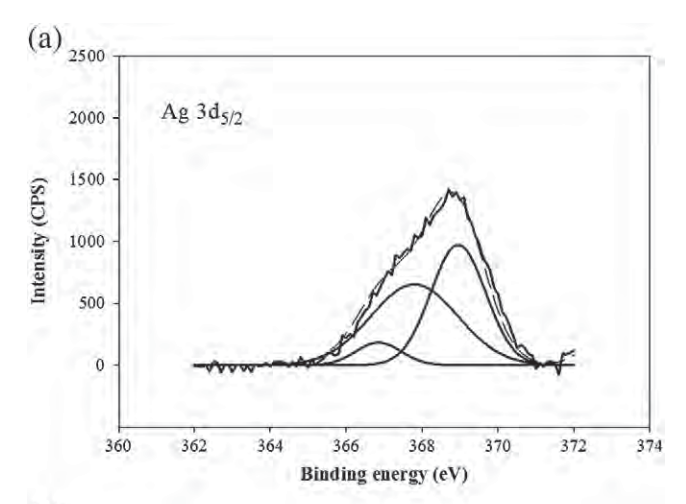


 $\textbf{Fig. 3.} \ \textbf{FT-IR} \ spectra \ of \ TiO_2 \ and \ P-modified \ TiO_2 \ with \ different \ phosphorus \ precursors.$

unmodified-TiO $_2$ support decreased from ~15 to ~11 nm when the TiO $_2$ support was modified with phosphorus. The particle sizes of Ag/Ag $_2$ O on the P-modified TiO $_2$ supports were determined to be ca. 2.3 nm which were smaller than those dispersed on the unmodified-TiO $_2$ (ca. 3 nm). The higher metal dispersion on the P-modified TiO $_2$ supported Ag catalysts was confirmed by the chemisorption results (see also Table 1). The amount of metal active sites on the P-modified TiO $_2$ supported Ag catalysts was nearly three times higher than the unmodified ones. However, the amount of metal active sites on the P-modified TiO $_2$ supported Ag catalysts prepared from different phosphorous precursors were found to be essentially similar in the range of 3.57–3.89 × 10 20 atoms Ag/g cat.

The FT-IR spectra of unmodified and P-modified TiO_2 are shown in Fig. 3. The spectra bands at ca. $1600~cm^{-1}$ and $3200~cm^{-1}$ were attributed to the surface-absorbed water and hydroxyl group, respectively [21,22]. The IR spectra bands at ca. $400-800~cm^{-1}$ were attributed to Ti–O–Ti bond. The bands in this range became weak when the TiO_2 support was modified with phosphorus while the bands corresponding to Ti–O–P appeared at ca. $1100~cm^{-1}$ [23–25]. It is likely that the formation of Ti–O–Ti was suppressed by the formation of Ti–O–P. The incorporation of phosphorus into TiO_2 support could inhibit the agglomeration of TiO_2 crystal, leading to a decrease of TiO_2 crystallite size. The FT-IR results support the characterization by XRD and TEM in which smaller TiO_2 crystallite size was obtained after P doping.

The oxidation state of element on the catalyst surface was examined by XPS and is summarized in Table 2. The binding energies of Ti 2p, O 1s, Ag 3d, and P 2p were slightly different among the various catalysts. The Ti 2p peaks consisting of Ti $2p_{3/2}$ and Ti $2p_{1/2}$, with a separation around 5.3 eV, were assigned to the Ti^{4+} in pure anatase TiO_2 [26,27]. The binding energy of O 1s in all the samples was at ca. 530.0 eV, which was assigned to the Ti-O-Ti lattice oxygen of TiO_2 [28]. The P 2p of all the P-modified TiO_2 shows only one peak in the range of 133.8–134.4 eV, indicating that the oxidation state of phosphorus in TiO_2 was P^{5+} . The absence of P 2p spectra at 129 eV suggested that Ti^{4+} in the lattice of TiO_2 was replaced by P^{5+} [29]. For all the samples, the binding energies of Ag $3d_{5/2}$ and Ag $3d_{3/2}$ were



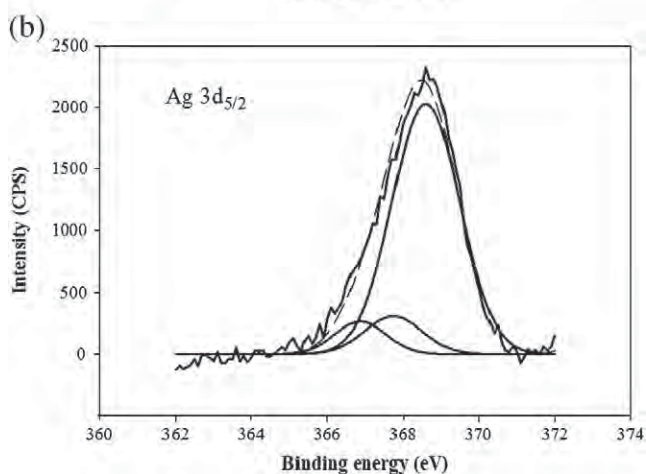


Fig. 4. The Ag 3d XPS spectra of (a) 10%Ag/unmodified-TiO $_2$ and (b) 10%Ag/TiO $_2$ – $(C_2H_5)_3PO_4$ catalysts.

centered at ca. 368 and 374 eV, respectively. According to the literature [30], the binding energy of Ag $3d_{5/2}$ at 368.2 eV and the splitting between Ag $3d_{5/2}$ and Ag $3d_{3/2}$ 6.0 eV indicates a normal state of Ag⁰. The deconvolution of Ag $3d_{5/2}$ of 10%Ag/unmodified-TiO₂ and 10%Ag/TiO₂-(C₂H₅)₃PO₄ is shown in Fig. 4. Three peaks at the binding energy of ca. 366.8 eV, 367.7 eV, and 368.5 eV were attributed to AgO, Ag₂O, and Ag⁰, respectively [31]. Base on the deconvolution analysis, the 10%Ag/TiO₂-(C₂H₅)₃PO₄ catalyst produced larger amount of Ag metallic (80%) than the 10%Ag/unmodified-TiO₂ (45%). Such results indicated that the P-modified TiO₂ promoted the Ag metallic formation on the TiO₂ support.

3.2. Effect of P doping on the activity of CO oxidation

Fig. 5 shows the CO conversion as a function of reaction temperature of the unmodified TiO_2 and P-modified TiO_2 supported Ag catalysts prepared with different types of phosphorus precursor.

Table 2Binding energies of 10 at.% Ag catalyst supported on TiO₂ and P-modified TiO₂ with different phosphorus precursors.

Sample	Ti 2p		O 1s	Ag 3d		P 2p	
	Ti 2p _{3/2}	Ti 2p _{1/2}		Ag 3d _{5/2}	Ag 3d _{3/2}	P 2p _{3/2}	P 2p _{1/2}
10%Ag/unmodified-TiO ₂	458.75	464.55	530.0	368.90	375.00	_	-
10%Ag/TiO ₂ -H ₃ PO ₄	459.85	465.65	531.1	368.70	375.00	133.4	-
10%Ag/TiO ₂ -(NH ₄) ₂ HPO ₄	459.35	465.15	530.70	368.70	374.60	133.80	-
10%Ag/TiO ₂ -(C ₂ H ₅) ₃ PO ₄	459.25	464.85	530.60	368.50	374.60	133.40	135.2
10%Ag/TiO ₂ -P ₂ O ₅	458.45	465.05	530.8	368.90	374.90	134.00	-

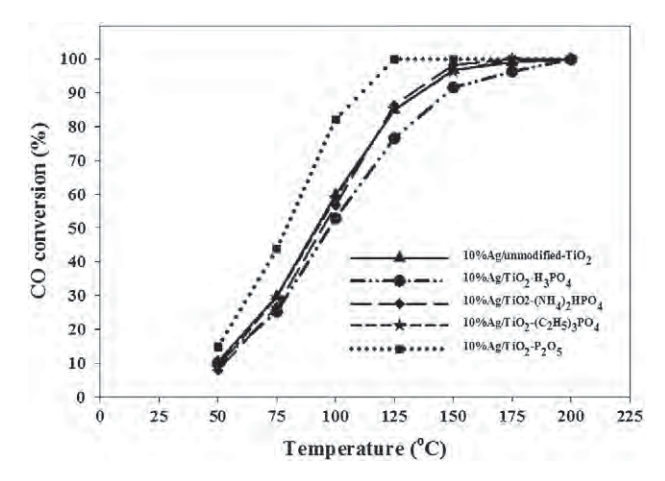


Fig. 5. CO conversion over 10 at.% Ag catalysts supported on ${\rm TiO_2}$ and P-modified ${\rm TiO_2}$ with different phosphorus precursors.

The results show that the type of phosphorus precursor affected the CO oxidation activity of the TiO_2 supported Ag catalysts. The P-modified TiO_2 supported Ag catalysts using the phosphorus precursor in the form of phosphate showed comparable (for $10\%Ag/TiO_2-(NH_4)_2HPO_4$ and $10\%Ag/TiO_2-(C_2H_5)_3PO_4$) or lower activity ($10\%Ag/TiO_2-H_3PO_4$) compared to the $10\%Ag/unmodified-TiO_2$ (light-off temperature ca. 92-97 °C). On the contrary, the catalyst prepared with the phosphorus precursor in the form of oxide ($10\%Ag/TiO_2-P_2O_5$) showed higher activity than the unmodified- TiO_2 supported catalyst (light-off temperature ~80 °C).

Since the physical properties of the P-modified TiO₂ supported Ag catalysts prepared from different phosphorous precursors were quite similar (i.e. in terms of BET surface area, crystallite size, and metal dispersion), the catalytic behaviors were correlated with the O₂ adsorption-desorption behavior on the catalyst surface. Fig. 6 shows the O₂-TPD patterns of the unmodified and P-modified TiO₂ supported Ag catalysts with different phosphorus precursors. The Ag catalyst modified with phosphorus exhibited lower desorption temperature compared to the unmodified ones. The desorption temperature of 10% Ag/TiO₂-(C₂H₅)₃PO₄ and 10%Ag/TiO₂-P₂O₅ catalyst appeared at lower temperature in comparison with the 10%Ag/unmodified-TiO2. The desorption peak appeared in the range of 250 to 265 °C was assigned to species [32]. For the 10%Ag/TiO₂-(NH₄)₂HPO₄ and 10%Ag/TiO₂- H_3PO_4 , a small shoulder of O_2 desorption peak at around 250–265 °C and large desorption peaks at higher temperature in the range of 300-320 °C and 400-430 °C were observed.

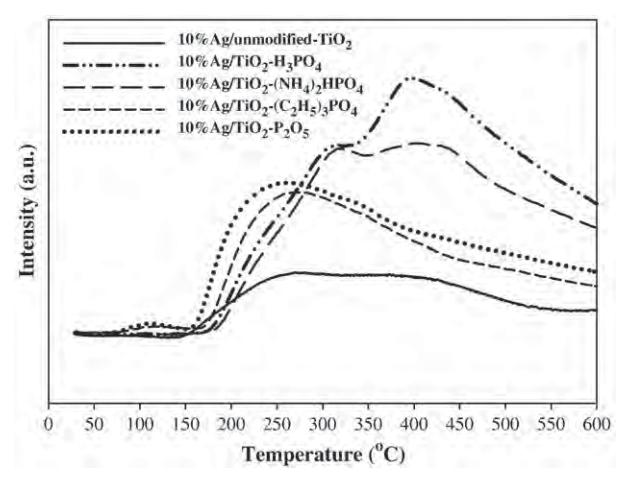
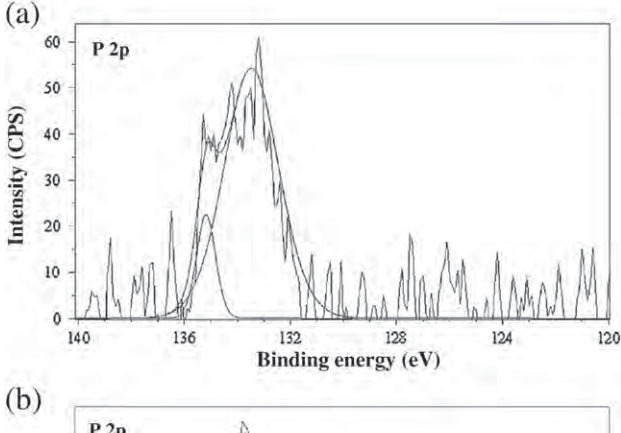


Fig. 6. O_2 -TPD patterns of 10 at.% Ag catalysts supported on TiO_2 and P-modified TiO_2 with different phosphorus precursors.



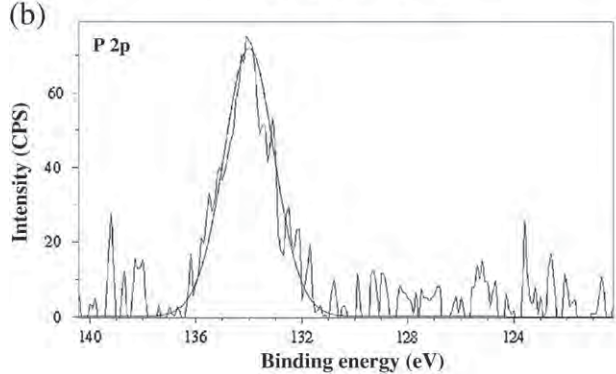


Fig. 7. The P 2p XPS spectra of (a) $10\% Ag/TiO_2-(C_2H_5)_3PO_4$ and (b) $10\% Ag/TiO_2-P_2O_5$ catalysts.

According to Masakazu et al. [33], there are three kinds of adsorbed oxygen species on TiO_2 surface. The adsorbed oxygen consists of weakly adsorbed surface oxygen, strongly adsorbed surface oxygen, and surface lattice oxygen, with the oxygen desorption temperature in the range of 220–250 °C, 470–490 °C, and 810–870 °C, respectively [34,35]. The strongly adsorbed surface oxygen species blocks the adsorption and diffusion of weakly adsorbed surface oxygen, causing a decrease in the CO oxidation activity [36]. It is clearly seen from the O_2 -TPD results that the $10\%\text{Ag/TiO}_2$ – $(NH_4)_2\text{HPO}_4$ and $10\%\text{Ag/TiO}_2$ – $H_3\text{PO}_4$ exhibited higher amount of strongly adsorbed oxygen than the other catalysts, thus lower CO oxidation activities were obtained. The desorption profiles of $10\%\text{Ag/TiO}_2$ – $(C_2H_5)_3\text{PO}_4$, however, was quite similar to the $10\%\text{Ag/TiO}_2$ – P_2O_5 , although the catalytic activities in CO oxidation were different.

Based on the XPS analysis (Fig. 7), the phosphate species on the P-modified TiO_2 surface were identified. The P 2p spectra of 10%Ag/ TiO_2 – $(C_2H_5)_3$ PO $_4$ were slightly different from those of 10%Ag/ TiO_2 – P_2O_5 in which a shoulder at a binding energy of 135.2 eV appeared in addition to the major peak at 133.4 eV. The P 2p spectra at a binding energy of 133.4 eV was assigned to the monodentate surface complex, which phosphate adsorbed to the surface hydroxyl ion with one coordination number. The shoulder peak at higher binding energy (135.2 eV) was assigned to the bidentate surface complex in which phosphate was bound to two surface hydroxyl

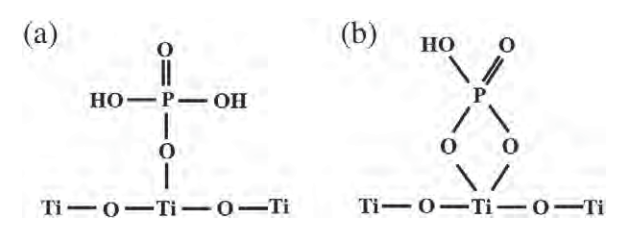


Fig. 8. Schematic illustration of (a) monodentate, (b) bidentate surface complex on the surface of ${\rm TiO_2}$ support.

ions. The formation of monodentate and bidentate surface complexes on TiO₂ support is illustrated in Fig. 8. The bidentate adsorption is very difficult to remove by a washing step during the preparation of P-modified TiO₂ [28,37]. In other words, the 10%Ag/TiO₂- $(C_2H_5)_3$ PO₄ produced bidentate of phosphate species on the surface of TiO₂ that could result in the blocking of active sites and lower activity in CO oxidation.

4. Conclusions

Modification of the TiO₂ supports with different phosphorus precursors altered the catalytic behaviors of Ag/TiO2 catalysts in the CO oxidation. The insertion of phosphorus into the TiO₂ lattice in the form of Ti–O–P not only increased the metal active sites by increasing the specific surface area of the catalyst and inhibiting the agglomeration of TiO₂ crystallites but also altered the strength of O2 adsorption—desorption behavior on the catalyst surface. The P-modified TiO2 supported Ag catalysts using the phosphorus precursor in the form of phosphate produced the strongly adsorbed oxygen species and/or the bidentate of phosphate species on the TiO₂ supports, which resulted in no improvement in the CO oxidation activity. On the other hand, the use of phosphorus precursor in the form of oxide enhanced the CO oxidation activity of Ag/TiO2 catalysts due to the promotion of weakly adsorbed oxygen species.

Acknowledgments

The financial support from the Thailand Research Fund (TRF) and the Office of Higher Education Commission (CHE), Ministry of Education, Thailand are gratefully acknowledged.

References

- S.J. Tauster, S.C. Fung, R.L. Garten, J. Am. Chem. Soc. 100 (1978) 170-175.
- [2] G.L. Haller, D.E. Resasco, H.P.D.D. Eley, B.W. Paul, Adv. Catal. 36 (1989) 173–235.
 [3] M.A. Vannice, B. Sen, J. Catal. 115 (1989) 65–78.
- [4] P. Claus, S. Schimpf, R. Schdel, P. Kraak, W. Mrke, D. Hnicke, Appl. Catal. A Gen. 165 (1997) 429-441.

- [5] L.L. Murrell, D.J.C. Yates, T. Seiyama, K. Tanabe, Stud. Surf. Sci. Catal. 7 (1981) 1470-1471.
- C.-S. Chen, J.-H. You, J.-H. Lin, Y.-Y. Chen, Catal. Commun. 9 (2008) 2381-2385.
- M.A. Vannice, C. Sudhakar, J. Phys. Chem. 88 (1984) 2429-2432.
- J. Yu, G. Wu, D. Mao, G. Lu, Acta Phys. Chim. Sin. 24 (2008) 1751-1755.
- C.L. Peza-Ledesma, L. Escamilla-Perea, R. Nava, B. Pawelec, J.L.G. Fierro, Appl. Catal. A Gen. 375 (2010) 37-48.
- [10] J.A. Hernandez, S. Gomez, B. Pawelec, T.A. Zepeda, Appl. Catal. B Environ. 89 (2009) 128–136.
- J.-N. Lin, J.-H Chen, C.-Y Hsiao, Y.-M. Kang, B.-Z. Wan, Appl. Catal. B: Environmental 36 (2002) 19–29.
- [12] J. Moma, M. Scurrell, W. Jordaan, Top. Catal. 44 (2007) 167-172.
- K. Ruth, M. Hayes, R. Burch, S. Tsubota, M. Haruta, Appl. Catal. B Environ. 24 (2000) L133-L138
- [14] M.R. Kim, S.I. Woo, Appl. Catal. A Gen. 299 (2006) 52-57.
- Z. Ma, S. Brown, S.H. Overbury, S. Dai, Appl. Catal. A Gen. 327 (2007) 226–237.
- W. Payakgul, O Mekasuwandumrong, V. Pavarajarn, P. Praserthdam, Ceram. Int. 31 (2005) 391-397.
- N. Comsup, J. Panpranot, P. Praserthdam, Catal. Lett. 133 (2009) 76-83.
- T. Nanba, S. Masukawa, J. Uchisawa, A. Obuchi, J. Catal. 259 (2008) 250-259.
- L. Ren, Y.-P. Zeng, D. Jiang, Catal. Commun. 10 (2009) 645-649.
- X. Fan, T. Yu, Y. Wang, J. Zheng, L. Gao, Z. Li, J. Ye, Z. Zou, Appl. Surf. Sci. 254 (2008) [20]
- [21] J. Zhu, J. Yang, Z.-F. Bian, J. Ren, Y.-M. Liu, Y. Cao, H.-X. Li, H.-Y. He, K.-N. Fan, Appl. Catal. B Environ. 76 (2007) 82–91.
- K. Nagaveni, M.S. Hegde, N. Ravishankar, G.N. Subbanna, G. Madras, Langmuir 20 (2004) 2900-2907.
- J.C. Yu, L. Zhang, J. Yu, Chem. Mater. 14 (2002) 4647-4653.
- A. Bhaumik, S. Inagaki, J. Am. Chem. Soc. 123 (2001) 691-696.
- [25] X. Zhang, J.C. Shen, Adv. Mater. 11 (1999) 1139-1143.
- G. Silversmit, G. De Doncker, R. De Gryse, Surf. Sci. Spectra 9 (2002) 21-29.
- C.K. Maiti, S.K. Samanta, G.K. Dalapati, S.K. Nandi, S. Chatterjee, Microelectron. Eng. 72 (2004) 253–256. D. Zhao, C. Chen, Y. Wang, H. Ji, W. Ma, L. Zang, J. Zhao, J. Phys. Chem. C 112 (2008)
- 5993-6001.
- Q. Shi, D. Yang, Z. Jiang, J. Li, J. Mol. Catal. B Enzym. 43 (2006) 44-48.
- H. Wang, J. Niu, X. Long, Y. He, Ultrason. Sonochem. 15 (2008) 386-392.
- B. Xin, L. Jing, Z. Ren, B. Wang, H. Fu, J. Phys. Chem. B 109 (2005) 2805–2809.
- [32] H. Chon, J. Pajares, J. Catal. 14 (1969) 257-260.
- [33] M. Iwamoto, Y. Yoda, N. Yamazoe, T. Seiyama, J. Phys. Chem. 82 (1978) 2564-2570.
- R. Li, J. Ma, J. Xu, X. Zhou, Z. Su, React. Kinet. Catal. Lett. 70 (2000) 363-370.
- L. Luo, G. Shao, Z. Duan, Turk. J. Chem. 29 (2005) 597-605.
- Q. Zhenping, C. Mojie, S. Chuan, B. Xinhe, J. Nat. Gas Chem. 14 (2005) 4-12.
- E.W. Shin, J.S. Han, M. Jang, S.-H. Min, J.K. Park, R.M. Rowell, Environ. Sci. Technol. 38 (2003) 912-917.

Provided for non-commercial research and education use.

Not for reproduction, distribution or commercial use.



This article appeared in a journal published by Elsevier. The attached copy is furnished to the author for internal non-commercial research and education use, including for instruction at the authors institution and sharing with colleagues.

Other uses, including reproduction and distribution, or selling or licensing copies, or posting to personal, institutional or third party websites are prohibited.

In most cases authors are permitted to post their version of the article (e.g. in Word or Tex form) to their personal website or institutional repository. Authors requiring further information regarding Elsevier's archiving and manuscript policies are encouraged to visit:

http://www.elsevier.com/copyright

Author's personal copy

Chemical Engineering Journal 164 (2010) 77-84

ELSEVIER

Contents lists available at ScienceDirect

Chemical Engineering Journal

journal homepage: www.elsevier.com/locate/cej

Chemical Engineering Journal

Effects of synthesis conditions and annealing post-treatment on the photocatalytic activities of ZnO nanoparticles in the degradation of methylene blue dye

Okorn Mekasuwandumrong^a, Pongsapak Pawinrat^b, Piyasan Praserthdam^b, Joongjai Panpranot^{b,*}

- ^a Department of Chemical Engineering, Faculty of Engineering and Industrial Technology, Silpakorn University, Nakorn Phathom 73000, Thailand
- b Center of Excellence on Catalysis and Catalytic Reaction Engineering, Department of Chemical Engineering,

Faculty of Engineering, Chulalongkorn University, Bangkok 10330, Thailand

ARTICLE INFO

Article history: Received 8 March 2010 Received in revised form 11 August 2010 Accepted 11 August 2010

Keywords: Flame-spray pyrolysis ZnO Particle size effect Photocatalysts Annealing

ABSTRACT

The effects of synthesis conditions (i.e., metal concentration, precursor flowrate, and O_2 dispersion) during flame-spray pyrolysis (FSP) and annealing post-treatment on the characteristics and photocatalytic activities of ZnO nanoparticles have been investigated. The average particle size of ZnO powder prepared by one-step FSP method were in the range of 8.8–47.0 nm and were found to be increased with increasing the enthalpy density, flame height, and high-temperature residence time during FSP synthesis. The larger particle size FSP-derived ZnO nanoparticles exhibited higher photocatalytic activities in the degradation of methylene blue (MB) dye. The degradation rate over FSP-ZnO-47.0 nm was 1.7 and 7.2 times higher than those of the commercially available photocatalysts Degussa P-25 and JRC-TiO2, respectively. The better photocatalytic performance of the FSP-ZnO was correlated well with the improved crystalline quality of ZnO nanoparticles as revealed by the X-ray diffraction (XRD) and the photoluminescence (PL) results. Further increase of FSP-ZnO particle size to 52.6–103.5 nm by annealing post-treatment at high temperatures (750–900 °C), however, gradually decreased their photocatalytic activities. Our results in this study suggest a balance between high crystalline quality that enhanced photo phenomena and the surface area available for substrate adsorption in order to obtain high photocatalytic activity of ZnO nanoparticles.

© 2010 Elsevier B.V. All rights reserved.

1. Introduction

Dye pollutants from textile paper and other industries are an important source of environmental contamination. Conventional treatment of such wastewater generally involves coagulation/flocculation [1,2], electrocoagulation [3], coagulation/carbon adsorption process [4] and so on. These methods, however, merely transfer dyes from the liquid-phase to the solid-phase, requiring further treatment and causing secondary pollution [5]. In the past two decades, photocatalysis by semiconductive materials such as TiO₂ and ZnO has attracted public concern as a promising tool among the advanced oxidation processes to substitute the traditional wastewater treatment due to their high photosensitivity, non-toxic nature, high stability, and wide band gap [6]. While TiO₂ is probably the most frequently used photocatalyst, ZnO is an alternative photocatalyst with low cost. It has a similar band gap energy compared to TiO₂ (3.2 eV) [7] and can adsorb over a larger frac-

tion of UV spectrum [8]. Higher photocatalytic efficiency of ZnO compared to TiO_2 has been reported especially for degradation of organics in aqueous solutions [5,9–13]. Our recent study showed that Au–ZnO and Pt–ZnO nanocomposites prepared by one-step flame-spray pyrolysis exhibited high photocatalytic activities in degradation of methylene blue dye [14].

For semiconductor photocatalysts, particle size is an important parameter for controlling surface area and electronic structure. When the catalyst particle size is reduced down to a few nanometers, an elevate density of active sites for substrate adsorption and/or catalysis can be guaranteed, as small particles possess a significantly higher surface-to-volume ratio compared to the bulk material. When the nanocrystal size is comparable or smaller than the bulk exciton diameter, the band-gap becomes size-dependent due to quantization effects [15,16]. Moreover, an efficient photocatalytic process requires highly crystalline semiconductors to minimize electron-hole pair loss owing to the trapping of either charge carriers at defect states [17,18].

The effect of particle size on photoactivity of ZnO has been addressed by a number of researchers [19–22]. For examples, among the three different particle sizes of ZnO nanoparticles (14,

^{*} Corresponding author. Tel.: +66 2218 6869; fax: +66 2218 6877. E-mail address: joongjai.p@chula.ac.th (J. Panpranot).

O. Mekasuwandumrong et al. / Chemical Engineering Journal 164 (2010) 77-84

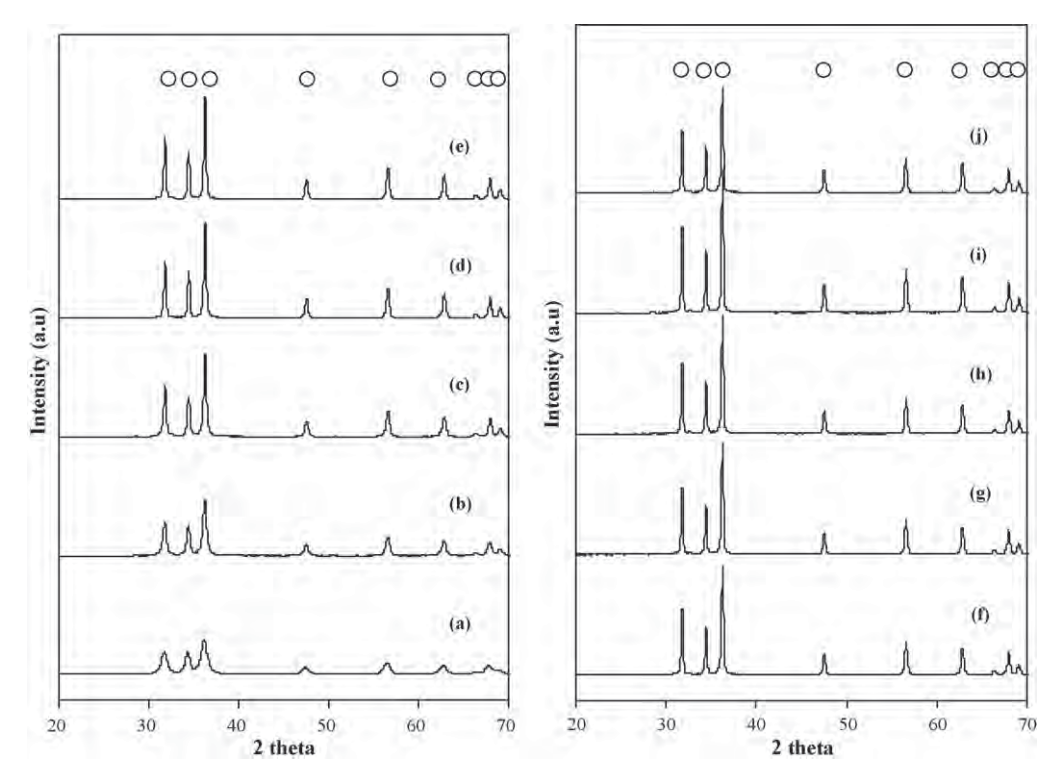


Fig. 1. XRD patterns of the as-prepared flame-made ZnO with various crystallite sizes: (a) 8.8 nm, (b) 19.4 nm, (c) 30 nm, (d) 40.7 nm, (e) 47 nm and the annealed flame-made ZnO particles: (f) 52.6 nm, (g) 67.1 nm, (h) 80.3 nm, (i) 90.6 nm, (j) 103.5 nm.

19, and 26 nm) prepared by precipitation process, the smaller one resulted in more surface oxygen vacancies, higher ESR intensity, stronger PL signal, and higher photocatalytic activity [20]. Dodd et al. [21] prepared ZnO nanoparticles with various particle sizes

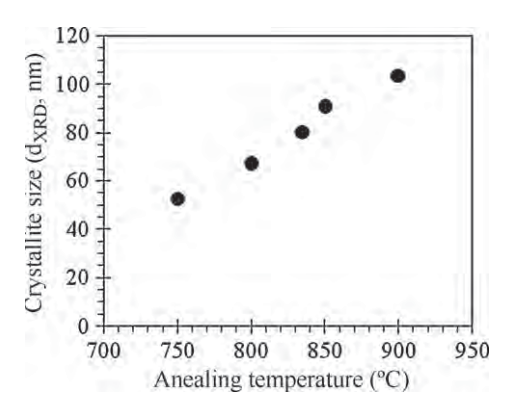


Fig. 2. Relationship between crystallite size of ZnO and annealing temperature.

in the range of 28-57 nm by mechanical milling and heat treatment. The authors found that there exists an optimum size of 33 nm for which the photocatalytic activity of ZnO is maximized. Li et al. [22] also obtained ZnO nanoparticles with average sizes 21–90 nm by varying the calcination temperature between 200 and 1000 °C and found that ZnO prismatic aggregated obtained by calcination at 800 °C demonstrated the highest photocatalytic activity. More recently, Xie et al. [19] showed that photocatalytic properties of various particle sizes of ZnO (15, 50, 200, and 1000 nm) synthesized by thermal evaporation and chemical deposition in UV-induced degradation of methyl orange depended on size, morphology, and preparation method of ZnO. Thus, in previous studies, it has clearly shown that efficiency of photocatalytic process can be maximized by optimizing the particle size of ZnO photocatalysts. However, preparation method as well as pretreatment conditions such as calcination temperature strongly affects the properties of ZnO photocatalysts.

In this report, ZnO nanoparticles with various particle sizes were obtained by flame-spray pyrolysis (FSP) method. Various particle sizes of the flame-made ZnO powder (8.8–103.5 nm) were obtained by varying the process conditions such as metal concentration in

Table 1Relationship between the synthesis conditions and ZnO crystallite sizes.

Metal concentration (molar)	Precursor flow rate (ml/min)	Dispersion oxygen flow rate (l/min)	Annealing temperature (°C)	Crystallite size d_{XRD} (nm)	Average primary particle size d_{TEM} (nm)	BET surface area (m²/g)
0.3	3	5	n/a	8.8	11.1	63.1
0.3	8	3	n/a	19.4	20.5	35.5
0.5	8	3	n/a	30.0	31.3	26.2
0.8	8	3	n/a	40.7	39.8	13.6
1	8	3	n/a	47.0	48.7	15.1
1	8	3	750	52.6	57.7	12.0
1	8	3	800	67.1	71.7	8.0
1	8	3	835	80.3	98.9	6.8
1	8	3	850	90.6	116.7	5.9
1	8	3	900	103.5	159.9	5.8

n/a = not applied.

feed, precursor flow rate, dispersion oxygen flow rate, and annealing temperature. The effects of both FSP synthesis conditions and annealing post-treatment on the characteristics and photocatalytic properties of the flame-made ZnO in photodegradation of methylene blue (MB) were discussed extensively.

2. Material and methods

2.1. Synthesis of ZnO nanoparticles by flame-spray pyrolysis

Synthesis of ZnO with various particle sizes by FSP technique were carried out using a spray flame reactor [24]. Zinc naphthanate (Aldrich; <50% in mineral spirits) was used as zinc precursor. The

precursor was dissolved in ethanol (J.T. Baker; 99.9%). To obtain different ZnO particle sizes during particle synthesis, precursor solution ranged from 0.3 to 1 mol/l and liquid precursor feed rates varied from 3 to 8 ml/min were fed to the flame by a syringe pump. Precursors were dispersed with 3-5 l/min oxygen forming fine spray droplets. The pressure drop at the capillary tip was maintained at 1.5 bar by adjusting the orifice gap area at the nozzle. The reactor was water-cooled to avoid evaporation or decomposition of the precursor within the feed lines. The flame was ignited by a concentric premixed methane/oxygen pilot flame (CH₄ 1.5 l/min, O₂ 3.0 l/min) that was sheathed further by flowing oxygen (25 l/min) through a sintered metal plate ring (8 mm wide,

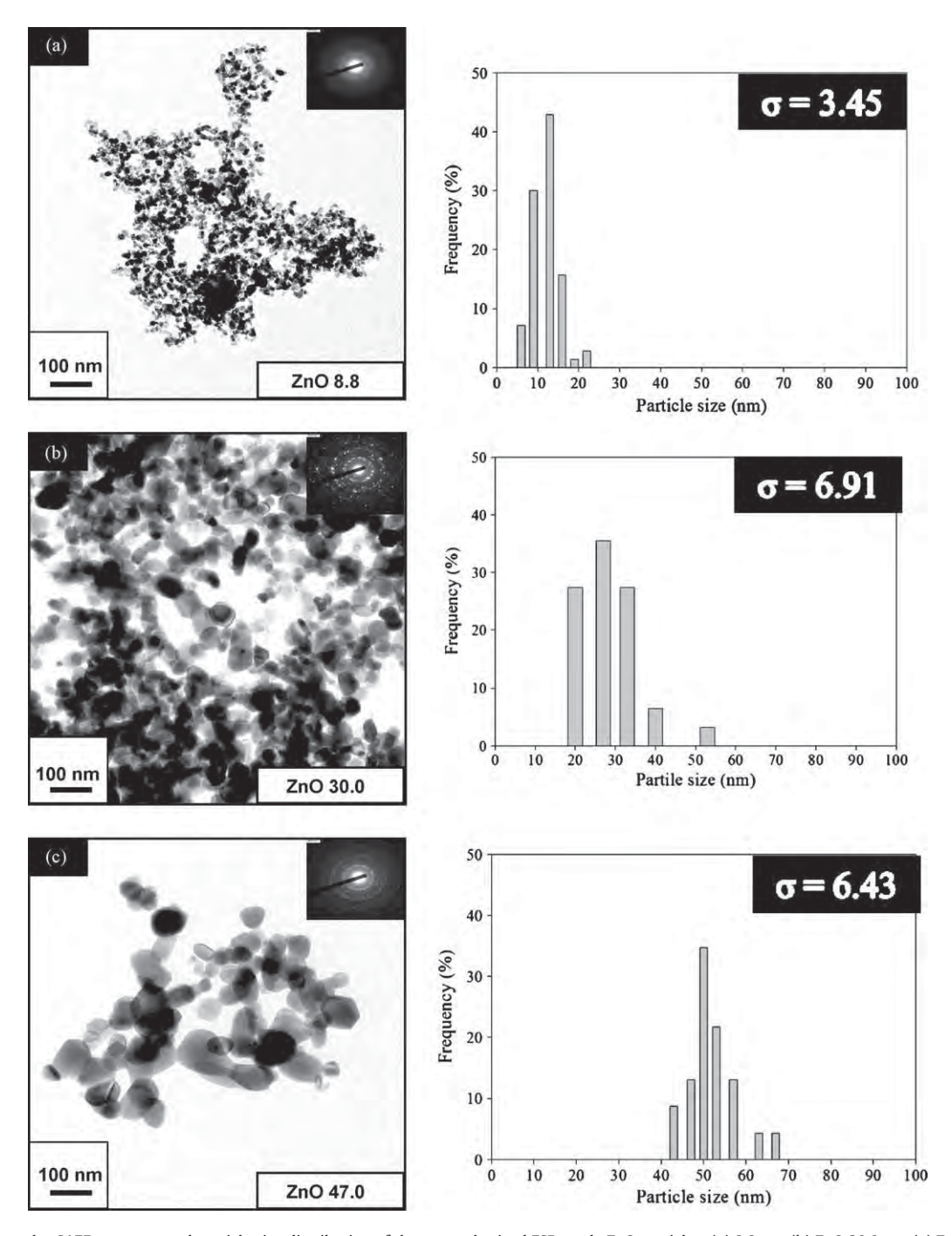


Fig. 3. TEM micrographs, SAED patterns, and particle size distribution of the as-synthesized FSP-made ZnO particles: (a) 8.8 nm, (b) ZnO 30.0 nm, (c) ZnO 47.0 nm and the annealed ZnO: (d) 67.1 nm, (e) 80.3 nm, (f) 103.5 nm.

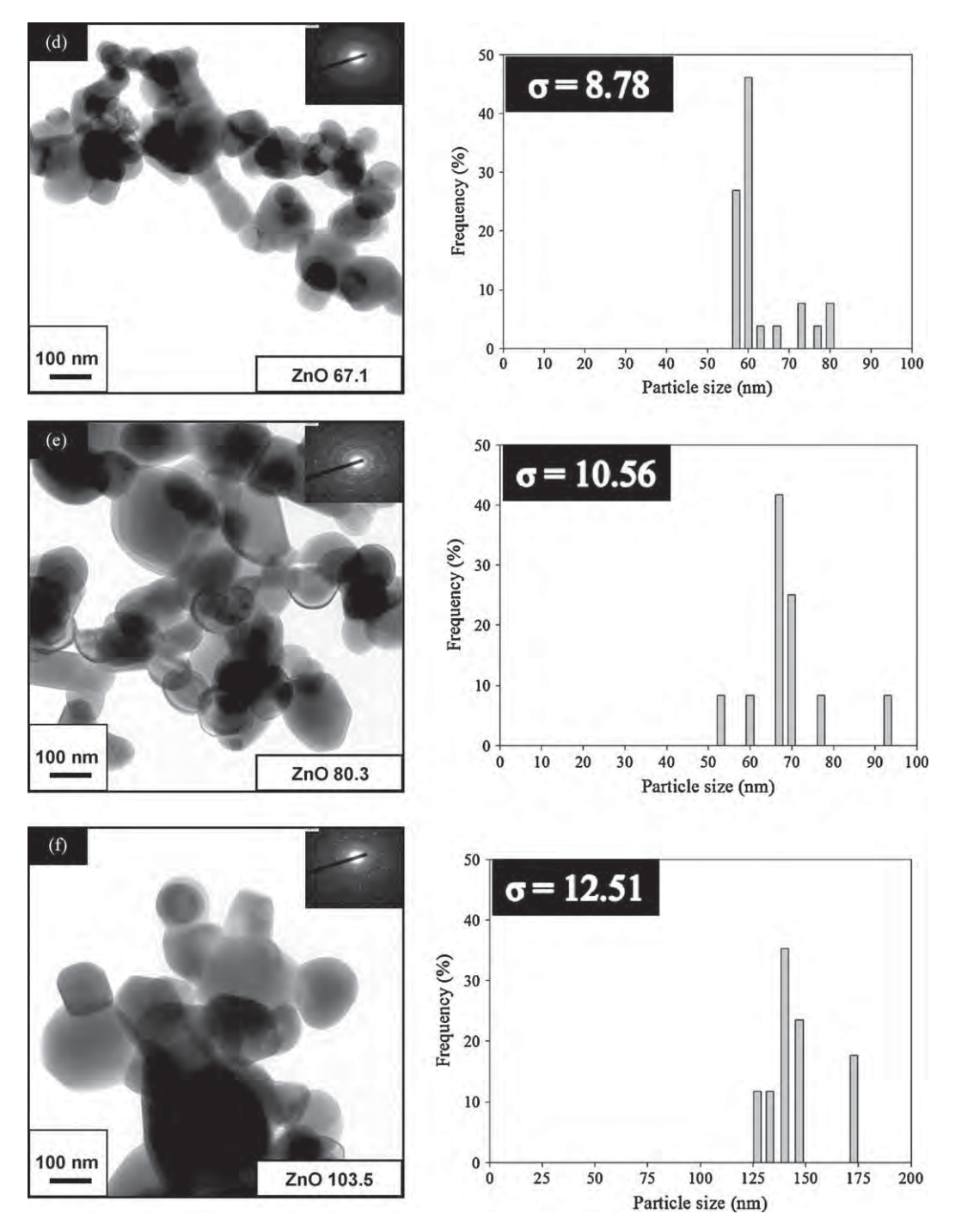


Fig. 3. (Continued)

starting at a radius of 8 mm). The powder particles were collected on a glass-fiber filter (GF/D Whatman; 257 mm diameter) with the aid of a vacuum pump.

2.2. Annealing of the flame-made ZnO

Annealing of the ZnO powders was performed in a Carbolite CWF1300 temperature programmed box furnace in static air, ZnO powders with the particle size of 47 nm produced by FSP method were heated at 10 °C/min to desired temperature (750, 800, 835, 850, or 900 °C) and maintained at that temperature for 1 h in order to form larger particles.

2.3. Characterization

Powder X-ray diffraction (XRD) was performed by a SIEMENS XRD D5000 diffractometer using Cu K α radiation. The crystallite size (d_{XRD}) of FSP-ZnO powders was estimated from the full-width half-maximum breadth of the (101) diffraction peak using the Scherrer equation. The specific surface area was measured by N $_2$ physisorption using a Micromeritics ASAP 2000 automated system and the Brunauer–Emmet–Teller (BET) method. Each sample was degassed under vacuum at <1 \times 10 $^{-5}$ bar in the Micromeritics system at 300 $^{\circ}$ C for 3 h prior to N $_2$ physisorption. The particle morphology was observed using JEOL Model JEM-

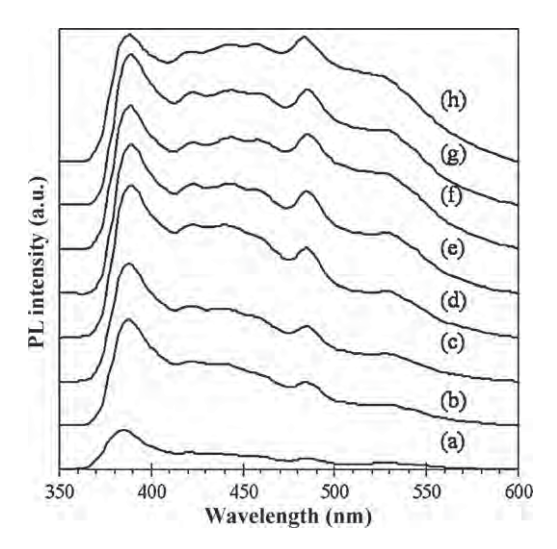


Fig. 4. PL spectra of various ZnO particle sizes prepared by FSP method (a) ZnO $8.8\,\text{nm}$, (b) ZnO $19.4\,\text{nm}$, (c) ZnO $30.0\,\text{nm}$, (d) ZnO $47.0\,\text{nm}$, (e) ZnO $67.1\,\text{nm}$, (f) ZnO $80.3\,\text{nm}$, (g) ZnO $90.6\,\text{nm}$, and (h) ZnO $103.5\,\text{nm}$ with the excitation wavelength of $325\,\text{nm}$

2010 transmission electron microscope (TEM) operated at 200 keV. Photoluminescence measurement (PL) was carried out on a fluorescence spectrophotometer (Perkin-Elmer LS-50) using a Xenon lamp as the excitation source at room temperature. The sample was dispersed in ethanol using ultrasonic bath and the excitation wavelength used in PL measurement was 325 nm.

2.4. Photocatalytic activity testing

A basic aniline dye, methylene blue (MB), from Unilab Asia Pacific Specialty Chemicals Limited was used as a probe molecule to evaluate the photocatalytic activities of the flame-made ZnO with various particle sizes. The photocatalytic reaction was conducted at room temperature under UV light 2 × 15 W UV tube predominantly emitting at 365 nm (Philips) with the average light intensity on the reaction beaker (pyrex) at a distance of 6 cm from the lamp was found to be $4.7 \times 10^{-4} \, \text{W cm}^{-2}$. The reaction was carried out with 20 mg of catalyst dispersed in 200 ml of 10 ppm methylene blue aqueous solution. The pH of solution was constant at 6.3 for all experiments. The reaction was operated with high stirring rate (1000 rpm) in order to eliminate the external mass transfer effect. Prior to irradiation, the suspensions were magnetically stirred in the dark for 15 min to establish the adsorption/desorption equilibrium of methylene blue. 2 ml samples were withdrawn every 10 min. Before analysis, the aqueous samples were centrifuged to remove any suspended solid catalyst particles. The residual concentration of methylene blue was measured at 665 nm using the UV-vis spectrophotometer (Perkin-Elmer lampda 650) in liquid cuvette configuration with de-ionized water as reference. The percentage of degradation was calculated using the equation given

Degradation (%) =
$$\frac{C_0 - C}{C_0} \times 100$$
 (1)

in which C_0 is the initial dye concentration and C is the dye concentration after the treatments.

3. Results and discussion

3.1. Particles characterization

Fig. 1a-e shows the XRD patterns of as-synthesized FSP-ZnO nanopowder with average crystallite sizes between 8.8 and

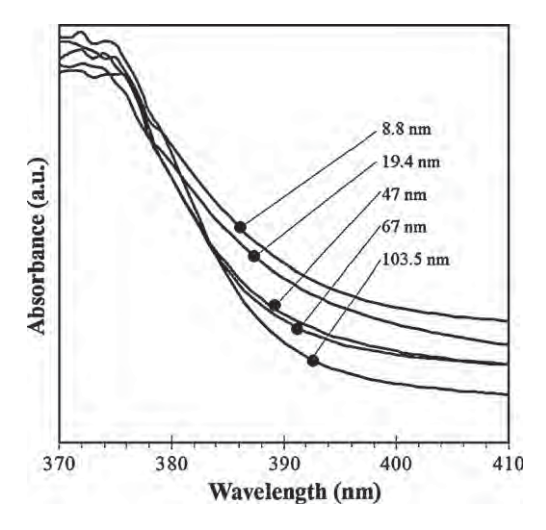


Fig. 5. UV-vis spectra of ZnO with various particle sizes.

47.0 nm. All of the indexed peaks are well matched with that of bulk ZnO (JCPDS Card No. 36-1451) possessing wurtzite hexagonal phase. No other diffraction peaks or amorphous phase was detected. The diffraction peak intensities were increased and the peaks became sharper with increasing ZnO particle sizes. The larger particle sizes of ZnO particles were obtained by increasing the precursor concentration, the ratio of the feed liquid, and decreasing the dispersion oxygen gas flow rates through the nozzle. Fig. 1f-j shows the XRD patterns of the annealed ZnO powders. The XRD characteristic peaks were similar to those of the as-synthesized ones. The calculated particle sizes of annealed ZnO were in the range of 52.6-103.5 nm indicating that annealing of the flame-made ZnO particles (47 nm) at relatively high temperature between 750 and 900 °C resulted in further crystal growth of ZnO. The relationship between synthesis conditions and corresponding ZnO particle sizes are summarized and illustrated in Table 1 and Fig. 2, respectively.

The TEM micrographs with selected area electron diffraction (SAED) patterns and particle size distribution of the as-synthesized and the annealed ZnO with various particle sizes are shown in Fig. 3. Frequency (%) was obtained by counting 50–100 ZnO particles from TEM images. All the samples consisted of polyhedral primary particles, typically seen in flame-made powders [23], with spheroidal particles and rod-like particles. The average primary particle diameters of ZnO with various particle sizes determined by TEM ($d_{\rm TEM}$) are also given in Table 1. The $d_{\rm TEM}$ data were in good agreement with the $d_{\rm XRD}$ values. The corresponding SAED patterns are shown in the

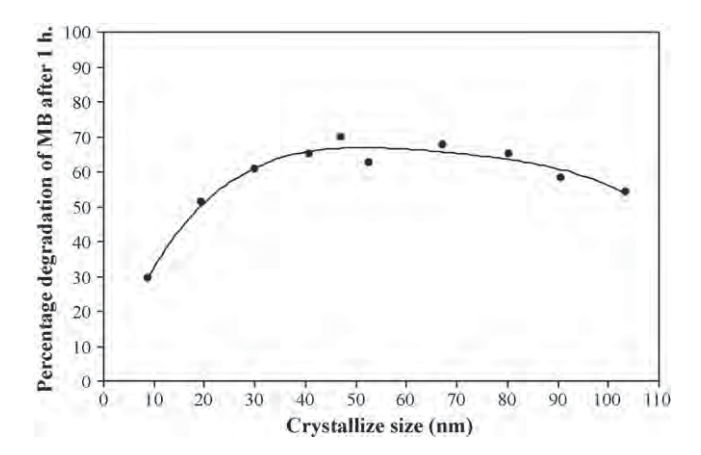


Fig. 6. Relationship between for the percentage of MB degradation after 1 h and the particle size of ZnO photocatalysts prepared by FSP method.

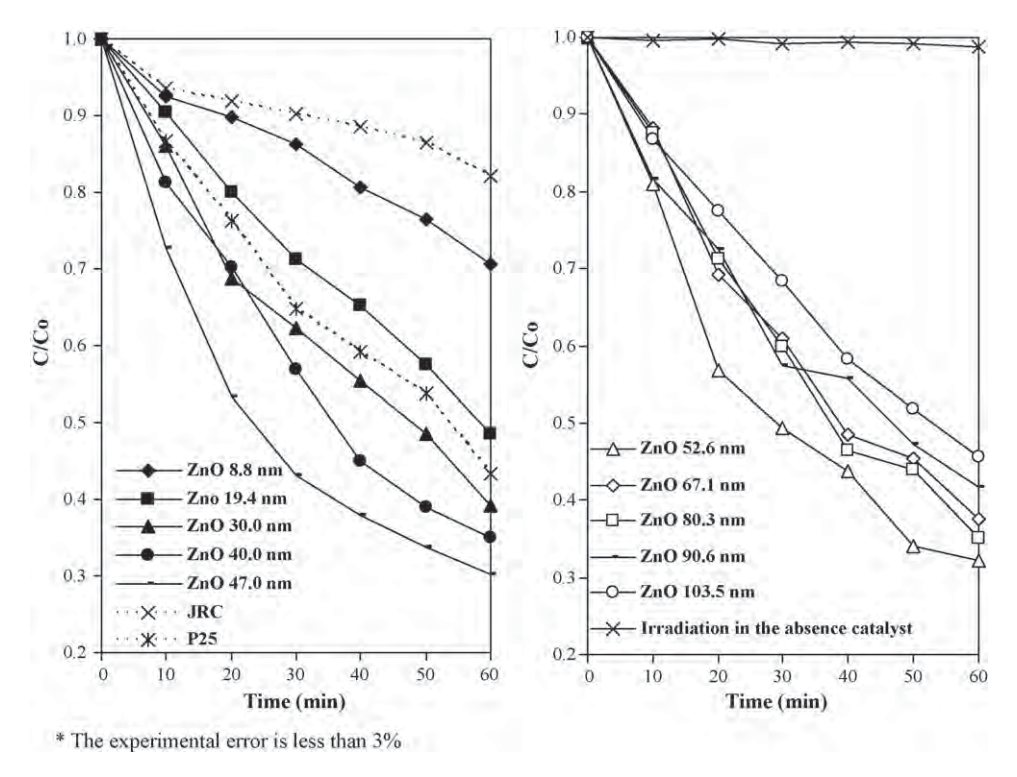


Fig. 7. The catalytic performances for photodegradation of methylene blue using FSP-made ZnO catalysts with various particle sizes (bold lines) and commercial catalysts for comparison (P25 and JRC titania) (dashed lines).

insets. The diffraction patterns of all the powders illustrate spot patterns of the hexagonal structure of ZnO, indicating that the ZnO nanoparticles are single crystalline. As also shown in Table 1, BET surface areas of the as-synthesized ZnO particles decreased from 63.1 to 15.1 m^2/g as the precursor concentration increased from 0.3 to 1 M and the feed rate increased from 3 to 8 ml/min. The result was consistent with previous studies of the flame-synthesized metal oxides such as TiO₂ [25], SiO₂ [26], CeO₂ [27], Pt/Al₂O₃ [28], and Ag/ZnO [29]. Typically, increasing of precursor feed flow rate and/or precursor concentration while keeping the oxygen flow rate constant results in higher enthalpy of flame, longer residence times and hotter flames [24,25]. This phenomenon is due to the fact that the combustion of the precursor is an exothermic reaction, contributing to overall increase in energy dissipation within the flame. Additionally, as the precursor feed flow rate and precursor concentration increased, Zn concentration within the flame also increased. This, coupled with the increased enthalpy content, residence time and higher flame temperature, resulted in increased coalescence and sintering of the particles. After high-temperature annealing (750-900°C), the BET surface areas decreased further from 15.1 to $5.8 \,\mathrm{m}^2/\mathrm{g}$ indicating that ZnO particles sintered by heat treatment.

Room temperature PL spectra of all the ZnO powders are shown in Fig. 4. The spectra mainly consisted of two emission bands. The first band is the UV near-band-edge emission (NBE) at ~385 nm [30,31]. Sharp NBE emission peak results from recombination of excitons and its position and structure is an indication of crystal quality [32,33]. The NBE emission intensities in the PL spectra increased as the particle size of as-synthesized ZnO increased. The highest value was found for the FSP-made ZnO with the crystallite size of 47 nm. Improvement of the crystal quality of ZnO can be attributed to the increase of flame enthalpy and Zn atomic concentration in gas phase that contributed typically to longer and hotter flames, which as a consequence, produced larger and more crystalline particles. However, the excitonic peak intensity for the annealed samples was remained constant and slightly decreased as the annealing temperature was raised higher than 835 °C. More-

over, the shift to the lower wavelength was also found in the FSP-made ZnO with the crystallite size of 8.8 nm. This result would be attributed to the quantum confinement effect of ZnO nanoparticles [34,35]. Madler et al. [35] prepared the ZnO quantum dots by spray combustion of Zn/Si precursors. These crystallites exhibit a quantum size effect due to the preventing of the growth and stabilized the ZnO crystals. The blue shift of the ultraviolet-vis absorption edge increased with decreasing ZnO crystal size. The other band observed in PL spectra was the visible emission that usually associates with the deep level emission (DLE) in ZnO. Most researchers believe that the DLE come from oxygen vacancies (V_0) . zinc vacancies (Zn₀), interstitial zinc (Zn_i), or interstitial oxygen (O_i) [36,37]. The blue emission at ~425 nm and weak blue at ~445 nm most likely occurs from the donor level of Zn interstitial (Zn_i) to acceptor energy level of Zn vacancy (Zn_0) [38]. The blue-green band around 470 nm was probably caused by radiative

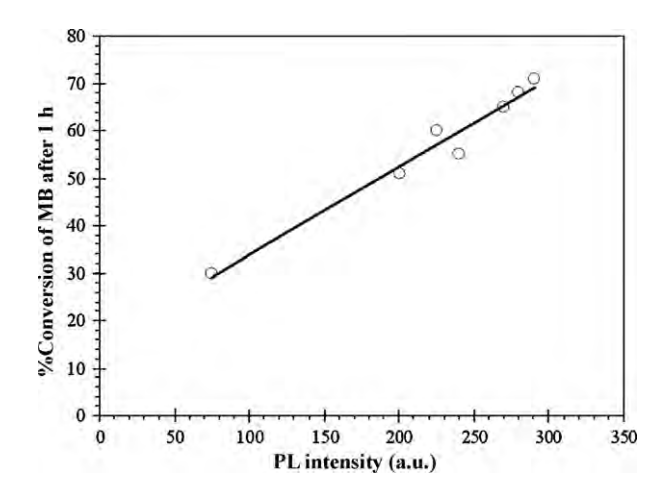


Fig. 8. Relationship between percentage of conversion of MB after 1 h of UV irradiation and PL intensity of the ZnO particles.

O. Mekasuwandumrong et al. / Chemical Engineering Journal 164 (2010) 77-84

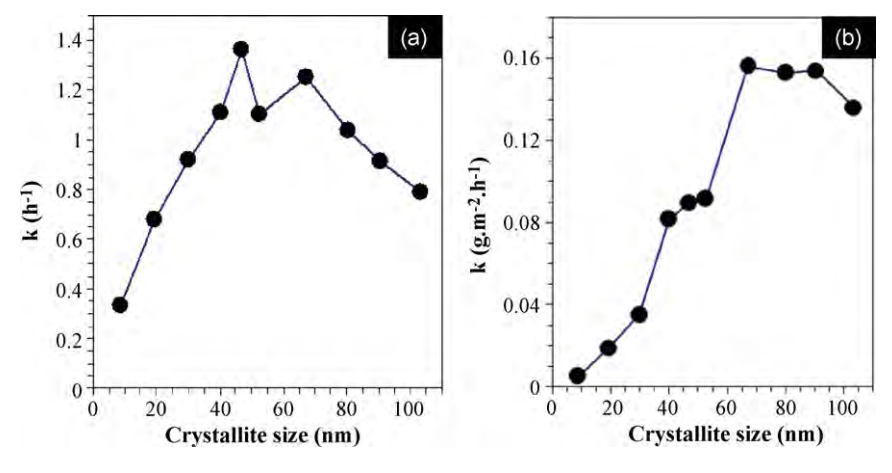


Fig. 9. Pseudo first-order rate constants for ZnO catalysts with various crystallite sizes on a mass (a) and SSA normalized (b) basis.

transition of electron from shallow donor levels, created by the oxygen vacancy to valence band [39]. The green emission at $\sim\!\!530$ is commonly observed for ZnO, and was attributed to the singly ionized oxygen vacancy in ZnO [40]. This emission results from the recombination of a photo-generated hole with the singly ionized charge state of the specific defect [41]. The peak intensity of the blue and weak blue peak light emission increased with increasing of ZnO crystallite size from 8.8 to 47.0 nm and then was found remained unchanged. The weak blue–green band and green band emission peaks intensity slightly increased with increasing crystallite size from 8.8 to 103.5 nm.

Fig. 5 shows UV–vis absorbance spectra of the FSP-made ZnO powders. It can be seen that the slope of UV–vis spectra of the FSP-made ZnO powder was steeper from the smallest size of 8.8 nm to the size of 47 nm before reaching a plateau. A sharp UV–vis absorption curve (steep slope) indicates a high degree of crystalline quality [29]. The improved crystal structure for the larger size ZnO was in good agreement with the XRD and PL-measurements.

3.2. Photocatalytic activity

The dependence of percent conversion of MB decomposition after 60 min on the particle size of ZnO powders is shown in Fig. 6. Irradiation in the absence of photocatalyst for 60 min revealed no change in the MB concentration, confirming that the MB cannot be degraded by 365 nm irradiation alone. The percentages of MB degradation increased from 30 to 70% when the particle size of as-synthesized ZnO powders increased from 8.8 to 47 nm. The photocatalytic performances for MB degradation of the as-synthesized and annealed FSP-ZnO catalysts are also shown as the plots of (C/C_0) versus time in Fig. 7 in which the results for commercial photocatalysts Degussa P25 ($d_{XRD} = 20.1 \text{ nm}$) and JRC-TiO-1 titania (d_{XRD} = 15.5 nm) and irradiation in the absence of catalyst are included. The photocatalytic activity of the as-synthesized flamemade ZnO powders was superior to both P25 and JRC-TiO-1 titania when their particle sizes were larger than 30 nm with the as-syn ZnO-47 nm showed the highest activity. The rate constant assuming first-order kinetics of ZnO-47 nm was determined to be 1.7 and 7.2 times higher than those of degussa P25 and JRC-TiO-1 titania, respectively. For the larger particle sizes of ZnO powder obtained by annealing post-treatment, the percentages of MB degradation gradually decreased from 70 to 55%. The lower photocatalytic efficiency can be ascribed by the decrease in BET surface area, which lowered the adsorption of dye molecules on the catalyst surface.

In general, photocatalysis can be considered to be dominated by two linked mechanisms, namely photo phenomena or the interaction of light with the material to form electron-hole pairs, and secondly surface catalytic effects [42]. The photo aspect is sensitive to crystal defects while the surface catalytic effect is mainly dominated by the specific surface area. In this study, the photocatalytic performance of FSP-ZnO nanoparticles was found to increase with increasing crystalline quality of ZnO as illustrated by a linear relationship between the PL intensity of NBE bands and the percent conversion of MB decomposition after 60 min (Fig. 8). It is suggested that the photo phenomena (the interaction of light with the material to form electron-hole pairs) played decisive role on the photocatalytic performance of FSP-ZnO nanoparticles than the surface area for the ZnO particle size range 8.8-47.0 nm. Fig. 9a shows the corresponding rate constants (on a fixed mass basis) as a function of ZnO crystallite size. The rate constant increased from 0.33 to $1.36 \,h^{-1}$ as the crystallite size increased from 8.8 to 47.0 nm and then slightly dropped when the crystallite size was further increased. On the other hand, when the rate constants are presented on an SSA normalized basis (Fig. 9b), an increase of photocatalytic activity of ZnO nanoparticles increased with increasing ZnO particle size from 8.8 to 67.1 nm and then remained relatively constant. The ZnO-47 nm performs best on a mass basis due to its optimum crystallinity and surface area while the ZnO-67.1 nm performs better on a surface area normalized basis, as the crystal quality within the ZnO particles was higher. For the flame-made materials, the crystalline quality would be expected to improve with increasing of the enthalpy density, flame height, and hightemperature residence time. The effect of the crystal size of ZnO on the photocatalytic activity has been reported by many researchers. They also reported the optimum size for which the photocatalytic activity of ZnO is maximized [19-23]. The optimum sizes of ZnO reported in literatures were varied depending on the preparation and pretreatment methods. The decrease of photocatalytic activity of ZnO when the particle size of ZnO was larger than optimum size was explained by the decrease of surface area.

4. Conclusions

The FSP-synthesized ZnO nanoparticles have shown to be better photocatalysts for the degradation of methylene blue dye under UV irradiation, compared to the Degussa P-25 and the JRC-TiO₂ commercial photocatalysts. The photocatalytic activities of the FSP-ZnO nanoparticles were found to be correlated well with their crystalline quality. For those prepared by one-step FSP method with average particle size 8.8–47.0 nm, improved crystal quality as well as higher photocatalytic activities were obtained by increasing flame enthalpy density, flame height, and high-temperature residence time during the FSP synthesis. However, the larger ZnO particle sizes (52.6–103.5 nm) obtained by anneal-

ing post-treatment of the FSP-ZnO at high temperature, showed a descending trend of the photocatalytic activity due to the significant decrease of surface availability for reactant adsorption and light absorption of the annealed ZnO particles.

Acknowledgements

The financial supports from the Thailand Research Fund (TRF) and the Office of Higher Education Commission are gratefully acknowledged.

References

- C. Allegre, M. Maisseu, F. Charbit, P. Moulin, Coagulation-flocculation-decantation of dye house effluents: concentrated effluents, J. Hazard. Mater. B 116 (2004) 57–64.
- [2] V. Golob, A. Vinder, M. Simonic, Efficiency of the coagulation/flocculation method for the treatment of dyebath effluents, Dyes Pigments 67 (2005) 93–97.
- [3] A. Alinsafi, M. Khemis, M.N. Pons, J.P. Leclerc, A. Yacoubi, A. Benhammou, A. Nejmeddine, Electro-coagulation of reactive textile dyes and textile wastewater, Chem. Eng. Proc. 44 (2005) 461–470.
- [4] S. Papic, N. Koprivanac, A. LoncaricBozic, A. Metes, Removal of some reactive dyes from synthetic wastewater by combined Al(III) coagulation/carbon adsorption process, Dyes Pigments 62 (2004) 291–298.
- [5] K. Tanaka, K. Padermpole, T. Hisanaga, Photocatalytic degradation of commercial azo dyes, Water Res. 34 (2000) 327–333.
- [6] N.S. Allen, M. Edge, J. Verran, J. Stratton, J. Maltby, C. Bygott, Photocatalytic titania based surfaces: environmental benefits, Polym. Degrad. Stab. 9 (2008) 1632–1646
- [7] S. Sakthivel, B. Neppolian, M.V. Shankar, B. Arabindoo, M. Palanichamy, V. Murugesan, Solar photocatalytic degradation of azo dye: comparison of photocatalytic efficiency of ZnO and TiO₂, Sol. Energy Mater. Sol. Cells 77 (2003) 65–82.
- [8] M.A. Behnajady, N. Modirshahla, R. Hamzavi, Kinetic study on photocatalytic degradation of C.I. Acid Yellow 23 by ZnO photocatalyst, J. Hazard. Mater. 133 (2006) 226–232.
- [9] A. Sharma, P. Rao, R.P. Mathur, S.C. Ameta, Photocatalytic reactions of xylidine ponceau on semiconducting zinc oxide powder, J. Photochem. Photobiol. A: Chem. 86 (1995) 197–200.
- [10] A.A. Khodja, T. Sehili, J.F. Pilichowski, P. Boule, Photocatalytic degradation of 2-phenylphenol on TiO₂ and ZnO in aqueous suspensions, J. Photochem. Photobiol. A: Chem. 141 (2001) 231–239.
- [11] A. Akyol, H.C. Yatmaz, M. Bayramoglu, Photocatalytic decolorization of Remazol Red RR in aqueous ZnO suspensions, Appl. Catal. B: Environ. 54 (2004) 19–24.
- [12] R. Kavitha, S. Meghani, V. Jayaram, Synthesis of titania films by combustion flame spray pyrolysis technique and its characterization for photocatalysis, Mater. Sci. Eng. B 139 (2007) 134–140.
- [13] N. Daneshvar, D. Salari, A.R. Khataee, Photocatalytic degradation of azo dye acid red 14 in water on ZnO as an alternative catalyst to TiO₂, J. Photochem. Photobiol. A: Chem. 162 (2004) 317–322.
- [14] P. Pawinrat, O. Mekasuwandumrong, J. Panpranot, Synthesis of Au–ZnO and Pt–ZnO nanocomposites by one-step flame spray pyrolysis and its application for photocatalytic degradation of dyes, Catal. Commun. 10 (2009) 1380–1385.
- [15] A.P. Alivisatos, Perspectives on the physical chemistry of semiconductor nanocrystals, J. Phys. Chem. 100 (1996) 13226–13239.
- [16] A. Henglein, Small-particle research: physicochemical properties of extremely small colloidal metal and semiconductor particles, Chem. Rev. 89 (1989) 1861–1873.
- [17] M.R. Hoffmann, S.T. Martin, W. Choi, D.W. Bahnemann, Environmental applications of semiconductor photocatalysis, Chem. Rev. 95 (1995) 69–96.
- cations of semiconductor photocatalysis, Chem. Rev. 95 (1995) 69–96.
 [18] D. Beydoun, R. Amal, G. Low, S. McEvoy, Role of nanoparticles in photocatalysis,
 J. Nanopart. Res. 1 (1999) 439.

- [19] H. Wang, C. Xie, W. Zhang, S. Cai, Z. Yang, Y. Gui, Comparison of dye degradation efficiency using ZnO powders with various size scales, J. Hazard. Mater. 141 (2007) 645–652.
- [20] L. Jing, F. Yuan, H. Hou, B. Xin, W. Cai, H. Fu, Relationships of surface oxygen vacancies with photoluminescence and photocatalytic performance of ZnO nanoparticles, Sci. China Ser. B Chem. 48 (2005) 25.
- [21] A.C. Dodd, A.J. McKinley, M. Saunders, T. Tsuzuki, Effect of particle size on the photocatalytic activity of nanoparticulate zinc oxide, J. Nanopart. Res. 8 (2006) 43–51.
- [22] D. Li, V. Balek, N. Ohashi, T. Mitsuhashi, S. Hishita, H. Haneda, Self-assembly prismatic aggregates formed during the calcination of ZnO powders: in situ monitoring by ETA technique and their photocatalytic properties, J. Colloid Interface Sci. 289 (2005) 472–478.
- [23] S.E. Pratsinis, Flame aerosol synthesis of ceramic powders, Prog. Energy Combust. Sci. 24 (1998) 197–219.
- [24] T. Tani, L. Ma'dler, S.E. Pratsinis, Homogeneous ZnO nanoparticles by flame spray pyrolysis, J. Nanopart. Res. 4 (2002) 337–343.
 [25] A. Teleki, S.E. Pratsinis, K. Kalyanasundaram, P.I. Goumab, Sensing of organic
- [25] A. Teleki, S.E. Pratsinis, K. Kalyanasundaram, P.I. Goumab, Sensing of organic vapors by flame-made TiO₂ nanoparticles, Sens. Actuators B 119 (2006) 683–690.
- [26] H. Briesen, A. Fuhrmann, S.E. Pratsinis, The effect of precursor in flame synthesis of SiO_2 , Chem. Eng. Sci. 53 (1998) 4105–4112.
- [27] L. M\u00e4dler, W.J. Stark, S.E. Pratsinis, Flame-made ceria nanoparticles, J. Mater. Res. 17 (2002) 1356–1362.
- [28] S. Hannemann, J. Grunwaldt, P. Lienemann, D. Günther, F. Krumeich, S.E. Pratsinis, A. Baiker, Combination of flame synthesis and high-throughput experimentation: The preparation of alumina-supported noble metal particles and their application in the partial oxidation of methane, Appl. Catal. A: Gen. 316 (2007) 226–239.
- [29] M.J. Height, S.E. Pratsinis, O. Mekasuwandumrong, P. Praserthdam, Ag–ZnO catalysts for UV-photodegradation of methylene blue, Appl. Catal. B: Environ. 63 (2006) 305–312.
- [30] B. Mariĭ, F.J. Manjoĭn, M. Mollar, J. Cembrero, R. Gómez, Photoluminescence of thermal-annealed nanocolumnar ZnO thin films grown by electrodeposition, Appl. Surf. Sci. 252 (2006) 2826–2831.
- [31] J. Lim, K. Shin, H.W. Kim, C. Lee, Effect of annealing on the photoluminescence characteristics of ZnO thin films grown on the sapphire substrate by atomic layer epitaxy, Mater. Sci. Eng. B107 (2004) 301–304.
- [32] N. Serpone, D. Lawless, R. Khairlutdinov, E. Pelizzetti, Subnanosecond relaxation dynamics in TiO2 colloidal sols (particle sizes Rp=1.0-13.4 nm). Relevance to heterogeneous photocatalysis, J. Phys. Chem. 99 (1995) 16655-16661.
- [33] A. Umar, S. Lee, Y.H. Im, Y.B. Hahn, Flower-shaped ZnO nanostructures obtained by cyclic feeding chemical vapour deposition: structural and optical properties, Nanotechnology 16 (2005) 2462–2468.
- [34] T.S. Vaishnavi, P. Haridoss, C. Vijayan, Optical properties of zinc oxide nanocrystals embedded in mesoporous silica, Mater. Lett. 62 (2008) 1649–1651.
- [35] L. Mädler, W.J. Stark, S.E. Pratsinis, Rapid synthesis of stable ZnO quantum dots, J. Appl. Phys. 92 (2002) 6537–6540.
- [36] F. Leiter, H. Alves, D. Pfisterer, N.G. Romanov, D.M. Hofmann, B.K. Meyer, Oxygen vacancies in ZnO, Physica B 340–342 (2003) 201–204.
- [37] X. Li, B. Zhang, H. Zhu, X. Dong, X. Xia, Y. Cui, K. Huang, G. Du, Properties of ZnO thin films grown on Si substrates by photo-assisted MOCVD, Appl. Surf. Sci. 254 (2008) 2081–2084.
- [38] X.Q. Wei, B.Y. Man, M. Liu, C.S. Xue, H.Z. Zhuang, C. Yang, Blue luminescent centers and microstructural evaluation by XPS and Raman in ZnO thin films annealed in vacuum, N-2 and O-2, Physica B 388 (2007) 145–152.
- [39] D. Chu, Y. Zeng, D. Jiang, Hydrothermal synthesis and optical properties of Pb²⁺ doped ZnO nanorods, Mater. Lett. 60 (2006) 2783–2785.
- [40] K. Vanheusden, W.L. Warren, C.H. Seager, D.R. Tallant, J.A. Voigt, B.E. Gnade, Mechanisms behind green photoluminescence in ZnO phosphor powders, J. Appl. Phys. 79 (1996) 7983–7990.
- [41] J. Wang, L. Gao, Hydrothermal synthesis and photoluminescence properties of ZnO nanowires, Solid State Commun. 132 (2004) 269.
- [42] Y.V. Kolenko, B.R. Churagulov, M. Kunst, L. Mazerolles, C. Colbeau-Justin, Photocatalytic properties of titania powders prepared by hydrothermal method, Appl. Catal. B: Environ. 54 (2004) 51–58.

Flow Pattern of Liquid Multiphase Flow in Microreactors with Different Guideline Structures

Chayanoot Kositanont¹, Sompong Putivisutisak², Piyasan Praserthdam¹, Suttichai Assabumrungrat¹, Hiroshi Yamada³ and Tomohiko Tagawa³

¹Department of Chemical Engineering, Faculty of Engineering, Chulalongkorn University, Bangkok 10330, Thailand

²Department of Mechanical Engineering, Faculty of Engineering, Chulalongkorn University, Bangkok 10330, Thailand

³Department of Chemical Engineering, Nagoya University, Chikusa-ku, Nagoya-shi, Aichi 464-8603, Japan

Keywords: Microstructure, Multiphase Flow, Guideline Structure, CFD, Flow Pattern

The present study investigates CFD simulation of aqueous-organic two phase flow in microreactors with a guideline structure. The guideline structure was developed in order to stabilize and to maintain parallel flow of liquids within the microreactors. The CFD simulation can well predict the flow patterns observed in experiments. Upon determining the flow pattern and stability, it is reported that, with the presence of guideline structure, the interface became more curved and stable. Finally, the role of the guideline structure on the flow development was also investigated.

Introduction

A microreactor such as a miniaturized reaction system with typical channel or chamber widths in a range of 10–500 µm (Lowe and Ehrfeld, 1999) offers some outstanding advantages over conventional reactor systems such as intensified mass and heat transport.

A number of reactions involving immiscible systems have been studied in microreactors over the past decade (Doku et al., 2005; Kiwi-Minsker and Renken, 2005; Aljbour et al., 2010). For multiphase liquid-liquid systems such as organic-aqueous reaction systems, low solubility results in very low rates of reaction and extended reaction times. Microreactors possessing a large surface-to-volume ratio can reduce the mass transfer limitations involved. A stable multiphase parallel flow in microchannels can provide a phase separation of the product mixture at the exit and then reduce the requirements of post-treatment unit operation. A microchannel with guideline structure has been proposed in order to stabilize the parallel flow for multiliquid phase systems (Surmeian et al., 2002; Tokeshi et al., 2002; Maruyama et al., 2003; Tagawa et al., 2007).

Computational fluid dynamics (CFD) is a powerful technique applying numerical methods to analyze the flow and performance of process equipment. There are

Received on April 20, 2011; accepted on June 21, 2011 Correspondence concerning this article should be addressed to T. Tagawa (E-mail address: tagawa@nuce.nagoya-u.ac.jp). many advantages in CFD over experimental approaches; for example, it can predict microscopic phenomena which occur in a very short interval. Although there are a number of works focusing on the fluid dynamics in microchannels, simulation works on the system with guideline structures are rather limited (Maruyama *et al.*, 2004). In our study, we used FLUENT (ANSYS Inc.), a well-established commercial CFD solver, to investigate the fluid dynamic behaviors of multiphase flow in microchannels with guideline structures. Different guideline structures were considered in order to achieve stable multiphase flow in the microchannels.

1. Simulation

In order to simulate multiphase flow through microchannels, a 2D geometrical model was generated using the pre-processor GAMBIT. The CFD simulation was carried out with FLUENT 6.3 (Fluent Inc., 2006).

The reliability of our approach was checked by performing a set of simulations with two-phase Taylor flow in the T-shaped microchannel model shown in **Figure 1** to compare with the results reported by Guo and Chen (2009). The fluid and surface properties were set according to those in the literature. The simulated slug lengths with the effect of both phase velocities were in good agreement with the experimental and numerical results of Guo and Chen, as shown in **Figure 2**.

In our study, a 2D geometrical model having 20,040 cells was generated for the microchannel, shown in



Fig. 1 The simulated Taylor flow in microchannel ($U_{\rm G} = 0.0694 \, {\rm m/s}, \, U_{\rm L} = 0.0764 \, {\rm m/s})$

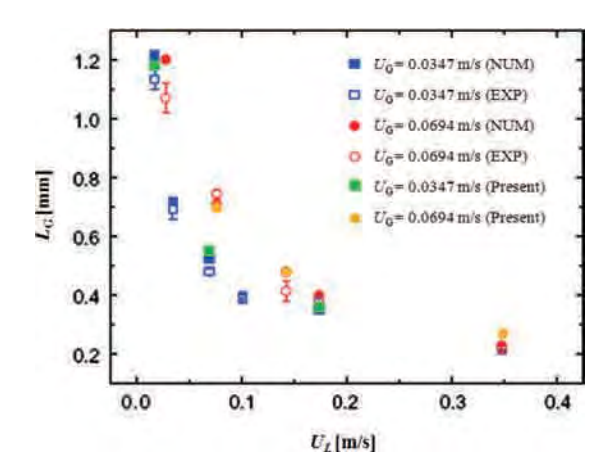


Fig. 2 Comparison of the slug length between the simulated results and results reported by Guo and Chen (2009)

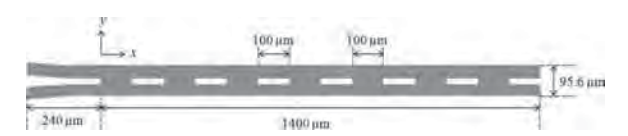


Fig. 3 The microchannel reactor with guideline structure (Model A)

Figure 3. The length and width were 1640 µm and 95.6 μ m, respectively. The grid sizes in the x direction for the reactor and the inlets were 5.56 and 7.00 µm, respectively. In the y direction, the maximum grid size was 2.51 µm and the minimum was 0.57 µm near the guideline walls. Pure water and toluene were used as aqueous and organic phases, respectively. The contact angle of water on glass in toluene and surface tension were measured at 37° and 0.0371 kg/s² (Aota et al., 2009; Dessimoz et al., 2008). The feed flow rates of both phases were set equal at 0.02 mL/min (0.2035 m/s). The volume of fluid (VOF) method was applied to track the interface. The channel was initialized with water. For the inflows, constant velocities were specified as the boundary conditions. Fully-developed conditions were applied at outflows, and no-slip boundary conditions were used on the walls of the microchannel and guideline structures. A simulation with refined grid was carried out to confirm that the solution was independent of grid resolution. The effect of the guideline was investigated by varying the guideline structure, as summarized in **Table 1**.

Table 1 Guideline structure

Model	Length [μm]	Interval [µm]
A	100	100
В	100	180
C (No guideline)	_	_

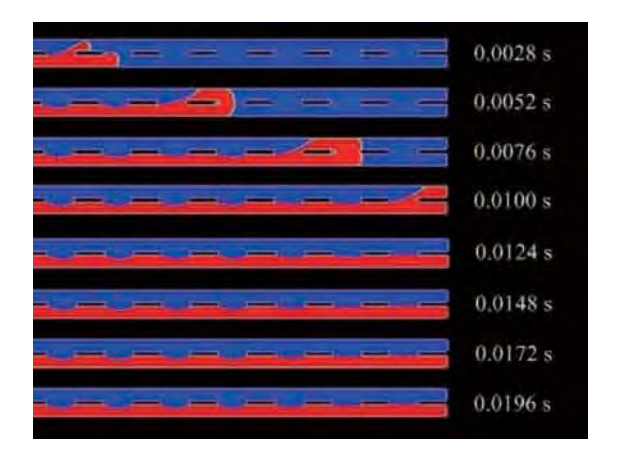


Fig. 4 The snapshots of flow development in Model A

Experiments were conducted with the microchannel sample represented by the model A under operational conditions reported in a previous paper (Tagawa *et al.*, 2007). The channel was washed and filled with distilled water before use.

2. Results and Discussion

2.1 Flow pattern and stability

The simulated flow development in the Model A microchannel is shown in **Figure 4**.

Before feeding the organic phase, the channel was filled with aqueous phase (blue). The top part of organic phase (toluene; red part) was spread over the entire channel and was divided from the aqueous phase to form two phase flow after passing a guideline. The parallel flow gradually stabilized with time. The flow pattern at 0.0148 s which offered the stabilized interface is compared with the experimental result under the same operation conditions in **Figure 5**. The stable interface was curved between the guideline structures (Figure 5(a)), which was in good agreement with that observed from the experiment (Figure 5(b)).

From the simulation results, the flow patterns for Models B and C are shown in **Figures 6** and **7**, respectively. For the cases with the existence of the guideline structure, Models A and B, the interface shape became more curved than the case without the guideline, Model C, at some positions along the channel length.

In Model A, which posses a smaller interval than

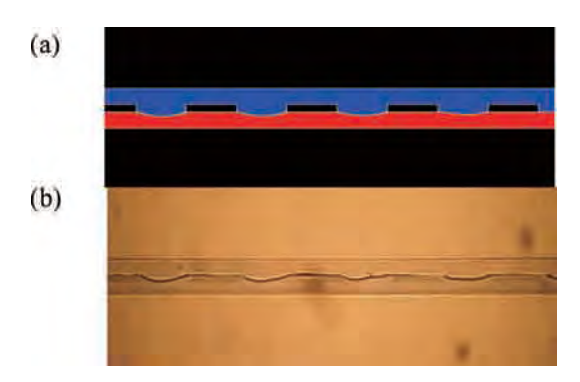


Fig. 5 (a) The simulated stable two phase flow pattern with Model A at 0.0148 s and (b) experimental observation

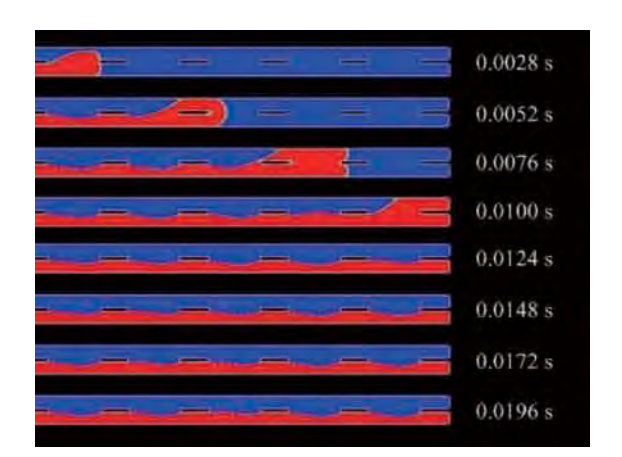


Fig. 6 The flow pattern at different times for Model B

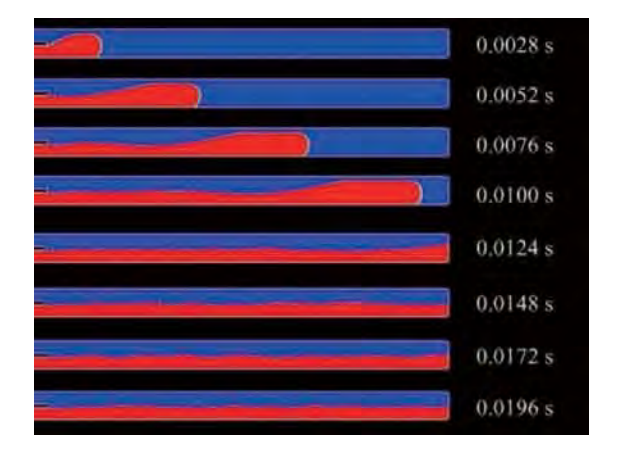


Fig. 7 The flow pattern at different times for Model C

Model B, the interface near the exits is much more flat and stable. Therefore Model A may provide better phase separation than Model B.

While the interface of Model A is stable after 0.0124 s, Model B seems to need more time to stabilize. On the other hand, the interface of Model C is more unstable with time as seen in Figure 7. Although the interface of Model C is near the center along the length of the microreactor, the instability with flow time makes



Fig. 8 The snapshots of flow developing with guideline structure in Model A

the separation uncontrollable.

2.2 The role of guideline structure

The role of guideline on the flow development in the Model A microchannel is shown in **Figure 8**. It is observed that the fluids were kept in their own lanes after passing each guideline wall. The toluene stream was divided into two parts when reaching each structure. After passing the wall, the interface was pushed toward the corner of the wall and broken. Then, the fluids were guided in their own lanes.

Conclusions

The guideline structures turn the flat interface into a curve shape, which becomes more stable with flow time. The fluids are kept in their own lines after passing each guideline wall. In the smaller interval case, the interface position near the exits is close to the centerline, which is believed to provide better separation function; however, the interface area is decreased with more guideline walls and, therefore, the reaction conversion may be reduced in the case of operation with reaction. Thus, the guideline structure geometry should be further studied in more detail in order to achieve an optimized design. It is important to note that the obtained design needs to be confirmed through experiment.

Acknowledgements

The support of Dusadeepipat, the Thailand Research Fund and Commission on Higher Education and Nagoya University Program for Academic Exchange (NUPACE) are gratefully acknowledged.

Literature Cited

Aota, A., K. Mawatari, S. Takahashi, T. Matsumoto, K. Kanda, R. Anraku, A. Hibara, M. Tokeshi and T. Kitamori; "Phase Separation of Gas-Liquid and Liquid-Liquid Microflows in Microchips," *Microchim. Acta*, 164, 249–255 (2009)

Aljbour, S., H. Yamada and T. Tagawa; "Mass Transfer Performance of a Capillary Microreactor during Ultrasound Assisted Phase Transfer Catalysis," J. Chem. Eng. Japan, 43, 429–434 (2010)

Dessimoz, A. L., L. Cavin, A. Renken and L. Kiwi-Minsker; "Liquid-Liquid Two-Phase Flow Patterns and Mass Transfer

VOL. 44 NO. 9 2011 651

- Characteristics in Rectangular Glass Microreactors," *Chem. Eng. Sci.*, **63**, 4035–4044 (2008)
- Doku, G. N., W. Verboom, D. N. Reinhoudt and A. V. D. Berg; "On-Microchip Multiphase Chemistry—A Review of Microreactor Design Principles and Reagent Contacting Modes," *Tetrahedron*, 61, 2733–2742 (2005)
- Fluent Inc.; FLUENT 6.3 Documentation, Fluent Incorporated, Lebanon, U.S.A. (2006)
- Guo, F. and B. Chen; "Numerical Study on Taylor Bubble Formation in a Micro-Channel T-Junction Using VOF Method," *Microgravity Sci. Technol.*, 21, S51–S58 (2009)
- Kiwi-Minsker, L. and A. Renken; "Microstructured Reactors for Catalytic Reactions," Catal. Today, 110, 2–14 (2005)
- Lowe, H. and W. Ehrfeld; "State-of-the-Art in Microreaction Technology: Concepts, Manufacturing and Applications," *Electrochim. Acta*, 44, 3679–3689 (1999)
- Maruyama, T., J. Uchida, T. Ohkawa, T. Futami, K. Katayama, K. Nishizawa, K. Sotowa, F. Kubota, N. Kamiya and M. Goto;

- "Enzymatic Degradation of *p*-Chlorophenol in a Two-Phase Flow Microchannel System," *Lab Chip*, **3**, 308–312 (2003)
- Maruyama, T., T. Kaji, T. Ohkawa, K. Sotowa, H. Matsushita, F. Kubota, N. Kamiya, K. Kusakabea and M. Goto; "Intermittent Partition Walls Promote Solvent Extraction of Metal Ions in a Microfluidic Device," *Analyst*, 129, 1008–1013 (2004)
- Surmeian, M., M. N. Slyadnev, H. Hisamoto, A. Hibara, K. Uchiyama and T. Kitamori; "Three-Layer Flow Membrane System on a Microchip for Investigation of Molecular Transport," *Anal. Chem.*, 74, 2014–2020 (2002)
- Tagawa, T., S. Aljbour, M. Matouq and H. Yamada; "Micro-Channel Reactor with Guideline Structure for Organic-Aqueous Binary System," Chem. Eng. Sci., 62, 5123–5126 (2007)
- Tokeshi, M., T. Minagawa, K. Uchiyama, A. Hibara, K. Sato, H. Hisamoto and T. Kitamori; "Continuous-Flow Chemical Processing on a Microchip by Combining Microunit Operations and a Multiphase Flow Network," Anal. Chem., 74, 1565–1571 (2002)



Article

The Influence of Mixed Activators on Ethylene Polymerization and Ethylene/1-Hexene Copolymerization with Silica-Supported Ziegler-Natta Catalyst

Nichapat Senso ¹, Supaporn Khaubunsongserm ², Bunjerd Jongsomjit ¹ and Pivasan Praserthdam ^{1,*}

- ¹ Center of Excellence on Catalysis and Catalytic Reaction Engineering, Department of Chemical Engineering, Faculty of Engineering, Chulalongkorn University, Bangkok 10330, Thailand
- ² PTT Research and Technology Institute, PTT Public Company Limited, Wangnoi, Ayuthaya 13170, Thailand
- * Author to whom correspondence should be addressed; E-Mail: piyasan.p@chula.ac.th; Tel.: +662-218-6869; Fax: +662-218-6868.

Received: 15 November 2010; in revised form: 10 December 2010 / Accepted: 14 December 2010 / Published: 16 December 2010

Abstract: This article reveals the effects of mixed activators on ethylene polymerization and ethylene/1-hexene copolymerization over MgCl₂/SiO₂-supported Ziegler-Natta (ZN) catalysts. First, the conventional ZN catalyst was prepared with SiO₂ addition. Then, the catalyst was tested for ethylene polymerization and ethylene/1-hexene (E/H) co-polymerization using different activators. Triethylaluminum (TEA), tri-n-hexyl aluminum (TnHA) and diethyl aluminum chloride (DEAC), TEA+DEAC, TEA+TnHA, TnHA+ DEAC, TEA+DEAC+TnHA mixtures, were used as activators in this study. It was found that in the case of ethylene polymerization with a sole activator, TnHA exhibited the highest activity among other activators due to increased size of the alkyl group. Further investigation was focused on the use of mixed activators. The activity can be enhanced by a factor of three when the mixed activators were employed and the activity of ethylene polymerization apparently increased in the order of TEA+ DEAC+TnHA > TEA+DEAC > TEA+TnHA. Both the copolymerization activity and crystallinity of the synthesized copolymers were strongly changed when the activators were changed from TEA to TEA+DEAC+TnHA mixtures or pure TnHA and pure DEAC. As for ethylene/1-hexene copolymerization the activity apparently increased in the order of TEA+DEAC+TnHA > TEA+TnHA > TEA+DEAC > TnHA+DEAC > TEA > TnHA > DEAC. Considering the

properties of the copolymer obtained with the mixed TEA+DEAC+TnHA, its crystallinity decreased due to the presence of TnHA in the mixed activator. The activators thus exerted a strong influence on copolymer structure. An increased molecular weight distribution (MWD) was observed, without significant change in polymer morphology.

Keywords: Ziegler-Natta catalyst; silica support; polyethylene; mixed activator; ethylene polymerization

1. Introduction

Progress in catalyst technology has lead to the synthesis of a rich set of new polymers with different structures and performances to meet the progressive demands of modern industry and life [1-12]. Recently, branched polyethylenes such as linear low-density polyethylene (LLDPE) have grown in importance in industry because of the specific properties that can be obtained by varying comonomer content and polymerization conditions. The recent development of homogeneous single-site catalyst makes it possible to synthesize the copolymers with completely different structures and performances from traditional polyethylenes [13]. The ethylene/α-olefin copolymers obtained by metallocene catalysts show homogeneous comonomer distribution and narrow molecular weight distributions in comparison with those obtained with traditional Ziegler–Natta (ZN) catalysts [14]. The correlation between the structures of the ethylene/α-olefin copolymers obtained with ZN catalysts and their properties has been extensively studied [15,16]. However, easy methods to control polymer properties and catalytic activity in polymerization system are still of concern to the industry.

One of the most important factors in ethylene and ethylene/ α -olefin polymerization is the choice of alkyl aluminum used to control the activity and polymer characteristics. The alkyl aluminums are often added to the reactor during slurry polymerization with ZN catalyst and conventional supported metallocene/MAO catalyst to scavenge impurities. In polymerization systems, alkyl aluminums also act as activators responsible for the generation of active sites. There are many reports on the use of alkyl aluminum as activators in the polymerization of ethylene and ethylene/α-olefins using ZN catalysts [17-23]. Trialkyl aluminum compounds are usually preferred over the halogen-containing analogues because higher polymerization rates can be obtained with the former. Alkyl aluminums such as trimethyl aluminum (TMA), triethyl aluminum (TEA), tri-n-hexyl aluminum (TnHA) and triisobutyl aluminum (TiBA), as well as diethyl aluminum chloride (DEAC) have been used in olefin polymerizations [24-31]. In general, it has been found that an increase in size of the alkyl groups (C_nH_{2n+1}) up to approximately n = 11 has enhanced catalytic activity. The study by Wanke et al. [18] revealed that increasing the size of alkyl group with n < 11 produces an increase in the activity and when a very large alkyl groups (n = 18) was used, the catalytic activity was very low upon when using the ZN catalyst for ethylene polymerization. An exception to these general trends was observed by Nooijen [17]. His results showed a strong effect of activators (TEA, TiBA, TnOA and IPRA) diffusion on the rate of activation of MgCl₂-supported Ziegler-Natta catalyst in slurry polymerization. At a constant ratio of activator to catalyst, the maximum activity depends on the diffusion of the activator.

The properties of polymer, such as the morphology of polymer product particles [22], were also controlled by type of activator, the product molar mass distribution, the average catalyst activity, and the shape of the activity-time profiles [22,23]. Increasing the size of the ligands attached to aluminium atoms increased the average molar masses and resulted in narrower molar weight distributions of polyethylene [18]. Terano *et al.* [23] reported that the molecular weight distribution (MWD) of the polyethylene obtained from the functionalized SiO₂-supported catalyst changed markedly from broad and multimodal to narrow and unimodal depending on the type of activator used. In the case of TEA, a broad trimodal MWD was observed, while for DEAC, the MWD of polyethylene was very narrow and unimodal [23]. In the case of poly[propylene-co-(7-methyl-1,6-otadiene)], the different activators produced polypropylene with a wide range of MWD [32].

Not only single activators are used in α-olefin polymerization, but also mixtures of alkyl aluminums are interesting subjects for improvement of the catalytic activity and polymer properties. Fan *et al.* [20] synthesized PE-PP copolymers using TEA, TIBA or TEA+TIBA mixtures as activators with MgCl₂/SiO₂/TiCl₄/diester-ZN catalyst in a slurry polymerization process. Their results showed that the behaviors of the TEA/TIBA mixture in catalytic systems were not a simple superposition of those activated by the TEA or TIBA alone. When a 50:50 TEA+TIBA mixture was used, the copolymerization activity became the highest, and the yields of both systems were highly random copolymers. In their articles, rapid exchange between the alkyl groups in mixtures of TEA with the *iso*-butyl group in TIBA may be an important reason for the increase in catalytic activity and yields of both the random copolymer and the segmented copolymer parts, which were close to the highest level in PE-PP copolymer.

In spite of these interesting results, the effect of mixed alkyl aluminum on catalytic activity of ethylene polymerization and ethylene/1-hexene copolymerization, and polymer properties has received little attention, even though it could be of crucial importance to successfully design and operate industrial polymerization processes. In the current study, the effect of various activator mixtures on activity, product morphology and molecular weight distribution of polyethylene and ethylene/1-hexene copolymere synthesized by the MgCl₂/SiO₂/TiCl₄/THF-ZN catalyst was investigated. The obtained polymers were characterized by means of X-ray diffraction (XRD), gel permeation chromatography and (GPC), differential scanning calorimetry (DSC), nuclear magnetic resonance (¹³C-NMR) techniques.

2. Results and Discussion

2.1. Catalyst characterization

In general, the MgCl₂/SiO₂/TiCl₄/THF-ZN catalyst has been developed for an excellent morphology control of polymer particles under the fluidized bed reactor conditions [33,34]. Kim *et al.* [34,35] reported that catalyst characteristics such as the ratio of SiO₂/MgCl₂ had an influence on the shape and size of the MgCl₂/SiO₂/TiCl₄/THF-ZN catalyst used for ethylene polymerization and ethylene/1-butene copolymerization. In this study, the MgCl₂/SiO₂/TiCl₄/THF-ZN catalyst was prepared as described in the experimental part using a SiO₂/MgCl₂ molar ratio of 1:1. Based on this preparation, the presence of Ti content in catalyst is 2.33 wt% (ICP). The shape and size of the catalyst were observed by SEM as

shown in Figure 1. The prepared catalyst exhibits a spherical shape and unimodal size distribution. Thus, the aggregated and melted form of catalyst particles seen in Figure 1 (top) are only present in a small amounts. These fractions possibly resulted from contact of catalyst particles with moisture and oxygen, when analyzed by SEM. The average diameter of obtained catalyst is approximately 30, µm as seen in Figure 1 (bottom).

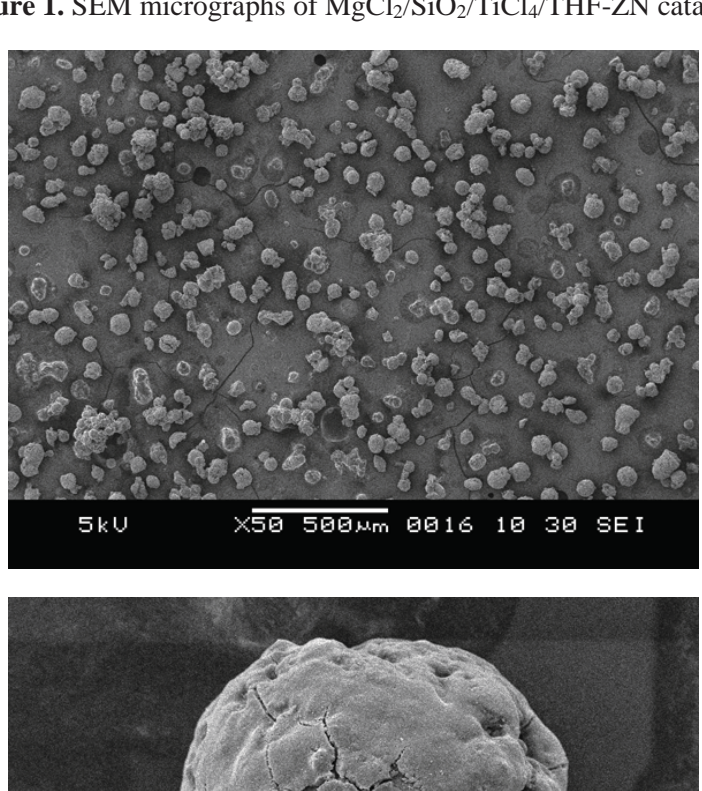
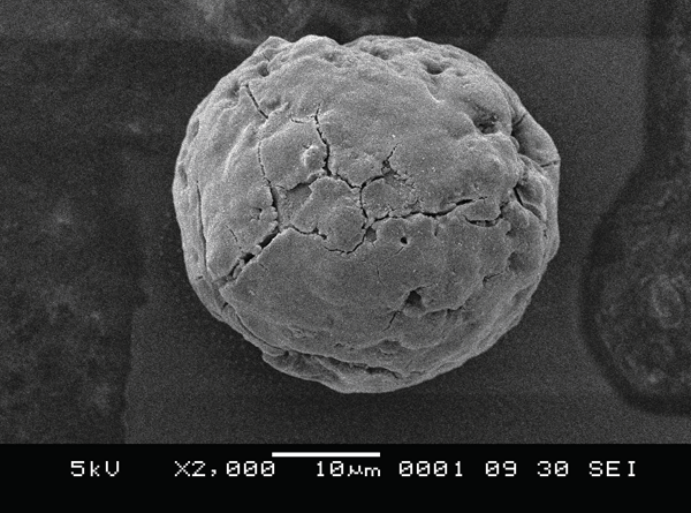


Figure 1. SEM micrographs of MgCl₂/SiO₂/TiCl₄/THF-ZN catalyst.

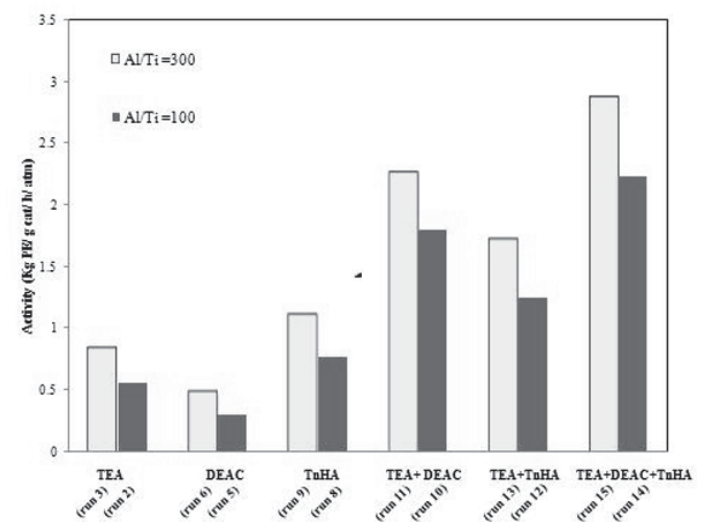


2.2. Ethylene homo-polymerization

For commercial production of polyethylene, the MgCl₂/SiO₂-supported ZN catalyst exhibits high catalytic activity when TEA is used as activator. This activator provides the highest activity among other activators, including diethyl aluminum chloride (DEAC) and tri-n-hexyl aluminum (TnHA) [24]. The MgCl₂/SiO₂/TiCl₄/THF-ZN catalyst shows high catalytic activity for ethylene polymerization. In this work, the effects of different types of alkyl aluminums including TEA, DEAC, TnHA and mixed

alkyl aluminums on activity were investigated. The Al/Ti molar ratio was fixed at 100 and 300. The polymerization activities with various activators are shown in Figure 2 and Table 1.

Figure 2. Effect of various activators on ethylene polymerization activity using MgCl₂/SiO₂/TiCl₄/THF-ZN catalyst.



Note: Total mass of supported catalyst = 0.006 mmol of Ti, titamiun content = 2.33 mmol Ti/ g cat; Polymerization temperature = 80 °C, $P_{tot} = 8$ bar, $P_{H2} = 3.5$ bar; Polymerization time = 2 h, ratio of Al/Ti = 100 and 300.

Table 1. Description of ethylene polymerization with various activators.

D		Activator ^a			A -4::4b
Run – number	TEA (mol%)	DEAC (mol%)	TnHA (mol%)	Al/Ti	Activity ^b (kg PE/ g cat/ h/ atm)
1	100	-	-	100	0.53
2	100	-	-	100	0.55
3	100	-	-	300	0.83
4	-	100	-	100	0.32
5	-	100	-	100	0.30
6	-	100	-	300	0.48
7	-	-	100	100	0.78
8	-	-	100	100	0.76
9	-	-	100	300	1.10
10	50	50	-	100	1.79
11	50	50	-	300	2.25
12	50	-	50	100	1.25
13	50	-	50	300	1.71
14	33	33	33	100	2.23
15	33	33	33	300	2.86

^a Concentrations of TEA, DEAC and TnHA are 0.300 mmol/mL; ^b Ti concentration is 0.006 mmol/mL.

Considering the single activators, the catalytic activity was the highest when TnHA was employed, whereas DEAC exhibited the lowest activity. A similar trend was observed with regards to change in Al/Ti ratio. These results were also consistent with those reported by Lynch $et\ al$. [18] and Hammawa $et\ al$. [22]. For trialkyl aluminum with n < 11, the activity increases with the size of alkyl group [22]. It was observed that DEAC was a less effective activator than TnHA, as reported by Haward $et\ al$. [24].

They explained that there was an optimal ligand size for producing maximum catalyst activity. Based on this work, by mixing activators having different sizes of alkyl groups, the catalytic activity of each system was in the order of; TEA+DEAC+TnHA > TEA+DEAC > TEA+TnHA, as listed in Table 1. In addition, the mixed DEAC+TnHA (50:50) was also tested for ethylene polymerization (data not shown), but it gave low activity than seen for DEAC or TnHA alone. Hence, the catalytic activity can be enhanced by a factor of three when the suitable mixed activators are employed.

These results can be described by: (i) each type of alkyl aluminum has different reducing ability towards the catalyst, and hence produces different types of active sites [22], (ii) the optimal ligand size for producing maximum catalyst activity can be obtained by mixing the various types of activator [24], and (iii) it is related to the real mechanistic roles of alkyl aluminum activator in the formation of the active site in heterogeneous Ziegler-Natta catalysis, using either a monometallic or bimetallic active site model. Besides, changes in forms of mixed alkyl aluminums during polymerization were also a possible reason. To determine the rapid exchange of alkyl groups in the mixed alkyl aluminums, ¹H-NMR measurements were performed by Hatada *et al.* [36]. They found that the ¹H-NMR spectrum of the mixture of TEA and DEAC at room temperature displayed a rapid intermolecular exchange of ethyl groups. However, a new ¹H-NMR signal occurred upon the measurement at low temperature. In Scheme 1, we propose that the formation of new alkyl groups after mixing various alkyl groups may occur through various possible mechanisms. It should be noted that besides the formation of Al-ABC (as shown), other forms of mixed activator such as Al-ACC, Al-BBC, Al-BCC, and so on can occur.

Scheme 1. The possible formation of new alkyl groups after mixing (A, B and C refer to ethyl, *n*-hexyl and Cl).

The new alkyl groups may be suitable for adding more steric hindrance to the surface of catalyst enhancing the performance of ethylene to occupy the active species, as illustrated in Scheme 2. Moreover, the formation of catalyst might have a reducing ability to produce active sites for ethylene polymerization.

Scheme 2. Suggested mechanism of active site formation activated by new alkyl aluminum type $(X: -Cl; A, B \text{ or } C: \text{ ethyl, } n\text{-hexyl or } Cl; \Box: \text{ coordination vacancy}).$

2.3. Ethylene/1-hexene copolymerization

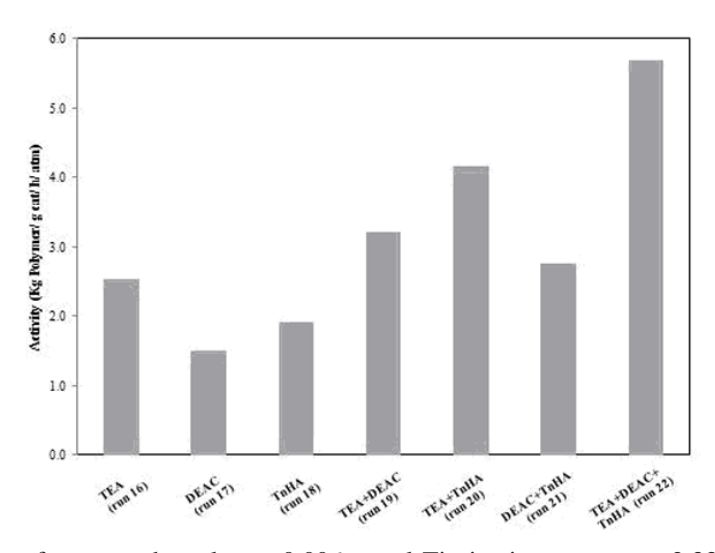
(EH) It is known that ethylene/1-hexene polymerization is also catalyzed MgCl₂/SiO₂/TiCl₄/THF-ZN catalyst in the slurry polymerization system using TEA as activator. However, the EH copolymerization with the catalyst activated by DEAC or TnHA has been found to exhibit different catalytic activity when compared to the system activated by TEA. To further explore the possibility of modifying catalytic activity and EH copolymer properties via changes in activator, TEA, DEAC, TnHA and their mixtures were employed in the equal molar ratio for each activator in the mixture. The Al/Ti molar ratio was kept constant at 300. The results are summarized in Table 2 and Figure 3.

Table 2. Activity of ethylene/1-hexene copolymerization with various ratios of activators and % 1-hexene insertion.

_		Activator ^a used		Activity (kg	1-hexene
Run number	TEA (mol%)	DEAC (mol%)	TnHA (mol%)	polymer/g cat/ h/ atm)	insertion (mol%) ^b
16	100	-	-	2.53	1.27
17	-	100	-	1.50	0.49
18	-	-	100	1.91	1.90
19	50	50	-	3.22	0.70
20	50	-	50	4.15	1.26
21	-	50	50	2.75	0.60
22	33	33	33	5.69	1.10

^a Ratio of Al/Ti =300; ^b 1-hexene insertion was determined by ¹³C-NMR.

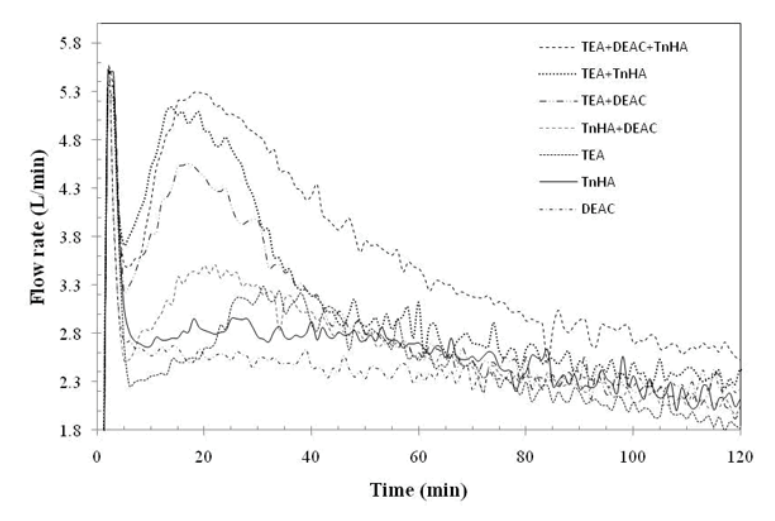
Figure 3. Effect of mixed activators on catalytic activity of MgCl₂/SiO₂/TiCl₄/THF-ZN catalyst for ethylene/1-hexene copolymerization.



Note: Total mass of supported catalyst = 0.006 mmol Ti, titanium content = 2.33 mmol Ti/ g-cat, 1-hexene = 50 mL, polymerization temperature = 80 °C, P_{tot} = 8 bar, P_{H2} = 3.5 bar, polymerization time = 2 h, ratio of Al/Ti = 300.

Interestingly, the kinetic profile behaviors of ethylene/1-hexene copolymerization with various activators were not a simple superposition of those activated by TEA, DEAC or TnHA alone, as shown in Figure 4. From this viewpoint, this result supports the notion of a change of alkyl groups in the alkyl aluminum mixture as mentioned before. From Table 2 and Figure 3, it was evident that the activator exerted strong influence on both catalytic activity and copolymer properties. The activity increased upon mixing TEA, DEAC and TnHA (TEA+DEAC, TEA+TnHA and TEA+DEAC+TnHA). The insertion of 1-hexene in copolymer increased in the order of TnHA > TEA > DEAC > mixed activators. No relationship between the catalytic activity and 1-hexene insertion was found with the different activators.

Figure 4. Kinetic profile based on ethylene consumption with various activators for ethylene/1-hexene copolymerization.



Note: Total mass of supported catalyst = 0.006 mmol Ti, titanium content = 2.33 mmol Ti/ g-cat, 1-hexene = 50 mL, polymerization temperature = 80 °C, P_{tot} = 8 bar, P_{H2} = 3.5 bar, polymerization time = 2 h, ratio of Al/Ti = 300.

Many explanations have been put forth for the reported co-monomer effects on the enhancement of catalytic activity and can be classified as follows: (i) chemical and physical effects of co-monomer on the catalyst generation of active sites [37], (ii) increasing propagation rate constant (*kp*) [37], (iii) enhancement of the diffusion due to lower crystallinity [38], (iv) fracturing the catalyst, and (v) changing the oxidation state of Ti [38]. It seems that some of these explanations cannot possibly explain the mixed activator behavior, which should be concerned with the change in the active sites for the ZN catalyst with using different types of alkyl aluminum. Based on 1-hexene insertion, it seems that DEAC can effectively activate those active sites that produce partly crystalline copolymer, whereas the other activators such as TEA and TnHA were more efficient activators of active sites that produce amorphous copolymer. In the case of TEA+DEAC+TnHA mixture, it was able to activate both types of active sites, leading to a copolymerization system with high activity and slightly lower content of 1-hexene insertion. On the other hand, TnHA itself can produce a copolymer having relatively higher degree of 1-hexene insertion.

2.4. Polymer characterization

2.4.1. Gel permeation chromatography (GPC) analysis

The M_w, M_n and MWD of the corresponding polymers are shown in Table 3. The MWD of the obtained polyethylene (Al/Ti ratio 300) gradually changed depending on the types of activator used. Apparently, TnHA produced polymers with a broader MWD as compared to polyethylene obtained from TEA and DEAC. Thus, the use of different types of activators in ethylene polymerization resulted in changes of the Mw and MWD values of polyethylene. The mixed alkyl aluminum system tended to exhibit a broad polyethylene MWD, as shown in Table 3. This result was also consistent with the dependence of MWD on the type of alkyl aluminum activator as shown in a previous report [24]. This interesting phenomenon was considered to stem from the existence of multiplicity in the nature of active sites with different propagation, termination and chain transfer rates on the surface of functionalized MgCl₂/SiO₂-supported ZN catalyst. According to the GPC profiles (not shown), it might be speculated that mainly two kinds of active titanium precursors exist on the surface of functionalized MgCl₂/SiO₂-supported ZN catalyst. The various alkyl aluminum activators may provide different types of active sites and different oxidation state of Ti. The M_w, M_n and MWD results of the copolymers are also given in Table 3. The TEA, DEAC and TnHA gave M_w of 295, 364 and 336 kg/mol, and MWD of 3.7, 3.6 and 4.2, respectively. The average molecular weights of copolymers obtained from mixed activators tended to decrease compared to those obtained with a single activator. On the contrary, the MWD of copolymers increased as the follows: TEA+DEAC+TnHA (5.6) > TEA+TnHA (4.5) > TnHA (4.3) > TnHA+DEAC (3.8) = TnHA+DEAC (3.8) > TEA (3.7) > DEAC (3.6). These results showed no relationship among the M_w, MWD, reducing power and activity in copolymerization system.

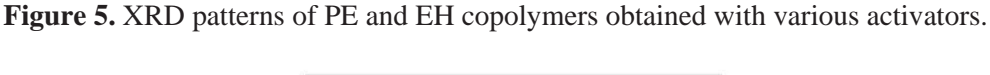
Table 3. M_W , M_n and polydispersity	(M_w/M_n) of	f polyethylene and		
3.7	7. //		TC.	C 4 111 14 (0)

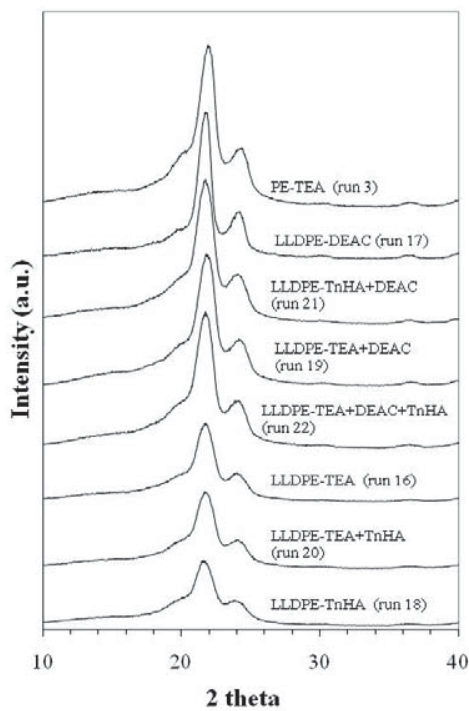
Run	Monomor	Activator	$\mathbf{M_n}$	\mathbf{M}_{w}	M _w /M _n ^a	T _m (°C)	d°	Crystallinity (%)	
Kuii	Monomer	Activator	(kg/ mol)	(kg/ mol)	IVI _W /IVI _n	I _m (C)	(g/mL)	DSC^d	X-ray ^e
3	Ethylene	TEA	74	299	4.0	136.5	0.955	66.0	71.3
6		DEAC	51	180	3.5	136.3	0.957	67.7	-
9		TnHA	103	474	4.6	135.9	0.956	66.3	-
11		TEA+ DEAC	31	175	5.6	136.3	0.957	67.7	-
13		TEA+ TnHA	86	344	4.0	135.9	0.957	67.7	-
15		TEA+ DEAC+	55	283	5.2	136.3	0.957	67.6	-
		TnHA							
16	Ethylene/	TEA	165	295	3.8	120.7	0.926	41.0	46.2
	1-hexene								
17		DEAC	56	364	6.5	124.4	0.943	55.5	60.1
18		TnHA	79	336	4.2	97.5	0.914	30.7	35.4
19		TEA+ DEAC	77	294	3.8	122.5	0.941	54.0	59.1
20		TEA+ TnHA	56	255	4.5	111.6	0.918	34.1	38.2
21		TnHA+ DEAC	54	209	3.8	123.7	0.943	55.3	60.3
22		TEA+ DEAC+	48	272	5.6	119.5	0.923	38.4	42.2
		TnHA							

^a Polydispersity index, evaluated as M_w/M_n , and determine by GPC analysis; ^b Melting temperature determined by DSC analysis; ^c Copolymer density determined according to the semi-empirical equation: $d = (2195 + \Delta H_m)/2500$; ^d Crystallinity degree determined according to the equation: $(\Delta H_m/\Delta H_m^{\circ}) \times 100$, assuming $\Delta H_m^{\circ} = 293$ J/g; ^e Crystallinity degree determined by XRD according to the equation: $W_{c,x} = (I_{110} + 1.42I_{200}) / (I_{110} + 1.42I_{200} + 0.68I_a)$.

2.4.2. X-ray diffraction (XRD) and thermal properties

It is well known that the melting enthalpy ($\triangle H_m$) of an EH copolymer decreases with increasing comonomer content [30]. The insertion of the α -olefin reduces both the degree of crystallinity and the melting temperature of the copolymer. Randall [39] found that for EH copolymer, the density of the sample decreases with increasing the comonomer content. Table 3 shows the melting temperatures of the EH copolymers obtained with different activators. It was very interesting that both melting temperature and enthalpy of melting decreased with TnHA. Figure 5 shows the XRD patterns of EH copolymers and homopolymer (PE) obtained with different activators. It was observed that the copolymers exhibit two crystalline peaks at 20 degree of 21.1 and 23.58 assigned to 110 and 200 spacing and one amorphous peak at 20 degree of 19.48. It was evident that the degree of crystallinity decreased with increasing comonomer content. The degrees of crystallinity calculated from both enthalpy and XRD are shown in Table 3. The results are very close to those reported by Mo et al. [14] and Quijada [1]. The values from XRD measurement are higher than those obtained from the DSC measurement. This can be attributed to different treatment of polymer samples prior to measurement for each technique. It can be accepted that different activators had no effect on the crystallinity of the polyethylene. However, in the case of EH copolymer, changes in activator can alter the crystallinity of copolymer due to different insertion of 1-hexene, as determined by the ¹³C-NMR.

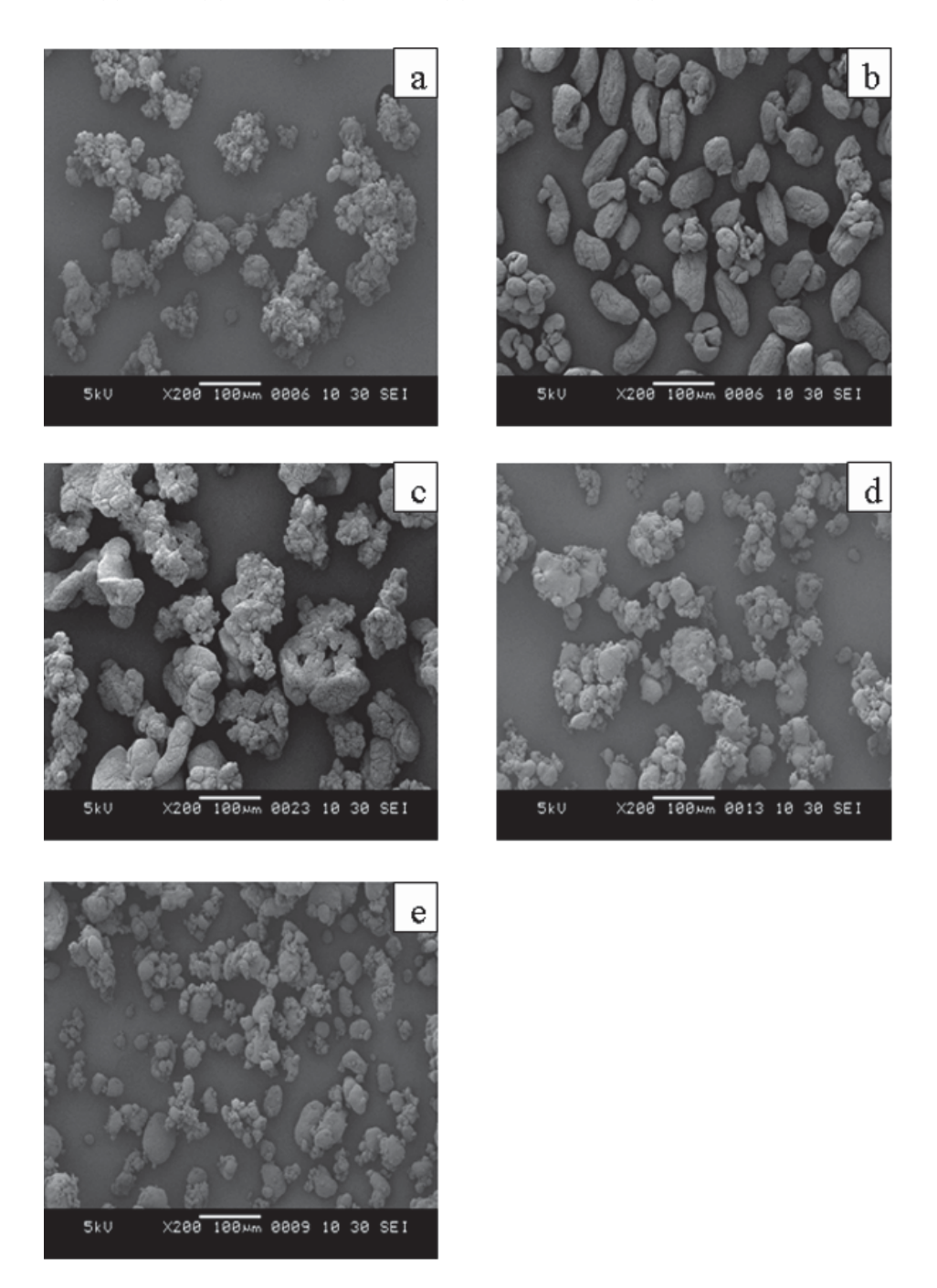




Different polymerization systems produced different polyethylene particle shapes, as seen by SEM in Figure 6. These results may result from the different reducing powers of the activators. In addition,

alkyl aluminums also participate in the termination of polymer chain growth, *i.e.* act as chain transfer agents, and/or reactivation of dormant sites [40].

Figure 6. SEM micrographs of secondary product particles obtained with different activators; (a) TEA, (b) DEAC, (c) TnHA, (d) TEA+DEAC, (e) TEA+DEAC+TnHA.



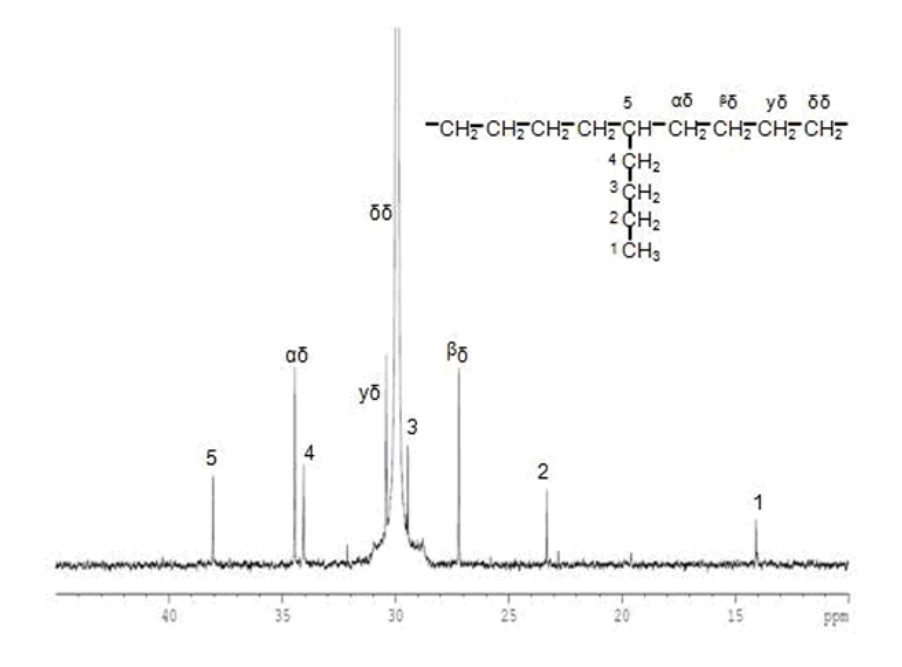
2.4.3. ¹³C-NMR analysis

The incorporation of 1-hexene in copolymers was determined by ¹³C-NMR spectroscopy. The chemical dislocations in the copolymers were calculated according to the work of Randall [39]. Table 4 shows 1-hexene incorporation in EH copolymers with different activators in the polymerization system. It was found that copolymers had 1-hexene insertion in the range of 0.49-1.90 mol%, depending on the type of activator used. Apparently, DEAC produced copolymer having the lowest 1-hexene insertion (0.49 mol%). On the contrary, TnHA gave the highest 1-hexene insertion in the copolymer (1.90 mol%). It is worth noting that the alkyl aluminum mixtures such as TEA+DEAC and TnHA+DEAC produced copolymer having 1-hexene insertion values around 0.70 and 0.60 mol%, respectively. Similarly, TEA and TEA+TnHA had a 1-hexene insertion that was very close to that of TEA alone. It should be noted that 1-hexene unit was isolated by ethylene units, and no sequence of double co-monomer units or alternating ethylene/1-hexene units were found, as shown in Figure 7. The same results were also obtained with other activators.

Table 4. Triad distribution based on ¹³C-NMR for EH copolymer obtained from different activators.

Run	Activator	[HHH]	[EHH]	[EHE]	[EEE]	[HEH]	[HEE]	%E	%Н
16	TEA	0.0	0.7	0.6	97.0	0.2	1.2	98.73	1.27
17	DEAC	0.0	0.2	0.3	98.8	0.1	0.6	99.51	0.49
18	TnHA	0.0	1.2	0.7	96.3	0.4	1.4	98.10	1.90
19	TEA+DEAC	0.0	0.2	0.5	98.2	0.1	1.0	99.30	0.70
20	TEA+TnHA	0.0	0.7	0.6	97.2	0.2	1.2	98.74	1.26
21	TnHA+DEAC	0.0	0.2	0.4	98.4	0.2	0.8	99.40	0.60
22	TEA+DEAC+TnHA	0.0	0.4	0.7	97.4	0.1	1.4	98.89	1.11

Figure 7. A typical ¹³C-NMR spectrum of EH copolymer obtained with TEA.



3. Experimental

3.1. Chemicals

All reactions were performed under purified argon atmospheres using a standard glove box and Schlenk techniques. Polymerization grade ethylene, donated by the PTT Company, was used as received. Triethylaluminum (TEA), tri-*n*-hexylaluminum (TnHA), diethyl aluminum chloride (DEAC), donated by Tosoh Akzo Corp., were stored in a glove box and used without further purification. TiCl₄ (Aldrich), MgCl₂ (anhydrous) was donated by Tosoh Akzo Corp. Silica (specific surface area of 150 m²/g), supplied by Grace Davision, was heated under vacuum at 400 °C for 6 h. Hexane purchased from Aldrich Chemical Company Inc., was purified by passing it through a 13X molecular sieves column. Tetrahydrofuran and 1-hexene were dried over dehydrated CaCl₂ and distilled over sodium/ benzophenone under an argon atmosphere prior to use. Ultra high purify (UHP) argon (99.999%) was purchased from Thai Industrial Gas Co., Ltd. and was further purified by passing through 3Å molecular sieves, BASF catalyst R3-11G, NaOH and phosphorus pentaoxide (P₂O₅) to remove traces of oxygen and moisture.

3.2. Catalyst preparation

The catalyst was prepared in a 500 mL vessel equipped with temperature control, and a turbine agitator. Anhydrous tetrahydrofuran (150 mL) was added to the vessel. The tetrahydrofuran was heated to 50 °C, and then magnesium metal (0.12 g) was added, followed by titanium tetrachloride (2 mL). The mixture was continuously agitated. The temperature was held at about 70 °C for 3 h. At the end of this time, magnesium dichloride (4.5 g) was added and heating was continued at 70 °C for another 3 h. Then, Grace Davision silica (4.5 g) was added over several minutes and the mixture was stirred for 1 h. This mixture was washed with hexane, and then dried under vacuum. The titanium content in the catalyst is 2.33 wt% (ICP).

3.3. Polymerization reaction

The slurry polymerization was performed in hexane solution (1,000 mL) with various activator mixtures as shown in Table 1 (Al/Ti molar ratio = 100 and 300). First hexane (1,000 mL) was added into the reactor under argon atmosphere. After that, activators and catalyst were introduced into a 2 L stainless steel reactor equipped with a magnetic stirrer, and the reactor was then evacuated to remove the argon. Hydrogen ($P_{H2} = 3.5$ bar) was fed into the reactor prior to the introduction of ethylene. The polymerization reaction was initiated by introducing the ethylene ($P_{C2H4} = 4.5$ bar). The total pressure in the reactor was 8 bar. The polymerization reaction was held constant at 80 °C and terminated after 2 h by quenching with dilute hydrochloric acid solution in methanol. The resulting polymer was isolated and dried under vacuum.

The EH copolymerization was performed as follows; the 2 L autoclave was evacuated and purged with argon several times similar to the ethylene polymerization. After hexane (950 mL) was added at 80 °C, the solution of activator such as TEA, DEAC, TnHA and TEA+DEAC+TnHA mixtures, 1-hexene (50 mL) and the catalyst (Al/Ti = 300) were added into reactor sequentially. Then, the 3.5 bar

of hydrogen was fed into the reactor. The ethylene gas was fed into reactor and the total pressure in reactor was raised to 8 bar and held constant by continuous feed. After 2 h, the copolymerization was terminated using the same procedure as mentioned for ethylene polymerization.

3.4. Polymer characterization

A high temperature GPC (PL-GPC220) equipped with a viscometric detector, differential optical refractometer and four Styragel HT type columns (HT3, HT4, HT5, and HT6) with a 1×10^7 exclusion limit for polystyrene was used to determine the molecular weight (M_W) and molecular weight distributions (MWD) of the polymers produced. The analyses were performed at 160 °C using 1,2,4-trichlorobenzene as the solvent. The columns were calibrated with standard narrow MWD polystyrene.

The comonomer contents of the resultant copolymers were determined by ¹³C-NMR spectroscopy. The measurements were performed at 110 °C on Bruker 400 MHz instrument using 1,2,4trichlorobenzene as solvent. The thermal behavior of polyethylene and EH copolymers was examined with a Perkin-Elmer Pyris Diamond DSC at standard heating/cooling rate of 10 °C/min, under N₂ flow. The samples were first melted to 180 °C (1st scan) and kept at this temperature for 3 min, then cooled to 50 °C, and again heated up to the melting with the same heating rate (2nd scan). The reported melting temperature values are referred to the second heating scan. The melting temperature (Tm) and the melting enthalpy (ΔH_m) were taken from the second heating curve. Temperatures and heats of phase transitions were determined, respectively, from the maxima and areas of the crystallization and melting peaks. In this context, it was possible to relate ΔH_m (J/g) to the density (d, g/mL) of the copolymer through the following semiempirical equation: $d = (2195 + \Delta H_m)/2500$ [41]. Finally, using standards of known composition, a linear correlation between sample density and its content in terms of 1-hexene co-units was found, at least in the 0.92-0.94 g/mL density range [41]. The degree of crystallinity, X_c of PE and its copolymers was calculated from the ratio between the values of melting enthalpy, $\triangle H_m$ (as calculated from the second heating scan) and the heat of fusion of 100% crystalline PE taken as $\triangle H_m = 293 \text{ J/g [42]}$.

X-ray diffraction patterns (XRD) analysis was carried out on a Siemens D-5000 apparatus working at 40 kV and 30 mA and using the Cu K_{α} radiation ($\lambda = 0.154439 \text{ Å}$) in the 10° - 40° 20 range with a scanning step of 0.01° in the reflection geometry. The crystalline degrees of the copolymers were calculated via Eq. (1) developed by Mo and Zhang [14]:

$$W_{c,x} = \frac{I_{110} + 1.42I_{200}}{I_{110} + 1.42I_{200} + 0.68I_a}$$
(1)

The morphological observations of polymers were carried out with a JEOL JSM-6400 scanning electron microscope (SEM). Micrographs were taken at a 5-kV acceleration voltage. Before SEM observations, the fracture surfaces of blends were coated with a thin layer of gold to avoid electrical charging and increase contrast during observation.

4. Conclusions

The use of suitable mixed activators such as TEA+DEAC+TnHA, can result in the significant increase in catalytic activity for the bi-supported Ziegler-Natta catalyst for ethylene polymerization and ethylene/1-hexene copolymerization. This can be attributed to the change in reducing power of the mixed activators leading to generation of different active forms of the catalyst or stabilization of the active center in ethylene polymerization. The activator type had an effect on the molecular weight and molecular weight distribution of polyethylene without any significant change in polymer morphology. In the case of copolymerization, there were no relationship among the $M_{\rm w}$, MWD and catalytic activity when the mixed activators were employed.

Acknowledgements

The authors thank the Thailand Research Fund (TRF), Office of the Higher Education Commission (CHE), Chulalongkorn University for Royal Golden Jubilee Fund under contract No. CU-CLUSTER-Advanced-4-54-53, and PTT Company for the financial support of this project.

References and Notes

- 1. Quijada, R.; Guevara, J.L.; Galland, G.B.; Rabagliati, F.M.; Lopez-Majada, J.M. Synthesis and properties coming from the copolymerization of propene with α-olefins using different metallocene catalysts. *Polymer* **2005**, *46*, 1567–1574.
- 2. Kawahara, N.; Kojoh, S.; Toda, Y.; Mizuno, A.; Kashiwa, N. The detailed analysis of the vinylidene structure of metallocene-catalyzed polypropylene. *Polymer* **2004**, *45*, 355–357.
- 3. Cruz, V.; Ramos, J.; Mun oz-Escalona, A.; Lafuente, P.; Pen a, B.; Martinez, S. 3D-QSAR analysis of metallocene-based catalysts used in ethylene polymerization. *Polymer* **2004**, *45*, 2061–2072.
- 4. Lee, H.W.; Chung, J.S.; Choi, K.Y. Physical transitions and nascent morphology of syndiotactic polystyrene in slurry polymerization with embedded Cp*Ti(OMe)3/methyl aluminoxane catalyst. *Polymer* **2005**, *46*, 5032–5039.
- 5. Nitta, K.H.; Shin, Y.W.; Hashiguchi, H.; Tanimoto, S.; Terano, T. Morphology and mechanical properties in the binary blends of isotactic polypropylene and novel propylene-co-olefin random copolymers with isotactic propylene sequence 1. Ethylene-propylene copolymers. *Polymer* **2005**, *46*, 965–975.
- **6.** Wooster, T.J.; Abrol, S.; Macfarlane, D.R. Cyanate ester polymerization catalysis by layered-silicates. *Polymer* **2004**, *45*, 7845–7852.
- 7. Chen, S.; Hua, Z.J.; Fang, Z.; Qi, G.R. Copolymerization of carbon dioxide and propylene oxide with highly effective zinc hexacyanocobaltate(III)-based coordination catalyst. *Polymer* **2004**, *45*, 6519–6524.
- 8. Bazzini, C.; Giarrusso, A.; Porri, L.; Pirozzi, B.; Napolitano, R. Synthesis and characterization of syndiotactic 3,4-polyisoprene prepared with diethylbis(2,2'-bipyridine)iron-MAO. *Polymer* **2004**, 45, 2871–2875.
- 9. Liu, J.Y.; Zheng, Y.; Li, Y.S. Polymerization of methyl methacrylate by iron(II) pyridinebisimine complexes. *Polymer* **2004**, *45*, 2297–2301.
- 10. Gao, M.Z.; Liu, H.T.; Wang, J.; Li, C.X.; Ma, J.; Wei, G.S. Novel MgCl₂-supported catalyst containing diol dibenzoate donor for propylene polymerization. *Polymer* **2004**, *45*, 2175–2180.

11. Kawahara, N.; Kojoh, S.I.; Toda, Y.; Mizuno, A.; Kashiwa, N. The detailed analysis of the vinylidene structure of metallocene-catalyzed polypropylene. *Polymer* **2004**, *45*, 355–357.

- 12. Lee, T.S.; Kim, J.W.; Bae, J.Y. Palladium-catalyzed selective dehalogenative homocoupling polymerization of AB2-type dihaloaryl sulfonate monomers. *Polymer* **2004**, *45*, 5065–5076.
- 13. Galland, G.B.; Quijada, R.; Rojas, R.; Bazan, G.; Zachary Komon, J.A. NMR Study of Branched Polyethylenes Obtained with Combined Fe and Zr Catalysts. *Macromolecules* **2002**, *35*, 339–345.
- 14. Mo, Z.S.; Zhang, H.F. The degree of crystallinity in polymers by wide-angle x-ray diffraction (WAXD). Macromol. *Chem. Phys.* **1995**, *C35*, 555–580.
- 15. Madri, S.; Xuejing, Z.; RoBert, B.J.; JOHN, C.C.; COR, E.K. Effect of 1-Hexene Comonomer on Polyethylene Particle Growth and Copolymer Chemical Composition Distribution. *J. Polym. Sci.: Part A: Polym. Chem.* **2006**, *44*, 2883–2890.
- 16. Yong, P.C.; Zhi, F. Ethylene/1-hexene copolymerization with TiCl4/MgCl2/AlCl3 catalyst in the presence of hydrogen. *Eur. Polym. J.* **2006**, *42*, 2441–2449.
- 17. Nooijen, G.A.H. On the importance of diffusion of cocatalyst molecules through heterogeneous ziegler/natta catalysts. *Eur. Polym. J.* **1994**, *30*, 11-15.
- 18. Lynch, T.D.; Jejelowo, M.O.; Wanke, S.E. The influence of aluminum alkyls on the polymerization of ethylene with silica/magnesium chloride-supported titanium tetrachloride catalysts. *Can. J. Chem. Eng.* **1991**, *69*, 657-664.
- 19. Siokou, A.; Ntais, S. Towards the preparation of realistic model Ziegler-Natta catalysts: XPS study of the MgCl₂/TiCl₄ interaction with flat SiO₂/Si(1 0 0). *Surf. Sci.* **2003**, *540*, 379-388.
- 20. Dong, Q.; Fu, Z.; Xu, J.; Fan, Z. Strong influences of cocatalyst on ethylene/propylene copolymerization with a MgCl₂/SiO₂/TiCl₄/diester type Ziegler-Natta catalyst. *Eur. Polym. J.* **2007**, *43*, 3442-3451.
- 21. Lynch, D.T.; Wanke, S.E. Reactor Design and Operation for Gas-Phase Ethylene Polymerization Using Ziegler-Natta Catalysts. *Can. J. Chem. Eng.* **1991**, *69*, 332-339.
- **22.** Hammawa, H.; Mannan, T.M.; Lynch, D.T.; Wanke, S.E. Effects of aluminum alkyls on ethylene/1-hexene polymerization with supported metallocene/MAO catalysts in the gas phase. *J. Appl. Polym. Sci.* **2004**, *92*, 3549-3560.
- 23. Fukuda, K.; Liu, B.; Nakatani, H.; Nishiyama, I.; Yamahiro, M.; Terano, M. Significant variation of molecular weight distribution (MWD) of polyethylene induced by different alkyl-Al cocatalysts using a novel surface functionalized SiO2-supported Ziegler-Natta catalyst. *Catal. Commun.* **2003**, *4*, 657-662.
- 24. Haward, R.N.; Roper, A.N.; Fletcher, K.L. Highly active catalysts for ethylene polymerization by the reduction of TiCl₄ with organomagnesium compounds. *Polymer* **1973**, *14*, 365-372.
- 25. Gardner, K.; Parsons, I.W.; Haward, R.N. Polymerization of propene with organomagnesium-reduced titanium (IV) chloride-based catalyst. *J. Polym. Sci.: Polym. Chem.* **1978**, *16*, 1683-1696.
- 26. Kashiwa, N. Super active catalyst for olefin polymerization. *Polymer* 1980, 12, 603-608.
- 27. Licchelli, J.A.; Haward, R.N.; Parsons, I.W.; Caunt, A.D. Polymerization catalysts for propene from the reduction of titanium tetrachloride with halogen-free magnesium alkyls. *Polymer* **1981**, 22, 667-672.
- 28. Machon, J.P.; Hermant, R.; Houzeaux, J.P. Study of the catalytic activity of violet titanium trichloride in the high-temperature polymerization of ethylene. *J. Polym. Sci. Symp. Ser.* **1975**, *52*, 107-117.

29. Munoz, E.A.; Hernandez, J.G.; Gallardo, J.A.; Keii. T.; Soga, K. Design of supported Ziegler-Natta catalysts using silica as carrier. *Stud. Surf. Sci. Catal.* **1986**, *25*, 123-125.

- 30. Munoz, E.A.; Garcia, H.; Albornoz, A. Homo- and copolymerization of ethylene with highly active catalysts based on titanium tetrachloride and Grignard compounds. *J. Appl. Polym. Sci.* **1987**, *34*, 977-988.
- 31. Zakharov, V.A.; Bukatov, G.D.; Ermakov, Y. The Mechanism of the Catalytic Polymerisation of Olefins Based on the Number of Active Centres and the Rate Constants for Individual Stages. *Russ. Chem. Rev.* **1980**, *49*, 1097-1111.
- 32. Mori, H.; Ohnishi, K.; Terano, M. Ethene polymerization with modified-polypropene-supported highly stable Ziegler catalyst. *Macromol. Rapid Commun.* **1996**, *17*, 25-29.
- 33. Zacca, J.J.; Debling, J.A.; Ray, W.H. Reactor residence time distribution effects on the multistage polymerization of olefins I. Basic principles and illustrative examples, polypropylene. *Chem. Eng. Sci.* **1996**, *51*, 4859-4886.
- 34. Kim, I.; Chung, M.C.; Choi, H.K.; Kim, J.H.; Woo, S.I. (1990) Homo- and Co-polymerization of Ethylene with the Highly Active TiCl₄/THF/MgCl₂ Catalyst. *Catal. Olefin Polym.* **1990**, 323.
- 35. Kim, I.; Kim, J.H.; Woo, S.I. Kinetic Study of Ethylene Polymerization by Highly Active Silica Supported TiCl₄ MgCl₂ Catalyst. *J. Appl. Polym. Sci.* **1990**, *39*, 837-854.
- 36. Hatada, K.; Yuki, H. Alkyl interchange in the mixture of triethyl aluminum and diethylaluminum chloride. *Tetrahedron Lett.* 1967, *51*, 5227-5231.
- 37. Calabro, D.C.; Lo, F.Y. A comparison of the reaction kinetics for the homo- and copolymerization of ethylene and hexene with a heterogeneous Ziegler catalyst. In *Transition Metal Cata lyzed Polymerizations: Ziegler–Natta and Methathesis Polymerization;* Quirk, R.P., Ed.; Cambridge University Press: New York, NY, USA, 1988; pp. 729-739.
- 38. Chien, J.C.W.; Nozaki, T. Ethylene-hexene copolymerization by heterogeneous and homogeneous Ziegler-Natta catalysts and the "comonomer" effect. *J. Polym. Sci.* **1993**, *31*, 227-237.
- 39. Randall, J.C. A review of high-resolution liquid carbon-13 nuclear magnetic resonance characterizations of ethylene-based polymers. *AJMS-REV. Macromol. Chem. Phys.* **1989**, *C*29, 201-317.
- 40. Zakharov, V.A.; Bukatov, G.D.; Yermakov, Y.I. On the mechanism of olefin polymerization by Ziegler-Natta catalysts. *Adv. Polym. Sci.* **1983**, *51*, 61-100.
- 41. Carlini, C.; Alessio, A.D.; Giaiacopi, S.; Po, R.; Pracella, M.; Galletti, A.M.R.; Sbrana, G. Linear low-density polyethylenes by co-polymerization of ethylene with 1-hexene in the presence of titanium precursors and organoaluminium co-catalysts. *Polymer.* **2007**, *48*, 1185-1192.
- 42. Wunderlich, B.; Czornyj, G. A study of equilibrium melting of polyethylene. *Macromolecules* **1977**, *10*, 906-913.

Sample Availability: Samples of the compounds (PEs and LLDPEs) are available from the authors.

© 2010 by the authors; licensee MDPI, Basel, Switzerland. This article is an open access article distributed under the terms and conditions of the Creative Commons Attribution license (http://creativecommons.org/licenses/by/3.0/).



Article

Observation of Different Catalytic Activity of Various 1-Olefins during Ethylene/1-Olefin Copolymerization with Homogeneous Metallocene Catalysts

Mingkwan Wannaborworn, Piyasan Praserthdam and Bunjerd Jongsomjit *

Center of Excellence on Catalysis and Catalytic Reaction Engineering, Department of Chemical Engineering, Faculty of Engineering, Chulalongkorn University, Bangkok 10330, Thailand

* Author to whom correspondence should be addressed; E-Mail: bunjerd.j@chula.ac.th; Tel.: +66 2 2186869; Fax: +66 2 2186877.

Received: 18 November 2010; in revised form: 28 December 2010 / Accepted: 5 January 2011 /

Published: 7 January 2011

Abstract: This research aimed to investigate the copolymerization of ethylene and various 1-olefins. The comonomer lengths were varied from 1-hexene (1- C_6) up to 1-octadecene (1-C₁₈) in order to study the effect of comonomer chain length on the activity and properties of the polymer in the metallocene/MAO catalyst system. The results indicated that two distinct cases can be described for the effect of 1-olefin chain length on the activity. Considering the short chain length comonomers, such as 1-hexene, 1-octene and 1-decene, it is obvious that the polymerization activity decreased when the length of comonomer was higher, which is probably due to increased steric hindrance at the catalytic center hindering the insertion of ethylene monomer to the active sites, hence, the polymerization rate decreased. On the contrary, for the longer chain 1-olefins, namely 1-dodecene, 1tetradecene and 1-octadecene, an increase in the comonomer chain length resulted in better activity due to the opening of the gap aperture between C_p(centroid)-M-C_p-(centroid), which forced the coordination site to open more. This effect facilitated the polymerization of the ethylene monomer at the catalytic sites, and thus, the activity increased. The copolymers obtained were further characterized using thermal analysis, X-ray diffraction spectroscopy and ¹³C-NMR techniques. It could be seen that the melting temperature and comonomer distribution were not affected by the 1-olefin chain length. The polymer crystallinity decreased slightly with increasing comonomer chain length. Moreover, all the synthesized polymers were typical LLDPE having random comonomer distribution.

Keywords: metallocene catalyst; homogeneous catalyst; long chain olefins; copolymerization

1. Introduction

Nowadays, polymers play a significant role in many applications, especially linear low-density polyethylene (LLDPE). The LLDPE has many advantages such as low density, good mechanical properties, and easy fabrication and recycling. Therefore, it has been used to produce many products such as shopping bags, food packaging film, plastic pipe and house appliances, *etc.* [1-3]. Thus, the demand for LLDPE is quite high compared with other polymers. For the production of LLDPE, the polymer can be synthesized by the polymerization of ethylene and short chain 1-olefins, namely 1-hexene, 1-octene and 1-decene, in the catalyst system for better activity. A low pressure slurry process, the gas phase process and the solution-phase process [4] can be employed for LLDPE. Some 15 million tons of LLDPE are produced worldwide using the metallocene catalyst system, since this catalyst can incorporate many types of comonomer. Moreover, it can give a narrow molecular weight distribution. Thus, there has been an increase in research and development on the synthesis of the LLDPE using metallocene catalysts [5,6].

However, the properties of LLDPE, such as the average molecular weight of the macromolecules and its distribution, the degree of crystallization, the melting temperature and the amount and distribution of the monomeric units, depend on a factor called "comonomer effect" [7-9]. Previous studies show that an increase in the quantities of 1-olefin provides higher activity which relates to a physical phenomenon improving the monomer diffusion in the lower crystalline copolymer structure. Besides the comonomer quantity, the length of the comonomer also affects the properties of LLDPE. Although short chain comonomers are normally used in the process, long chain comonomers can provide different LLDPE properties. Therefore, the use of long chain comonomers is also attractive for future production.

In this work, the effects of short and long comonomer chain length on the polymerization activity and the properties of the resulting copolymers were investigated. The synthesis of the LLDPE was performed by copolymerization of ethylene and various 1-olefins, namely 1-hexene (1- C_6), 1-octene (1- C_8), 1-decene (1- C_{10}), 1-dodecene (1- C_{12}), 1-tetradecene (1- C_{14}) and 1 -octadecene (1- C_{18}), with a metallocene catalyst.

2. Results and Discussion

2.1. Homo- and co-polymerization activities

This study is aimed to investigate the polymerization of ethylene with short and long chain 1-olefins, namely 1-hexene, 1-octene, 1-decene, 1-dodecene, 1-tetradecene and 1-octadecene. The catalytic activities obtained with different 1-olefins are shown in Table 1.

Table 1. Copolymerization of ethylene with long chain 1-olefins using *rac*-Et[Ind]₂ZrCl₂/MAO, as the catalytic system.

Run number	Olefin type	Polymerization time (s)	Polymer yield ^a (g)	Catalytic activity ^b (×10 ⁻⁴ kgPol/molZr h)
1	-	115	0.8703	1.8
2	1-C ₆	124	1.4781	2.9
3	1-C ₈	97	1.5529	3.8
4	$1-C_{10}$	115	1.6783	3.5
5	$1-C_{12}$	109	1.6134	3.6
6	$1-C_{14}$	89	1.3704	3.7
7	$1-C_{18}$	123	2.3157	4.5

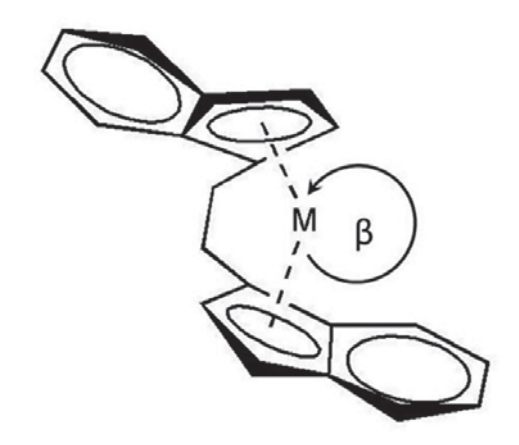
^a The polymer yield was limited by the amount of ethylene fed (0.018 mol). The molar ratio of ethylene:comonomer was 2:1; ^b Activities were measured at polymerization temperature of 343 K, [ethylene]= 0.018 mol, [Al]_{MMAO} / [Zr]_{cat} = 1135, in toluene with total volume = 30 mL and [Zr]_{cat} = 5×10^{-5} M.

From Table 1, when comparing the activities between homo-polymerization and co-polymerization, it can be seen that the addition of the comonomer in the system yields better activity. The enhancement of polymerization rate by 1-olefin comonomers, well documented for both titanocene [7,10,11] and zirconocene catalysts [7,12,13], is called the "comonomer effect". This phenomenon in copolymerization involving the zirconocene catalysts may be related to the perturbations of the ion pairs at the active sites. Karol et al. [13] have proposed that 1-olefins can function as ligands. By coordination to the active center, the 1-olefin can alter the charge density on the cationic zirconocenium ion. Metal centers with higher mobility, lower steric interference, and higher electrophilicity are believed to form stronger ion pairs. Monomers that cause a greater separation between the cationic metal centers and the MAO aggregates can enhance the activity of the catalyst, consequently increase the rate polymerization. On the other hand, two distinct cases can be described for the effect of the comonomer length. Considering the short chain length comonomers (runs 2-4), the results indicated that the increase of the comonomer length (from C₈ to C₁₀) resulted in lower activity due to increased steric hindrance. The longer chain comonomer can hinder the insertion of ethylene, and slow the propagation reaction process. This leads to lower catalytic activity for polymerization [12-15]. On the contrary, for the long chain length 1-olefins (runs 5-7), we observed an increase of polymerization activity when the length of 1-olefin was increased. This may be attributed to the opening of the gap aperture between C_p(centroid)-M-C_p-(centroid) in metallocene complex, which forced the coordination site to open more (Figure 1). This effect caused ethylene monomer to polymerize easier at the catalytic sites, and thus the activity increased [16,17]. A similar behavior was observed by Kaminsky et al. [17] for ethylene/ long chain 1-olefins copolymerization with a [Ph₂C(2,7-di-tert-BuFlu)(Cp)]ZrCl₂/MAO catalyst system, under different experimental conditions (T = 60 °C and the presence of hydrogen), but no reason was given for the trend.

The obtained result is also consistent with the study of Braunschweig and Breitling [18], which revealed that opening of the βC_p (centroid)-M- C_p -(centroid) angle can be found in the polymerization

of ethylene and long chain olefins. Moreover, they also reported that a longer 1-olefin chain can open the C_p (centroid)-M- C_p -(centroid) angle wider in metallocene complexes.

Figure 1. Structure of the opening gap aperture between C_p (centroid)-M- C_p -(centroid) in metallocene complex, redrawn from the conceptual idea by Braunschweig and Breitling [18].



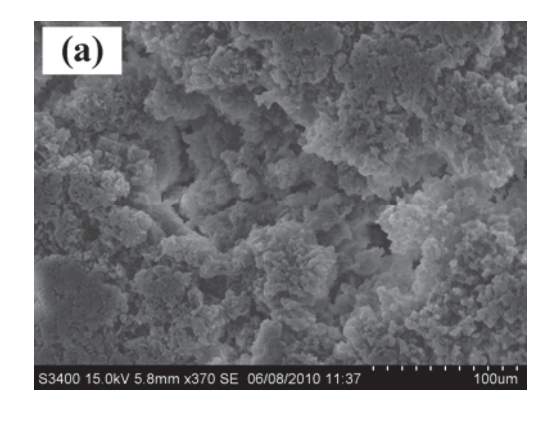
2.2. Polymer properties

Homo- and copolymers with different 1-olefins (copolymers containing 6 to 18 carbon atoms), synthesized by a metallocene catalyst, have been analyzed using four characterization techniques.

2.2.1. SEM measurements

Figure 2 presents the scanning electron micrograph (SEM) of the polymers obtained by homo- and co-polymerization. Considering the effect of the length of comonomer on morphology, the results indicated that the crystalline structure of the obtained polymer seems to be lower with increased comonomer chain length. This is probably due to more steric hindrance caused upon introducing a longer chain length comonomer. Therefore, the amount and chain length of comonomer apparently affected on the morphology of the resulting polymer.

Figure 2. SEM micrograph of LLDPE produced with metallocene catalyst. (a) homopolymer (b) ethylene/1-hexene copolymer (c) ethylene/1-octadecene copolymer.



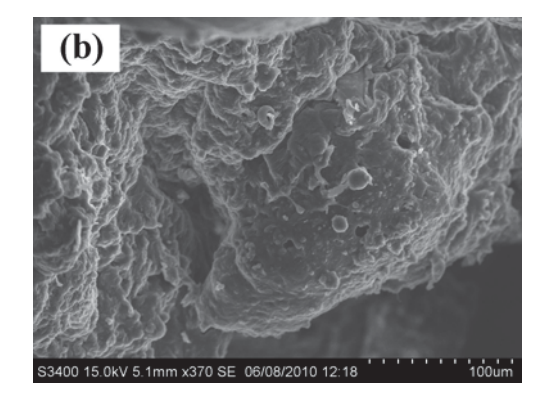
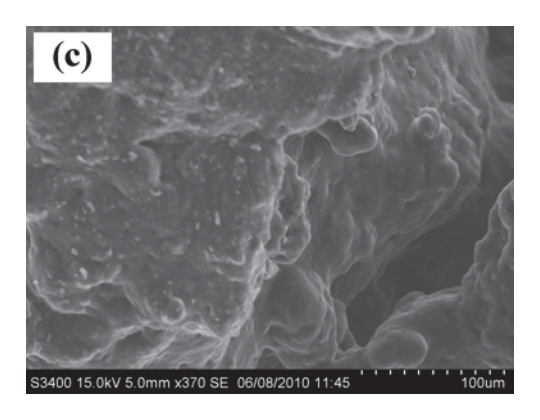


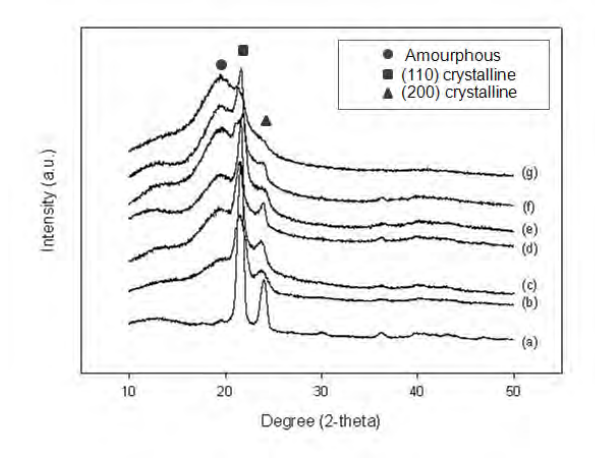
Figure 2. Cont.



2.2.2. X-ray Diffraction (XRD) analysis

For XRD results, the diffractograms of the different samples, which were acquired at room temperature, are shown in **Figure 3**. As expected, it can be seen that all samples display XRD peaks at three positions. A broad amorphous peak was evident centered around 19.5-20 degrees. A previous work suggested this peak as indicative of the side branches of 1- olefin participating in the crystalline structure. While the other two peaks appeared at $2\theta = 21.8$ and 24.3 degrees are the (110) and (200) reflections, assigned to the characteristic orthorhombic cell of polyethylene [19-21]. Moreover, the longer chain length of the additional comonomers seemed to disturb the polymer recrystallization, which can probably be attributed to the increased steric hindrance, leading to a reduction in crystalline peak intensity, but clearly increasing the intensity of the amorphous peak [19,22].

Figure 3. X-ray diffractograms of different samples. From bottom to top. (a) homopolymer (b) ethylene/1- C_6 (c) ethylene/1- C_8 (d) ethylene/1- C_{10} (e) ethylene/1- C_{12} (f) ethylene/1- C_{14} and (g) ethylene/1- C_{18} copolymers.



2.2.3. NMR analysis

In order to determine the influence of chain length on the comonomer distribution, the obtained copolymers were also characterized by 13 C-NMR measurements. The chemical-shift assignments of ethylene/ 1-C₁₂ to ethylene/ 1-C₁₈ copolymer and some resonances of the main and side chains are

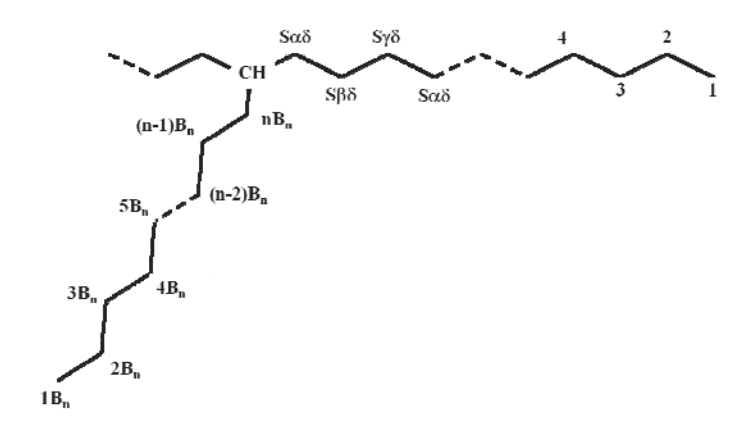
shown in Table 2 and Figure 4. The quantitative analysis of triad distribution for all copolymers is reported in Table 3.

Table 2. Chemical-shift assignment in ¹³C-NMR spectra of ethylene/1-dodecene, ethylene/1-tetradecene and ethylene/1-octadecene copolymers [23].

Combon		Chemical shift ^b (ppm)	
Carbon type ^a	ethylene/1-dodecene	ethylene/1-tetradecene	ethylene/1-octadecene
туре	$(1-C_{12})$	$(1-C_{14})$	$(1-C_{18})$
$1B_n$	14.10	14.10	14.10
$2 B_n$	22.80	22.80	22.80
$3 B_n$	32.13	32.13	32.13
$4 B_n$	29.50	29.50	29.50
$5 B_n$	29.85	29.85	29.85
6 B _n	29.90^{c}	29.90°	29.90°
$7 B_n$	29.90 °	29.90°	29.90°
$8 B_n$	30.36	29.90°	29.90°
9 B _n	27.18	29.90°	29.90°
10 B _n	34.45	30.37	29.90 °
11 B _n	-	27.18	29.90 °
12 B _n	-	34.46	29.90°
13 B _n	-	-	29.90°
14 B _n	-	-	30.37
15 B _n	-	-	27.18
16 B _n	-	-	34.46
CH	38.11	38.11	38.11
Sαδ	34.49	34.49	34.49
Sβδ	27.20	27.20	27.20
$S\gamma\delta$	30.38	30.38	30.38
Sδδ	29.90	29.90	29.90

^a See Scheme 1; ^b According to Randall [26]; ^c Overlapped to S δδ peak at 29.90 ppm.

Figure 4. Resonance of the main chain methylenes and the side chain of the ethylene/1-olefin copolymer.



_ Olefin			Triad distribution ^a					C_n	$T_{\rm m}$	χ_c	d ^e
Entry	type	[EEE]	[XEE]	[EXE]	[XEX]	[EXX]	[XXX]	(mol%) ^b		(%) ^d	(g/mL)
2	1-C ₆	0.775	0.142	0.052	0.017	0.014	0.000	7	121.64	7.36	0.88
3	$1-C_8$	0.412	0.379	0.164	0.045	0.000	0.000	16	113.62	2.44	0.88
4	$1-C_{10}$	0.471	0.310	0.176	0.043	0.000	0.000	18	116.25	2.33	0.88
5	$1-C_{12}$	0.499	0.331	0.135	0.035	0.000	0.000	13	117.61	6.21	0.89
6	$1-C_{14}$	0.604	0.154	0.091	0.087	0.064	0.000	20	112.98	1.33	0.87
7	$1-C_{18}$	0.591	0.214	0.152	0.043	0.000	0.000	15	117.58	4.34	0.88

Table 3. Triad distribution and properties of the resulting ethylene/1-olefin copolymers.

 a Obtained from $^{13}\text{C-NMR},$ where E refers to ethylene monomer and X refers to 1-olefin comonomer; b Content of 1-olefin in the copolymer from $^{13}\text{C-NMR};$ c Melting temperature from DSC; d Crystallinity degree: χ_c =100 \times ($\Delta H/\Delta H^\circ$) , where ΔH° = 290 J/g for linear polyethylene; e Copolymer density calculated from the semi-empirical equation: d = (2,195 + ΔH)/2,500.

From the table, it is found that ethylene incorporation in all systems gave copolymers with similar triad distribution, and only random copolymers can be produced in all systems. However, the olefin length has no effect on the comonomer distribution [12,23-25]. It should be noted that the comonomer content depends on different variables; for example, a long 1-olefin chain length forces the angle of the metallocene complex to open more. However, at the same time it causes steric hindrance to the incoming ethylene monomer. Therefore, the two effects (chain length and opened angle) can be superimposed on each other.

2.2.4. Differential scanning calorimetric analysis

When dealing with the thermal properties of the polymer, DSC measurements are usually considered the second melting of the sample. All the experimental results, including melting temperature (T_m), % crystallinity (χ_c), and density are also reported in Table 3. The PE sample (run 1) is a high density polymer with a linear microstructure, a high melting temperature (Tm~135 °C), a degree of crystallinity of 65% and a high density (0.95 g/mL) (data not shown in the Table). Based on Table 3, it can be observed that the polymer with higher incorporation of comonomers exhibited less crystallinity and lower melting temperature. This is in correspondence with the percent insertion from ¹³C-NMR results. In addition, when the crystallinity results obtained from DSC measurements are considered, they indicate that the length of the comonomer did not affect the crystallization behavior, which was different from the XRD results. This was due to the fact that XRD was analyzed the assynpolymers at ambient conditions, whereas the DSC measurement was performed upon heating the samples. For DSC, the determination relies on the measurement of the enthalpy of melting and on the assumption of a unique enthalpy of melting for the crystal. Thus, the enthalpy of melting of long 1olefin side chains had to be taken into account for the determination of crystallinity. Therefore, the crystallinity value may be different between the various determinations. [12,13,27-29]. However, it can be concluded that the increase in the length of the comonomer chain can result in a decrease of the melting temperature. The density of all samples is in the range of 0.87-0.95 g/cm³ indicating a typical LLDPE structure.

3. Experimental

3.1. Materials

Chemicals and polymerizations were handled and operated under an argon atmosphere, using a glove box and/or Schlenk techniques. Toluene was dried over dehydrated CaCl₂, and then distilled over sodium/benzophenone before use. The zirconocne, (*rac*-Et[Ind]₂ZrCl₂) was supplied by the Aldrich Chemical Company, Inc. Modified methylaluminoxane (MMAO) in hexane was donated by Tosoh (Akso, Japan). 1-Olefins were purchased from Aldrich Chemical Company, Inc. Ethylene gas (99.96% pure) was donated by the National Petrochemical Co., Ltd., Thailand. Ultrahigh purity argon was further purified by passing it through columns packed with BASF R3-11G catalyst (molecular-sieved to 3 Å), sodium hydroxide (NaOH), and phosphorus pentaoxide (P₂O₅) to remove traces of oxygen and moisture.

3.2. Homo- and co-polymerization

Ethylene/1-olefin copolymerizations was carried out in a 100 mL semi-batch stainless steel autoclave reactor equipped with a magnetic stirrer. In the glove box, the desired amounts of *rac*-Et[Ind]₂ZrCl₂ and MMAO were introduced into the autoclave and then, toluene was added (to make a total volume of 30 mL). After that, the reactor was frozen in liquid nitrogen to stop any reactions and the proper amount of the comonomer was injected into the reactor (the molar ratio of ethylene:comonomer was fixed at 2:1). The reactor was evacuated to remove argon. Then, it was heated up to polymerization temperature (343 K) and the polymerization was started by feeding ethylene gas until the consumption of 0.018 mol of ethylene (6 psi was observed from the pressure gauge) was reached. The polymerization was terminated by addition of acidic methanol [30]. The time of reaction was recorded for purpose of calculating the activity. The precipitated polymer was washed with acidic methanol and dried at room temperature. Based on the system as mentioned above, the polymer yield was fixed by the amount of ethylene fed (0.018 mol). Experimentally, the polymerization was performed at least three times for each run and only the average yield and activity are reported. The error was found to be within less than 5% based on this polymerization system.

3.3. Polymer characterization

Scanning electron microscopy (SEM) was used to determine the morphology of the polymeric samples. The samples were sputter-coated with a fine layer of platinum in an Edward Sputter Coater and analyzed with a JEOL (mode JSM-6400) electron microscope.

X-ray diffraction (XRD) was performed to determine the bulk crystalline phases of samples. Diffraction patterns were recorded in the reflection mode at room temperature using a Siemens D-5000 instrument. Ni-filtered Cu K_{α} ($\lambda = 1.54439$ Å) was used. The diffraction scans were collected over a period of 2.4° min⁻1 of 2θ from 10 to 80° .

¹³C-NMR spectroscopy was used to determine the triad distribution and 1-olefin insertion indicating the copolymer microstructure. Chemical shifts were referenced internally to the CDCl₃ peak and calculated according to the method described by Randall [26]. Sample solutions were prepared by

dissolving copolymer (50 mg) in 1,2,4-trichlorobenzene and CDCl₃ (0.5 mL). ¹³C-NMR spectra were taken at 383 K using a Bruker Avance II 400 operating at 100 MHz with an acquisition time of 1.5 s and a delay time of 4 s.

The thermal properties were measured by a PerkineElmer Pyris Diamond Differential Scanning Calorimeter at a standard heating/cooling rate of 20K/min, under nitrogen flow. Both first and second melting temperatures have been analyzed. The reported melting temperature values are referred to the second heating scan. The peak temperature was assumed as melting temperature (T_m) and the area was corresponding to the global melting enthalpy (ΔH). The crystallinity, χ_c , was calculated from DSC data by using the formula $\chi_c = 100 \cdot \times (\Delta H/\Delta H^{\circ})$ where $\Delta H^{\circ} = 290$ J/g is the enthalpy of fusion for linear polyethylene as reported in ref. [31]. Approximately, 5-10 mg of sample was used for each DSC measurement. Moreover, it was possible to relate ΔH (J/g) to the density (d, g/mL) of the copolymer through the following semiempirical equation: $d = (2,195 + \Delta H)/2,500$.

4. Conclusions

In this article, we have reported the synthesis of LLDPE from the copolymerization of ethylene/1-olefin via metallocene/MAO catalysts by varying the comonomer (1-olefin) chain length. The results show that the increase in the short chain length 1-olefns (from 1-C₈ to 1-C₁₀) can cause more steric hindrance of the catalytic center leading to decreased activity. However, when a long chain comonomer was used, a block of long chain 1-olefin can force the opening of the supplementary angle, therefore the coordination site was more open, resulting in increased activity. However, the increase of the chain length has no significant effects on the melting temperature and comonomer distribution. The crystallinity tended to decrease with increased chain length of comonomer, based on the XRD measurements.

Acknowledgements

We thank the Thailand Research Fund (TRF), the Office of Higher Education Commission (CHE) of Thailand for the financial support of this project.

References

- 1. Chum, P.S.; Swogger, K.W. Olefin polymer technologies-History and recent progress at The Dow Chemical Company. *Prog. Polym. Sci.* **2008**, *33*, 797-819.
- 2. Cano, J.; Kunz, K. How to synthesize a constrained geometry catalyst (CGC) A survey. *J. Organomet. Chem.* **2007**, *692*, 4519-4527.
- 3. Bensason, S.; Minick, J.; Moet, A.; Chum, S.; Hiltner, A.; Baer, E. Classification of homogeneous ethylene-octene copolymers based on comonomer content. *J. Polym. Sci., Part A: Polym. Phys.* **1996**, *34*, 1301-1315.
- 4. Ali, E.M.; Abasaeed, A.E.; Al-Zahrani, S.M. Optimization and control of industrial gas-phase ethylene polymerization reactors. *Ind. Eng. Chem. Res.* **1998**, *37*, 3414-3423.
- 5. Halterman, R.L. Synthesis and applications of chiral cyclopentadienylmetal complexes. *Chem. Rev.* **1992**, *92*, 965.

6. Brintzinger, H.; Beck, S.; Leclerc, M.; Stehling, U.; Röll, W. Reaction Mechanisms in Metallocene-Catalyzed Olefin Polymerization. *Stud. Surf. Sci. Catal.* **1994**, *89*, 193-200.

- 7. Chien, J.C.W.; Nozaki, T. Ethylene-hexene copolymerization by heterogeneous and homogeneous Ziegler-Natta catalysts and the "comonomer effect". *J. Polym. Sci., Part A: Polym. Chem.* **1993**, *31*, 227-237.
- 8. Simanke, A.G.; Galland, G.B.; Freitas, L.; Da Jornada, J.A.H.; Quijada, R.; Mauler, R.S. Influence of the comonomer content on the thermal and dynamic mechanical properties of metallocene ethylene/1-octene copolymers. *Polymer* **1999**, *40*, 5489-5495.
- 9. Shan, C.L.P.; Soares, J.B.P.; Penlidis, A. Ethylene/1-octene copolymerization studies with in situ supported metallocene catalysts: Effect of polymerization parameters on the catalyst activity and polymer microstructure. *J. Polym. Sci., Part A: Polym. Chem.* **2002**, *40*, 4426-4454.
- 10. Jaber, I.A.; Ray, W.H. Polymerization of olefins through heterogeneous catalysis. XIII. The influence of comonomer in the solution copolymerization of ethylene. *J. Appl. Polym. Sci.* **1993**, 49, 1709-1724.
- 11. Kim, I.; Woo, S.I. Homo- and co-polymerization of ethylene with highly active Ti/Mg bimetallic complexes Effect of crystallization conditions on structure and productivity. *Polym. Bull.* **1989**, 22, 239-246.
- 12. Koivumäki, J.; Fink, G.; Seppälä, J.V. Copolymerization of ethene/1-dodecene and ethene/1-octadecene with the stereorigid zirconium catalyst systems iPr[FluCp]ZrCl₂/ MAO and Me₂Si[Ind]₂ZrCl₂/MAO: Influence of the comonomer chain length. *Macromolecules* **1994**, 27, 6254-6258.
- 13. Karol, F.J.; Kao, S.-C.; Cann, K.J. Comonomer effects with high-activity titanium- and vanadium-based catalysts for ethylene polymerization. *J. Polym. Sci., Part A: Polym. Chem.* **1993**, *31*, 2541-2553.
- 14. Bialek, M.; Czaja, K. The effect of the comonomer on the copolymerization of ethylene with long chain α-olefins using Ziegler-Natta catalysts supported on MgCl₂(THF)₂. *Polymer* **2000**, *41*, 7899-7904.
- 15. Awudza, J.A.M.; Tait, P.J.T. The "comonomer effect" in ethylene/α-olefin copolymerization using homogeneous and silica-supported Cp₂ZrCl₂/MAO catalyst systems: Some insights from the kinetics of polymerization, active center studies, and polymerization temperature. *J. Polym. Sci.*, *Part A: Polym. Chem.* **2008**, *46*, 267-277.
- 16. McKnight, A.L.; Waymouth, R.M. Group 4 ansa-cyclopentadienyl-amido catalysts for olefin polymerization. *Chem. Rev.* **1998**, *98*, 2587-2598.
- 17. Kaminsky, W.; Piel, C.; Scharlach, K. Polymerization of ethene and longer chained olefins by metallocene catalysis. *Macromol. Symp.* **2005**, 226, 25-34.
- 18. Braunschweig, H.; Breitling, F.M. Constrained geometry complexes-synthesis and applications. *Coord. Chem. Rev.* **2006**, *250*, 2691-2720.
- 19. Pérez, E.; Benavente, R.; Quijada, R.; Narváez, A.; Barrera Galland, G. Structure characterization of copolymers of ethylene and 1-octadecene. *J. Polym. Sci., Part B: Polym. Phys.* **2000**, *38*, 1440-1448.
- 20. Li, K.-T.; Dai, C.-L.; Kuo, C.-W. Ethylene polymerization over a nano-sized silica supported Cp₂ZrCl₂/MAO catalyst. *Catal. Commun.* **2007**, *8*, 1209-1213.

21. Krimm S.; Tobolsky A.V. Quantitative x-ray studies of order in amorphous and crystalline polymers. Quantitative x-ray determination of crystallinity in polyethylene. *J. polym. Sci.* **1951**, *7*, 57-76.

- 22. Hong, H.; Zhang, Z.; Chung, T.C.M.; Lee, R.W. Synthesis of new 1-decene-based LLDPE resins and comparison with the corresponding 1-octene- and 1-hexene-based LLDPE resins. *J. Polym. Sci., Part A: Polym. Chem.* **2007**, *45*, 639-649.
- 23. Camurati, I.; Cavicchi, B.; Dall'Occo, T.; Piemontesi, F. Synthesis and characterization of ethylene/1-olefin copolymers obtained by "single centre" catalysis. *Macromol. Chem. Phys.* **2001**, 202, 701-709.
- 24. Koivumäki, J. Properties of ethylene/1-octene, 1-tetradecene and 1-octadecene copolymers obtained with Cp2ZrCl2/MAO catalyst: Effect of composition and comonomer chain length. *Polym. Bull.* **1996**, *36*, 7-12.
- 25. Starck, P.; Löfgren, B. Thermal properties of ethylene/long chain α-olefin copolymers produced by metallocenes. *Eur. Polym. J.* **2002**, *38*, 97-107.
- 26. Randall, J.C. Carbon-13 NMR of ethylene-1-olefin copolymers: extension to the short-chain branch distribution in a low-density polyethylene. *J. Polym. Sci., Part A-2: Polym. Phys.* **1973**, *11*, 275-287.
- 27. Kim, C.; Kim, H. Copolymerization of propylene with various higher α-olefins using silica-supported *rac*-Me₂Si(Ind)₂ZrCl₂. *J. Polym. Sci.*, *Part A: Polym. Chem.* **2001**, *39*, 3294-3303.
- 28. Quijada, R.; Galland, G.B.; Mauler, R.S. The influence of the comonomer in the copolymerization of ethylene with α-olefins using C₂H₄[Ind]₂ZrCl₂/ methylaluminoxane as catalyst system. *Macromol. Chem. Phys.* **1996**, *197*, 3091-3098.
- 29. Clas, S.D.; Mcfaddin, D.C.; Russell, K.E.; Scammell-Bullock, M.V.; Peat, I.R. Melting points of homogeneous random copolymers of ethylene and 1-alkenes. *J. Polym. Sci., Part A: Polym. Chem.* **2000**, *41*, 7899-7904.
- 30. Jongsomjit, B.; Kaewkrajang, P.; Shiono, T.; Praserthdam, P. Supporting effects of silica-supported methylaluminoxane (MAO) with zirconocene catalyst on ethylene/1-olefin copolymerization behaviors for linear low-density polyethylene (LLDPE) production. *Ind. Eng. Chem. Res.* **2004**, *43*, 7959-7963.
- 31. Carlini, C.; D'Alessio, A.; Giaiacopi, S.; Po, R.; Pracella, M.; Raspolli Galletti, A.; Sbrana, G. Linear low-density polyethylenes by co-polymerization of ethylene with 1-hexene in the presence of titanium precursors and organoaluminium co-catalysts. *Polymer* **2007**, *48*, 1185-1192.

Sample Availability: Samples of the compounds (LLDPEs) are available from the authors.

© 2011 by the authors; licensee MDPI, Basel, Switzerland. This article is an open access article distributed under the terms and conditions of the Creative Commons Attribution license (http://creativecommons.org/licenses/by/3.0/).







Journal of Natural Gas Chemistry 21(2012)83-90

iai of Natural Gas Chemistry 21(2012)85–90

Production of propylene from an unconventional metathesis of ethylene and 2-pentene over Re₂O₇/SiO₂-Al₂O₃ catalysts

Weena Phongsawat¹, Benjamas Netivorruksa¹, Kongkiat Suriye², Siraprapha Dokjampa², Piyasan Praserthdam¹, Joongjai Panpranot^{1*}

1. Center of Excellence on Catalysis and Catalytic Reaction Engineering, Department of Chemical Engineering, Faculty of Engineering, Chulalongkorn University, Bangkok 10330, Thailand; 2. SCG Chemicals CO., LTD. 1 Siam Cement Rd., Bangsue, Bangkok 10800, Thailand

[Manuscript received May 12, 2011; revised August 4, 2011]

Abstract

An unconventional metathesis of ethylene and 2-pentene over Re_2O_7/SiO_2 - Al_2O_3 catalysts has been studied as an alternative route for the production of propylene. Complete conversion of 2-pentene and propylene yield as high as 88 wt% were obtained under mild reaction conditions at 35 °C and atmospheric pressure. Unlike the conventional metathesis of ethylene and 2-butenes in which isomerization is a competing side reaction, the isomerization of 1-butene product from the unconventional metathesis of ethylene and 2-pentene to 2-butenes can further react with excess ethylene in the feed, resulting in additional increase in propylene yield. The secondary metathesis reaction was found to be favored under ethylene/2-pentene (E/2P) molar ratio \geqslant 3 and gas hourly space velocity (GHSV) \leqslant 1000 h⁻¹ at the reaction temperature of 35 °C. No catalyst deactivation was observed during the 455 min time-on-stream under the selected reaction conditions.

Key words

metathesis; propylene production; 2-pentene; rhenium; silica-alumina

1. Introduction

Propylene is one of the most important feedstocks for petrochemical industries. The average annual growth of propylene global demand from 2009 to 2014 is expected to be around 5.1% per year [1-4]. Propylene supply-demand conditions and pricing are strongly dependent on refinery production, operating rates and feedstocks slates in the ethylene industry [5,6]. The main source of propylene is a byproduct from the thermal cracking of liquid feedstocks such as naphtha and LPGs. Propylene can also be produced using on-purpose technologies such as propane dehydrogenation and metathesis. The technology of propylene production from metathesis has received much attention in recent years. The commercial processes for conversion of ethylene and 2-butenes to propylene via cross-metathesis over heterogeneous catalysts have been developed [5,7-10]. This route, however, has some drawbacks because it needs access to large C4 streams that are free of isobutylene and butadiene [4]. Moreover, both cost and demand of butenes industrial feedstock increase continuously [7,11]. Metathesis between ethylene and 2-pentene is, therefore, considered as an alternative route to produce propylene from cheaper raw materials. As shown in Equation 1, the main products from ethylene and 2-pentene are propylene and 1-butene. 1-Butene is also an important feedstock for the production of linear low density polyethylene.

$$CH_2 = CH_2 + CH_3 - CH = CH - CH_2 - CH_3 \rightarrow$$
 $CH_2 = CH - CH_3 + CH_2 = CH - CH_2 - CH_3$
(1)

Generally, the catalysts for olefin metathesis are based on transition metals Mo, W, Re, and Ru [7,12–16]. The catalytic systems can be carried out in both homogeneous and heterogeneous systems. The homogeneous catalysts are usually Mo, W, Re and Ru in the form of organometallic complexes while the most successful heterogeneous catalysts include Mo, W and Re in oxide form supported on high surface area inorganic oxides such as silica and alumina [7,17,18]. Due to their better handling properties and low separation problems, supported metal oxide catalysts are commercially more attractive. Industrial applications of olefin metathesis have been reviewed by Mol et al. [10].

This work was supported by the financial supports from the Thailand Research Fund (TRF), the Office of Higher Education Commission, and the NRU-CU (AM1088A).

^{*} Corresponding author. Tel: +66-2218-6869; Fax: +66-2218-6877; E-mail: joongjai.p@chula.ac.th

Supported Re oxide catalysts are known to be highly active for olefins metathesis under very mild reaction conditions even at room temperature [19] whereas supported W and Mo oxide catalysts requires much higher reaction temperature (150-500 °C) [7,20]. The major negative effects under high operating temperature over an acidic support were that isomerization readily occurs and as a consequence, selectivity to the primary metathesis product is much lowered [21]. High reaction temperature also leads to heavy coke formation on the metathesis active sites [22]. Another advantage of supported Re oxide catalysts is the higher tolerance to several poisons such as alkoxycarbonyl and alkoxy groups [7]. Since 1980s, the improvement of olefin metathesis over Re-based catalysts has been extensively reported. A number of studies have concluded that acidity of the support is an important factor for the active sites formation [23-29]. Recently, it has been reported that the use of mesoporous alumina supports for Re oxides has shown significant improvement in several metathesis reactions including metathesis of terminal olefins, internal olefins, α -, ω -dienes as well as ring opening metathesis polymerization (ROMP) of cycloalkenes and cross-metathesis of cycloalkenes with linear olefins [12,30-33]. Besides feed impurities, catalyst poisons, and the nature of catalysts, the activity and product selectivity in conventional olefins metathesis for propylene production depend largely on the reaction conditions such as the molar ratio of ethylene to 2-butene, GHSV, and reaction temperature.

In the present study, the gas-phase olefin metathesis between ethylene and 2-pentene as an alternative route for propylene production was investigated for the first time over the Re₂O₇/SiO₂-Al₂O₃ catalysts. The Re₂O₇/SiO₂-Al₂O₃ catalysts were selected because they have shown to produce high catalytic activity and good propylene yields under mild reaction conditions in the conventional cross metathesis between ethylene and 2-butene [19,34,35]. Moreover, reaction at relatively low temperature would be of industrial interest and more practical for the use of the alternative feed in an existing system. The catalytic performances of Re₂O₇/SiO₂-Al₂O₃ catalysts in the metathesis of ethylene and 2-pentene were investigated under wide operating conditions (i.e., the reaction temperature ranging from 35 to 150 °C, molar ratio of ethylene to 2-pentene (E/2P) from 2 to 6, and gas hourly space velocity (GHSV) from $500 \text{ to } 3000 \text{ h}^{-1}$). The propylene yield, 2-pentene conversion and product distribution during 455 min time-on-stream were reported.

2. Experimental

2.1. Catalyst preparation

SiO₂-Al₂O₃ (99.9% Grade 135) from Aldrich was used as the support for the preparation of Re_2O_7/SiO_2 -Al₂O₃ catalysts. The catalysts were prepared by the incipient wetness impregnation method using an aqueous solution of ammonium perrhenate (NH₄ReO₄, 99.999%, Aldrich). When the solution amount of the desired metal species was greater than that of the pore volume of the support, the impregnation procedure was repeated several times with drying (6 h, 110 °C) between each cycle to eliminate excess solvent. The catalysts were dried overnight at 110 °C in air and calcined at 550 °C for 8 h under oxygen flow with a heating rate of 10 °C/min. The actual amount of Re loading was determined by the inductive coupled plasma optical emission spectrometer (ICP-OES, PerkinElmer).

2.2. Reaction test

Gas-phase metathesis reactions between ethylene and 2-pentene were carried out in a fixed-bed down flow stainless steel reactor with an i.d of 0.7 cm at atmospheric pressure. The reactant feed was composed of 6.75 vol% of 2pentene (>99% mixture of isomers, Aldrich) pre-mixed with 2.25 vol% ethylene (99.999%, SCG Chemicals Co., Ltd.) in N₂ balance. All the reactants used in this work were in high purity grade without impurity such as oxygen, CO, water, S, and oxygenates hydrocarbons. In each experiment, approximately 1 g of the catalyst sample was placed in the middle of the reactor. A temperature sensor (type K thermocouple) was mounted into the reactor at the middle. The catalyst was first pretreated at 550 °C under nitrogen down flow for 1 h and then cooled down under the same gas to the desired operating temperature. Then, the reactant feed was introduced and both feed and reaction products were followed and analyzed every half an hour using an on-line gas chromatograph (Agilent GC 7820A) equipped with a capillary GS-Gaspro113-4362 column (60 m×0.32 mm). The GC signals were collected using an EZChrom Elite integrated peak program integrator. The conversion of limited 2-pentene reactant and the yield of products were calculated using the following equations:

Yield of component i (%) = 2-Pentene conversion $\times \frac{\text{Amount of component } i \text{ in products}}{\text{Amount of total products}}$ (2)

3. Results and discussion

3.1. Effect of E/2P mole ratio

The physical properties of SiO_2 - Al_2O_3 and Re_2O_7/SiO_2 - Al_2O_3 catalysts are summarized in Table 1.

As shown in Equation (3), the theoretical stoichiometric value of reactants in the olefin metathesis reaction is equimolar [11]. However, in the conventional metathesis process of ethylene and 2-butene, the optimal molar ratio of ethylene to 2-butene to produce high propylene yield was determined to be in excess but not more than 2.5 [36].

$$RCH=CHR+R'CH=CHR' \longrightarrow RCH=CHR \\ \vdots \\ R'CH=CHR'$$
 (3)
$$\longrightarrow 2RCH=CHR'$$

Table 1. The properties of the support and supported rhenium oxide catalyst

Properties	Sample			
Troperties	SiO ₂ -Al ₂ O ₃	Re ₂ O ₇ /SiO ₂ -Al ₂ O ₃		
BET surface area (m ² ·g ⁻¹)	547.8	395.6		
Pore volume ($cm^3 \cdot g^{-1}$)	0.8	0.6		
Average pore size (nm)	5.6	5.9		
Al ₂ O ₃ support composition (wt%)	13	13		
Actual Re-metal loading (wt% Re) ^a	_	5.83		

^a The actual amount of Re-metal loading after calcination was determined by ICP-OES

In order to investigate the effect of E/2P molar ratio in the metathesis of ethylene and 2-pentene on Re₂O₇/SiO₂-Al₂O₃ catalysts, the reaction temperature and GHSV were set at 35 °C and 3000 h⁻¹, respectively. All the reaction data were taken at 455 min time-on-stream. Changes of the catalyst activities in terms of 2-pentene conversion during 455 min timeon-stream were determined to be less than 5% under the selected reaction conditions. The 2-pentene concentration was kept constant while changing excess ethylene concentration to obtain the required molar ratios. The E/2P molar ratios were varied in the range of 2-6. The 2-pentene conversions under different E/2P molar ratios are shown in Figure 1. It is clear from Figure 1 that 2-pentene conversion increases from 77% to 87% with the increasing of E/2P molar ratio from 2 to 3. However, only a slight increase of 2-pentene conversion (to ca. 92%) could be observed with further increase of the E/2P molar ratio from 3 to 6. The main product yields in term of weight percent from the metathesis of ethylene and 2-pentene over Re₂O₇/SiO₂-Al₂O₃ catalysts as a function of time-onstream for different E/2P mole ratios are shown in Figure 2. The propylene yield increased from 39% to 59% with increasing E/2P from 2 to 3. There was no increase in propylene yield when E/2P was further increased from 3 to 6.

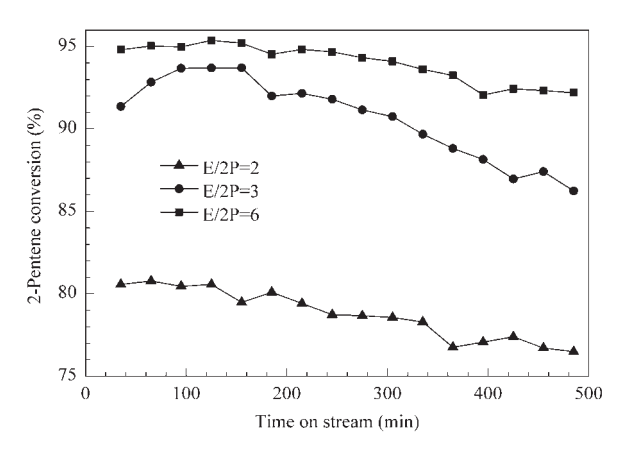
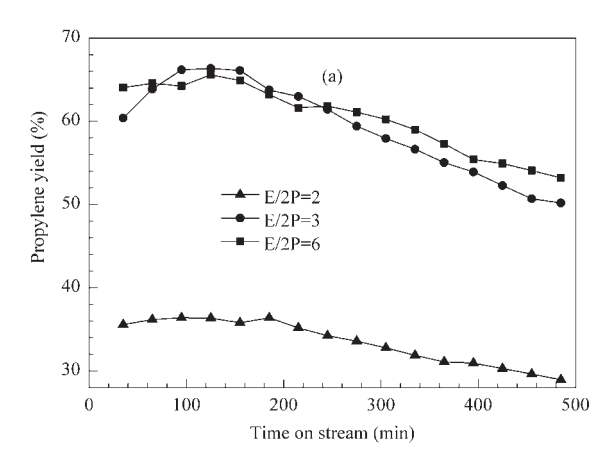


Figure 1. Effect of ethylene/2-pentene mole ratio on the 2-pentene conversion on $Re_2O_7/SiO_2-Al_2O_3$ catalysts. Reaction conditions: Pressure = 0.1 MPa, GHSV = 3000 h^{-1} , Temperature = 35 $^{\circ}C$



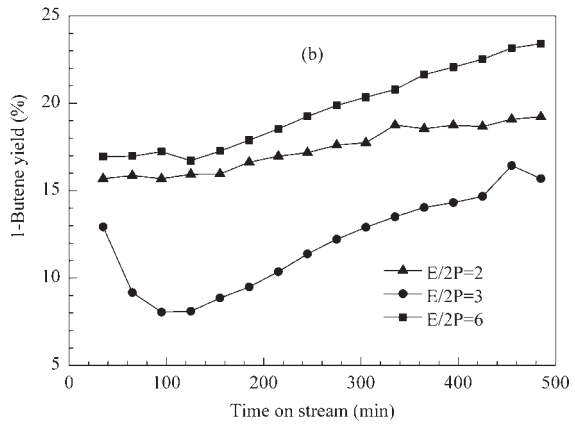


Figure 2. Yield of the primary metathesis products in the metathesis of ethylene and 2-pentene over Re_2O_7/SiO_2 - Al_2O_3 catalysts. Reaction conditions: Pressure = 0.1 MPa, $GHSV = 3000 \text{ h}^{-1}$, $Temperature = 35 \,^{\circ}\text{C}$

Besides propylene and 1-butene primary metathesis products, the other by-products were also produced including cisand tran-2-butene, 1-pentene, and C₅₊ hydrocarbons. The product distribution (yield percentage) from the metathesis reaction of ethylene and 2-pentene at 455 min time-on-stream obtained under different E/2P ratios and 35 °C are shown in Figure 3. It is known that 2-butene is more stable than 1butene so the double-bond isomerization of 1-butene to 2butene is inevitable over acidic catalyst systems even at low reaction temperature. In the conventional feed, double-bond isomerization also occurred at 21-25 °C [12,37,38]. The major C₅₊ hydrocarbon in this set of reactions was 3-hexene which were produced by self-metathesis of 2-pentene. Higher amount of C₅₊ hydrocarbons were produced at lower E/2P mole ratio (E/2P = 2). It is suggested that excess ethylene could prevent the self-metathesis reaction of 2-pentene on the Re₂O₇/SiO₂-Al₂O₃ catalysts. Moreover, the amount of 2butenes was decreased with increasing E/2P mole ratio. The 2-butenes products could easily undergo a subsequent secondary metathesis reaction with excess ethylene, resulting in an additional propylene formation. The propylene yields for all the cases far exceeded the stoichiometric values (propylene selectivity of 50% (mole) or $\sim 43\%$ (weight)). It is suggested that the isomerization of 1-butene to 2-butene was a useful side reaction assisting propylene formation in this alternative feed in the present work. A possible reaction scheme for propylene formation in the metathesis of ethylene and 2-pentene is shown in Equations (4) to (6):

Main reaction (primary metathesis)

$$CH_2 = CH_2 + CH_3 - CH = CH - CH_2 - CH_3 \rightarrow CH_2 = CH - CH_3 + CH_2 = CH - CH_2 - CH_3$$
 (4)

Double-bond isomerization of the primary metathesis product (1-butene)

$$\begin{aligned} CH_2 &= CH - CH_2 - CH_3 \rightarrow \\ CH_3 - CH &= CH - CH_3 \end{aligned} \tag{5}$$

Secondary metathesis reaction

$$CH = CH + CH_3 - CH = CH - CH_3 \rightarrow$$

$$2CH_2 = CH - CH_3$$
(6)

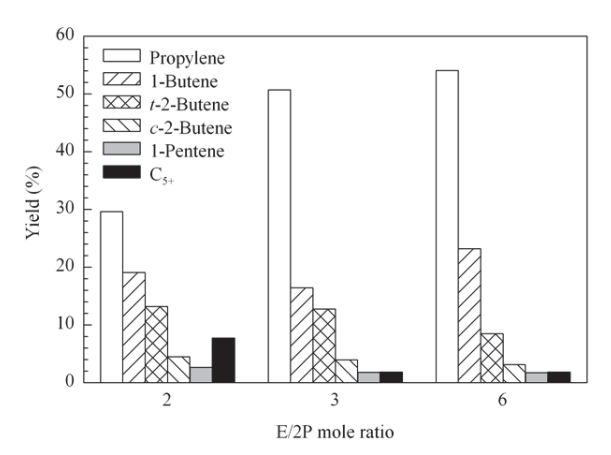


Figure 3. Product distribution in the metathesis reaction of ethylene and 2-pentene at different ethylene/2-pentene mole ratio at 455 min on stream. Reaction conditions: Pressure = $0.1\,$ MPa, GHSV = $3000\,h^{-1}$, Temperature = $35\,$ °C

3.2. Effect of GHSV

The effect of GHSV in the range of $500-3000 \,h^{-1}$ on the catalytic performances of Re₂O₇/SiO₂-Al₂O₃ in the metathesis of ethylene and 2-pentene was investigated under the E/2P molar ratio of 3 and at 35 °C. As shown in Figure 4, the conversion of 2-pentene increased drastically from 87% to 100% when the GHSV was decreased from 3000 to $500 \, h^{-1}$ at 455 min time-on-stream. The main product yields of the metathesis reaction between ethylene and 2-pentene as a function of time-on-stream under various GHSV are shown in Figure 5. Both propylene and 1-butene yields did not follow their stoichiometric amounts (43 wt% of propylene and 57 wt% of 1-butene) and higher amount of propylene and lower amount of 1-butene were obtained. As mentioned earlier, the isomerization of 1-butene to 2-butenes and the subsequent secondary metathesis reaction between ethylene and 2-butenes occurred readily under the selected reaction conditions, resulting in an increase in propylene yield. Table 2 summarizes the activities and the product yields obtained over Re₂O₇/SiO₂-Al₂O₃ catalysts at 35 °C under different GHSVs. It was found that at higher GHSV the secondary metathesis became less

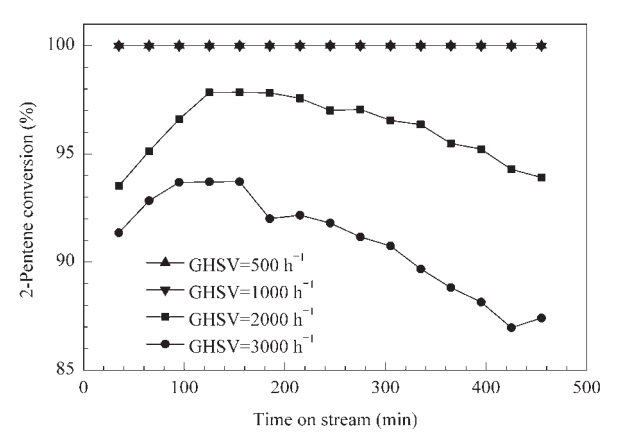
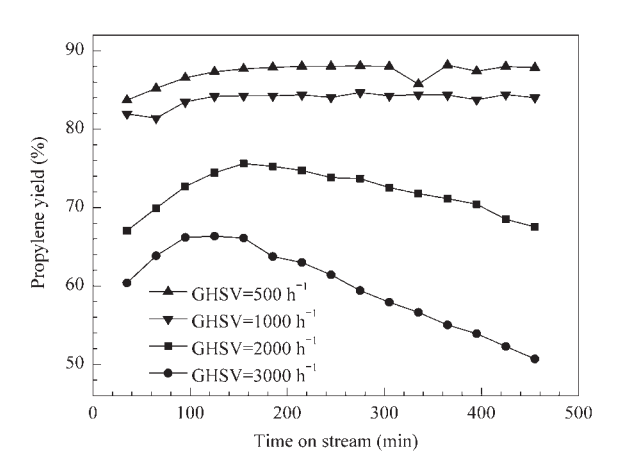


Figure 4. Effect of gas hourly space velocity on the 2-pentene conversion over Re_2O_7/SiO_2 - Al_2O_3 catalysts. Reaction conditions: Pressure = 0.1 MPa, E/2P mole ratio = 3, Temperature = 35 °C



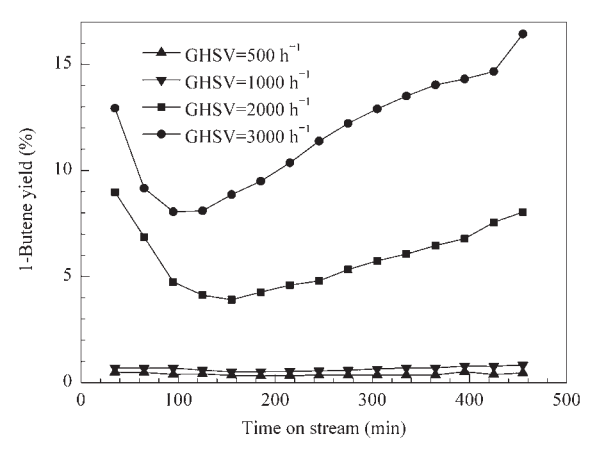


Figure 5. Yield of the primary metathesis products in the metathesis of ethylene and 2-pentene over Re_2O_7/SiO_2 - Al_2O_3 catalysts. Reaction conditions: Pressure = 0.1 MPa, E/2P mole ratio = 3, Temperature = 35 °C

pronounced while the other side reactions such as self-metathesis of 2-pentene was favored. Probably, due to the slow desorption rate of 2-pentene as compared with smaller hydrocarbon molecules such as ethylene [39–43], some of the 2-pentenes that adsorbed on the catalyst surface could interact themselves (self-metathesis reaction), forming 2-butene

and 3-hexene when the contact time was relatively short. It is noted that under the low reaction temperature conditions, oligomerization rate may be low so that the weight percentage of C_{5+} formed was mainly the 3-hexene products from 2-pentene self-metathesis reaction. Complete conversion of 2-pentene and propylene yield as high as 88% were achieved under the lowest GHSV $(500\,h^{-1})$ and were found to be stable during the 455 min time-on-stream.

Table 2. Catalytic performance of Re₂O₇/SiO₂-Al₂O₃ catalyst with different GHSVs

GHSV	2-C ₅ =		Selectivity (%)				
(h^{-1})	conversion (%)	C ₃ =	$1-C_4^=$	$2-C_4^=$	1-C ₅	C ₅₊	
500	100	88.0	0.5	11.7	_	_	
1000	100	83.9	0.8	15.2	_	_	
2000	93.9	70.9	8.6	19.5	_	_	
3000	87.4	58.2	8.8	19.1	2.0	2.1	

Reaction conditions: P=0.1 MPa, ethylene/2-pentene = 3 (mole ratio), $T=35\,^{\circ}$ C, Time on stream = 455 min

3.3. Effect of reaction temperature

The metathesis of simple linear olefins is not accompanied by significant structural changes. Therefore, the reaction is almost a thermally neutral process and the variation of temperature has a negligible influence in view of the thermodynamics aspect [44]. However, for the operation aspect, it needs to know the effect of reaction temperature in the range of 35 to 150 °C on the catalytic performance of the metathesis of ethylene and 2-pentene over Re₂O₇/SiO₂-Al₂O₃ catalyst. And the results are shown in Figure 6. It is clear from Figure 6 that the reaction at 150 °C caused catalyst much faster deactivation than at the other temperatures. A fast drop of 2-pentene conversion from 99% to 83% was observed within the first 120 min time-on-stream. Then, it was gradually decreased to ca. 75% after 455 min time-on-stream. The main product yields of the metathesis reaction between ethylene

and 2-pentene at different reaction temperatures as a function of time-on-stream are shown in Figure 7. A trend similar to the conversion of 2-pentene was observed. If the reaction was proceeded at 150 °C, the propylene yield dramatically decreased from 70% to 37% within 120 min time-on-stream. On the other hand, 1-butene products were gradually increased along with the time-on-stream especially when the reaction was carried out at high reaction temperature. Deactivation of Re-based catalysts under high reaction temperature has been reported in Refs. [40,45-47]. The deactivation of the Rebased catalysts can mainly attribute to many aspects such as the structure change of active center, coke deposition, impurity in reactants, excessively reduction, adsorption of products and byproducts, etc. However, the reactants used in this study were high purity grade without impurity such as H₂O, S, and oxygen-containing hydrocarbon so that the effect of impurity in the reactants on the catalyst activity would be minimized.

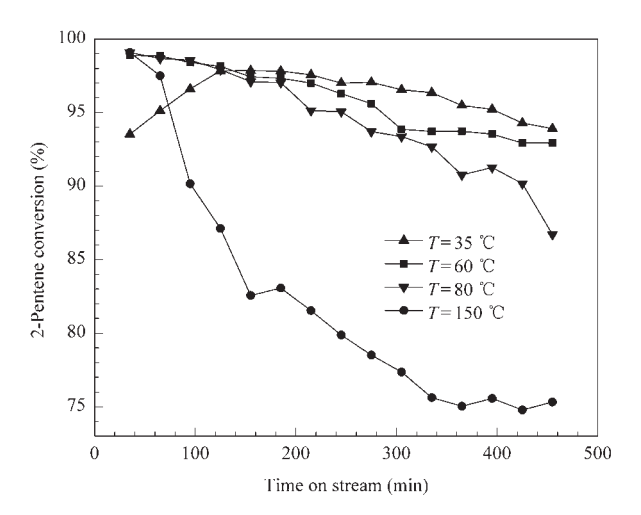
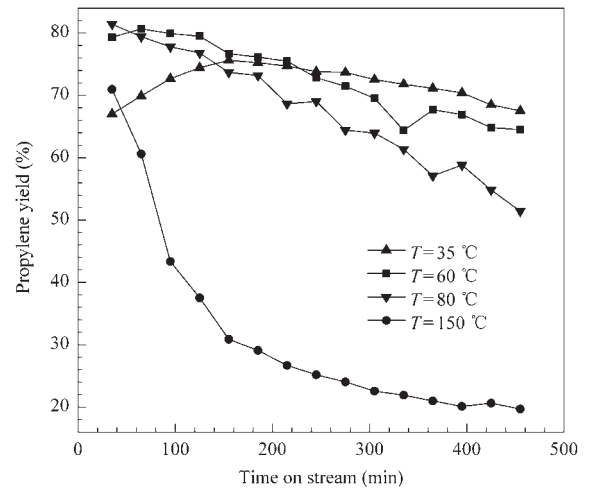


Figure 6. Effect of reaction temperature on the 2-pentene conversion over $Re_2O_7/SiO_2-Al_2O_3$ catalysts. Reaction conditions: Pressure = 0.1 MPa, E/2P mole ratio = 3, GHSV = $2000 \ h^{-1}$



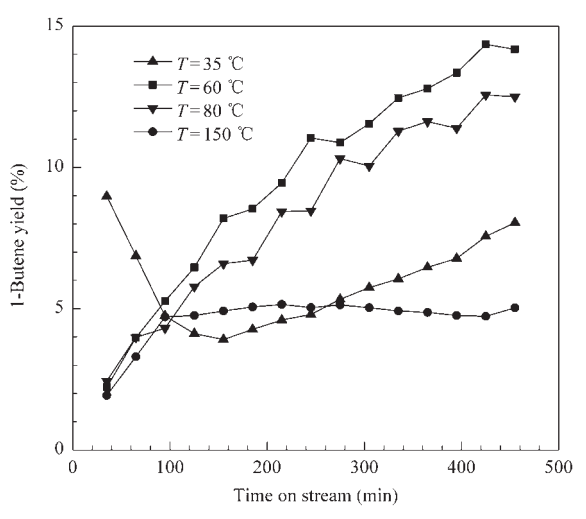


Figure 7. Yield of the primary metathesis products in the metathesis of ethylene and 2-pentene over $Re_2O_7/SiO_2-Al_2O_3$ catalysts. Reaction conditions: Pressure = 0.1 MPa, E/2P mole ratio = 3, E/2P mole ratio = 3,

The product distributions in term of yield percentage produced after running the reaction for 35, 245, and 455 min on stream at various reaction temperatures are shown in Figure 8. It was found that much more side reactions, such as isomerization of butenes products and isomerization of 2-pentene reactant, could be observed over Re₂O₇/SiO₂-Al₂O₃ catalysts at the temperature higher than 60 °C. Moreover, the propylene yield decreased gradually with time-on-stream if the reaction temperature was higher than 60 °C. When the reaction temperature set at 150 °C, the propylene yield decreased by almost 40%, whereas the propylene yield remained constant

at ca. 70% – 72% when the reaction temperature set at 35 °C after running the reaction for 455 min. It has been reported that the deactivation of Re-based catalysts occurred as soon as they were in contact with alkenes and was accelerated under higher reaction temperatures [40,47]. On the one hand, larger amount of 2-butenes products were obtained at 150 °C, since most of 2-butenes did not further react with ethylene to form propylene in the subsequent secondary metathesis, resulting in poor propylene yield. On the other hand, isomerization and oligomerization were also dominated at higher reaction temperature. Although, 1-pentene product was not detected

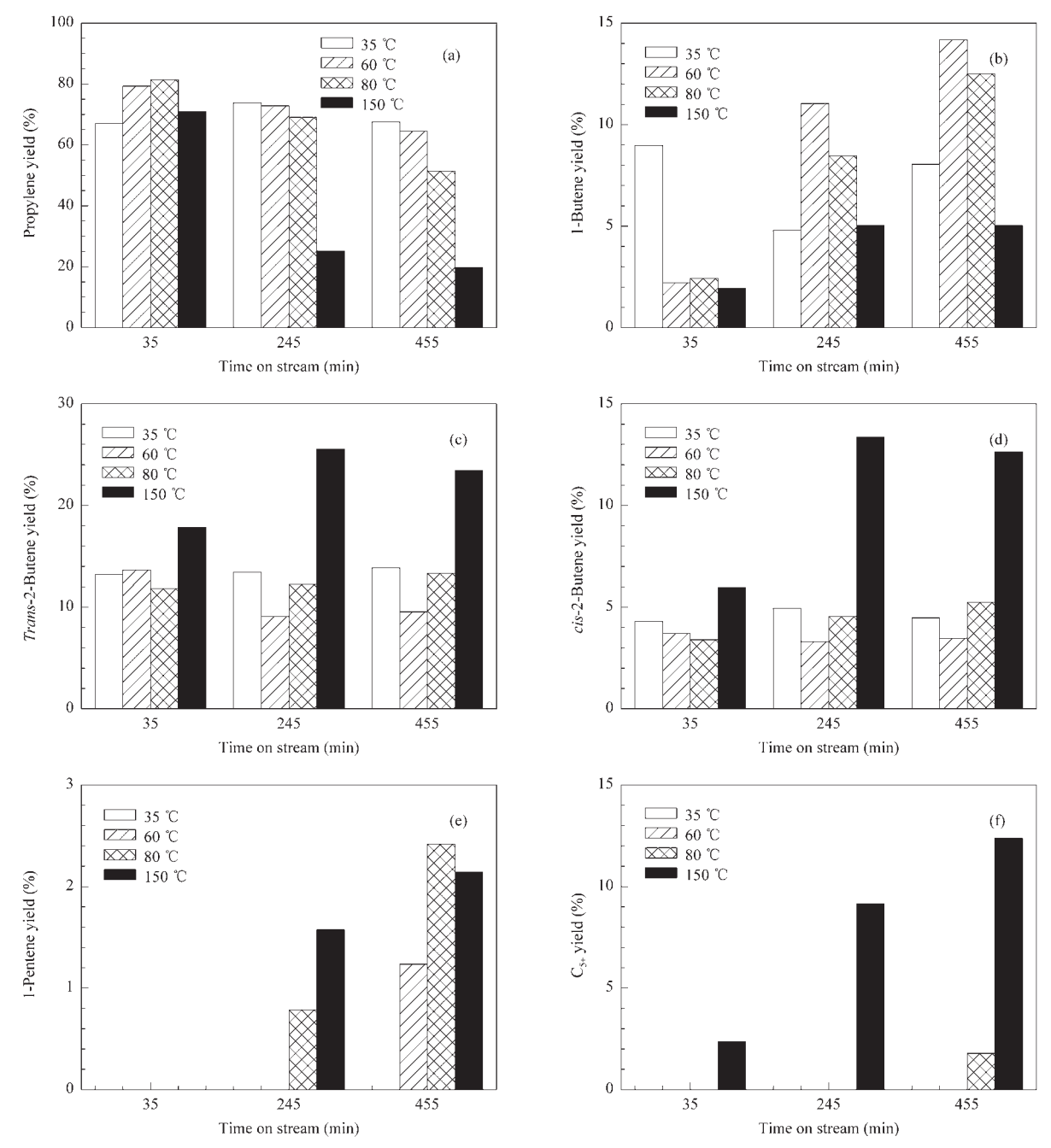
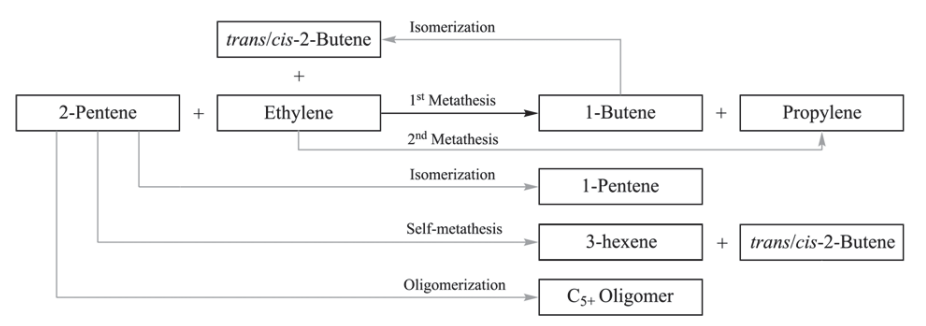


Figure 8. Product distributions along time on stream in the metathesis reaction of ethylene and 2-pentene at different reaction temperatures. Reaction conditions: Pressure = 0.1 MPa, E/2P (mole ratio) = 3, GHSV = 2000 h^{-1}

during the first 35 min on stream at all the reaction temperatures, it became apparent (less than 2%) during 245 min on stream for the reaction temperatures at 80 and 150 °C. If the reaction temperature set at 60 °C, 1-pentene (ca. 1.2%) also produced after running the reaction for 455 min. There were very small amounts of branched isomers of butenes and hexene in the products because skeletal isomerization were also detected at the early stage of the reaction (during the first 90 min) when the reaction temperature was higher than 60 °C (results not shown), but they disappeared when the reaction time was prolonged. The results suggest that the modification of rhenium species on the catalyst surface may happen upon contacting with the reactants. It has been reported that skeletal isomerization was induced by unreduced rhenium oxide species [48]. After the rhenium-carbene species were formed, metathesis reaction was dominated and the skeletal isomerization became less pronounced. In the metathesis of 1-butene, iso-butene was found over the catalysts with relatively low activity and decreased with increasing metathesis activity [49].

As far as the formation of higher hydrocarbons is concerned, the C_{5+} products can be formed during the first 35 min on stream only at the reaction temperature as high as $150\,^{\circ}$ C. Both 1-pentene and C_{5+} were increased with time-on-stream at high reaction temperature. Since much faster catalyst deactivation rate could be observed at $150\,^{\circ}$ C, it is suggested that besides the self-metathesis of 2-pentene leading to the formation of 3-hexene, the formation of larger hydrocarbons via oligomerization reaction would occur under high reaction temperatures, leading to the formation of carbonaceous deposits and blocking the Re-active sites. Various reaction pathways in the metathesis of ethylene and 2-pentene over $Re_2O_7/SiO_2-Al_2O_3$ catalysts are illustrated in Scheme 1.



Scheme 1. Various reaction pathways in the metathesis of ethylene and 2-pentene over $Re_2O_7/SiO_2-Al_2O_3$ catalysts. Dotted line represents the conventional metathesis of ethylene and 2-butenes

4. Conclusions

The metathesis of ethylene and 2-pentene to propylene and 1-butene over Re₂O₇/SiO₂-Al₂O₃ catalysts with Re loading of 5.83 wt% has shown to be an effective alternative route for propylene production. The catalyst activity increases with increase of the reaction temperature, however, much faster catalyst deactivation is observed at 150 °C due to side reactions such as oligomerization and self-metathesis of 2pentene. The propylene yield at reaction temperature of 35 °C can be further improved when the mole ratio of E/2P higher than 3 and GHSV lesser than $1000 \,\mathrm{h^{-1}}$ are used. The propylene yield of 88% at a 2-pentene conversion of 100% can be obtained under the optimized reaction conditions (i.e., with E/2P mole ratio of 3, GHSV of $500 \, h^{-1}$, and at the reaction temperature of 35 °C) without catalyst deactivation during 455 min on stream. Although double bond isomerization of 1-butene to 2-butenes occurred at the reaction temperature of 35 °C, they could further interact with excess ethylene, resulting in an increase in propylene selectivity.

Acknowledgements

The financial supports from the Thailand Research Fund (TRF), the Office of Higher Education Commission, and the NRU-CU (AM1088A) are gratefully acknowledged. The authors would like to thank the Royal Golden Jubilee Ph. D. scholarship from TRF and

SCG Chemicals for W. P.

References

- [1] Gartner E. World Petrochemicals Coverage of Propylene. World Petrochemicals. United States: IHS, Inc., 2010. 1
- [2] Eramo M. Oil Gas J, 2005, 103(45): 52
- [3] Jiao Y. Petrochem Ind Trends, 2004, (9): 9
- [4] Park Y K, Lee C W, Kang N Y, Choi W C, Choi S, Oh S H, Park D S. Catal Surv Asia, 2010, 14(2): 75
- [5] Parkinson G. Chem Eng, 2001, 108(8): 27
- [6] Mol J C. J Mol Catal, 1991, 65(1-2): 145
- [7] Ivin K J, Mol J C. Olefin Metathesis and Metathesis Polymerization. San Diego: Academic Press, 1997. 93
- [8] Taoufik M, Le Roux E, Thivolle-Cazat J, Basset J M. Angew Chem Int Ed, 2007, 46(38): 7202
- [9] Connon S J, Blechert S. Angew Chem Int Ed, 2003, 42(17): 1900
- [10] Mol J C. J Mol Catal A: Chem, 2004, 213(1): 39
- [11] Cornil B, Herrmann A W, Schogl R. Wong C. A Concise Encyclopedia Catalysis from A to Z. New York: Wiley-VCH, 2000
- [12] Balcar H, Hamtil R, Zilkova N, Cejka J. Catal Lett, 2004, 97(1-2): 25
- [13] Topka P, Balcar H, Rathousky J, Zilkova N, Verpoort F, Cejka J. Microporous Mesoporous Mater, 2006, 96(1-3): 44
- [14] Buchmeiser M R. New J Chem, 2004, 28(5): 549

- [15] Rhers B, Salameh A, Baudouin A, Quadrelli E A, Taoufik M, Coperet C, Lefebvre F, Basset J M, Solans-Monfort X, Eisenstein O, Lukens W W, Lopez L P H, Sinha A, Schrock R R. Organomet, 2006, 25(15): 3554
- [16] Rendon N, Berthoud R, Blanc F, Gajan D, Maishal T, Basset J M, Coperet C, Lesage A, Emsley L, Marinescu S C, Singh R, Schrock R R. Chem Eur J, 2009, 15(20): 5083
- [17] Li X, Zhang W, Li X, Liu S. Prog Chem, 2009, 20: 1021
- [18] Lokhat D, Starzak M, Stelmachowski M. Appl Catal A, 2008, 351(2): 137
- [19] Mol J C. Catal Today, 1999, 51(2): 289
- [20] Amigues P, Chauvin Y, Commereuc D, Hong C T, Lai C C, Liu Y H. *J Mol Catal*, 1991, 65(1-2): 39
- [21] Van Roosmalen A J, Mol J C. J Catal, 1982, 78(1): 17
- [22] Bartholomew C H. Appl Catal A, 2001, 212(1-2): 17
- [23] Duquette L G, Cieslinski R C, Jung C W, Garrou P E. *J Catal*, 1984, 90(2): 362
- [24] Piquemal J Y, Briot E, Vennat M, Bregeault J M, Chottard G, Manoli J M. Chem Commun, 1999, (13): 1195
- [25] Xiaoding X, Mol J C, Boelhouwer C. J Chem Soc, Faraday Trans 1 F, 1986, 82(9): 2707
- [26] Hsu C C. [PhD Dissertation]. Oklahoma: Oklahoma University,
- [27] Buffon R, Auroux A, Lefebvre F, Leconte M, Choplin A, Basset J M, Herrmann W A. J Mol Catal, 1992, 76(1-3): 287
- [28] Amigues P, Chauvin Y, Commereuc D, Hong C T, Lai C C, Liu Y H. J Mol Catal, 1991, 65(1-2): 39
- [29] Schekler-Nahama F, Clause O, Commereuc D, Saussey J. Appl Catal A, 1998, 167(2): 237
- [30] Onaka M, Oikawa T. Chem Lett, 2002, (8): 850
- [31] Oikawa T, Ookoshi T, Tanaka T, Yamamoto T, Onaka M. Microporous Mesoporous Mater, 2004, 74(1-3): 93

- [32] Balcar H, Cejka J. Macromol Symp, 2010, 293(1): 43
- [33] Martin-Aranda R M, Cejka J. Top Catal, 2010, 53(3-4): 141
- [34] Mitra B, Gao X T, Wachs I E, Hirt A M, Deo G. Phys Chem Chem Phys, 2001, 3(6): 1144
- [35] Mol J C, Imamoglu i Y, Zumreoglu-Karan B, Amass A J. Olefin Metathesis and Polymerization Catalysis. Netherlands: Kluwer Academic, 1989. 173
- [36] Garside R J, Greene M I. US Patent 0124839 A1. 2005
- [37] Andreini A, Xu X D, Mol J C. Appl Catal, 1986, 27(1): 31
- [38] Mol J C, Andreini A. J Mol Catal, 1988, 46(1-3): 151
- [39] Moodley D J, van Schalkwyk C, Spamer A, Botha J M, Datye A K. Appl Catal A, 2007, 318: 155
- [40] Spronk R, Andreini A, Mol J C. J Mol Catal, 1991, 65(1-2): 219
- [41] Aguado J, Escola J M, Castro M C, Paredes B. Appl Catal A, 2005, 284(1-2): 47
- [42] Spronk R, Mol J C. Appl Catal, 1991, 70(2): 295
- [43] Hamtil R, Zilkova N, Balcar H, Cejka J. Appl Catal A, 2006, 302(2): 193
- [44] Huang S J, Liu S L, Xin W J, Xie S J, Wang Q X, Xu L Y. J Nat Gas Chem, 2006, 15(2): 93
- [45] Salameh A, Baudouin A, Soulivong D, Boehm V, Roeper M, Basset J M, Coperet C. J Catal, 2008, 253(1): 180
- [46] Stoyanova M, Rodemerck U, Bentrup U, Dingerdissen U, Linke D, Mayer R W, Lansink Rotgerink H G J L, Tacke T. Appl Catal A, 2008, 340(2): 242
- [47] Behr A, Schuller U, Bauer K, Maschmeyer D, Wiese KD, Nierlich F. Appl Catal A, 2009, 357(1): 34
- [48] Logie V, Maire G, Michel D, Vignes J L. J Catal, 1999, 188(1): 90
- [49] Harmse L, Van Schalkwyk C, Van Steen E. Catal Lett, 2010, 137(3-4): 123



Article

Behaviors in Ethylene Polymerization of MgCl₂-SiO₂/TiCl₄/THF Ziegler-Natta Catalysts with Differently Treated SiO₂

Nichapat Senso, Bunjerd Jongsomjit and Piyasan Praserthdam *

Center of Excellence on Catalysis and Catalytic Reaction Engineering, Department of Chemical Engineering, Faculty of Engineering, Chulalongkorn University, Bangkok 10330, Thailand

* Author to whom correspondence should be addressed; E-Mail: piyasan.p@chula.ac.th; Tel.: +662-218-6869; Fax: +662-218-6868.

Received: 17 January 2011; in revised form: 24 January 2011 / Accepted: 27 January 2011 /

Published: 28 January 2011

Abstract: The present research focuses on investigation of the catalytic behaviors of MgCl₂-SiO₂/TiCl₄/THF Ziegler-Natta (ZN) catalysts with fumed SiO₂ variously treated with silane compounds. The non-treated silica (NTS) and other silicas treated with dimethylsilicone fluid (TSDMSF), dimethyldichlorosilane (TSDMDCS), and hexamethyldisilazane (TSHMDS) were employed. It was found that the Cat-TSDMDCS and Cat-TSHMDS exhibited remarkably high activity, even with a similar bulk Ti content as the others. Thus, the more powerful technique of XPS analysis was used to determine the Ti content at the catalyst surface. It was evident that the surface concentrations of Ti could play important role on the catalyst activity. As the result, the increased activity is proportional to the surface concentration of Ti. It was mentioned that the change in surface concentration of Ti with different treated silica can be attributed to the effect of silane spacer group and steric hindrance. The distribution of Ti on the external surface can be also proven by means of EDX mapping, which matched the results obtained by XPS analysis. The treated silica also resulted in narrower molecular weight distribution (MWD) due to the more uniform active sites produced. There was no significant change in polymer morphology upon treatment of the silica.

Keywords: Ziegler-Natta catalyst; polyethylene; silica; alkyl silane; XPS

1. Introduction

In the polyolefin industry, the significant role of the Ziegler-Natta (ZN) catalysts is remarkable as are both industrial and academic interest in their reaction engineering [1-4]. In the production of polyolefins, the polymer particle morphology strongly affects the plant operation. The loss of polymer morphological control leads to many industrial operating problems, such as fouling and broadening reactor residence-time distribution. It is widely accepted that the polymer particle morphology is mainly determined by the morphology of a parent catalyst through the replication phenomenon [5,6]. The modification of supported-ZN catalyst is a preferred way to increase the morphology control of the polymers, increase the catalytic activity as well as increase catalytic stability.

Anhydrous magnesium dichloride (MgCl₂) has been known as a preferred support for highly efficient ZN catalysts for the polymerization of olefins. MgCl₂ is often convenient to use in producing ZN catalysts with good morphology and the high rates of polymerization activity [7-8]. However, the frailty of MgCl₂ during preparation is still a problem for controlling the morphology of ZN when used in olefin polymerization. To overcome these problems, MgCl₂-SiO₂-bisupported titanium catalyst is preferred, especially when it is used in a gas-phase polymerization system [9-11]. For example, UCC has developed a series of MgCl₂-SiO₂/THF/TiCl₄ four-component catalyst systems for gas-phase ethylene polymerization and ethylene/1-hexene copolymerization [12-13]. This catalyst exhibits good comonomer incorporation properties, and the polyethylene products show good morphology control. Somehow, the catalytic activity of MgCl₂-SiO₂/THF/TiCl₄ system is lower than that without SiO₂ added. To increase the catalytic activity, the properties of SiO₂ such as type, shape, surface area [14] and OH content on the surface, should be considered in order to prepare a catalyst that is completely satisfactory for all purposes [15].

As is well known SiO₂ has OH groups on the surface, which are a very important poison for ZN catalysts. Preheated SiO₂ with different calcination temperatures (110-820 °C) is necessary to control the OH content on the surface of SiO₂. The relationship between calcination temperature and TiCl₄ reaction temperature was observed by Hornytzkyj et al. [16]. It was found that the lower reaction temperature of 175 and 125 °C led to amorphous titanium species, whereas the temperature of 350 °C or higher resulted in amorphous and agglomerated titanium species. The amount of amorphous titanium species present in the high temperature samples is a function of the reaction temperature of TiCl₄ and of the preheat temperature of the SiO₂ determined by etching with sulfuric acid. Consequently, suitable calcination methods can also decrease the OH groups on the surface, but it consumes much energy and increases the production cost, so chemical treatment is one of the promising ways to decrease the OH groups on the surface of SiO₂ and it is practical. Hexamethyldisilazane (HMDS) and other organosilicon compounds (OSC), such as butyl dimethylsilyl (BDMS), dimethylsilicone fluid (DMSF), dimethyldichlorosilane (DMDCS), octadecyl dimethylsilyl (ODDMS) and trimethylsilyl (TMS) are commonly employed for the treatment of SiO₂. This treated SiO₂ has a wide variety of applications, including as a support for ZN catalysts. Although the properties of surface-modified solids can be predicted, observed changes often differ from expectations. Predictions of structural changes, for instance, are almost always related to primary particles [17-19], but structural changes of highly dispersed or porous solids are often hierarchal. In the case of fumed oxides, structures are dictated by aggregates of primary particles and agglomeration of aggregates.

This hierarchal structure is difficult to predict, as it is dependent upon a balance of forces, which are altered as a result of surface modification [20,21]. This often results in unexpected changes to the modified surface of SiO₂. Hertl and Hair [22] studied the treatment of silica with HMDS and used it as a support in ZN catalyst. They proposed that the reaction of HMDS occurs almost exclusively with isolated OH groups, leaving the H-bonded OH groups unoccupied. This property of HMDS has been applied successfully to study the bi-functional reactivity of TiCl4 toward H-bonded OH groups on silica in both vapor phase [22] and organic solution [23]. There were no changes of HMDS coverages on the HMDS-modified silica after the reaction with TiCl₄ at 175 °C [24]. Instead, the number of titanium atoms were half of that reacted without silylation, and the reaction led exclusively to doubly bonded titanium species. Consequently, the attainable trimethylsilyl surface coverage was not only determined by the steric hindrance, but also by the lower reactivity of HMDS toward H-bonded in OH groups. However, from the previous research, there is still little information about the effects of SiO₂ treated with different functional ethyl groups, such as dimethylsilicone fluid (DMSF), dimethyldichlorosilane (DMDCS) and hexamethyldisilazane (HMDS) on ZN catalyst properties and polymer properties although this information is of interest in both academia and industryl, especially in the surface study area. The XPS, SEM and EDX techniques were used in this investigation. Four types of CAB-O-SIL fumed silica were chosen for study based on the fact that they have well defined surface structures. They can be prepared by reproducible procedures and they are commonly used as catalyst supports. In this study, the influence of different silane compounds employed for the treatment of fumed silica in MgCl₂-SiO₂/TiCl₄/THF catalysts on ethylene polymerization was examined The properties obtained were also determined and are discussed in detail.

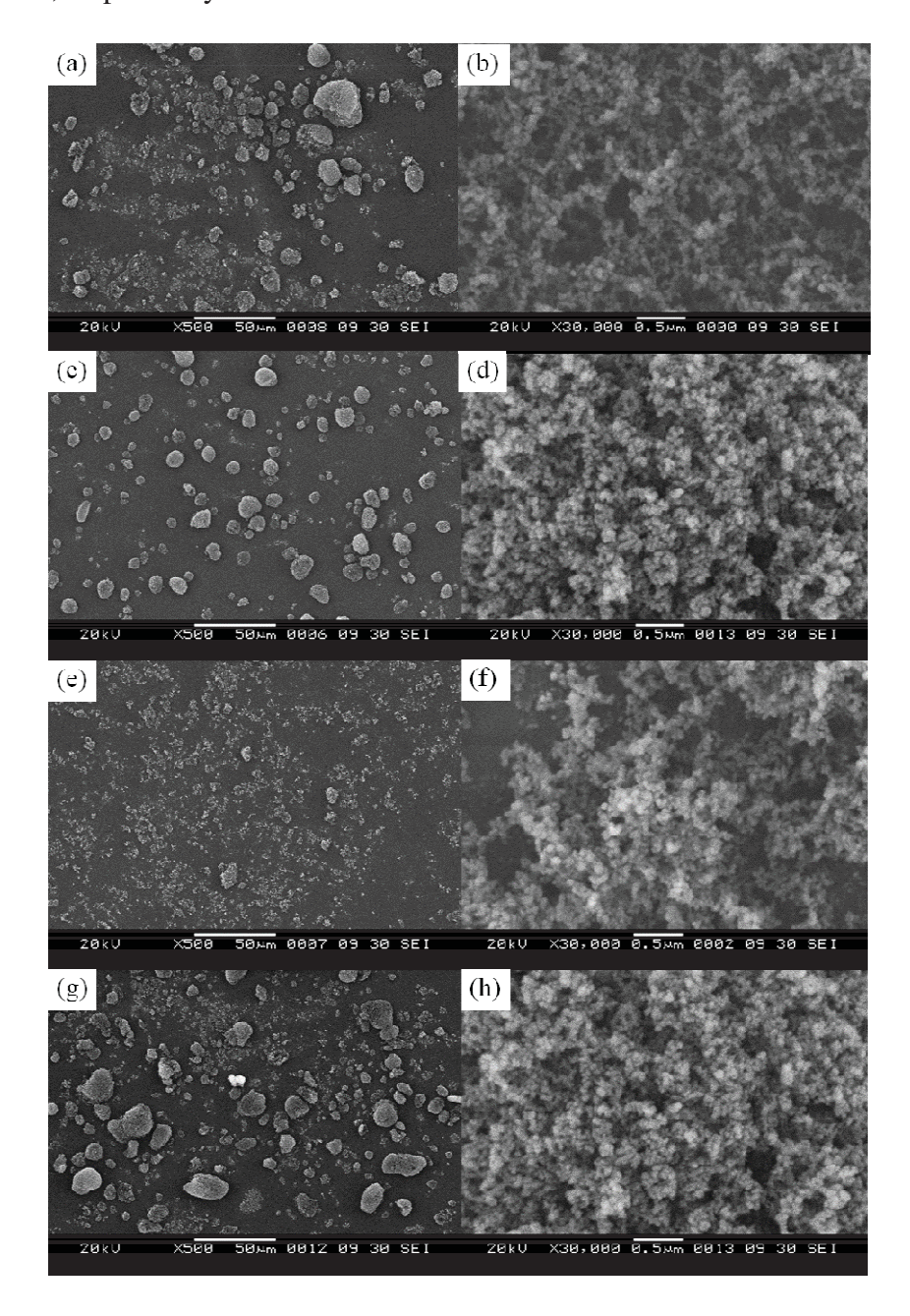
2. Results and Discussion

The structures of various treated fumed silicas used as supports in ZN catalysts are shown in Figure 1. There were four modified surface fumed silicas: (i) untreated SiO₂ (NTS); (ii) SiO₂ treated with dimethylsilicone fluid (TSDMSF); (iii) SiO₂ treated with dimethyldichlorosilane (TSDMDCS); and (iv) SiO₂ treated with hexamethyldisilazane (TSHMDS).

Figure 1. Different organo-silicon groups on the surface of variously treated fumed silicas.

The SEM images of all the samples are shown in Figure 2. It can be seen that the primary particles of fumed SiO₂ [Figures 2(b), (d), (f), and (h)] display no change in shape and size after treatment. A little agglomeration of particles occurred in TSDMSF and TSHMDS. The agglomeration of TSDMSF and TSHMDS particles results from the balance of force and type of chemical treatment. This result is supported by other research [20,21].

Figure 2. SEM images of different treated silicas; (a) NTS; (c) TSDMSF; (e) TSDMDCS; (g) TSHMDS; and (b), (d), (f), and (h) represent the primary particles of corresponding treated silicas, respectively.



After making the ZN catalysts with different treated SiO₂ supports, the bulk Ti content for all catalysts (Cat-NTS, Cat-TSDMSF, Cat-TSDMDCS, and Cat-TSHMDS) was analyzed by ICP. The results are shown in Table 1.

Sample	Treatment	Ti in bulk of catalysts (wt %) ^a	Activity b (kg PE/ mol-Ti/ h)
Cat-NTS	Untreated silica	2.27	1,570
Cat-TSDMSF	Dimethylsilicone Fluid	2.32	1,370
Cat-TSDMDCS	Dimethyldichlorosilane	2.34	6,370
Cat-TSHMDS	Hexamethyldisilazane	2.11	5,620

Table 1. Ti content in bulk and activity of different catalysts.

It was found that the Ti contents in all catalyst samples were similar and within the 2.11–2.34 wt % range. Then, all catalyst samples were tested for ethylene polymerization under the specified conditions. The activity results are also shown in Table 1. It can be observed that the silica treated with silane compounds tends to show increased catalytic activity due to the effect of the spacer groups introduced by silane treatment [25]. It was also surprising that although all catalysts had similar amount of Ti contents in bulk, they exhibited different catalytic activity. As seen, Cat-TSDMDCS, and Cat-TSHMDS exhibited the remarkably high activity (about four times higher than Cat-NTS). For elucidation, another parameter such as the Ti content at surface needed to be verified. One of the most powerful techniques used to determine the surface properties is X-ray photoelectron spectroscopy (XPS). The oxidation state related to the binding energy of Ti and other elements was evaluated. Ti exhibited its binding energy at ca. 459 eV, indicating the Ti 2p state in all catalyst samples.

The surface concentrations obtained from the XPS measurements for Ti and other elements are also shown in Table 2. It was found that the surface concentrations for Ti 2p in the Cat-TSDMDCS and Cat-TSHMDS samples were remarkably high. On the other hand, for both samples Ti was located on the outer surface of the catalysts. This is probably due to less steric hindrance of the Cat-TSDMDCS and Cat-TSHMDS samples compared to the Cat-TSDMSF sample, as seen in Figure 1. The large amounts of Ti located on the surface are the main reason for the very high activities obtained from the Cat-TSDMDCS and Cat-TSHMDS samples as seen in Table 1. Therefore, the high activity of the ZN catalysts can be attributed to the large amounts of Ti content on surface, not in the bulk of catalysts.

Table 2. Surface concentrations of Ti, Si and Mg in all catalysts obtained by XPS analysis.

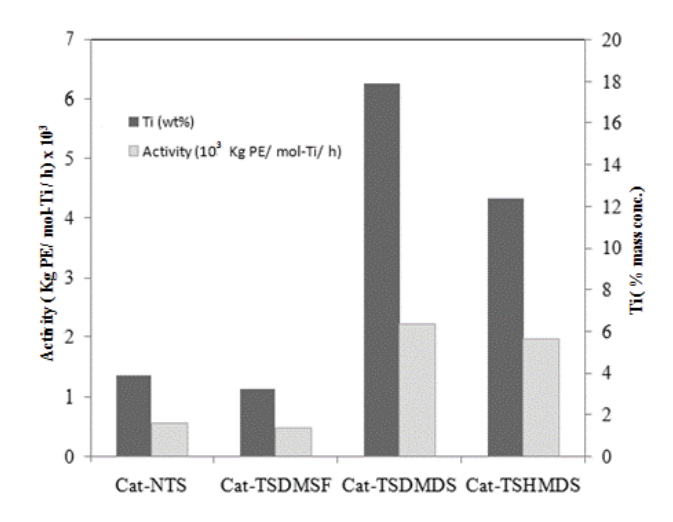
Peak	Cat-NTS	Cat-TSDMSF	Cat-TSDMDCS	Cat-TSHMDS
Ti2p	3.10	3.22	17.90	12.40
Si2p	64.05	88.55	37.81	56.13
Mg2s	32.85	8.23	44.30	31.47

In order to illustrate the relationship between the surface concentrations of Ti and the activities of catalysts, Figure 3 is constructed. It can be seen that the activities of catalysts are proportional to the surface concentrations of Ti present on the catalyst, as mentioned before.

Besides XPS measurements, the other powerful techniques used to determine the morphology and elemental distribution are SEM and EDX, respectively.

^a Obtained by ICP analysis; ^b Ethylene polymerization at 50 psi, 80 °C, Al/Ti = 100.

Figure 3. Relationship between the surface concentrations of Ti and the activities of catalysts.



The SEM and EDX mapping for all catalyst samples are shown in Figures 4 to 7 displaying the external surface of the catalysts and distribution of Mg, Si, and Ti on them. It should be mentioned that EDX only measures the concentrations in a layer less than 1 micrometer from the surface [26,27]. As a matter of fact, for whole catalyst particles, EDX measures the concentration on external surface of the particles. Figures 4–7 were all obtained with identical magnification. Considering the Ti distribution on the external surface of each catalyst represented by yellow patches (e), it can be clearly seen that the intensities of yellow patches (Ti at surface) in Figures 4 (Cat-NTS) and 5 (Cat-TSMDSF) are very low compared with those in Figures 6 (Cat-TSDMDCS) and 7 (Cat-TSDMDCS) corresponding to the XPS measurements as mentioned before. Therefore, both XPS and EDX mapping results can be used to confirm the rich Ti surface contents on the Cat-TSDMDCS and Cat-TSDMDCS samples leading to high catalytic activity. It is known that generally, TiCl₄ can bind to OH groups in the untreated silica. However, after treatment, it is mostly located on the MgCl₂ support as seen in the EDX mapping.

Figure 4. SEM micrograph and elemental distribution on Cat-NTS; (a) SEM image; (b) external surface; (c) Mg distribution; (d) Si distribution and (e) Ti distribution.

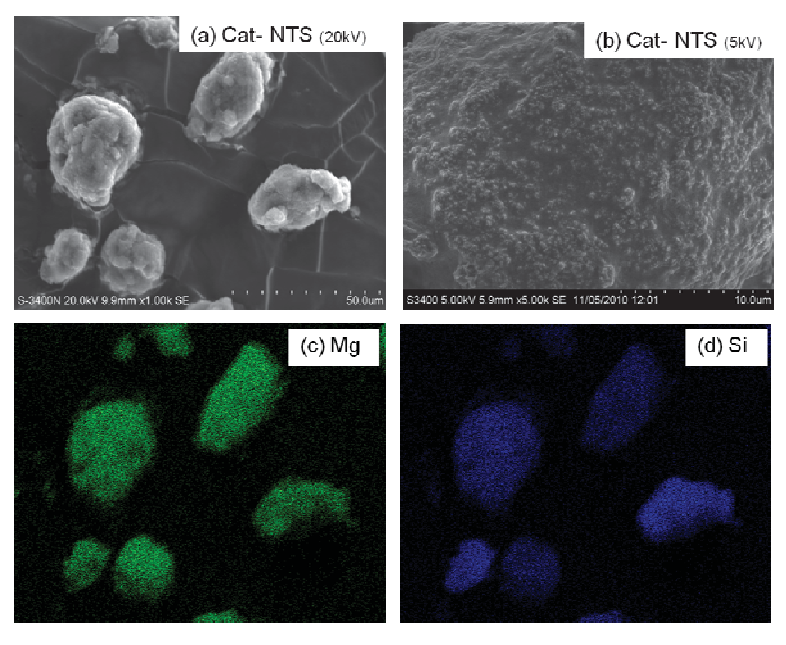


Figure 4. Cont.

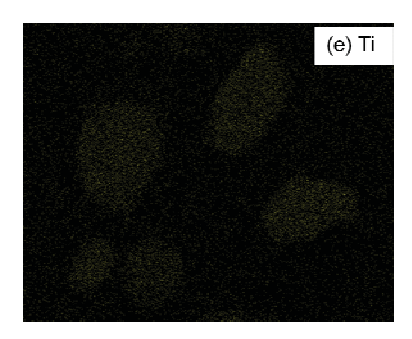


Figure 5. SEM micrograph and elemental distribution on Cat-TSDMSF; (a) SEM image; (b) external surface; (c) Mg distribution; (d) Si distribution and (e) Ti distribution.

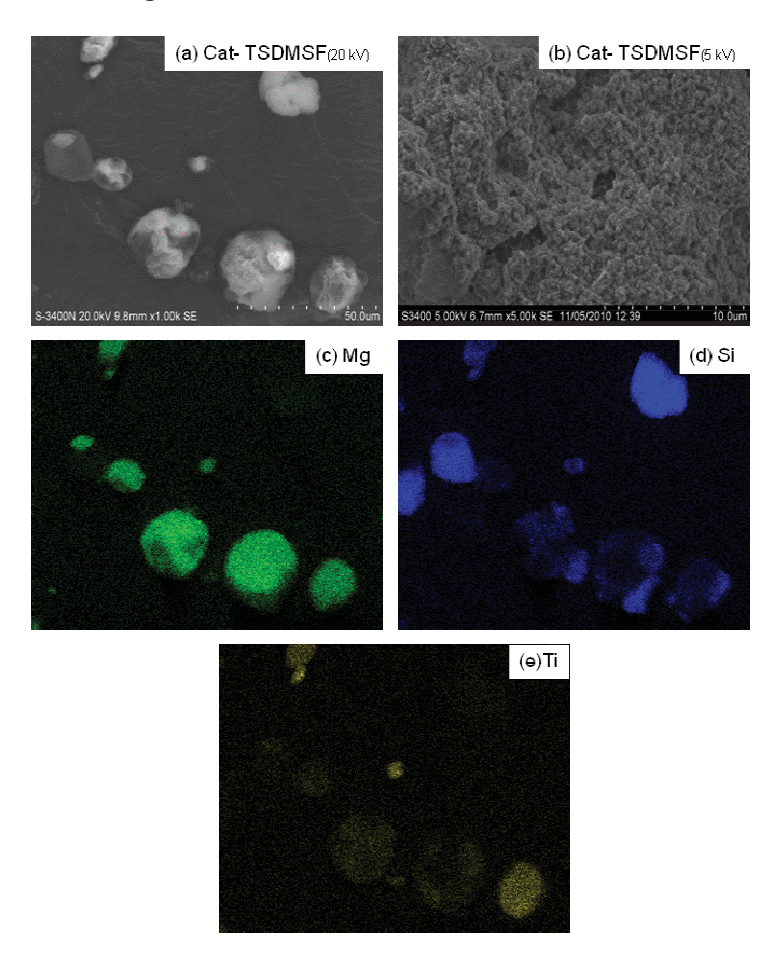


Figure 6. SEM micrograph and elemental distribution on Cat-TSDMDCS; (a) SEM image; (b) external surface; (c) Mg distribution; (d) Si distribution and (e) Ti distribution

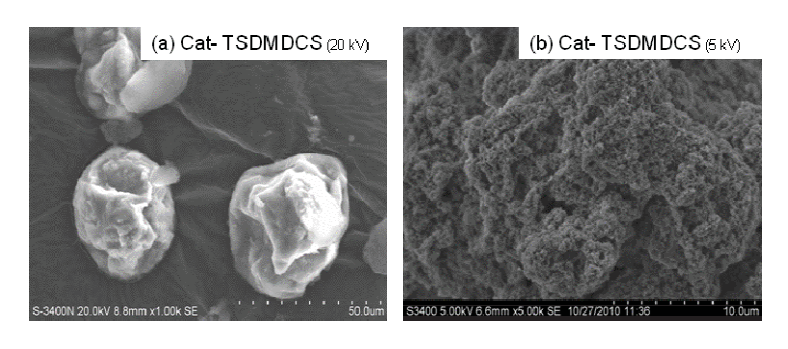


Figure 6. Cont.

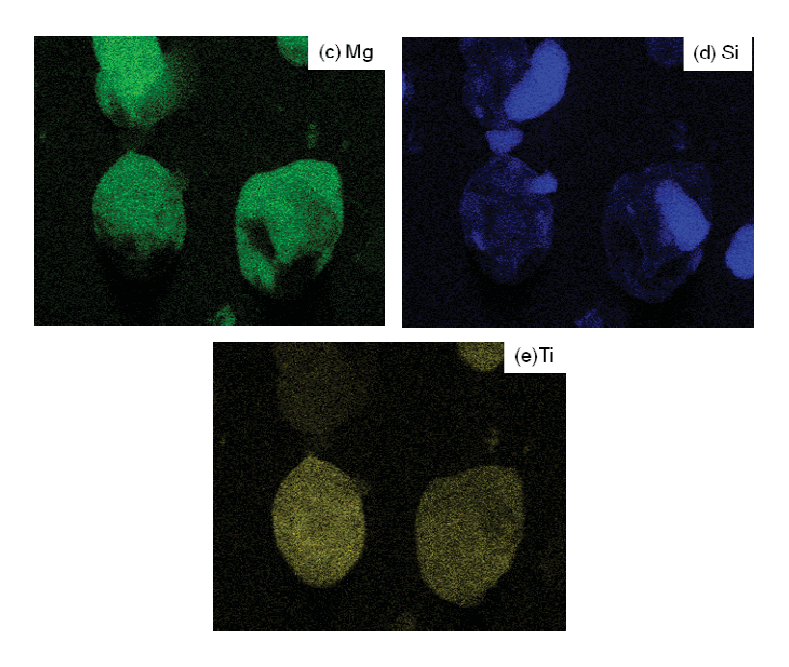
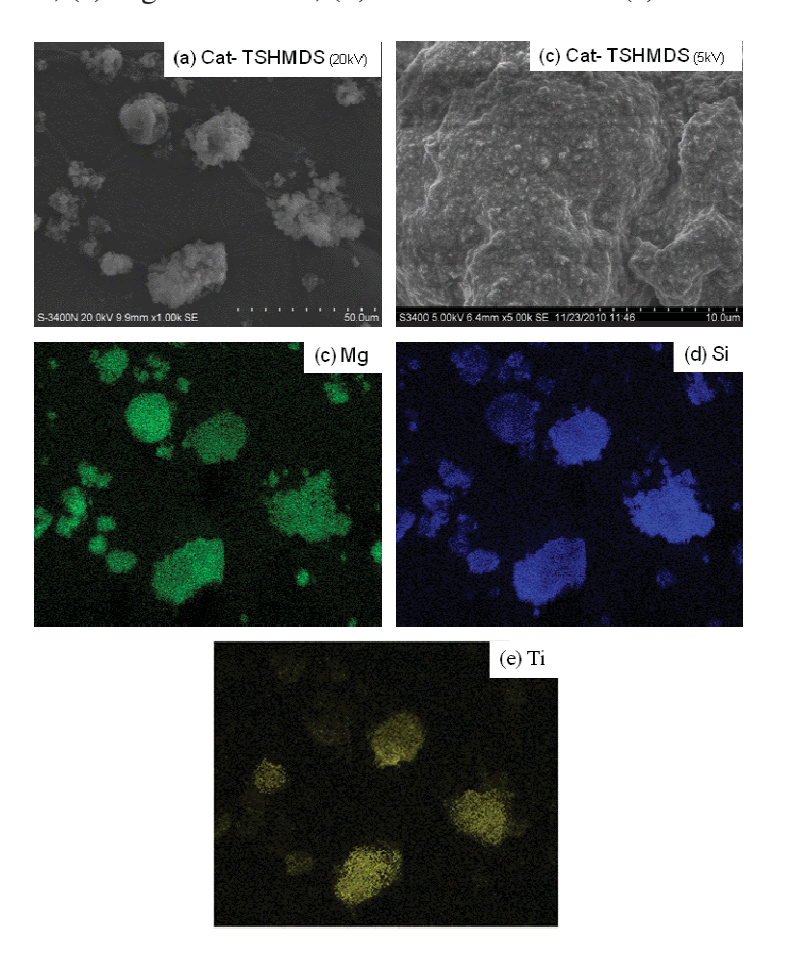


Figure 7. SEM micrograph and elemental distribution on Cat-TSHMDS; (a) SEM image; (b) external surface; (c) Mg distribution; (d) Si distribution and (e) Ti distribution.



The molecular weight (M_w) and molecular weight distribution (MWD) of polymers obtained from different catalysts as analyzed by GPC are listed in Table 3. It can be seen that Cat-NTS produced polymer having the highest M_w , M_z , and MWD compared to polymers obtained from other catalysts.

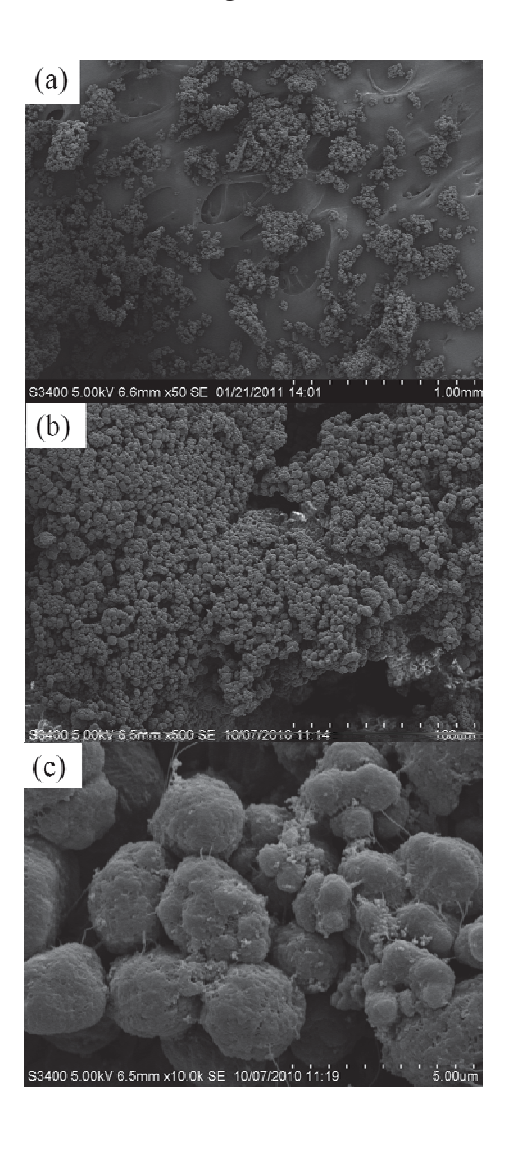
The broad MWD for Cat-NTS can be also attributed to the high molecular weight tail (M_z). It can be observed that all treated silica for ZN catalysts apparently resulted in narrower MWD, as also reported in our previous work [25]. It was suggested that the treatment of silica with silane can result in more uniform active centers leading to narrower MWD.

Table 3. Molecular weights and	their distribution of p	olymers obtained from	different catalysts.

Comple	$\mathbf{M}_{\mathbf{n}}$	$M_{\rm w}$	M_z	$M_{\rm v}$	MWD
Sample	(kg/mol)	(kg/mol)	(kg/mol)	(kg/mol)	(M_w/M_n)
Cat-NTS	40	1,028	4,574	739	25.7
Cat-TSDMSF	23	359	4,073	339	15.6
Cat-TSDMDCS	55	787	3,086	595	14.3
Cat-TSHMDS	24	437	4,064	405	18.2

A typical SEM micrograph of polymer obtained from all catalysts, which was similar, is shown in Figure 8. Hence, it indicates that the treated silica has no effect on the polymer morphologies.

Figure 7. A typical SEM micrograph of polyethylene samples of the treated silica ZN catalyst; (a) polyethylene at \times 50 magnification; (b) polyethylene at \times 500 magnification; and (b) surface of polyethylene at \times 10k magnification.



3. Experimental

3.1. Chemicals

Polymerization grade ethylene and triethylaluminum (TEA) donated by PTT Chemical Plc., were used without further purification. TiCl₄ (Aldrich) and MgCl₂ (anhydrous) were donated by Toho Catalyst Co., Ltd. Fumed silica [non-treated (NTS), surface area 149.35 m²/g] and silica treated with different organic compounds [dimethylsilicone fluid (TSDMSF, surface area 121.60 m²/g), with dimethyldichlorosilane (TSDMDCS, surface area 112.00 m²/g), and with hexamethyldisilazane (TSHMDS, surface area 130.95 m²/g)] were supplied by Cabot Corporation and average particle size of all silicas were 0.2–0.3 μm as reported by the supplier. All types of silica were heated under vacuum at 120 °C for 2 h. Hexane and tetrahydrofuran were dried over dehydrated CaCl₂ and distilled over sodium benzophenone under an argon atmosphere prior to use. Ultra high purify (UHP) argon (99.999%) was purchased from Thai Industrial Gas Co., Ltd. and was further purified by passing through 3 Å molecular sieves., BASF catalyst R3-11G, NaOH and phosphorus pentaoxide (P₂O₅) to remove traces of oxygen and moisture. All chemicals were manipulated under an inert atmosphere using a vacuum glove box and Schlenk techniques.

3.2. Catalyst Preparation

The catalyst was prepared in a 500 mL vessel equipped with temperature control, and a turbine agitator. First, anhydrous tetrahydrofuran (150 mL) was added into the vessel and heated up to a 50 °C. Then, magnesium metal (0.12 g) was added, followed by titanium tetrachloride (2 mL). The mixture was continuously agitated and the temperature was held at about 70 °C. After that, magnesium dichloride (4.5 g) was added, and the heating process was continued at 70 °C for another 3 h. Then different treated silicas (NTS, TSDMSF, TSDMDCS and TSHMDS, 4.5 g) were slowly added to the mixture, which was stirred for 1 h to thoroughly disperse the silica in the solution. The temperature of mixture was held at 70 °C throughout this period and an argon atmosphere was maintained for all time. This mixture was washed, and then dried under vacuum.

3.3. Polymerization Reaction

Ethylene polymerization was carried out in a 100 mL stainless steel autoclave reactor equipped with magnetic stirrer. The prescribed amount of hexane (30 mL), TEA and the SiO₂-MgCl₂-supported ZN catalysts, such as Cat-NTS, Cat-TSDMSF, Cat-TSDMDCS and Cat-HMDS (Al/Ti molar ratio = 100) were added into the reactor. The ethylene pressure and reactor temperature were kept constant during polymerization [pressure in reactor = 50 psi and polymerization temperature was held at 80 °C]. Due to the fixed ethylene consumption (at 0.018 moles), the polymerization time was defined as the time that all ethylene gas was totally consumed [the equivalent pressure drop of 42 kPa (6 psi) was observed]. The polymerization time was recorded to calculate the activity. The reaction was terminated by adding acidic methanol and polymer was stirred for 30 min. After filtration, the polymer obtained was washed with methanol and dried at room temperature.

3.4. Polymer and Catalyst Characterization

3.4.1. Scanning electron microscopy and energy dispersive X-ray spectroscopy (SEM/EDX)

The morphological observations of polymers were carried out with a JEOL JSM-6400 scanning electron microscope. Micrographs were taken at 5-kV and 20-kV acceleration voltage. Before scanning electron microscopy (SEM) observations, the fracture surfaces of blends were coated with a thin layer of gold to avoid electrical charging and increase contrast during observation. The EDX was performed using Link Isis series 300 program, to determine the elemental distribution in catalysts.

3.4.2. Inductively coupled plasma (ICP)

Titanium content was measured using inductively coupled plasma atomic emission spectroscopy equipment (ICP-OES optima 2100 DV from PerkinElmer). In order to digest the sample, the catalyst was dissolved in hydrofluoric acid. The mixtures were stirred over a night. After the catalyst was completely dissolved, the solution was diluted with ID water to a volume of 100 mL.

3.4.3. X-ray photoelectron spectroscopy (XPS)

The chemical states and surface concentration of the elements were measured by the XPS technique using an Amicus photoelectron spectrometer with Mg K_{α} X-ray source at current of 20 mA and 10 keV, resolution of 0.1 ev/step, and pass energy of 75 eV. The binding energy was calibrated by the C 1s peak at 285.0 eV. In this study, the sample was always treated under argon to prevent the sample from damage by moisture and oxygen in the atmosphere.

3.4.4. Gel permeation chromatography (GPC)

A high temperature GPC (Waters 150-C) equipped with a viscometric detector, differential optical refractometer and four Styragel HT type columns (HT3, HT4, HT5, and HT6) with 1×107 exclusion limit for polystyrene was used to determine the molecular weight (M_W) and molecular weight distributions (MWD) of the polymers produced. The analyses were performed at 140 °C using 1, 2, 4-trichlorobenzene as the solvent. The columns were calibrated with standard narrow MWD polystyrene.

4. Conclusions

In summary, the catalytic behaviors of MgCl₂-SiO₂/TiCl₄/THF catalysts with different treated silicas, such as Cat-NTS, Cat-TSDMSF, Cat-TSDMDCS, and Cat-TSHMDS were investigated. Although all catalysts exhibited the similar bulk Ti content, their activities were different. Therefore, the measurement of surface concentrations of Ti by means of XPS techniques was crucial. It was found that Cat-TSDMDCS and Cat-TSHMDS rendered high activities due to the large amounts of Ti at the surface of the catalyst. This could be also confirmed by the EDX mapping of Ti on the external surface. It can be concluded that for each catalyst the increased activity is proportional to the surface concentration of Ti. It is worth noting that the increased activity for the treated silica for Cat-TSDMDCS and Cat-TSHMDS catalysts can be attributed to both the effects of the silane spacer group and less steric hindrance. The treated silica in MgCl₂-SiO₂/TiCl₄/THF catalysts apparently resulted in

narrower MWD due to the increased uniformity of the active sites. However, there was no significant change in polymer morphology with the treated silicas as seen by SEM.

Acknowledgements

The authors thank the Thailand Research Fund (TRF), Office of the Higher Education Commission (CHE), Chulalongkorn University for Royal Golden Jubilee Fund under contract No. CU-CLUSTER-Advanced-4-54-53, Chula Unisearch (AM1088A), PTT Company and SCG chemical for the financial support of this project.

References and Notes

- 1. Moore, E.P., Jr. *Polypropylene Handbook*, 1st ed.; Hanser Publishers: New York, NY, USA, 1996; pp. 86-87.
- 2. Ray, W.H. *Transition Metal Catalyzed Polymerizations*, 1st ed.; Quirk, R.P., Ed.; Cambridge University Press: New York, NY, USA, 1988; pp. 563-567.
- 3. Simonazzi, T.; Cecchin, G.; Mazzaulo, S. An outlook on progress in polypropylene-based polymer technology. *Prog. Polym. Sci.* **1991**, *16*, 303-329.
- 4. Senso, N.; Khaubunsongserm, S.; Jongsomjit, B.; Praserthdam, P. The influence of mixed activators on ethylene polymerization and ethylene/1-hexene copolymerization with silica-supported ziegler-natta catalyst. *Molecules* **2010**, *15*, 9323-9339.
- 5. Hock, C.W. How titanium chloride catalysts control the texture of as-polymerized polypropylene. *J. Polym. Sci. A-Polym. Chem.* **1966**, *4*, 3055-3064.
- 6. Kakugo, M.; Sadatoshi, H.; Sakai, J.; Yokoyama, M. Growth of polypropylene particles in heterogeneous Ziegler-Natta polymerization. *Macromolecules* **1989**, *22*, 3172-3177.
- 7. Kashiwa; N. The discovery and progress of MgCl₂-supported TiCl₄ catalysts. *J. Polym. Sci. A-Polym. Chem.* **2004**, *42*, 1-8.
- 8. Nejad, M.H.; Ferrari, P.; Pennini, G.; Cecchin, G. Ethylene homo- and copolymerization over MgCl₂-TiCl₄ catalysts: Polymerization kinetics and polymer particle morphology. *J. Appl. Polym. Sci.* **2008**, *108*, 3388-3402.
- 9. Lu, H.; Xiae, S. Highly isospecific silica/magnesium chloride bisupported catalyst for propene polymerization. *Makromol. Chem.* **1993**, *194*, 2095-2102.
- 10. Kim, I.I.; Woo, S.I. Morphological study of HDPE prepared with the highly active silica-supported titanium tetrachloride/magnesium chloride catalyst. *Polym. J.* **1989**, *21*, 697-707.
- 11. Pasquet, V.; Spitz, R. Preparation of bisupported catalysts for ethylene polymerization. *Makromol. Chem.* **1990**, *191*, 3084-3096.
- 12. Robert, J.J.; Belle Mead, N.J.; Elton, D.F.; Victoria, T. George, L.G.; Belle Mead, N.J. Process for producing ethylene polymers having reduced hexane extractable content. *US Patent No.* 5,290,745, 1994.
- 13. Isaac, J.L.; Frederick, J.K.; Belle Mead, N.J. Processes for preparing polyethylene catalysts by heating catalyst precursors. *US Patent No. 4,719,193*, 1988.
- 14. Lakomaa, E-L.; Haukka, S.; Suntola, T. Atomic layer growth of titania on silica. *Appl. Surf. Sci.* **1992**, 742, 60-61.

15. Haukka, S.; Lakomaa, E.-L.; Suntola, T. Analytical and chemical techniques in the study of surface species in atomic layer epitaxy. *Thin Solid Films* **1993**, 280, 225.

- 16. Haukka, S.; Lakomaa, E-L.; Jylha, O.; Vilhunen, J.; Hornytzkyj, S. Dispersion and distribution of titanium species bound to silica from TiCl₄. *Langmuir* **1993**, *9*, 3497-3506.
- 17. Legrand, A.P. *The Surface Properties of Silicas*, 1st ed.; Wiley: New York, NY, USA, 1998; pp. 415-464.
- 18. Adamson, A.W.; Gast, A.P. *Physical Chemistry of Surface*, 6th ed.; Wiley: New York, NY, USA, 1997, pp. 365-369.
- 19. Gregg, S.J.; Sing, K. S.W. *Adsorption Surface Area and Porosity*, 2nd ed.; Academic Press: London, UK, 1982.
- 20. Barthel, H.; Rosch, L.; Weis, J. *Organosilicon Chemistry II. From Molecules to Materials*; Auner, N., Weis, J., Eds.; VCH: Weinheim, Germany, 1996; pp. 761-778.
- 21. Degussa, A.G. Basic Characteristics of Aerosil, Tech. Bull. Pigment. 1997, 997, 11-12.
- 22. Hertl, W.; Hair, M.L. Reaction of hexamethyldisilazane with silica, *J. Phys. Chem.* **1971**, *75*, 2181-2185.
- 23. Haukka, S.; Lakomaa, E.L. An IR and NMR study of the chemisorption of titanium tetrachloride on silica. *J. Phys. Chem.* **1993**, *97*, 5085-5094.
- 24. Blitz, J.P. Reactions of titanium tetrachloride with modified silica gel surfaces studied by diffuse reflectance FTIR spectroscopy. *Colloids Surf.* **1990**, *63*, 11-19.
- 25. Jongsomjit, B.; Kaewkrajang, P.; Wanke, S.E.; Praserthdam, P. A comparative study of ethylene/α-olefin copolymerization with silane-modified silica-supported MAO using zirconocene catalysts. *Catal. Lett.* **2004**, *94*, 205-208.
- 26. Tangjituabun, K.; Jongsomjit, B.; Praserthdam, P. Catalytic behaviors of SiO₂-supported various aluminoxanes as coactivator in MgCl₂/DEP/TiCl₄-TEA catalysts for propylene polymerization. *Catal. Commun.* **2009**, *10*, 1319-1323.
- 27. Jongsomjit, B.; Ngamposri, S.; Praserthdam, P. Catalytic activity during copolymerization of ethylene and 1-hexene via mixed TiO₂/SiO₂-supported MAO with *rac*-Et[Ind]₂ZrCl₂ metallocene catalyst, *Molecules* **2005**, *10*, 672-678.

Sample Availability: Samples of the polyethylene compounds are available from the authors.

© 2011 by the authors; licensee MDPI, Basel, Switzerland. This article is an open access article distributed under the terms and conditions of the Creative Commons Attribution license (http://creativecommons.org/licenses/by/3.0/).



Article

The Influence of Comonomer on Ethylene/ α -Olefin Copolymers Prepared Using [Bis(N-(3-tert butylsalicylidene)anilinato)] Titanium (IV) Dichloride Complex

Patcharaporn Kaivalchatchawal ¹, Pattiya Suttipitakwong ², Sutheerawat Samingprai ², Piyasan Praserthdam ¹ and Bunjerd Jongsomjit ¹,*

- ¹ Center of Excellence on Catalysis and Catalytic Reaction Engineering, Department of Chemical Engineering, Faculty of Engineering, Chulalongkorn University, Bangkok 10330, Thailand
- Innovation & Technology, PTT Chemical Public Company Limited, Tambon Map Ta Phut, Amphoe Mueang Rayong, Rayong 21150, Thailand
- * Author to whom correspondence should be addressed; E-Mail: bunjerd.j@chula.ac.th; Tel.: +66 2 2186869; Fax: +66 2 2186877.

Received: 25 November 2010; in revised form: 11 February 2011 / Accepted: 14 February 2011 / Published: 15 February 2011

Abstract: We describe the synthesis of [bis(*N*-(3-*tert*-butylsalicylidene)anilinato)] titanium (IV) dichloride (Ti-FI complex) and examine the effects of comonomer (feed concentration and type) on its catalytic performance and properties of the resulting polymers. Ethylene/1hexene and ethylene/1-octene copolymers were prepared through copolymerization using Ti-FI catalyst, activated by MAO cocatalyst at 323 K and 50 psi ethylene pressure at various initial comonomer concentrations. The obtained copolymers were characterized by DSC, GPC and ¹³C-NMR. The results indicate that Ti-FI complex performs as a high potential catalyst, as evidenced by high activity and high molecular weight and uniform molecular weight distribution of its products. Nevertheless, the bulky structure of FI catalyst seems to hinder the insertion of α -olefin comonomer, contributing to the pretty low comonomer incorporation into the polymer chain. The catalytic activity was enhanced with the comonomer feed concentration, but the molecular weight and melting temperature decreased. By comparison both sets of catalytic systems, namely ethylene/1-hexene and ethylene/1-octene copolymerization, the first one afforded better activity by reason of easier insertion of short chain comonomer. Although 1-hexene copolymers also exhibited higher molecular weight than 1-octene, no significant difference in both melting temperature and crystallinity can be noticed between these comonomers.

Keywords: post metallocene catalyst; homogeneous catalyst; FI catalyst; copolymerization

1. Introduction

Nowadays, polymers and plastics, especially linear low-density polyethylene (LLDPE), are playing the important role on the material industry due to their low density, high strength and cost-effectiveness. It is generally known that a common means of generating LLDPE is the copolymerization of ethylene and α-olefins such as 1-butene, 1-hexene, 1-octene and 1-decene [1]. The catalytic systems used have an effect on the structure and properties of the synthesized copolymers, therefore, much effort has been directed towards the development of highly active olefin polymerization catalysts. Normally, Ziegler-Natta catalysts produce copolymers with a wide molecular weight distribution (MWD) and chemical composition distribution (CCD) as a result of their multiple active sites [2,3]. Conversely, homogeneous metallocenes and post metallocenes are single sites, leading to very uniform polymers with narrow MWD and CCD. Particularly, the FI complexes (Fujita group invented catalysts) bearing phenoxyimine ligands that have been fully developed by Fujita and coworkers may be regarded in the forefront of these developments and have gained much attention in both academia and industry as potential olefin polymerization catalysts. This is probably because of high activities comparable to or exceeding those of the group 4 metallocene catalysts and the uniform properties of the polymers produced [4].

Concerning linear low-density polyethylene, it is normally accepted that comonomers (both type and concentration) play an important role in the properties of the resulting copolymers in terms of melting behavior, density, crystallinity and mechanical properties [5,6]. For instance, the introduction of short-chain branching derived from the comonomer decreases the crystallinity and melting temperature of the copolymer. In other words, the comonomer contents, which in turn are sensitive to a large number of factors, namely the catalyst and cocatalyst structure and the initial comonomer concentration in the polymerization system, govern the copolymer melting behavior [7]. Furthermore, a number of recent studies have been revealed that the film performance, such as impact and tensile strength, increases with the comonomer length [6]. The size and concentration of comonomer units also affects the catalytic activities in homogeneous metallocene systems. Hence, in this present study, in order to investigate the influence of the initial comonomer concentration and the type of comonomer (1-hexene or 1-octene) on the catalytic performance of the catalyst and the copolymer properties, the synthesis of ethylene/ α -olefins with Ti-FI catalysts have been performed using ethylene/comonomer in different proportions.

2. Results and Discussion

2.1. Synthesis and characterization of titanium complex (Ti-FI catalyst)

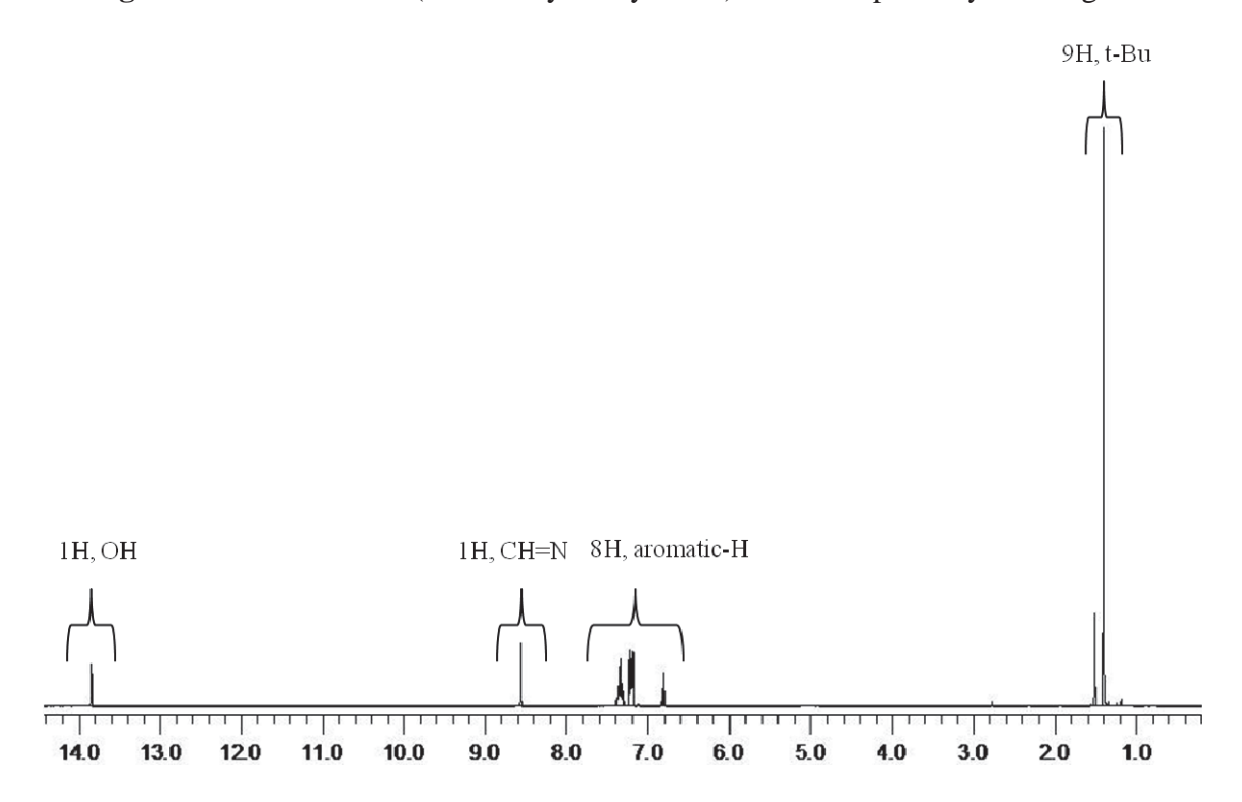
The synthetic route for titanium complex is depicted in **Scheme 1**. 3-t-Butylsalicylaldehyde reacted with a primary amine via Schiff base condensation in ethanol to yield a *N*-(3-tertbutylsalycilidene)

aniline or phenoxyimine ligand. The titanium complex was obtained as reddish brown crystals by reaction of two equivalents of the lithium salt of the phenoxyimine ligand with TiCl₄.

Scheme 1. Synthetic route to the titanium complex.

The 1 H-NMR spectra of the phenoxyimine chelate ligand N-(3-tertbutylsalicylidene) aniline and Ti-FI complexes having phenoxyimine ligands are shown in **Figures 1** and **2**, respectively.

Figure 1. ¹H-NMR of *N*-(3-*tert*-butylsalicylidene) aniline or phenoxyimine ligand.



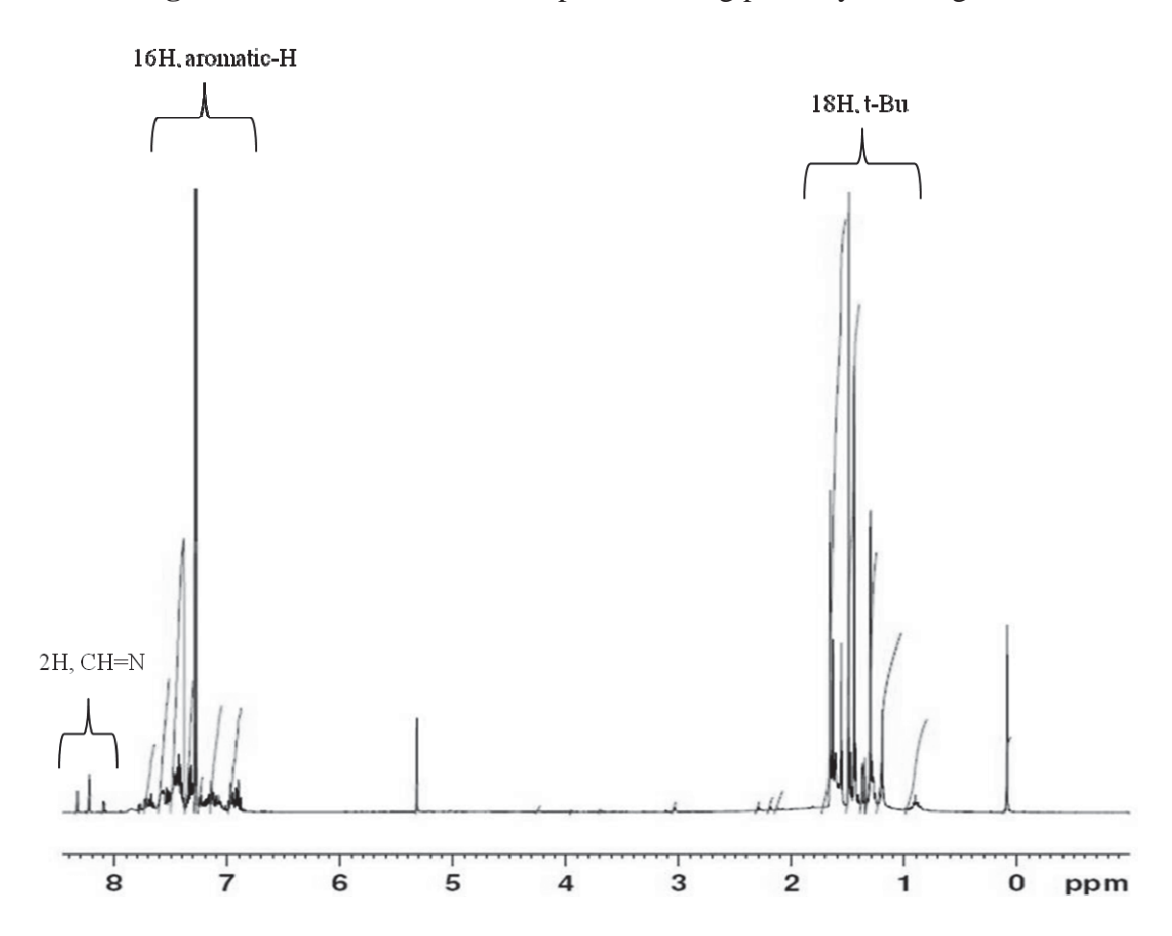


Figure 2. ¹H-NMR of Ti-FI complexes having phenoxyimine ligands.

In addition, using to the synthesis method mentioned, the Ti-FI ligand and complex can be crystallized into crystals and further characterized by optical microscopy to examine their morphologies, as shown in **Figure 3**. It can be seen from this figure that both of them exhibited the needle-like crystals of yellow and reddish brown color, respectively.

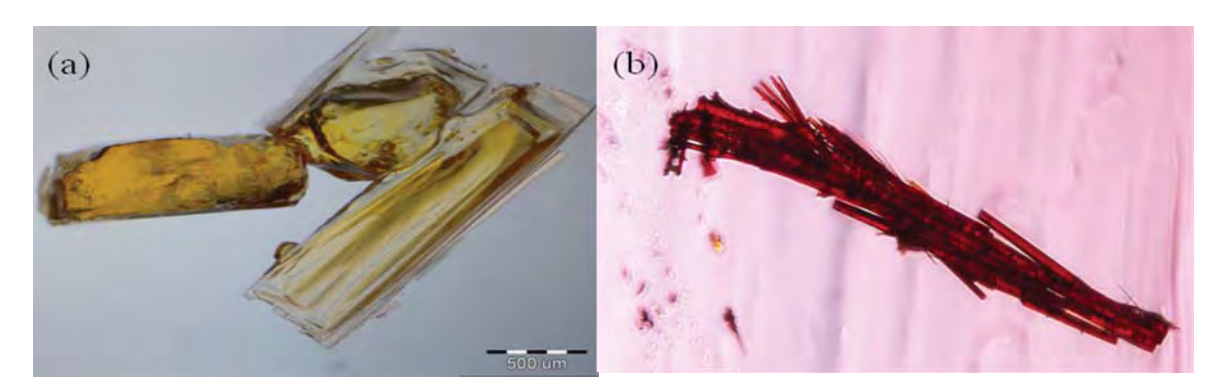


Figure 3. Optical microscope photographs of (a) Ti-FI ligand (b) Ti-FI complex.

2.2. Catalytic properties of ethylene and ethylene/α-olefins copolymerization

The laboratory scale Ti-FI catalyst/MAO catalyzed ethylene/ α -olefin copolymerization reaction was carried out at 323 K with constant ethylene pressure (50 psi). After filtration and drying, polymer was weighed and analyzed by 13 C-NMR, GPC and DSC. The results are summarized in **Table 1**.

Entry ^a	Ethylene ^b	Comonomer	Time	Weight	Activity ^c
Entry	[mol/L]	[mol/L]	[s]	[g]	[kg polymer/mol Ti·h]
E-1	0.6	0	146.4	0.2881	2833
E-2	0.6	0	133.2	0.3230	3491
H-1	0.6	0.3	91.2	0.3496	5520
H-2	0.6	0.45	91.8	0.3647	5720
H-3	0.6	0.6	83.4	0.3766	6502
H-4	0	0.6	n.a. ^d	n.a. ^d	n.a. ^d
O-1	0.6	0.3	180	0.4405	3524
O-2	0.6	0.45	135.6	0.3748	3980
O-3	0.6	0.6	142.2	0.4470	4526
O-4	0	0.6	n.a. ^d	n.a. ^d	n.a. ^d

Table 1. Summary of ethylene/ α -olefins copolymerization catalytic activities.

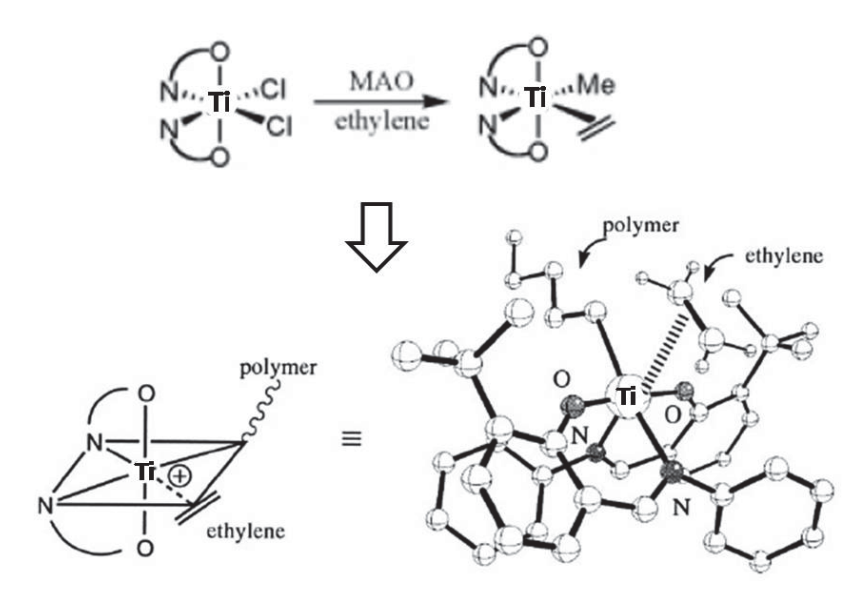
^a run E1 used commercial *rac*-Et[Ind]₂ZrCl₂ as catalyst; runs E2, H1-H4 and O1-O4 used Ti-FI as catalyst; comonomer of runs H1-H4 is 1-hexene; comonomer of runs O1-O4 is 1-octene; ^b Ethylene addition into the system; ^c Polymerization condition: [Ti] = 2.5 μmol, MAO as cocatalyst, [Al]/[Ti] = 250, liquid volume (toluene) = 30 mL, temperature = 323 K, ethylene pressure = 349 kPa (50 psi); ^d n.a. means not applicable (no observed polymer)

Concerning **Table 1**, the combination of Ti-FI catalyst with MAO in toluene solvent exhibited high activity (3,491 kg PE/mol Ti·h). To compare the catalytic activity of this catalyst with a metallocene catalyst, the commercial *rac*-Et[Ind]₂ZrCl₂ catalyst was used to produce polyethylene under the same polymerization conditions. It was found that the activity value exceeded the activity obtained with the commercial cyclopentadienyl ligand metallocene catalyst, indicating that phenoxyimine chelate ligands have good potential as olefin polymerization catalysts. This may be attributed to the fact that these ligands posses moderate electron-donating properties species as well as a pair of available *cis*-located sites for polymerization [2,8]. In order to obtain more detailed insights into the catalytic activity during the polymerization, the possible active species of the titanium complex as determined by Fujita *et al.* from DFT calculations and X-ray crystallographic analysis [4,8] and the ethylene polymerization mechanism can be represented in the **Figure 4**. The mechanism begins with the activation of the catalyst with an appropriate cocatalyst – MAO in this case – to form an alkyl cationic complex, having the two available *cis*-located sites needed for polymerization. As a result, two chlorine bound sites were turned into polymerization sites, in other words, a growing polymer chain site and an ethylene coordination site, leading to the propagation of growing polymer chain.

Moreover, it can be observed from **Table 1** that no polymer was obtained from the system that was composed of only 1-hexene or 1-octene as monomer (entry H4 or O4). This result corresponded to the finding of Chaichana *et al.* [5] who examined the catalytic behavior of constrained geometry catalyst (CGC). They reported that the system presented no catalytic activity for in 1-hexene polymerization. Conversely, entry E2, which performs the ethylene homopolymerization is capable of attaining high polymer yields, suggesting that TiC₃₄H₃₆Cl₂N₂O₂ (Ti-FI) acts as a high potential catalyst for ethylene polymerization, despite its poor performance for 1-hexene or 1-octene homopolymerization. This may be ascribed to the fact that ethylene is the most active monomer; thus, it can insert into the active site and then form polymer chains by itself, whereas the other monomers, namely 1-hexene and 1-octene,

are too large and less active; accordingly, the initiation polymerization step cannot occur because of a lack of space for insertion of a bulkier monomer. On the other hand, when the system contains both ethylene and a bulky comonomer like 1-hexene or 1-octene, it turns out that the initiation step can be accomplished by the displacement of ethylene. This step provides higher space for longer 1-alkene and after that the propagation can proceed into the growing chain of copolymer.

Figure 4. Structure and possible active species of titanium complex [8].



The comparison of catalytic activities of two sets of catalytic system, containing using 1-hexene (H1-H4) and 1-octene (O1-O4) as comonomers by using Ti-FI as catalyst can be obtained from **Table 1**. The activities of both copolymerization systems were higher than in ethylene homopolymerization, a feature generally known as the "comonomer effect", which is a quite general effect of many comonomer pairs. Moreover, the catalytic activity increases with the increase of comonomer feed concentration. Several possible causes have been proposed to explain this behavior; however, the simplest and most supported is the improvement of monomer diffusion to the catalyst center on account of the crystallinity reduction in polymer structures when introducing a small amount of comonomer [7]. Another explanation for this phenomenon is that the inserted comonomer may resulted in the ion separation between the cationic active species and anionic cocatalyst providing more space for polymerization, thus enhancing the activity.

With regard to **Table 1**, the catalytic activity shows a general trend of 1-hexene > 1-octene under the same conditions with a fixed [ethylene]/[α -olefin] monomer feed ratio. Thereby, it is fair to say that the bigger size of 1-octene comonomer has a negative effect on ethylene/ α -olefin copolymerization, which is probably due to more steric hindrance at the catalytic center.

2.3. Properties of polymers

The properties of the obtained homo and copolymers are gathered in **Table 2**. Comparing the PE obtained with both catalysts, it can be observed that the molecular weight of the homopolymer obtained with Ti-FI catalyst was considerably higher than that resulting from use of the metallocene catalyst. Besides, the commercial catalyst furnished quite high polydispersity when compared with the

corresponding value with the FI catalyst. The uniform molecular weight distribution results were also seen in all the copolymers having 1-hexene and 1-octene units synthesized with Ti-FI catalyst, implying the single site polymerization mechanism of this catalyst. Another interesting point dealing with the molecular weight result is that the average molecular weight of the copolymer decreased with the increase of comonomer feed concentration. This might suggest that 1-hexene and 1-octene incorporation promotes chain termination reactions, consequently contributing to formation of lower molecular weight copolymers [9]. Furthermore, it can be seen from **Table 2** that the copolymers derived from using 1-octene as comonomer had a lower molecular weight than those obtained from 1-hexene.

Regarding the thermal properties, 1-hexene and 1-octene incorporation resulted in a noticeable reduction of the melting temperature and crystallinity of the copolymers, when compared to the homopolymer (entry E-2), but the type of comonomer does not seem to influence both properties. This was in accord with the Flory's theory [1] that described the relationship between the melting behavior and comonomer of copolymerization system. However, this decrease was less pronounced in the case of higher comonomer feed concentration, suggesting that the bulky structure of the Ti-FI catalyst possibly reduces and limits the accessibility of the comonomer incorporation onto the active sites, especially for high comonomer concentrations, thus having a small effect on the properties.

Entry ^a	Feed ratio [E]/[α-olefin] [mol/mol]	Melting point ^c $(T_m)[^{\circ}C]$	Crystallinity ^d (X _c)[%]	Molecular weight ^e (M _w)[kg/mol]	PDI ^e (M _w /M _n)
E-1	1/0	134.5	38.78	432	2.5
E-2	1/0	134.3	64.01	920	1.60
H-1	1/0.5	128.7	41.94	729	1.66
H-2	1/0.75	126.3	44.93	768	1.69
H-3	1/1	127.0	43.21	675	1.67
H-4	0/1	n.a. ^b	n.a. ^b	n.a. ^b	n.a. ^b
O-1	1/0.5	128.0	42.21	668	1.64
O-2	1/0.75	127.2	48.13	641	1.63
O-3	1/1	128.3	50.37	633	1.65
O-4	0/1	n.a. ^b	n.a. ^b	n.a. ^b	n.a. ^b

Table 2. Properties of resulting polymers.

^a run E1 used commercial *rac*-Et[Ind]₂ZrCl₂ as catalyst; runs E2, H1-H4 and O1-O4 used Ti-FI as catalyst; comonomer of runs H1-H4 is 1-hexene; comonomer of runs O1-O4 is 1-octene; ^b n.a. means no observed polymer; ^c determined by DSC; ^d estimated by dividing the heat of fusion of polymer (measured by DSC) by 294 J/g of the theoretical value for 100% crystalline PE homopolymer; ^e determined by GPC

2.4. Microstructure of the polymers

The microstructure of copolymers, including the incorporation of comonomer and the comonomer triad distribution, can be determined from 13 C-NMR spectroscopy. Nonetheless, in this work there was no peak which indicated the comonomer branch in the backbone for all copolymers, presumably due to the presence of only a small amount of α -olefin insertion, contrary to the α -olefin incorporation ability

of commercial rac-Et[Ind]₂ZrCl₂. Jongsomjit et~al. found that this commercial complex possessed a high insertion ability for 1-hexene and 1-octene, at around 40 and 29%, respectively [10-14]. In addition, this problem might occur because of the ultra high molecular weight of the resulting copolymers and the too low sample preparation temperature. Thereby, other techniques, such as CRYSTAF, infrared spectroscopy and pyrolysis gas chromatography mass spectrometry, should be further applied to investigate the copolymer microstructure in this case.

2.5. Morphology of polymers

The SEM micrographs of polymers are shown in **Figure 5**, indicating the typical morphologies of copolymers obtained from this catalytic system. There was no significant change in copolymer morphologies with the different comonomer lengths and initial comonomer concentrations employed. On the contrary, the morphology of polymers generated from Ti-FI catalyst seems to more rod-like comparing to those obtained from metallocene catalyst, suggesting that the catalyst microstructure might have an effect on the polymer morphology.

(e) (f)

Figure 5. SEM photographs of polymers (a) E-1 (b) E-2 (c) H-1 (d) H-2 (e) H-3 (f) O-1.

3. Experimental

3.1. Materials

All operations were handled under an argon atmosphere using glove box and/or standard Schlenk techniques. Ethylene (polymerization grade) was obtained from the National Petrochemical Co. Ltd., Thailand. 3-*tert*-Butylsalicylaldehyde, aniline and TiCl₄ (99+%) were purchased from Aldrich Chemical Company, Inc., and used without further purification. Hexane, diethyl ether and dichloromethane (anhydrous grade) were purchased from Aldrich Chemical Company.

Methylaluminoxane, (MAO, 10% in toluene) was donated BY PTT Research and Technology Institute (Thailand). Toluene was obtained by the Exxon Chemical, Thailand Co., Ltd. It was dried over dehydrated CaCl₂ and distilled over sodium/benzophenone. Ultra-high purify (UHP) argon (99.999%) was purchased from Thai Industrial Gas Co., Ltd.. 1-Hexene and 1-octene (≥97%) was purchased from Aldrich Chemical Company, Thailand and further purified by distilling over CaH₂ for 6 h. Commercial metallocene catalyst, rac-Et[Ind]₂ZrCl₂, was purchased from Aldrich Chemical Company (Thailand). ¹H-NMR was used to investigate the structure of the ligand and catalyst complex. The spectra were recorded at ambient probe temperature (298K) using a Bruker AVANCE II 400 instrument operating at 400 MHz with an acquisition time of 1.5 s and a delay time of 4 s. Ligands and titanium complex solution were prepared using tetramethylsilane as solvent and deuterated chloroform for an internal lock. An Olympus BX51 instrument was employed to investigate the morphology of the ligand and the catalyst crystals by optical microscopy.

3.2. Titanium-FI complex synthesis

Bis[*N*-(3-*tert*-butylsalicylidene) anilinato]titanium (IV) dichloride (Ti-FI complex) was synthesized according to the procedure described by Saito *et al.* [15]. The synthesis of Ti-FI complex can be divided into two main steps, as follows:

3.2.1. Synthesis of N-(3-tert-butylsalicylidene) aniline

Firstly, a stirred mixture of 3-*tert*-butylsalicylaldehyde (2.34 g, 13.4 mmol) and 3Å molecular sieves (2 g) in ethanol (20 mL), a solution of aniline (1.41 g, 15.1 mmol) in ethanol (10 mL) was added dropwise over a 1-min period at room temperature. Then, the mixture was stirred for 16 h and filtered. The 3Å molecular sieves were washed with ethyl acetate (20 mL). The combined organic filtrates were concentrated *in vacuo* to afford the crude imine compound. Finally, purification by column chromatography on silica gel using hexane/ethyl acetate (10:1) as eluent gave *N*-(3-*tert*-butylsalicylidene) aniline as orange crystals. 1 H-NMR (CDCl₃) δ = 1.45 (s, 9H, t-Bu), 6.81–7.35 (m, 8H, aromatic-H), 8.56 (s, 1H, CH=N), 13.84 (s, 1H, OH).

3.2.2. Synthesis of Bis[N-(3-tert-butylsalicylidene)anilinato] titanium (IV) dichloride

To a stirring solution of N-(3-*tert*-butylsalicylidene) aniline (1.552 g, 6.13 mmol) in dried diethyl ether (50 mL) at 195 K, a 1.61 M hexane solution of *n*-butyllithium (3.80 mL, 6.08 mmol) was added dropwise over a 5-min period. The solution was allowed to warm to room temperature and stirred for 4 h. The resulting solution was added dropwise over a 30 min period to a stirred solution of TiCl₄ (0.58 g, 3.06 mmol) in dried diethyl ether (90 mL) at 195 K. The mixture was allowed to warm to room temperature and stirred over night. After removal of the solvent, the product was extracted with CH₂Cl₂. Filtration following removal of the volatile gave a reddish brown solid. The solid was recrystallized from a dried dichloromethane/dried pentane (1:1) solution at room temperature to give bis[*N*-(3-*tert*-butylsalicylidene) anilinato] titanium (IV) dichloride. ¹H-NMR (CDCl₃): $\delta = 1.26-1.66$ (m, 18H, t-Bu), 6.90–7.67 (m, 16H, aromatic-H), 8.22–8.33 (m, 2H, CH=N).

3.3. Polymerization procedure

The ethylene/ α -olefin [(1-hexene, H) and (1-octene, O)] copolymerization reactions were carried out in a 100 mL semi-batch stainless steel autoclave reactor equipped with a magnetic stirrer. At first, the desired amounts of MAO ([Al]_{MAO}/[Ti]_{cat} = 250) and the toluene were introduced into the reactor. The Ti-FI complex in toluene was put into the reactor to make the amount of catalyst 2.5 μ mol. After that, the reactor was immersed in liquid nitrogen, followed by addition of the α -olefins into the frozen reactor. The reactor was heated up to the polymerization temperature at 323 K. By feeding a fixed amount of ethylene (0.018 mole ~ 6 psi) into the reaction mixture, the ethylene consumption can be observed corresponding to the ethylene pressure drop. Lastly, the reaction was terminated by adding acidic methanol. After filtration, the resulting polymers were washed with methanol and dried at room temperature.

3.4. Characterization of polymers

Differential scanning calorimetry: DSC thermal analysis was used to examine the thermal properties (T_m and heat of fusion) via a DSC 204 F1 Phoenix®. The DSC measurements were recorded during the second heating/cooling cycle with the heating rate of 10 °C/min during the range of temperature 30–200 °C.

Gel Permeation Chromatography: A high temperature GPC (Waters 2200) equipped with a viscometric detector, differential optical refractometer and four Styragel HT type columns (HT3, HT4, HT5 and HT6) was used to determine the molecular weight (MW) and molecular weight distribution (MWD) of polymer. The measurement was taken at 135 °C using 1,2,4-trichlorobenzene as a solvent and a mobile phase of 1 mL/min flow rate

Scanning electron microscopy: SEM was used to determine the sample morphologies using a JEOL mode JSM-5800LV instrument.

Nuclear magnetic resonance spectroscopy: ¹³C-NMR spectroscopy was used to determine the α-olefin incorporation and copolymer microstructure. Comparison of the positions of peak in the ¹³C-NMR spectra of polymer sample with characteristic leads to identification of the sequence of the comonomer incorporation, referring to Randall [16]. The spectra were recorded at room temperature using a Bruker AVANCE II 400 instrument operating at 100 MHz with an acquisition time of 1.5 s and a delay time of 4 s. The samples were prepared from using 1,2,4-trichlorobenzene as a solvent and deuterated chloroform for an internal lock.

4. Conclusions

This article has reported the preparation of LLDPE copolymer from ethylene/ α -olefin copolymerization using TiC₃₄H₃₆Cl₂N₂O₂ (Ti-FI catalyst) by varying the initial comonomer concentration and the comonomer type. The results reveal that all copolymers achieved very high activity, high molecular weight and narrow molecular weight distribution; on the other hand, the bulkiness of the catalyst structure is likely the main feature limiting the incorporation of comonomer into the polymer backbone. The increase of initial comonomer concentration caused an increase in catalytic activity; conversely, it led to a decrease in molecular weight and melting temperature. In

addition, concerning the impact of the comonomer type on the catalytic behavior, 1-hexene exhibited apparently higher activity and molecular weight with corresponding 1-octene based copolymer. However, both melting temperature and crystallinity appeared to be independent of comonomer type.

Acknowledgements

We gratefully thank the Dusadeepipat scholarship (Chulalongkorn University Fund), the graduate school of Chulalongkorn University, Innovation & Technology of PTT Chemical Public Company Limited, the Thailand Research Fund (TRF), the Office of Commission on Higher Education (CHE) and NRU of CU (AM1088A) for the financial support of this work.

References

- 1. Hung, J.; Cole, A.P.; Waymouth, R.M. Control of sequence distribution of ethylene copolymers: Influence of comonomer sequence on the melting behavior of ethylene copolymers. *Macromolecules* **2003**, *36*, 2454-2463.
- 2. Makio, H.; Kashiwa, N.; Fujita, T. FI Catalysts: A New family of high performance catalysts for olefin polymerization. *Adv. Syn. Catal.* **2002**, *344*, 477-493.
- 3. Grieken, R.V.; Carrero, A.; Suarez, I.; Paredes, B. Effect of 1-hexene comonomer on polyethylene particle growth and kinetic profiles. *Macromol. Sym.* **2007**, 259, 243-252.
- 4. Ishii, S.; Saito, J.; Mitani, M.; Mohr, J.; Matsukawa, N.; Tohi, Y.; Matsui, S.; Kashiwa, N.; Fujita, T. Highly active ethylene polymerization catalysts based on titanium complexes having two phenoxy-imine chelate ligands. *J. Mol. Catal. A Chem.* **2002**, *179*, 11-16.
- 5. Chaichana, E.; Khaubunsongserm, S.; Prasethdam, P.; Jongsomjit, B. Ethylene-hexene copolymer derived from [t-butylfluorenylsilyl-amido] dimethyl titanium complex. *Express Polym. Lett.* **2010**, *4*, 94-100.
- 6. Hong, H.; Zhang, Z.; Chung, T.C.M.; Lee, R.W. Synthesis of new 1-decene-based LLDPE resins and comparison with the corresponding 1-octene- and 1-hexene-based LLDPE resins. *J. Polym. Sci. Part A Polym. Chem.* **2007**, *45*, 639-649.
- 7. Forlini, F.; Fan, Z.Q.; Tritto, I.; Locatelli, P.; Sacchi, M.C. Metallocene-catalyzed propene/1-hexene copolymerization: Influence of amount and bulkiness of cocatalyst and of solvent polarity. *Macromol. Chem. Phys.* **1997**, *198*, 2397-2408.
- 8. Matsui, S.; Fujita, T. FI Catalysts: Super active new ethylene polymerization catalysts. *Catal. Today* **2001**, *66*, 63-73.
- 9. Galland, G.B.; Seferin, M.; Mauler, R.S.; Santos, J.H.Z. Linear low-density polyethylene synthesis promoted by homogeneous and supported catalysts. *Polym. Inter.* **1999**, *48*, 660-664.
- 10. Desharun, C.; Jongsomjit, B.; Praserthdam, P. Study of LLDPE/alumina nanocomposites synthesized by in situ polymerization with zirconocene/d-MMAO catalyst. *Catal. Commun.* **2008**, *9*, 522-528.
- 11. Wongwaiwattanakul, P.; Jongsomjit, B. Copolymerization of ethylene/1-octene via different pore sized silica-based-supported zirconocene/dMMAO catalysts. *Catal. Commun.* **2008**, *10*, 118-122.

12. Bunchongturakarn, S.; Jongsomjit, B.; Praserthdam, P. Impact of bimodal pore MCM-41-supported zirconocene/dMMAO catalyst on copolymerization of ethylene/1-octene. *Catal. Commun.* **2008**, *9*, 789-795.

- 13. Jongsomjit, B.; Kaewkrajang, P.; Shiono, T.; Praserthdam, P. Supporting effects of silica-supported methylaliminoxane (MAO) with zirconocene catalyst on ethylene/1-olefin copolymerization behaviors for linear low-density polyethylene (LLDPE). *Ind. Eng. Chem. Res.* **2004**, *43*, 7959-7963.
- 14. Jongsomjit, B.; Ngamposri, S.; Praserthdam, P. Catalytic activity during copolymerization of ethylene and 1-hexene via mixed TiO₂/SiO₂-supported MAO with rac-Et[Ind]₂ZrCl₂ metallocene catalysts. *Molecules* **2005**, *10*, 672-678.
- 15. Saito, J.; Mitani, M.; Matsui, S.; Tohi, Y.; Makio, H.; Nakano, T.; Tanaka, H.; Kashiwa, N; Fujita, T. A new titanium complex having two phenoxy-imine chelate ligands for ethylene polymerization. *Macromol. Chem. Phys.* **2002**, *203*, 59-65.
- 16. Randall, J.C. A review of high resolution liquid ¹³carbon nuclear magnetic resonance characterizations of ethylene-based polymers. *J. Macromol. Sci. Rev. Macromol. Chem. Phys.* **1989**, 29, 201-317.

Sample Availability: Samples of the compounds are available from the authors.

© 2011 by the authors; licensee MDPI, Basel, Switzerland. This article is an open access article distributed under the terms and conditions of the Creative Commons Attribution license (http://creativecommons.org/licenses/by/3.0/).



Contents lists available at ScienceDirect

Fuel Processing Technology

journal homepage: www.elsevier.com/locate/fuproc



Effect of calcination treatment of zirconia on W/ZrO₂ catalysts for transesterification

Nichapat Senso, Bunjerd Jongsomjit*, Piyasan Praserthdam

Center of Excellence on Catalysis and Catalytic Reaction Engineering, Department of Chemical Engineering, Faculty of Engineering, Chulalongkorn University, Bangkok 10330, Thailand

ARTICLE INFO

Article history: Received 15 November 2010 Received in revised form 22 February 2011 Accepted 27 March 2011 Available online 17 April 2011

Keywords: Zirconia Tungsten Biodiesel Transesterification Calcination

ABSTRACT

In this present study, the nanocrystalline ZrO_2 particles synthesized by the solvothermal method were calcined in reductive (H_2) , inert (N_2) and oxidative $(O_2$ and air) atmospheres prior to impregnation with tungsten (W) in order to produce the W/ZrO_2 (WZ) catalysts. Based on the ESR measurement, it revealed that only the ZrO_2 samples calcined in H_2 and N_2 exhibited the F-center (single charged oxygen vacancy) at g=2.003. None of Zr^{3+} defect was detected for all calcined ZrO_2 samples. After impregnation with tungsten, the WZ catalysts were also characterized. It was present as the polycrystal, which can be seen by the selected area electron distribution (SAED). However, the presence of Zr^{3+} defect was evident in all WZ catalysts, while the F-center was absent. The highest Zr^{3+} intensity detected in the WZ catalyst using ZrO_2 under H_2 calcination atmosphere can be attributed to the transformation of F-center to Zr^{3+} defect. It revealed that the WZ-H2 catalysts exhibited the highest conversion under transesterification of triacetin and methanol among other WZ catalysts. This can be attributed to the high surface acidity, which was probably induced by large amounts of Zr^{3+} defect.

© 2011 Elsevier B.V. All rights reserved.

1. Introduction

Recently, the prices of energy from natural sources, such as petroleum gas and oil are increasing everyday because of the demand of energy for serving industries in many countries. Biodiesel is one of those renewable energy sources, which are attracted by many researchers because it can be made of bioresources, such as vegetable oils or fats from animal. Moreover, they can be readily converted to biodiesel comparing to petroleum oil and natural gas. Biodiesel itself will provide many advantages since it is effective fuel and it can reduce production cost. However, these feed stocks often contain a lot of free fatty acids (FFAs) and water, which are not suitable for homogeneous alkaline-catalyzed process and needed to pretreatment for disposal free fatty acids at the preliminary process of biodiesel production. The main reactions which play important roles on produce biodiesel are "esterification" and "transesterification", which require strong liquid acid catalysts such as sulfuric acid [1–6]. However, the use of strong liquid acid catalysts essentially causes side effects, such as high corrosive, hard to separate and having expensive cost because those catalysts are not reusable. Besides, the solid acid catalysts can be used in biodiesel production by transesterification of feedstock containing a high content of FFAs, such as waste cooking oils [7]. Hence, there are new investigation for solid acid and base catalysts, such as sulfated zirconia (SZ) and tungstated zirconia (WZ) catalysts [8] because these catalysts provide esterification and

transesterification reaction at the same time. The strong acidity of SZ catalyst has attracted much attention because of its ability to catalyze a wide range of reactions, such as cracking, alkylation, and isomerization, all needing solid acids as catalysts [9–12]. Since the SZ catalyst promoted with noble metals are subject among others to sulfate reduction and subsequent poisoning of the metallic function under reductive atmospheres [13], the W-based metal oxides originally proposed by Hino and Arata [14], seem to be good candidates for the skeletal isomerization of alkanes higher than C₄ requiring strong acid sites.

It is known that anionic dopants create additional electrondeficient regions that increase the Bronsted acid strength of a metal oxide surface by improving the ability of neighboring hydroxyl groups to act as proton donors [15]. As an alternative to sulfated zirconia (SZ), tungstated zirconia (WZ) was also reported to be active for the isomerization of C₄-C₈ alkanes [14,16-19]. Although the WZ catalyst was less active than SZ, the former shows several advantages over the latter. For instance, the WZ catalyst is much more stable than the SZ one at high temperatures [12] and it undergoes significantly less deactivation during catalytic reaction [20]. Lopez et al. [8] reported that the use of WZ catalyst has active sites equal to sulfuric acid for catalyzing biodiesel-forming transesterification reaction. Another advantage of WZ catalyst is that its deactivation appears to be not rapid for transesterification reaction of triglycerides with methanol [8,21]. Ramu et al. [22] also reported that the various W loadings on zirconia and various calcination temperatures affected the phase change of zirconia and consequently the catalyst activity on esterification reaction for biodiesel production process. In addition, some papers reveal that surface structure and phase of zirconia have

^{*} Corresponding author. Tel.: +66 2 218 6869; fax: +66 2 218 6766. E-mail address: bunjerd.j@chula.ac.th (B. Jongsomjit).

effects on the catalyst activity as well [23–25]. Since nature of surface and defects of zirconia can affect on its properties. Therefore, it is of great benefits to investigate the deep impact of nature of surface and defect of zirconia on its catalytic properties. Among studies, Lui et al. [26] created defection on zirconia surface by calcination at different temperatures. Another research [24] showed that the surface defect of zirconia can be created by altering the calcination atmospheres.

In this present work, the nanocrystalline zirconia particles were first synthesized via the solvothermal method, and then calcined upon different atmospheres using H₂, N₂, O₂ and air. The obtained zirconia samples as supports were further impregnated with tungsten (VI) chloride to produce WZ catalyst and being used for transester-ification of triacetin with methanol. In fact, the triacetin was used in this study since it is a model compound for larger triglycerides that has been found in many vegetable oils and fats [8]. Besides, it is also used to minimize the side effect of FFAs from crude oil. The effects of different calcination atmospheres of zirconia samples on the characteristics and catalytic properties of WZ catalysts were elucidated by means of various techniques, such as N₂ physisorption, X-ray diffraction (XRD), transmission electron microscopy (TEM) with the selected area electron distribution (SAED) and electron spin resonance (ESR).

2. Experimental

2.1. Preparation of nanocrystalline ZrO₂

The nanocrystalline ZrO₂ particles were prepared using the solvothermal method in the same manner as that of Kongwudthiti et al. [27]. Zirconium n-butoxide (97%, Aldrich) was used as the starting material. Approximately, 25 g of zirconium n-butoxide was suspended in 100 ml of 1,4-butanediol (Aldrich) in a test tube, which was then placed in a 300 ml autoclave. The 25 ml of the same solvent was filled in the gap between the test tube and the autoclave wall. The autoclave was purged completely by nitrogen after that it was heated up to the desired temperature at 300 °C with the rate of 2.5 °C min $^{-1}$. The temperature was held constant at 300 °C for 2 h, and then cooled down to room temperature. After the autoclave was cooled to room temperature, the resulting product was repeatedly washed with methanol by vigorous mixing and centrifuging. In fact, methanol was used to remove the impurity from the precursor during synthesis of zirconia and it is easy to evaporate during the drying process. The obtained powders were then dried in oven at 100 °C for 1 day. Finally, the obtained sample was calcined in a tube furnace in different atmospheres (H2, N2, O2, and Air, solely with the flow rate of $30 \text{ cm}^3 \text{min}^{-1}$) by heating to $500 \,^{\circ}\text{C}$ with a rate of $10 \,^{\circ}\text{C} \,^{\circ}\text{min}^{-1}$ and holding at that temperature for 2 h.

2.2. Preparation of tungstated zirconia (WZ) catalyst

The WZ catalysts were prepared by the incipient wetness impregnation of the calcined zirconia samples obtained from section 2.1 with a desired amount of an aqueous solution of tungsten (VI) chloride (99 wt.%, Aldrich) to produce the WZ catalyst having 15 wt.% of W loading. The catalysts were dried at 110 °C for 24 h and calcined in air at 500 °C for 3 h.

2.3. Catalyst nomenclature

The following nomenclature was used for samples in this study. The ZrO_2 –X sample refers to the ZrO_2 support calcined under X (H_2 , N_2 , O_2 , and Air) atmosphere. The WZ–X sample refers to the WZ catalyst using ZrO_2 support calcined under X atmosphere.

2.4. Catalyst characterization

X-ray diffraction (XRD) patterns were recorded with a Siemens D5000 using nickel filtered CuK_{α} radiation. The crystallite size was determined using the Scherrer equation by using α -alumina as the external standard. The surface area of solid was determined by physisorption of nitrogen (N₂) using Micromeritics ASAP 2020.

The amounts of acidity were measured by using the titration technique involved an ion-exchange step [8]. First, 0.2 g of catalyst was dissolved in 10 ml of 3.43 M NaCl solution. Stirring was taken place for 30 h at 28 °C, which caused the interchange ion between H⁺ of catalyst and Na⁺ of solution. Then, the solid phase was filtered out. Solution was next titrated with 0.05 M of NaOH solution. The endpoint for this titration was measured by pH meter (pH~7). The defected surface zirconia (${\rm Zr^{3+}}$ and F-center) was investigated by the electron spin resonance spectrometer (ESR). It was conducted on ESR spectrometer of JEOL model (JES-RE2X) on ES-IPRIT program with the X band microwave unit and frequency of 8.8–9.6 GHz. The cavity is cylindrical and it is operating in TE ₀₁₁ mode. Transmission electron microscope (TEM) and selected area electron distribution (SAED) used to characterize the morphology, crystallite size, and diffraction patterns of the primary particles of the WZ samples were obtained using the JEOL JEM-2010 transmission electron microscope operated at 200 kV with an optical point to point resolution of 0.23 nm. The sample was dispersed in ethanol prior to measurement.

2.5. Reaction study

The liquid phase transesterification reaction was carried out on well-mixed batch reactor. Hot plate and stirrer were used for heat generation and mixing. First, the solution of triacetin and methanol at molar ratio of 1:6 were mixed in the reactor [8]. The reactor was heated to 60 °C and the solid catalyst having the amounts of 2 wt.% of triacetin employed was added. Sample aliquot (1 ml) was withdrawn periodically from the reactor, quenched to room temperature, and centrifuged in order to separate out the solid catalyst and prevent further reaction. Reaction sample concentrations were determined using an SHIMADZU gas chromatograph GC-14B. The reaction was continuous on going through the stable conversion (7 h).

3. Results and discussion

3.1. Characteristics of zirconia calcined under different atmospheres

In this present study, the nanocrystalline ZrO_2 particles were synthesized via the solvothermal method. After drying, the samples were calcined under reductive (H_2), inert (N_2), and oxidative (O_2 and air) atmospheres. The characteristics of samples after calcinations are shown in Table 1. It was found that after calcination, all ZrO_2 samples exhibited the lower surface area due to sintering at high temperature (SO_2 °C). It should be noted that the ZrO_2 - O_2 sample had the lowest surface area (SO_2) among other samples indicating that the SO_2 0 atmosphere apparently resulted in more sintering. In order to identify the crystallite phases of SO_2 0, the XRD was performed. The XRD

Table 1 Characteristics of ZrO₂ calcined at different atmospheres.

Sample	SA	Crystal phase ^a		Crystallite size ^a	ESR signal (a.u.)	
	(m^2/g)	%t-ZrO ₂	%m-ZrO ₂	(nm)	F-center	Zr ³⁺
ZrO ₂ -H ₂	90.5	87.6	12.4	3.8	22,000	_
ZrO_2-N_2	90.1	87.4	12.6	3.6	15,510	-
ZrO_2-O_2	76.4	70.6	29.4	6.9	-	-
ZrO ₂ -Air	94.9	78.8	21.2	4.1	-	-
ZrO ₂ -As-syn	120.2	90.2	9.8	3.5	-	-

^a Based on the XRD measurement.

patterns for all calcined samples are shown in Fig. 1. Prior to calcination, the ZrO_2 sample exhibited the XRD peaks at 30.2° , 35.3° and 49.8° (strong) assigned to the tetragonal phase and at 28.2° and 33.1° (weak) assigned to the monoclinic phase. The percents of tetragonal and monoclinic phases in ZrO_2 (as also shown in Tables 1 and 2) were calculated by a comparison of the area for the characteristic peaks of the tetragonal and monoclinic phases. The percent of each phase was determined by means of the Gaussian areas $h \times w$, where h and w are the height and half-height width of the corresponding XRD characteristic peaks as follows [28]:

% tetragonal phase;

$$= \frac{\sum (h \times w) tetragonal\ phase}{\sum (h \times w) tetragonal\ phase\ and\ monoclinic\ phase}$$

% monoclinic phase;

$$= \frac{\sum (h \times w) monoclinic\ phase}{\sum (h \times w) tetragonal\ phase\ and\ monoclinic\ phase}$$

It was found that only small fraction of monoclinic phase was present prior to calcination. However, after calcination under different atmospheres, all samples exhibited the higher fractions of monoclinic phase. It revealed that calcination under oxidative atmosphere apparently resulted in significant higher fraction of monoclinic phase present as seen for Zr-O2 and Zr-Air samples. Only small change was found in the samples calcined under reductive (Zr-H₂) and inert (Zr-N₂) atmospheres. In our previous works [29,30], the similar synthesized zirconia samples were calcined at only 400 °C for 2 h in the reductive and oxidative atmospheres. However, no phase transformation from tetragonal to monoclinic was observed. Thus, in this study, the increased calcination temperature at 500 °C was performed to further investigate the effect of phase transformation of zirconia along with the calcination in inert atmosphere. Upon increased calcination temperature (500 °C), the phase transformation from tetragonal to monoclinic was more pronounced under the oxidative atmosphere. The crystallite size of sample was also obtained by the XRD line broadening using Scherrer equation. As seen in Table 1, only the ZrO₂-O₂ samples exhibited the remarkable change (largest) in the crystallite size corresponding to the lowest surface area observed. Hence, the sintering effect was more pronounced under oxidative atmosphere.

The ESR was used to identify the surface nature of ZrO₂ calcined under different atmospheres. The ESR spectra for all ZrO₂ samples are

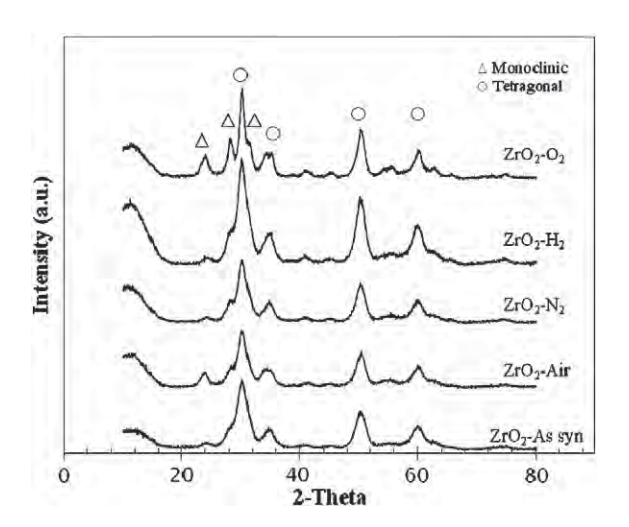


Fig. 1. XRD patterns of different ZrO_2 samples.

Table 2Characteristics of WZ catalysts obtained from different ZrO₂ samples.

Sample	SA	Acidity ^a	idity ^a Crystal phase ^b		Crystallite size ^b	ESR signal (a.u.)	
	(m²/g)	(µmol/g)	%t-ZrO ₂	%m-ZrO ₂	(nm)	F-center	Zr^{3+}
WZ-H ₂	90.2	200	76.0	24.0	3.8	_	2362
$WZ-N_2$	90.5	150	81.4	18.6	3.6	-	2105
$WZ-O_2$	69.8	100	68.7	31.3	6.7	-	1260
WZ-Air	85.5	125	85.2	14.8	3.9	-	1315

^a Obtained from the ion-exchange titration.

shown in Fig. 2. It revealed that no strong ESR signals can be detected for the dried-ZrO₂ (As-syn), ZrO₂–O₂, and ZrO₂–Air samples. However, the strong ESR signals for ZrO₂–H₂ and ZrO₂–N₂ samples were observed at g=2.003 assigned to F-center (single charged oxygen vacancy) [24]. This is confirmed that the calcination of zirconia under reductive atmosphere would lead to the formation of F-center as following reaction;

$$Zr^{4+} + OH^{-} + \frac{1}{2}H_{2} \rightarrow Zr^{4+} + F^{-} + H_{2}O$$

It is also worth noting that the intensity of F-center of ZrO_2-H_2 sample was higher than that of ZrO_2-N_2 sample as also shown in Table 1. Therefore, ZrO_2 was hardly reduced by H_2 due to strong Zr—O bond energy. Thus, the F-center was probably produced by the reduction of hydroxyl group on ZrO_2 surface [24]. It should be noted that no Zr^{3+} (g = 1.975) ESR signal as seen from ZrO_2 calcined at 400 °C [29,30] under oxidative atmosphere was observed. This is probably due to the presence of monoclinic phase after calcination at 500 °C inhibits the formation of Zr^{3+} . However, the existence of F-center was not affected by the presence of monoclinic phase under reductive and inert atmosphere.

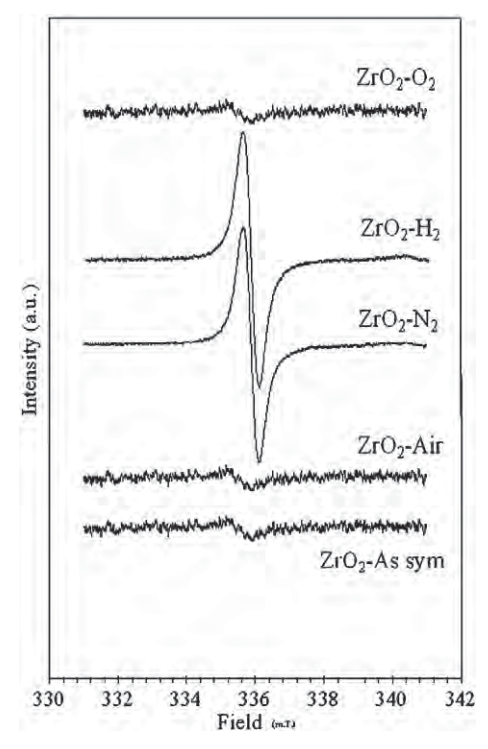


Fig. 2. ESR spectra of different ZrO₂ samples.

b Obtained from the XRD measurement.

3.2. Characteristics of tungstated zirconia (WZ) catalysts

Then, the different ZrO_2 samples were impregnated with W to produce the WZ catalysts. The characteristics of different WZ catalysts are shown in Table 2. The XRD patterns of WZ catalysts are shown in Fig. 3. They are similar to the XRD patterns of the ZrO_2 samples as seen in Fig. 1 indicating that tungsten is well dispersed onto the ZrO_2 support and cannot be detected by XRD. Considering the characteristics of WZ catalysts, it showed that the surface area, phase composition, and crystallite size of samples were not affected by W loading. The acidity of WZ catalysts was determined using chemical titration techniques [20]. The results, as also shown in Table 2, indicated that the acidity of WZ catalysts increased within the order of WZ-H₂>WZ-N₂>WZ-Air>WZ-O₂.

In order to elucidate the effect of W loading on surface nature of ZrO₂, the ESR measurement of WZ catalysts was also performed. The ESR spectra for all WZ catalysts are shown in Fig. 4. All samples exhibited the characteristic ESR signals for Zr^{3+} at g=1.975 and g = 1.957 [24,26], while the ESR signals for F-center for ZrO_2-H_2 and ZrO_2-N_2 samples were absent. Zhao et al. [24] reported that the Zr^{3+} detected by ESR can be described as the oxygen coordinatively unsaturated zirconium sites on the ZrO₂ surface. The intensity of Zr³⁺ obtained from ESR signal was determined and reported in Table 2. It increased upon the following order; WZ-H₂>WZ-N₂>WZ-Air>WZ-O₂, which was related to increased acidity of WZ catalysts. It is known that the intensity of F-center signal (as seen only in ZrO₂-H₂ and ZrO₂-N₂ samples) on zirconia surface is disproportional to that of Zr³⁺ signal. The appearance of these two signals is related in adverse effect. It may be because the electronic density redistribution can be relocated between Zr³⁺ and the closest oxygen vacancy. By calcination in reductive and oxidative (calcination of WZ catalysts) atmospheres, the electronic density can move to F-center and Zr³⁺, respectively. Hence, this reaction can be altered by calcination condition. The results of the disappearance of the F-center (V_0^-) in oxidative atmosphere can be drawn based on the work reported by Frolova and Ivanovskaya [31] as follows;

$$Zr^{3+} \, - [V_0] \mathop{\to}\limits_{\stackrel{\leftarrow}{\circ}_2}^{\stackrel{\scriptscriptstyle H_2}{\circ}} Zr^{4+} \, - [V_0^-]$$

TEM images along with SAED for all WZ catalysts are shown in Fig. 5. They are almost similar. Primarily, the spheroid shape with

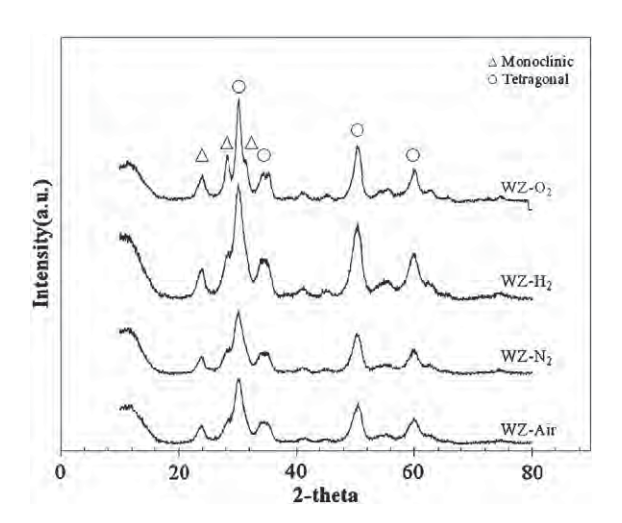


Fig. 3. XRD patterns of different WZ catalysts.

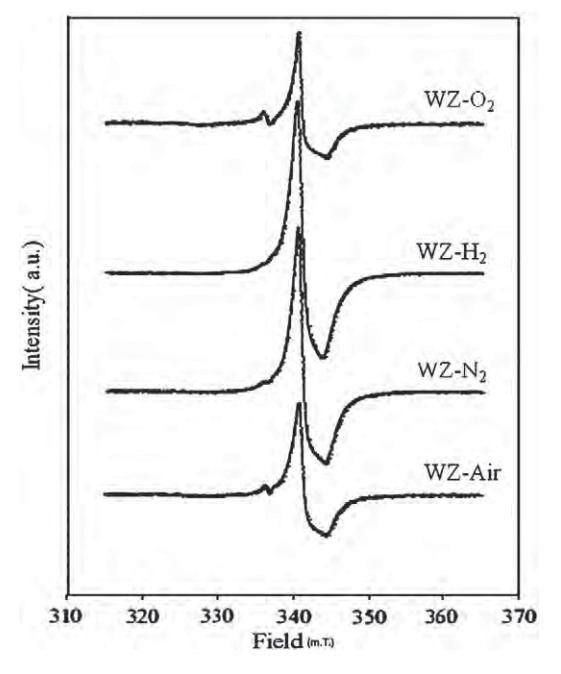


Fig. 4. ESR spectra of different WZ catalysts.

average size around 3 to 15 nm and irregular large shape overlayer are observed. From SAED analysis, the spheroid shape particles could be assigned to $\rm ZrO_2$ particles and the irregular shape overlayer was assigned to tungsten oxide. The crystallite sizes calculated by TEM image were also in good agreement with the crystallite sizes obtained from XRD. The WZ catalysts only consisted of irregular bulk solids trapped inside the small crystal. From EDX analysis, all bulk solids comprised of tungsten and zirconium atoms, where W atoms were mixed with the Zr atoms within the crystal. This result agrees with several works, which propose that tungsten species are entrapped inside the $\rm ZrO_2$ bulk forming a solid solution [22,25]. The results suggested that there were more dispersion of $\rm WO_x$ species on $\rm ZrO_2-H_2$ and $\rm ZrO_2-N_2$ supports. All TEM images of WZ catalysts clearly display crystalline $\rm ZrO_2$ lattice fringes.

3.3. Reaction study

The liquid phase transesterification of triacetin and methanol at 60 °C was used as the model reaction for comparing the catalytic activity of all WZ catalysts. The catalytic activities of WZ catalysts are displayed in Fig. 6. The conversions were in the range of WZ-H₂ $(53\%)>WZ-N_2$ $(40\%)>WZ-O_2$ $(17\%)\approx WZ-Air$ (16%). The results were in good agreement with the acidity contents of catalyst, which were related to the intensity of Zr³⁺ in WZ catalysts after calcination. The increased acidity for WZ catalysts can be explained by the formation of WO₃ nanoparticles, which can be observed by Raman spectroscopy and being more acidic than the surface WO_x species [32]. In earlier works, when the impregnated tungsten contents on ZrO₂ support increased, the tungsten species were changed from monotungstate to polytungstate surface WO_x and finally to form WO₃ nanocrystal. However, based on this work, the W loading was fixed at 15 wt.%. Thus, the changes in the formation of WO_x species should be due to the different surface structure of ZrO2 after calcination. Based on different characteristics of ZrO₂, especially for the F-center that was only present in ZrO₂-H₂ and ZrO₂-N₂ supports, it revealed that the presence of F-center in ZrO2 can facilitate the formation of Zr³⁺, and then more acidity tungsten species can be formed.

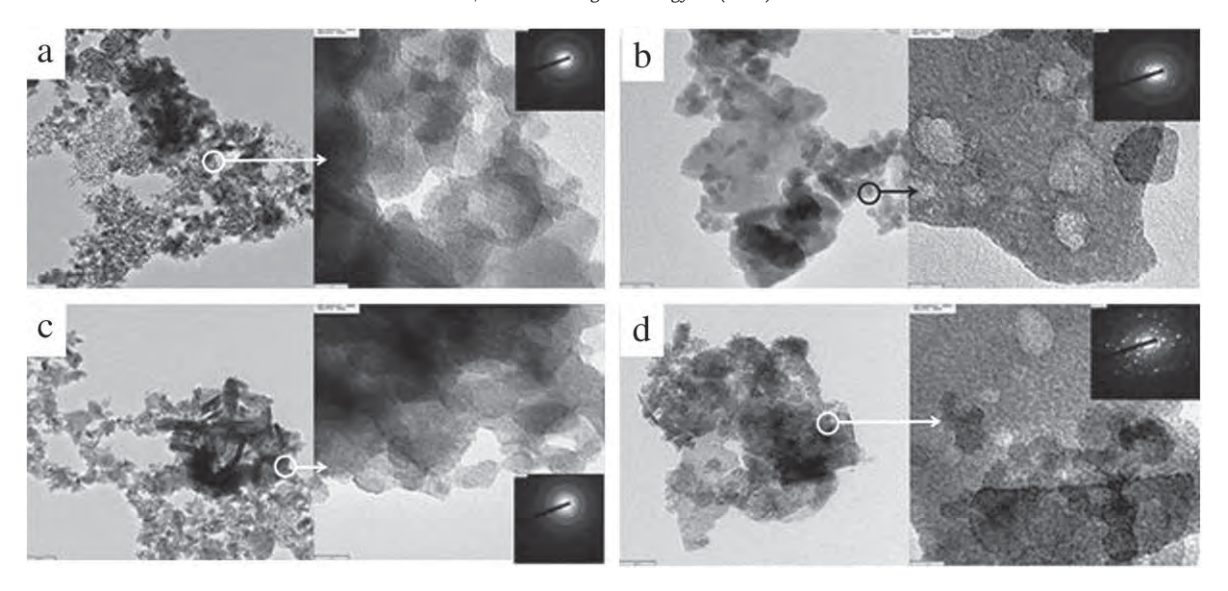


Fig. 5. TEM micrographs of (a) WZ-Air, (b) WZ-O₂, (c) WZ-N₂, and (d) WZ-H₂.

4. Conclusions

This present study revealed the effect of different calcination atmospheres on the nanocrystalline ZrO_2 particles. It indicated that only ZrO_2 calcined in H_2 and N_2 exhibited the F-center based on ESR measurement. No Zr^{3+} signal based on ESR was observed for ZrO_2 calcined in O_2 and air probably due to the presence of monoclinic phase. The F-center present under reductive and inert atmospheres can transform to Zr^{3+} after W loading and calcination. The large amount of Zr^{3+} apparently facilitates the formation of high acidic tungsten species that can increase the catalytic activity of WZ catalyst via transesterification.

Acknowledgments

The authors thank the Thailand Research Fund (TRF), Office of the Higher Education Commission (CHE) and NRU-CU (AM1088A) for the financial support of this project.

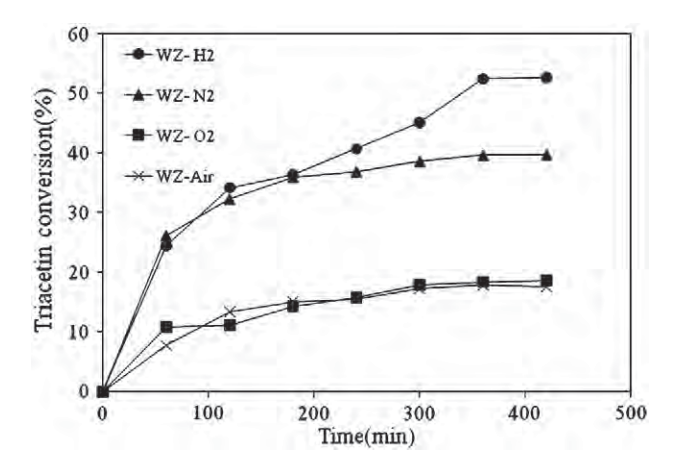


Fig. 6. Triacetin conversion upon different WZ catalysts; conditions: methanol:triacetin molar ratio = 6:1, reaction temperature = 60 °C, solid acids = 2 wt.% of triacetin employed, and running time = 7 h.

References

- M.L. Pisarello, C.B. Dalla, G. Mendow, C.A. Querini, Esterification with ethanol to produce biodiesel from high acidity raw materials: kinetic studies and analysis of secondary reactions, Fuel Process. Technol. 91 (2010) 1005–1014.
- [2] B. Sarkar, S. Sridhar, K. Saravanan, V. Kale, Preparation of fatty acid methyl ester through temperature gradient driven pervaporation process, Chem. Eng. J. 162 (2010) 609–615.
- [3] M. Canakci, G.J. Van, Biodiesel production via acid catalysis, TASAE 42 (1999) 1203–1210.
- [4] M. Canakci, G.J. Van, Biodiesel production from oils and fats with high free fatty acids, TASAE 44 (2001) 1429–1439.
- [5] M.J. Goff, N.S. Bauer, S. Lopes, W.R. Sutterlin, G.J. Suppes, Acid-catalyzed alcoholysis of soybean oil, JAOCS 81 (2004) 415–420.
- [6] E. Lotero, Y. Liu, D.E. Lopez, K. Suwannakarn, D.A. Bruce, J.G. Goodwin Jr., Synthesis of biodiesel via acid catalysis, Ind. Eng. Chem. Res. 44 (2005) 5353–5363.
- [7] C. Komintarachat, S. Chuepeng, Solid acid catalyst for biodiesel production from waste used cooking oils, Ind. Eng. Chem. Res. 48 (2009) 9350–9353.
- [8] D.E. Lopez, J.G. Goodwin Jr., D.A. Bruce, E. Lotero, Transesterification of triacetin with methanol on solid acid and base catalysts, Appl. Catal. A:Gen. 295 (2005) 97–105.
- [9] E. Iglesia, S.L. Soled, G.M. Kramer, Isomerization of alkanes on sulfated zirconia: promotion by Pt and by adamantyl hydride transfer species, J. Catal. 144 (1993) 238–253.
- [10] K.F. Yee, J. Kansedo, K.T. Lee, Biodiesel production from palm oil via heterogeneous transesterification: optimization study, Chem. Eng. Commun. 197 (2010) 1597–1611.
- [11] K. Suwannakarn, E. Lotero, J.G. Goodwin Jr., C. Lu, Stability of sulfated zirconia and the nature of the catalytically active species in the transesterification of triglycerides, J. Catal. 255 (2008) 279–286.
- [12] M. Busto, K. Shimizu, C.R. Vera, J.M. Grau, C.L. Pieck, M.A. D'Amato, M.T. Causa, M. Tovar, Influence of hydrothermal aging on the catalytic activity of sulfated zirconia, Appl. Catal. A: Gen. 348 (2008) 173–182.
- [13] X. Li, K. Nagaoka, L.J. Simon, R. Olindo, J.A. Lercher, Influence of calcination procedure on the catalytic property of sulfated zirconia, Catal. Lett. 113 (2007) 34–40.
- [14] M. Hino, K. Arata, Synthesis of solid superacid of tungsten oxide supported on zirconia and its catalytic action for reactions of butane and pentane, J. Chem. Soc. Chem. Commun. 18 (1988) 1259–1260.
 [15] E. Iglesia, D.G. Barton, S.L. Soled, S. Miseo, J.E. Baumgartner, W.E. Gates, G.A.
- [15] E. Iglesia, D.G. Barton, S.L. Soled, S. Miseo, J.E. Baumgartner, W.E. Gates, G.A. Fuentes, G.D. Meitzner, Selective isomerization of alkanes on supported tungsten oxide acids, Stud. Surf. Sci. Catal. 101 (1996) 533–542.
- [16] J.G. Santiesteban, J.C. Vartuli, S. Han, R.D. Bastian, C.D. Chang, Influence of the preparative method on the activity of highly acidic WO_x/ZrO₂ and the relative acid activity compared with zeolites. J. Catal. 168 (1997) 431–441
- activity compared with zeolites, J. Catal. 168 (1997) 431–441.

 [17] M. Busto, M.E. Lovato, C.R. Vera, K. Shimizu, J.M. Grau, Silica supported tungstazirconia catalysts for hydroisomerization-cracking of long alkanes, Appl. Catal. A: Gen. 355 (2009) 123–131.
- [18] X. Chen, C. Chen, N. Xu, C.Y. Mou, Catalytic activity of Al₂O₃/WO₃/ZrO₂ strong solid acid catalyst for n-butane isomerization, Chin. J. Catal. 24 (2003) 924–928.
- [19] X.R. Chen, C.L. Chen, N.P. Xu, C.Y. Mou, Al- and Ga-promoted WO₃/ZrO₂ strong solid acid catalysts and their catalytic activities in n-butane isomerization, Catal. Today. 93 (2004) 129–134.
- 20] D.E. López, J.G. Goodwin Jr., D.A. Bruce, S. Furuta, Esterification and transesterification using modified-zirconia catalysts, Appl. Catal. A: Gen. 339 (2008) 76–83.

- [21] S. Furuta, H. Matsuhashi, K. Arata, Biodiesel fuel production with solid superacid catalysis in fixed bed reactor under atmospheric pressure, Catal. Commun. 5 (2004) 721–723.
- [22] S. Ramu, N. Lingaiah, B.L.A.P. Devi, R.B.N. Prasad, I. Suryanarayana, P.S.S. Prasad, Esterification of palmitic acid with methanol over tungsten oxide supported on zirconia solid acid catalysts: effect of method of preparation of the catalyst on its structural stability and reactivity, Appl. Catal. A: Gen. 276 (2004) 163–168.
- [23] D.E. López, K. Suwannakarn, D.A. Bruce, J.G. Goodwin Jr., Esterification and transesterification on tungstated zirconia: effect of calcination temperature, J. Catal. 247 (2007) 43–50.
- [24] Q. Zhao, X. Wang, T. Cai, The study of surface properties of ZrO₂, Appl. Surf. Sci. 225 (2004) 7–13.
- [25] V. Lebarbier, G. Clet, M.A. Houalla, Comparative study of the surface structure, acidity, and catalytic performance of tungstated zirconia prepared from crystalline zirconia or amorphous zirconium oxyhydroxide, J. Phys. Chem. B 110 (2006) 13,905–13,911.
- [26] H. Liu, L. Feng, X. Zhang, Q. Xue, ESR characterization of ZrO₂ nanopowder, J. Phys. Chem. 99 (1995) 332–334.

- [27] S. Kongwudthiti, P. Praserthdam, P. Silveston, M. Inoue, Influence of synthesis conditions on the preparation of zirconia powder by the glycothermal method, Ceram. Int. 29 (2003) 807–814.
- [28] C. Su, J. Li, D. He, Z. Cheng, Q. Zhu, Synthesis of isobutene from synthesis gas over nanosize zirconia catalyst, Appl. Catal. A: Gen. 202 (2000) 81–89.
- [29] P. Wongmaneenil, B. Jongsomjit, P. Praserthdam, Influence of calcinations treatment on the activity of tungstated zirconia catalysts towards esterification, Catal. Commun. 10 (2009) 1079–1084.
- [30] K. Ngaosuwan, B. Jongsomjit, P. Praserthdam, The role of zirconia surface on catalytic activity of tungstated zirconia via two-phase esterification of acetic acid and 1-heptanol, Catal. Lett. 136 (2010) 134–140.
- [31] E.V. Frolova, M.I. Ivanovskaya, The origin of defects formation in nanosized zirconia, Mater. Sci. Eng. C 26 (2006) 1106–1110.
- [32] A. Martínez, G. Prieto, M.A. Arribas, P. Concepción, J.F. Sánchez-Royo, Influence of the preparative route on the properties of WO_x–ZrO₂ catalysts: a detailed structural, spectroscopic, and catalytic study, J. Catal. 248 (2007) 288–302.

ORIGINAL PAPER

Effect of Ga modification on different pore size silicas in synthesis of LLDPE by copolymerization of ethylene and 1-hexene with [t-BuNSiMe₂Flu]TiMe₂/MMAO catalyst

Ekrachan Chaichana ·
Supaporn Khaubunsongserm ·
Piyasan Praserthdam · Bunjerd Jongsomjit

Received: 2 June 2010/Revised: 27 December 2010/Accepted: 30 December 2010/

Published online: 19 January 2011 © Springer-Verlag 2011

Abstract Copolymerization of ethylene and 1-hexene for obtaining the linear low-density polyethylene was conducted along with silicas as supports for [t-BuN-SiMe₂Flu]TiMe₂/MMAO catalyst. Two silicas with different pore sizes were used to investigate the effect of pore sizes on copolymerization. In addition, gallium was also introduced into both silicas to improve their properties and enhance the catalytic activities of the system. It was found that before modification, the larger pore silica exhibited higher catalytic activity than the smaller one due to low internal diffusion resistance. After modification, both silicas exhibited higher catalytic activity comparing to their pristine condition. However, 1-hexene incorporation in the obtained copolymers was lower. The reduced surface area of silica after modification was the main reason for the decrease in 1-hexene incorporation. The properties of the copolymers by means of differential scanning calorimetry, gel permeation chromatography, and ¹³C NMR spectroscopy were further discussed in more detail.

Keywords Polymer synthesis · Silica · Metallocene · LLDPE

Introduction

First commercialize in the late 1970s by Union Carbide and Dow Chemical [1], linear low-density polyethylene (LLDPE) has continued a fast growth rate in usage

Center of Excellence on Catalysis and Catalytic Reaction Engineering, Department of Chemical Engineering, Faculty of Engineering, Chulalongkorn University, Bangkok 10330, Thailand e-mail: bunjerd.j@chula.ac.th

S. Khaubunsongserm

PTT Public Company Limited, PTT Research and Technology Institute, Wangnoi, Ayuthaya 13170, Thailand



E. Chaichana · P. Praserthdam · B. Jongsomjit (🖂)

from that time to this day. For using LLDPE in an efficient way, the specific properties of LLDPE, such as molecular weight (M_w) distribution, stereoregularity, and comonomer content need to be considered carefully. Metallocene is one of the most widely used catalysts for control those properties, and thus, many studies have been conducted with this type of catalyst [2-4]. However, the industrial application of metallocene is usually processed in a gas or slurry phase, so the development of supported metallocene is very important. Inorganic materials, such as SiO₂, Al₂O₃, and ZrO2 were applied for supported metallocene. It was, nevertheless, SiO2 that has been reported as the most attractive support. Therefore, the studies of silica on the role of support for metallocene catalyst have been conducted by many researchers in many aspects. Silveira et al. [5] have reported that textural properties of silica support were shown to influence several parameters and properties of supported metallocene catalysts, for example, the particle size influencing on catalytic activity. Besides the particle size, pore size is another factor that has been investigated. Kumkaew et al. [6, 7] have discovered that pore sizes influence the nature of the catalytic sites for supported metallocene catalyst, and then, also influence the comonomer incorporation rate of copolymerization. Ko et al. [8] reported that the certain pore size of support had different levels of impact on different sizes of (co)monomer. The effect of pore size not only exists in a system during copolymerization, but also does previously during preparation or modification of support. Therefore, properties of support before and after modification need to be considered to further clarify all phenomena occurring in the supported system.

In our previous study, the copolymerization of ethylene/1-hexene using the [t-BuNSiMe₂Flu]TiMe₃/MMAO catalyst under homogeneous system was investigated [9]. However, in this study, the similar copolymerization under the heterogeneous or supported system using silica support was further investigated. In addition, the effects of pore size of silica were studied by using different pore size silica-supported MMAO. Moreover, the effect of gallium (Ga) modification on silica was also examined to give a better understanding on how the catalytic activity apparently changes with Ga modification on different pore size silicas. In fact, the Ga modification on silica was chosen because it can enhance activity in zirconocene/ MMAO catalytic system as reported by Wannaborworn et al. [10].

Experimental

Materials

All operations were manipulated under an argon atmosphere using glove box and/or standard Schlenk techniques. [t-BuNSiMe₂Flu]TiMe₂ was synthesized according to the procedure described by Hagihara et al. [11]. Ethylene was obtained from the National Petrochemical Co. Ltd., Thailand. 1-Hexene was purchased from Aldrich Chemical Company. Modified methyl aluminoxane (MMAO) (1.86 M in toluene) was donated by Tosoh Akzo, Japan. Toluene was donated by the Exxon Chemical, Thailand Co. Ltd. It was dried over dehydrated CaCl₂ and distilled over sodium/ benzophenone. Silica gel from Fuji Silysia Chemical Ltd., Japan (Cariact Q-50 and



P-10) was calcined at 400 °C for 6 h under vacuum. Gallium nitrate was purchased from Aldrich Chemical Company, Inc., and use as received.

Preparation of Ga-modified silica support

The Ga modification of the silica support was prepared by the conventional incipient-wetness impregnation method according to the procedure described previously [12]. The Ga source in this case was $Ga(NO_3)$. Ga was impregnated onto silica gel (Cariact Q-50 and P-10) by 1.0 wt% of Ga. The support was dried in oven at 110 °C for 12 h, and then calcined in air at 400 °C for 2 h.

Preparation of supported MMAO

The silica supports were prepared by in situ impregnation method which was described by Wannaborworn et al. [10]. Silica (0.1 g) was allowed in contact with 4 mmol of MMAO for at least 2 h in a reactor with magnetic stirring, and then the slurry of MMAO/support was obtained and ready to be used in polymerization. To verify that all MMAO was immobilized onto the support, a batch test was conducted together with the preparation method for the entire samples. For the batch test, after stirring the mixture of support and MMAO for 2 h and leaving for precipitate for 1 h, 1 mL of clarified liquid was taken and injected into the polymerization reactor, where a desired amount of catalyst was already present. If no formation of any amount of polymer is observed, it will be evident that this clarified liquid does not contain the free MMAO. Thus, all MMAO was immobilized on the supports completely.

Polymerization procedure

The prepared MMAO/support (0.1 g support and 4 mmol MMAO) and toluene were introduced into the reactor. The titanium complex in toluene (10 μ mol mL⁻¹) was put into the reactor to make the [Al]_{MMAO}/[Ti]_{cat} = 400. Then, the reactor was immersed in liquid nitrogen. 0.018 mol of 1-hexene was added into the frozen reactor (to stop or prevent possible polymerization of 1-hexene). The reactor was heated up to the polymerization temperature at 70 °C. The polymerization was started by feeding ethylene into the reactor, and then stopped when ethylene consumption reached to 0.018 mol (6 psi on the pressure gauge). The reactor temperature was kept constant during the polymerization. The reaction was terminated by adding acidic methanol and the material was stirred for 30 min. After filtration, the copolymer obtained was washed with methanol and dried at room temperature.

Characterization

Characterization of supports

 N_2 physisorption: Measurement of BET surface area, average pore diameter, and pore size distribution were determined by N_2 physisorption using a Micromeritics



ASAP 2000 automated system. *X-ray diffraction*: XRD was performed to determine the bulk crystalline phases of samples. It was conducted using a SIEMENS D-5000 X-ray diffractometer with Cu K_{α} (l=1.54439~Å). The spectra were scanned at a rate of 2.4 min⁻¹ in the range of $2\theta=10^{\circ}-80^{\circ}$.

Characterization of polymers

¹³C NMR spectroscopy: The copolymers were characterized using ¹³C NMR spectroscopy (BRUKER AVANCE II 400) to determine the 1-hexene incorporation. Each sample solution was prepared by dissolving 50 mg of copolymer in 1,2,4-trichlorobenzene and CDCl₃. Spectra were taken at 60 °C operated at 100 MHz with an acquisition time of 1.5 s and a delay time of 4 s.

Differential scanning calorimetry (DSC): Thermal analysis measurements were performed using a Perkin-Elmer DSC P7 calorimeter. The DSC measurements reported here were recorded during the second heating/cooling cycle with the rate of 20 °C/min. This procedure ensured that the previous thermal history was erased and provided comparable conditions for all samples. Approximately, 10 mg of sample was used for each DSC measurement.

Gel permeation chromatography (GPC): The $M_{\rm w}$ of polymer was determined using GPC (GPC, PL-GPC-220). Samples were prepared having approximately concentration of 1–2 mg/mL in trichlorobenzene (mobile phase) by using the sample preparation unit (PL-SP 260) with filtration system at a temperature of 140 °C. The dissolved and filtered samples were transferred into the GPC instrument at 140 °C. The calibration was conducted using the universal calibration curve based on narrow polystyrene standards.

Results and discussion

Characterization of supports

In this study, two kinds of silica with different pore diameters were used as a supporting material for catalyst. By investigating their porous properties with N₂ physisorption, they were classified according to the size of pores. Large pore (LP) denotes the Q-50 silica having an average pore diameter of 380 Å, and small pore (SP) denotes the P-10 silica having an average pore diameter of 170 Å. Besides using both silicas in pristine condition, they were modified by gallium (SP-Ga and LP-Ga) for improving some specific properties before use. Thus, there were four kinds of supports used in this polymerization system. The specific properties of them are shown in Table 1. It can be seen from this table that after modification by Ga, both supports (SP and LP) exhibited decreased surface area and also pore volume compared to the supports before modification (SP-Ga and LP-Ga). This was due to the partial blockage of pore by Ga nitrate used for the modification procedure. In addition, according to the XPS investigation on Ga-modified supports conducted by Campos et al. [13], it was suggested that Ga modifiers were mostly deposited at the surface of the supports, but some of them can penetrate into the



Table 1 Specific properties of various supports obtained from N2 physisorption

Supports	Pore diameter (Å)	Pore volume (cm ³ /g)	Surface area (m ² /g)
SP	171	6.5	216.8
LP	369	1.36	70.9
SP-Ga	190	1.4	169.7
LP-Ga	320	0.2	68.8

surface and being present in the bulk of the support. The average pore diameters of the supports before and after modification slightly changed. The XRD patterns (not shown) for all supports were similar exhibited only a board peak between 20° and 30°, as seen typically for the conventional amorphous silica. No XRD peaks of Ga were observed after impregnation due to its highly dispersed form.

Effect of pore size of silica supports

As seen in Table 2, the LP silica exhibited higher catalytic activity than that of the SP silica. Although most MMAO is presumed located mostly at the external surface [10], some is located at the internal surface too. This can be observed from the effect of pore size of the silica support which still existed in this comparison. To grasp the effect of pore size, the internal diffusion resistance needs to be considered. In general, the supports with SP size result in poor intra-pellet diffusion efficiency and slow transportation of reactants and products due to strong diffusion resistance [14], contrasting with the supports with LP size, which are able to diminish the diffusion resistance by their large pores. Then, copolymerization conducted with LP size support exhibited higher catalytic activity than that with SP size support. Another parameter which provides compelling evidence is the copolymerization time of the systems. It can be obviously seen that copolymerization time of the LP silica system (LP and LP-Ga) was shorter than that of the SP silica system (SP and SP-Ga) indicating that propagation rate of system with the LP silica was higher, due to monomer and comonomer being able to reach to the catalytic active sites more easily even located inside the pores. In addition, silica with smaller diameters could

Table 2 Catalytic activities in ethylene/1-hexene copolymerization with different supports

Supports	Time ^a (s)	Yields (g)	Catalytic activity ^b (kg polymer/mol Ti h)
SP	233	0.8681	1341
LP	170	0.7941	1682
SP-Ga	186	0.9919	1920
LP-Ga	140	0.7632	1893
SP-Ga	186	0.9919	1920

^a Time when all ethylene (0.018 mol) was consumed

 $^{^{\}rm b}$ Copolymerization condition: Ti = 10 μ mol, Al/Ti = 400, temperature = 70 $^{\circ}$ C, 50 psi of ethylene pressure was applied



display the lower catalytic activities probably due to the higher probability of formation for the bimolecular species as described by Silveira et al. [15].

Effect of Ga modification on silica surface

To investigate an effect of Ga as modifying agent for silica support, comparisons were drawn between modified and unmodified supports on both types of silica. As seen from Table 2 (SP vs. SP-Ga, LP vs. LP-Ga), Ga modification can increase catalytic activity in both types of silica. It has been known that adding Ga into silica surface normally increases acidic sites to the silica support [13, 16]. These sites are required to activate metallocene catalyst to be an active species in supported system. Many inorganic supports which possess the strong Lewis acidic property, such as Al₂O₃ and MgCl₂ have been used as support for this purpose [17]. For silica, directly using as a support for metallocene catalysts preparation resulted in inactive catalysts formation [18]. However, in this method, MMAO took charge of main activating agent as usual in metallocene catalyst system and Ga can assist in the activation by increase Lewis acidity in support as mentioned. Furthermore, Ga can be anchored on the surface of silica, thus lower interaction between active sites and support. The result of higher catalytic activity by Ga modification accorded with the finding of Campos et al. [19], which found that introducing Ga into supports can improve the ability of the supports to immobilize metallocene, and then enhancing the catalytic activity of the systems. Improving ability to immobilize (grafting the substances) by Ga was also reported by Morrow and McFarlane [20]. They found that the introduction of species such as PH3 and AsH3 into the silica surface was more strongly adsorbed when silica was first reacted with the Ga.

When comparing the activities of system with Ga modification on both silica types, it revealed that the SP silica showed slightly higher catalytic activity. This was opposite to the result of activities before modifying the support. This is because the SP silica has higher surface area than that of the LP silica. Then, Ga modification, which mainly affected on the surface properties of support, can more efficiently influence catalytic behavior in higher surface area support than the lower surface area support. Therefore, after modification the SP silica would give the higher activity than that of the LP silica due to higher surface area.

Characterization of copolymers

The triad distribution for all copolymers investigated by 13 C NMR is also shown in Table 3. The triad block of comonomer (HHH) was not detected for all samples. This suggests that the good distribution of comonomer throughout the copolymer chain existed in the systems. In addition, the products of reactivity ($r_{\rm E}r_{\rm H}$) of some sample (SP-Ga) also showed the characteristic of random copolymers ($r_{\rm E}r_{\rm H} > 1$), and the rest of them showed the typical alternating copolymer character ($r_{\rm E}r_{\rm H} < 1$). Both silicas provided higher $M_{\rm w}s$ for the copolymers after Ga modification. This was probably due to Ga modifier enhanced propagation rate, but reduced termination rate (chain transfer) in polymerization. It was also observed that Ga



had more effect on the $M_{\rm w}$ of polymer obtained by the smaller pore silica than the larger one due to higher surface area of the smaller pore silica as mentioned earlier.

Effect of pore size of silica supports

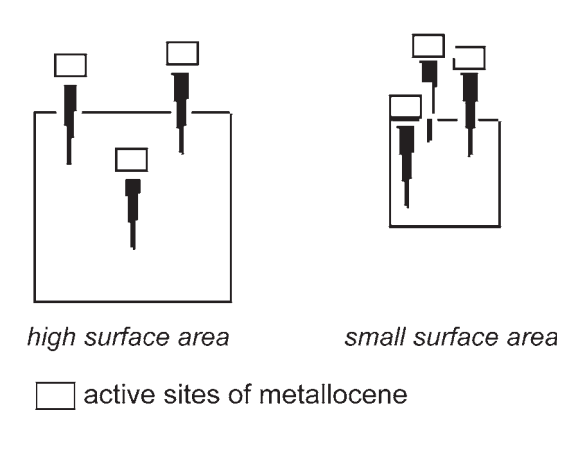
It can be observed from Table 3 that both pore size silicas produced copolymers with nearly the same incorporations of 1-hexene (SP and LP). In general, the LP silica should supply more comonomer for propagating the copolymer chain than the SP silica due to lower diffusion resistance within the pores. However, another factor which can influence on the incorporation of comonomers is the surface area of the supports. Regarding to surface area, the support with large surface area is expected to produce copolymers with high incorporation of comonomer as a result of more space between active sites dispersed on its surface area compared to the support with smaller surface area, as seen in Fig. 1. Then, the SP size silica with higher surface area would probably result in high comonomer incorporation with this effect. Therefore, from the result that showed a roughly equal amount of 1-hexene comonomer incorporation for two different textures of silicas indicated that both effects (pore size and surface area) have a profound impact at the same level upon the incorporation of 1-hexene in the obtained copolymers.

Table 3 Properties of the obtained copolymers examined by ¹³C-NMR and GPC

Supports	EEE	EEH	HEH	EHE	EHH	ННН	$r_{\rm E}r_{\rm H}^{\rm a}$	% H ^b	$M_{\rm w}^{\rm c}$
SP	0.367	0.269	0.041	0.156	0.166	0.000	0.969	32.2	26
LP	0.359	0.272	0.046	0.163	0.159	0.000	0.873	32.3	24
SP-Ga	0.410	0.246	0.038	0.149	0.157	0.000	1.108	30.6	37
LP-Ga	0.422	0.280	0.039	0.159	0.099	0.000	0.737	25.8	27
Lr-Ga	0.422	0.280	0.039	0.139	0.099	0.000	0.737	23.8	21

^a Relative comonomer reactivities ($r_{\rm E}$ for ethylene and $r_{\rm H}$ for 1-hexene) calculated by $r_{\rm E}=2$ [EE]/[EH]X, $r_{\rm H}=2$ X[HH]/[EH], [EE] = [EEE] + 0.5[HEE], [HH] = [HHH] + 0.5[EHH], [EH] = [HEH] + 0.5[HEE] + [EHE] + 0.5[EHH]

Fig. 1 Comparison of active site dispersion on the different surface areas





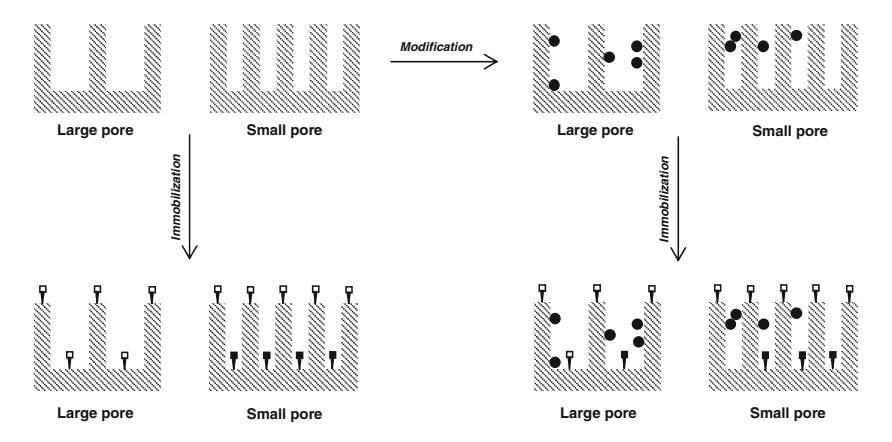
^b 1-Hexene incorporation

^c Molecular weight (kg/mol) obtained from GPC

Effect of Ga modification on silica surface

Comparing between SP and SP-Ga alongside LP and LP-Ga, we found that when modifying surface of silica support with Ga, the 1-hexene incorporations were decreased in both types of silica. This can be explained by the effect of surface area. Since both silicas had lower surface area through modifying procedure by Ga as follows; in LP 70.9 to 68.8 m²/g and in SP 216.8 to 169.7 m²/g. Although incipientwetness impregnation used in the modification is the easiest method of introducing a metal precursor, it results in the precipitation of small particles of the salt onto the support surface [21]. Therefore, the decrease in the surface area may be due to the partial blockage of pore by excess Ga nitrate. As seen from Fig. 2, the excess substances more seriously affect on the decrease in surface area of the SP silica than the LP silica because the SPs can be blocked by the deposit easier compared to the LP. Therefore, after modification with Ga, the significant decrease in surface area occurs in the SP silica, contrasting to that with the LP silica, which has only slight decrease. The average pore diameter shown in Table 1 also reveals that the blockage seriously affects on the smaller pore sizes by decreasing the population of the smaller pore sizes (the SPs become shallower until disappear), and then the average pore sizes are shifted to higher value (from 171 to 190 Å).

The decrease in 1-hexene incorporation in the copolymer obtained from both silicas after modification by Ga was opposite to the decrease in surface area. The significant decrease was observed for the LP silica instead. The reason for this can be explained as seen in Fig. 2. The active sites with high enough space for high 1-hexene incorporation were indicated in the figure by an open square while a filled square indicated the active sites with insufficient space for high 1-hexene incorporation. It can be seen that high space sites (open square) in the LP silica



- : Low space active site
- : Gallium nitrate salt

Fig. 2 Conceptual model for impact of pore blockage on supports with different pore sizes



were decreased noticeably after modification, whereas the number of the high space sites in the SP silica remained the same. The high space sites in the SP silica are always located outside the pores, and therefore they can not be affected by the deposit of excess Ga inside the pores. On the other hand, in the LP silica, these sites are sometimes located inside the pores, then the deposit on the wall of pores can hinder them from being reached by a large size molecules, especially for 1-hexene comonomer. Hence, the incorporation of 1-hexene in the LP silica system decreased significantly after the support was modified by Ga.

In addition, this proposed model (Fig. 2) can explain the previous results reported by our research group that sites with no or low 1-hexene incorporation rates (insufficient space site, filled square) were more prevalent at short polymerization times [7]. It can be seen from the model that the said sites usually located inside the pore, so therefore at initial time of polymerization it still had an impact in polymerization. After the long period of polymerization, the supports were covered by the growing chain of polymer and then, hindered the (co)monomer to reach inside of pores, thus decreasing the impact of the sites located inside the pores in polymerization. So if the polymerization time was longer, it would be found the fraction of polymer producing from sites with no or low 1-hexene incorporation rates. However, this model should be used together with the multigrain model [22] and the fragmentation of the particles should be neglected.

The model in Fig. 2 also indicated that different types of catalytic sites are present in these catalysts, according to the findings of Kumkaew et al. [7] which suggested that pore sizes can influence the type of catalytic sites present in the supports. The various sites derived from different environments which mainly point to steric hindrance as seen in the model. The hindrance is not just to the monomer to attack the site, but also to MMAO in forming cocatalysts-counterion fit and salvation, which plays a significant role in the structures and energetic of the ion pairing proposed by Lanza et al. [23]. Therefore, the alteration of selectivity by different pore sizes may be one of the reasons for the change in 1-hexene incorporations.

To support that the copolymers were obtained from different catalytic sites, one simple technique that can be used for this purpose is the DSC. As known, the DSC endotherms were influenced by many factors such as the crystallinity and $M_{\rm w}$ of polymer, then being difficult to identify each peak occurring clearly. However, they could brief necessary information about characteristic of catalyst as recommended by Kumkaew et al. [7] that DSC of nascent polymer may provide information on heterogeneity of supported polymerization catalysts.

From Fig. 3, it can be seen that the copolymers obtained from the unmodified supports exhibited several DSC endotherm peaks, whereas the ones obtained from the Ga-modified supports exhibited broader peaks. Nevertheless, all of them indicate multiple types of catalytic sites. The slight difference in characteristic of peaks between the Ga-modified support and the unmodified one may be derived from the change in surface nature of the support after modification, particularly the heterogeneous nature. Another parameter that provides information about heterogeneity of the support is the molecular weight distribution (MWD) of the obtained polymers. The MWD as measured by GPC of the samples are; SP = 2.8, SP-Ga = 2.9, LP = 1.8, and LP-Ga = 2.3. It can be seen that after modification both silicas



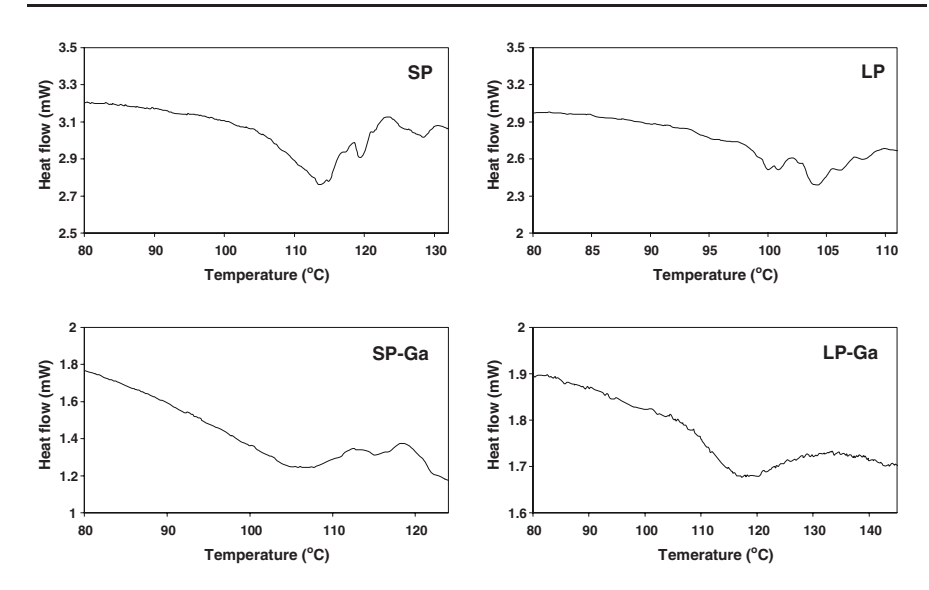


Fig. 3 DSC endotherms of LLDPE synthesized with various SiO₂ supports

exhibited broader MWD values, suggesting more heterogeneous nature. This may imply that silicas after modification by Ga have a greater degree of heterogeneity in catalytic sites. Therefore, it can be concluded that Ga addition into silica also changed the nature of catalyst and provide more heterogeneity in catalytic sites to supported system.

Conclusion

The higher catalytic activity of the LP silica was observed as a result of low internal diffusion resistance. However, after Ga modification, the SP silica exhibited higher catalytic activity. This is because Ga modification, which mainly improves properties of surface, more efficiently influences properties on silica with higher surface area. Then, the SP silica with higher surface can receive more improvement from Ga and raising more catalytic activities than the LP silica with lower surface area. Moreover, effect of surface area also caused change in 1-hexene incorporation, where a decrease in 1-hexene incorporation was evident with decreased surface area. In addition, different types of catalytic sites were observed, and then used to construct a model which helped explain the results.

Acknowledgments The authors thank the Thailand Research Fund (TRF), Office of the Higher Education Commission (CHE) and PTT Public Company Limited for the financial support of this project.

References

 Simpson DM, Vaughan GA (2003) Ethylene polymers, LLDPE. In: Mark HF (ed) Encyclopedia of polymer science and technology. Wiley, New York, pp 441–482. doi:10.1002/0471440264.pst122



- Severn JR, Chadwick JC, Duchateau R, Friederichs N (2005) "Bound but not gagged"—Immobilizing single-site a-olefin polymerization catalysts. Chem Rev 105:4073–4147. doi:10.1177/0010414 001034005002
- Kaminsky W, Albers I, Vathauer M (2002) New copolymers of olefins and styrene by metallocene catalysis. Des Monomers Polym 5:155–162. doi:10.1163/156855502760157881
- Shiono T, Yoshida S, Hagihara H, Ikeda T (2000) Additive effects of trialkylaluminum on propene polymerization with (t-BuNSiMe2Flu)TiMe2-based catalysts. Appl Catal A Gen 200:145–152. doi: 10.1016/S0926-860X(00)00633-5
- Silveira F, Pires GP, Petry CF, Pozebon D, Stedile FC, Santos JHZd, Rigacci A (2007) Effect of the silica texture on grafting metallocene catalysts. J Mol Catal A Chem 265:167–176. doi:10.1016/j. molcata.2006.10.008
- Kumkaew P, Wanke SE, Praserthdam P, Danumah C, Kaliaguine S (2002) Gas-phase ethylene polymerization using zirconocene supported on mesoporous molecular sieves. J Appl Polym Sci 87:1161–1177. doi:10.1002/app.11515
- 7. Kumkaew P, Wu L, Praserthdam P, Wanke SE (2003) Rates and product properties of polyethylene produced by copolymerization of 1-hexene and ethylene in the gas phase with (n-BuCp)₂ZrCl₂ on supports with different pore sizes. Polymer 44:4791–4803. doi:10.1016/S0032-3861(03)00473-7
- Ko YS, Woo SI (2003) Shape and diffusion of the monomer-controlled copolymerization of ethylene and a-olefins over Cp₂ZrCl₂ confined in the nanospace of the supercage of NaY. J Polym Sci Pol Chem 41:2171–2179. doi:10.1002/pola.10762
- Chaichana E, Khaubunsongserm S, Praserthdam P, Jongsomjit B (2010) Ethylene–hexene copolymer derived from [t-butylfluorenylsilyl-amido] dimethyl titanium complex. Express Polym Lett 4:94–100. doi:10.3144/expresspolymlett.2010.14
- Wannaborworn M, Jongsomjit B (2009) Ethylene/1-octene copolymerization over Ga-modified SiO₂supported zirconocene/MMAO catalyst using in situ and ex situ impregnation methods. Iran Polym J
 18:969–979
- Hagihara H, Shiono T, Ikeda T (1998) Living polymerization of propene and 1-hexene with the [t-BuNSiMe₂Flu]TiMe₂/B(C6F5) 3 catalyst. Macromolecules 31:3184–3188. doi:10.1021/ma971697k
- Pothirat T, Jongsomjit B, Praserthdam P (2008) Effect of Zr-modified SiO₂-supported metallocene/ MAO catalyst on copolymerization of ethylene/1-octene. Catal Lett 121:266–273. doi:10.1007/s 10562-007-9327-y
- Campos JM, Lourenco JP, Fernandes A, Rego AM, Ribeiro MR (2009) Mesoporous Ga-MCM-41 as support for metallocene catalysts: acidity-activity relationship. J Mol Catal A Chem 310:1–8. doi: 10.1016/j.molcata.2009.05.012
- Iglesia E, Reyes SC, Madon RJ (1991) Transport-enhanced a-olefin readsorption pathways in Ru-catalyzed hydrocarbon synthesis. J Catal 129:238–256. doi:10.1016/0021-9517(91)90027-2
- Silveira F, MdCM Alves, Stedile FC, Pergher SB, Rigacci A, JHZd Santos (2009) Effect of the silica texture on the structure of supported metallocene catalysts. J Mol Catal A Chem 298:40–50. doi: 10.1016/j.molcata.2008.10.011
- Takahara I, Saito M, Inaba M, Murata K (2004) Effects of pre-treatment of a silica-supported gallium oxide catalyst with H₂ on its catalytic performance for dehydrogenation of propane. Catal Lett 96:29–32, doi:10.1023/B:CATL.0000029525.33197.89
- Finch WC, Gillespiy RD, Hedden D (1990) Organometallic molecule-inorganic surface coordination and catalytic chemistry, in Situ CPMAS NMR delineation of organoactinide adsorbate structure, dynamics, and reactivity. J Am Chem Soc 112:6221–6232. doi:10.1021/ja00173a009
- Jongsomjit B, Kaewkrajang P, Shiono T, Praserthdam P (2004) Supporting effects of silica-supported methylaluminoxane (MAO) with zirconocene catalyst on ethylene/1-olefin copolymerization behaviors for linear low-density polyethylene (LLDPE) production. Ind Eng Chem Res 43:7959–7963. doi: 10.1021/ie049548v
- Campos JM, Lourenco JP, Fernandes A, Ribeiro MR (2008) Mesoporous Ga-MCM-41: a very efficient support for the heterogenisation of metallocene catalysts. Catal Commun 10:71–73. doi: 10.1016/j.catcom.2008.07.038
- Morrow BA, McFarlane RA (1986) Trimethylgallium adsorbed on silica and its reaction with phosphine, arsine, and hydrogen chloride: an infrared and Raman study. J Phys Chem 90:3192–3197. doi:10.1021/j100405a029
- 21. Hegedus LL (1987) Catalyst design, progress and perspectives. Wiley, New York



- Laurence RL, Chiovetta MG (1983) Heat and mass transfer during olefin polymerization from the gas phase. In: Reichert KH, Geiseler W (eds) Polymer reaction engineering. Hanser, New York, pp 73–111
- pp 73–111

 23. Lanza G, Fragala' IL, Marks TJ (2002) Energetic, structural, and dynamic aspects of ethylene polymerization mediated by homogeneous single-site "constrained geometry catalysts" in the presence of cocatalyst and solvation: an investigation at the ab initio quantum chemical level. Organometallics 21:5594–5612. doi:10.1021/om0207764





Article

The Influence of *t*-Butyl and Cyclododecyl Substitution on Ethylene/1-Hexene Copolymerization Using Ansa-Fluorenylamidodimethyltitanium Derivatives

Patcharaporn Kaivalchatchawal 1 , Piyasan Praserthdam 1 , Yuuichi Sogo 2 , Zhengguo Cai 2 , Takeshi Shiono 2 and Bunjerd Jongsomjit 1,*

- ¹ Center of Excellence on Catalysis and Catalytic Reaction Engineering, Department of Chemical Engineering, Faculty of Engineering, Chulalongkorn University, Bangkok 10330, Thailand
- ² Department of Applied Chemistry, Graduate School of Engineering, Hiroshima University, Higashi-Hiroshima 739-8527, Japan
- * Author to whom correspondence should be addressed; E-Mail: bunjerd.j@chula.ac.th; Tel.: +66 2 2186869; Fax: +66 2 2186877.

Received: 9 March 2011; in revised form: 9 May 2011 / Accepted: 12 May 2011 / Published: 19 May 2011

Abstract: In the present study, copolymerization of ethylene and 1-hexene was conducted with a series of ansa-fluorenylamidodimethyltitanium complexes, including [t-BuNSiMe₂Flu]TiMe₂ (complex 1), [cyclododecylNSiMe₂Flu]TiMe₂ (complex 2) and [t-BuNSiMe₂(2,7-t-Bu₂Flu)]TiMe₂ (complex 3), activated by MMAO. The effect of these catalysts on catalytic behavior, namely activity, molecular weight and monomer reactivity ratios, has been investigated. The results showed that all of them acted by a single site polymerization mechanism and the molecular weight distribution is independent of catalyst structure. Based on the study, it revealed that the introduction of a t-butyl at the 2,7 position on the fluorenyl ligand is able to enhance both catalytic activity and copolymer molecular weight more than introducing a cyclododecyl on the amine, which is probably associated with the electronic effect exerted by the t-butyl substituent. The comonomer incorporation content was controllable over a wide range by adjusting the comonomer feed ratio. Moreover, referring to monomer reactivity ratio exploration, it seems that the substitution on the ansa-fluorenylamidodimethyltitanium complex tends to hinder the insertion of 1-hexene into the polymer chain, leading to the highest 1-hexene content for traditional complex 1.

Keywords: polymer synthesis; catalytic synthesis; polyolefins; metallocene catalyst; CGC catalyst

1. Introduction

At present, linear low density polyethylene (LLDPE) is regarded as an important type of polyethylene and is also well recognized as economically attractive, accounting for more than half of the annual worldwide polymer production due to its distinctive processing and mechanical properties [1]. Copolymerization of ethylene and α -olefins, such as 1-butene, 1-hexene and 1-octene, is a general way to generate LLDPE with short chain branching. This copolymerization usually involves a constrained geometry catalyst (CGC) which has opened active sites for easy insertion of high α -olefins [2-5]. Superior to conventional Zeigler-Natta and metallocene catalysts, CGCs are capable of improving products in terms of much higher comonomer incorporation, narrower comonomer and molecular weight distribution which leads to better mechanical and physical properties. However, the incorporation of α -olefins that would result in the polymer properties depends on the structure of catalyst employed during copolymerization [1,6,7]. In fact, small variations of the ligand structure or ligand substituents may cause profound changes in the catalytic activity, copolymerization behavior and properties of the resulting polymer [3-5,8]. Therefore, by knowing the nature of catalysts, properties can be controlled and altered in order to achieve the desired LLDPE.

In this research, complexes 1, 2 and 3 (Scheme 1) were synthesized and further used as the catalysts for ethylene/1-hexene copolymerization to investigate the effect of the CGC-titanium complex on the copolymerization behavior.

Scheme 1. Ethylene/1-hexene copolymerization system.

2. Results and Discussion

The ethylene/1-hexene copolymerization with catalyst complexes 1, 2 and 3 was carried out at 273 and 298 K under atmospheric pressure whereas the polymerization time of each batch was adjusted so as to keep the comonomer conversion relatively constant for the purpose of acceptable reactivity ratio evaluation. The catalytic results are tabulated in Table 1.

Table 1. Summary of ethylene/1-hexene copolymerization catalytic activities and properties of copolymers.

Entry a)	1- hexenem ol'L ⁻¹	Time s	Yield g	Activity b) kg·mol ⁻¹ Ti·h ⁻¹	cont	$\mathbf{M}\mathbf{w}^{\mathrm{d})}$ $\mathbf{k}\mathbf{g}\mathbf{m}\mathbf{ol}^{-1}$	MWD e)
Т	0.75	60	0.6832	2050	-	-	-
1-1	0.075	210	0.0265	23	37.2	27	1.44
1-2	0.15	240	0.0835	63	37.8	25	1.53
1-3	0.45	360	0.2477	122	62.1	44	1.73
1-4	0.75	200	0.3688	221	74.3	49	1.53
1-5	1.5	180	0.3691	369	72.1	60	1.51
2-1	0.075	180	0.0813	81	30.1	26	1.61
2-2	0.15	120	0.1514	227	40.7	35	1.47
2-3	0.45	120	0.2250	338	57.9	36	1.54
2-4	0.75	150	0.3399	408	66.9	38	1.58
2-5	1.5	180	0.6160	616	78.0	71	1.48
3-1	0.075	45	0.0856	342	33.8	37	1.7
3-2	0.15	45	0.1167	467	47.2	64	1.48
3-3	0.45	40	0.2089	940	64.1	166	1.83
3-4	0.75	35	0.5272	2711	63.0	329	1.70
3-5	1.5	30	0.6006	3604	68.3	415	1.50

^{a)} Entry T, 1-1, 1-2, 1-3, 1-4 and 1-5 used complex 1 as catalyst; Entry 2-1, 2-2, 2-3, 2-4 and 2-5 used complex 2 as catalyst; Entry 3-1, 3-2, 3-3, 3-4 and 3-5 used complex 3 as catalyst; b) polymerization condition: [Ti] = 20 μmol, MMAO as cocatalyst, [Al]/[Ti] = 400, liquid volume (toluene) = 30 mL, ethylene pressure = 1 atm, temperature = 273 K (except Entry T (293 K)); c) 1-hexene content in copolymer determined by ¹³C NMR; d) molecular weight determined by GPC using PS standard; e) molecular weight distribution (Mw/Mn) determined by GPC using PS standard.

Regarding the result of Entry T in Table 1, it can be seen that the activity of the complex **1** when the reaction was performed at 293 K was very high (2,050 kg·mol⁻¹ Ti·h⁻¹), leading to difficulty in controlling the comonomer conversion. As a consequence, the other polymerization temperature conditions were reduced to 273 K. For comparison of the three sets of catalytic systems, including using catalyst complexes **1**, **2** and **3**, the activity towards ethylene/1-hexene was in the order complex **3** > complex **2** > complex **1**. In detail, the attachment of *t*-butyl groups at the 2,7 positions of the fluorenyl ring significantly impacted the catalytic behavior of the CGC complex, causing about 7–10 times higher activity than that obtained from the original nonsubstituted complex **1**. This was in good agreement with the previous research on propylene polymerization under the specified polymerization conditions [9]. It also showed that this increased catalytic activity is presumably due to an enhancement of the propagation rate by the electronic effect of the alkyl groups. The introduction of cyclododecyl on the amine group also resulted in an increase of activity, but less pronounced.

Likewise, a similar trend in copolymerization activity for these complexes can be observed. As the 1-hexene feed concentration rose, the catalytic activity increased. Relating to Table 1, it is fair to say that the activity displayed by complex 3 was more sensitive to the comonomer concentration. This phenomenon has been generally known as "comonomer effect" and has been described in a large number of reports [2,10]. The rate-time profiles of copolymerization demonstrated that all profiles were similar, starting with the minimum initial value and then gradually increasing with time, proposing that no deactivation of catalyst occurred during the copolymerization.

The relevant GPC results of obtained copolymers are collected in Table 1. All of resultant polymers possessed middle to high molecular weight and unimodal molecular weight distribution (Mw/Mn < 2), conforming the single site polymerization behavior of the three complexes. Nevertheless, it is noticeable that the molecular weight of copolymer obtained with complex 3 was 3–5 times higher than that of the corresponding copolymers obtained with the remaining complexes. Therefore, we may concluded that the 2,7 *t*-butyl substituent has a profound effect on a molecular weight increase. This is probably ascribable to the fact that the electronic effect exerted by the substituent reduces the rate of chain termination. Considering the relationship between the molecular weight and comonomer feed concentration, the molecular weight of all copolymers produced by the three titanium complexes increased with the rise of concentration, contrary to the literature [2]. This trend was rather unexpected since comonomer incorporation usually favors chain termination on account of terminal double bonds formed by hydride β -elimination which are mainly between comonomer units, consequently causing lower molecular weight copolymers.

A quantitative analysis of triad distribution was carrried out using ¹³C-NMR spectra assignment [11] of ethylene/1-hexene copolymer and is shown in Table 2. As expected, for each catalyst complex employed, the incorporation of comonomer increased with an increase in 1-hexene concentration in the reaction medium. Even though the content was slightly dependent on the complex used, all CGC complexes yielded the copolymers with high 1-hexene content (>30% mol).

The best way to investigate a copolymerization is to measure the reactivity ratios of the ethylene monomer (\mathbf{r}_E) and 1-hexene comonomer (\mathbf{r}_H) which are defined as the ratio of homopropagation to the crosspropagation rate constants. Thus, in this work, the reactivity ratios were calculated from the Fineman-Ross method and also from the Kelen-TÜdÖs method [12,13].

Table 2. Triad distributions of obtained copolymers determined by ¹³C NMR.

Entry	1-hexene	[HHH]	[EHH]	[EHE]	[EEE]	[HEH]	[HEE]	[H]
	mol'L ⁻¹	%	%	%	%	%	%	%
1-1	0.075	0.0	23.8	13.4	15.8	10.5	36.5	37.2
1-2	0.15	0.0	21.9	15.9	19.4	10.8	32.0	37.8
1-3	0.45	19.9	32.5	9.7	4.7	18.8	14.4	62.1
1-4	0.75	36.8	33.3	4.2	0.0	15.9	9.8	74.3
1-5	1.5	28.7	37.4	3.5	0.0	14.0	16.4	72.1
2-1	0.075	0.0	11.7	18.4	28.4	7.0	34.5	30.1
2-2	0.15	7.8	14.8	18.1	21.8	13.5	24.0	40.7
2-3	0.45	16.5	28.4	13.0	6.3	18.6	17.2	57.9
2-4	0.75	48.3	11.6	7.0	13.4	19.7	0.0	66.9
2-5	1.5	43.8	34.1	0.0	0.0	12.1	9.9	78.0
3-1	0.075	4.6	10.4	18.8	28.2	10.0	27.9	33.8
3-2	0.15	8.8	20.6	17.8	11.7	15.1	26.0	47.2
3-3	0.45	29.8	24.5	9.8	5.6	13.7	16.7	64.1
3-4	0.75	27.1	25.8	10.0	6.6	15.4	15.0	63.0
3-5	1.5	31.4	32.3	4.6	2.1	11.8	17.8	68.3

For the calculations, all copolymerizations of each series were used, except the one with the lowest concentration due to the fact it was the most affected by the experimental error. Figures 1 and 2 show the Fineman-Ross and the Kelen-TÜdÖs plots for the complexes 1, 2 and 3, respectively, and the least squares best fit line. In general, a good fit of the experimental results in the straight line was observed in most cases. Table 3 gathers the reactivity ratios that were calculated from the mentioned methods. As seen on the Fineman-Ross and Kelen-TÜdÖs plots in Figures 1 and 2, the values of r_E and r_H determined by the former fitted the experimental data obtained. Thus, a straighter line can be observed. In other words, the Fineman-Ross model was likely to give a better fit to the real data than the Kelen-TÜdÖs model. In fact, the 1-hexene reactivity ratio (r_H) is able to describe the preference of 1-hexene incorporation into a polymer chain compared with the ethylene in the same chain end. Hence, with regard to Table 3, it can be observed that, all employed titanium complexes resulted in a tendency of ethylene incorporation into the polymer chain in comparison with 1-hexene. Furthermore, the difference in r_H owing to the structure of the CGC catalyst was found. The increasing ratio of 1-hexene reactivity (r_H) along with the enhancing capability of catalyst complexes to provide higher 1-hexene

content in copolymer can be concluded as follows: complex 1 > complex 2 > complex 3. According to this result, it can be proposed that the attachment of each substituent group on ansa-fluorenyl amidodimethyltitanium complex seems to be an obstacle for higher α -olefin insertion. Overall, the values of $r_E r_H$ of the polymers obtained from all titanium complexes suggested a tendency of the formation of alternating copolymer structure ($r_E r_H < 1$).

Figure 1. Fineman-Ross plots for the copolymers obtained with \mathbf{a}) complex 1 \mathbf{b}) complex 2 and \mathbf{c}) complex 3 where $\mathbf{F} =$ the mole ratio of ethylene and 1-hexene in the feed and $\mathbf{f} =$ the mole ratio of ethylene and 1-hexene in the copolymer.

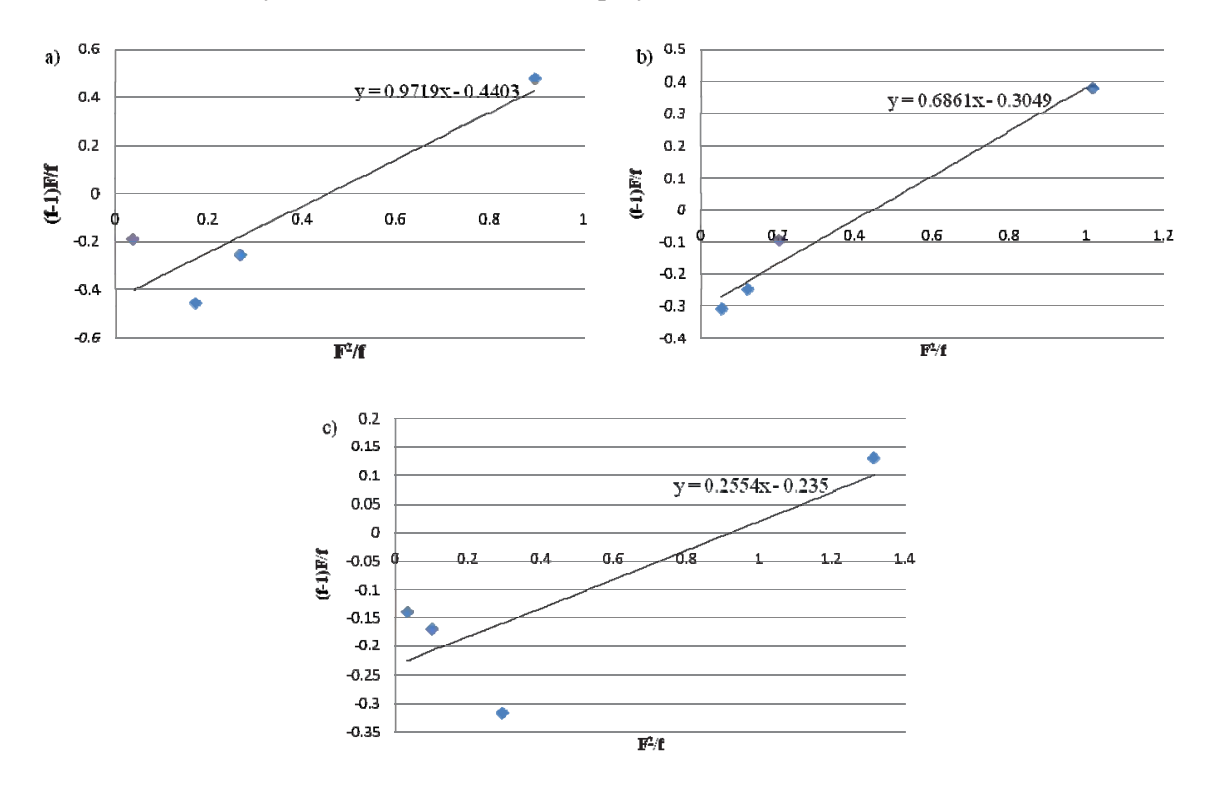
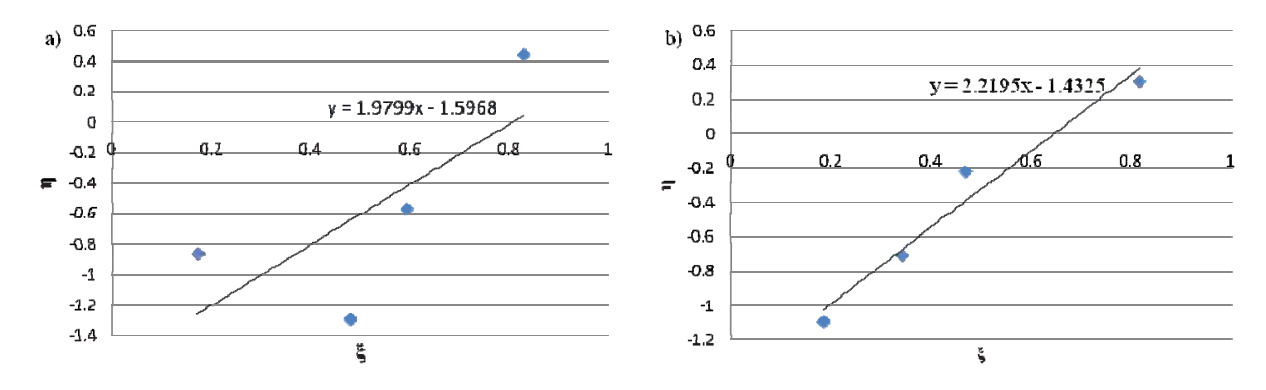


Figure 2. Kelen-TÜdÖs method plots for the copolymers obtained with **a**) complex 1 **b**) complex 2 and **c**) complex 3 where $\eta = G/(\alpha + F')$, $\xi = F'/(\alpha + F')$, G = (f-1)F/f, $F' = F^2/f$, $\alpha = (F'_{max}F'_{min})^{0.5}$, F = the mole ratio of ethylene and 1-hexene in the feed and f = the mole ratio of ethylene and 1-hexene in the copolymer.



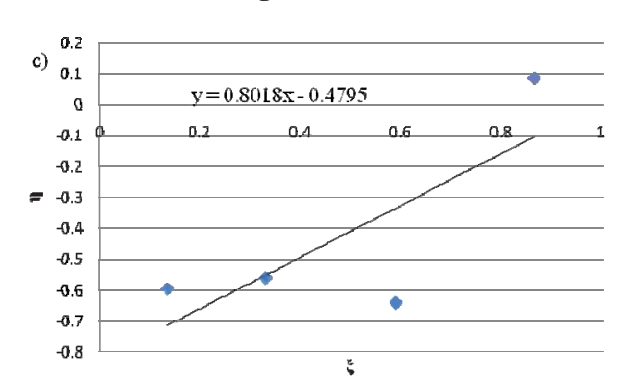


Figure 2. Cont.

Table 3. Reactivity ratios for each copolymerization system.

Complex	r _E ^{a)}	r _H b)	r _E c)	$r_{H}^{d)}$	_
1	0.97	0.44	0.76	0.30	
2	0.69	0.30	0.79	0.33	
3	0.26	0.24	0.32	0.10	

^{a)} Ethylene reactivity ratio calculated by Fineman-Ross method; ^{b)} 1-hexene reactivity ratio calculated by Fineman-Ross method; ^{c)} Ethylene reactivity ratio calculated by Kelen-TÜdÖs method; ^{d)} 1-hexene reactivity ratio calculated by Kelen-TÜdÖs method.

3. Experimental

3.1. Materials

All operations were performed under nitrogen gas using Schlenk techniques and all solvents were dried by usual procedures and freshly distilled before use. MMAO was donated by Tosoh-Finechem Co. Ltd. Research grade ethylene (Takachiho Chemicals Co.) was purified by passing it through columns of NaOH, P₂O₅, and 3Å molecular sieves, followed by bubbling through a NaAlH₂Et₂/1,2,3,4,-tetrahydronaphthalene solution. CGC complexes were synthesized according to procedures reported previously [14,15].

3.2. Polymerization Procedure

Ethylene/1-hexene copolymerization was performed in a 100 mL glass reactor equipped with a magnetic stirrer. After a desired amount of 1-hexene was dissolved in a toluene solution of MMAO, copolymerization was started by adding 1 mL solution of catalyst (20 μ mol). The polymerization was conducted for a certain time, and then was terminated by adding HCl/methanol solution. The obtained polymers were dried under vacuum at 333 K for 6 h.

3.3. Analytical Procedure

The molecular weight and molecular weight distribution were determined by GPC Waters 150 CV at 408 K using o-dichlorobenzene as a solvent and calibrated with polystyrene standards. The 13 C-NMR spectra of copolymers were recorded at 403 K on a JEOL GX 500 spectrometer operated at 125.65 MHz in the pulse Fourier-transform mode. The samples were prepared from using 1,1,2,2-tetrachloroethane- d_2 and the central peak of the solvent (74.47 ppm) was used as an internal reference.

4. Conclusions

Three CGC complexs, comprising complex 1 (unsubstituted complex), complex 2 (cyclododecyl substituent on the amine group) and complex 3 (2,7 *t*-butyl substituents on the fluorene ring), activated by MMAO were employed for ethylene/1-hexene copolymerization at 273 K to produce LLDPE. The introduction of both substituents is able to improve the activity and copolymer molecular weight. Nonetheless, it can be noticed that the 2,7 *t*-butyl group considerably impacted those features, achieving the highest activity of 3604 kg·mol⁻¹ Ti·h⁻¹ and the highest molecular weight of 415 kg·mol⁻¹. The polydispersity values of all obtained copolymers are less than 2, suggesting the single site behavior of all three titanium catalyst complexes. Moreover, the 1-hexene content of copolymers can be controlled by changing the comonomer feed concentration and is dependent on the catalyst structure as well. The comonomer reactivity ratio (r_H) result revealed that nonsubstituted titanium CGC complex yielded the highest tendency to incorporate 1-hexene into the copolymer chain.

Acknowledgements

The authors gratefully thank the *Dusadeepipat* scholarship (Chulalongkorn University Fund), Graduate school of Chulalongkorn University and Hiroshima University for the financial support of this work. The authors also extend the thankful for the Thailand Research Fund (TRF), Office of the Higher Education Commission (CHE), and CU-NRU (AM1088A).

References

- 1. Mulhaupt, R. Catalytic polymerization and post polymerization catalysis fifty years after the discovery of Ziegler's catalysts. *Macromol. Chem. Phys.* **2003**, *204*, 289-327.
- 2. Hong, H.; Zhang, Z.; Chung, T.; Lee, W. Synthesis of new 1-decene-based LLDPE resins and comparison with the corresponding 1-octene- and 1-hexene-based LLDPE resins. *J. Polym. Sci. A Polym. Chem.* **2007**, *45*, 639-649.
- 3. Cano, J.; Sudupe, M.; Royo, P. How to synthesize a constrained geometry catalyst (CGC) A survey. *J. Organomet. Chem.* **2007**, *692*, 4441-4423.
- 4. Braunschweig, H.; Breitling, F.M. Constrained geometry complexes Synthesis and applications. *Coord. Chem. Rev.* **2006**, *250*, 2691-2720.
- 5. Chum, P.S.; Swogger, K.W. Olefin polymer technologies-History and recent progress at The Dow Chemical Company. *Prog. Polym. Sci.* **2008**, *33*, 797-819.

6. Schellenberg, J. Influence of the catalyst on monomer insertion in the syndiospecific copolymerization of styrene and para-methylstyrene. *J. Polym. Sci. A Polym. Chem.* **2005**, *43*, 2061-2067.

- Wang, W.; Kolodka, E.; Zhu, S.; Hamielec, A.E. Continuous solution copolymerization of ethylene and octene-1 with constrained geometry metallocene catalyst. *J. Polym. Sci. A Polym. Chem.* **1999**, *37*, 2949-2957.
- 8. Liu, S.R.; Li, B.X.; Liu, J.Y.; Li, Y.S. Synthesis, structure and ethylene (co)polymerization behavior of new nonbridged half-metallocene-type titanium complexes based on bidentate beta-enaminoketonato ligands. *Polymer* **2010**, *51*, 1921-1925.
- 9. Cai, Z.; Ikeda, T.; Akita, M.; Shiono, T. Substituent effects of tert-butyl groups on fluorenyl ligand in syndiospecific living polymerization of propylene with ansa-fluorenylamidodimethyltitanium complex. *Macromolecules* **2005**, *38*, 8135-8139.
- 10. Grieken, R.V.; Carrero, A.; Suarez, I.; Paredes, B. Effect of 1-hexene comonomer on polyethylene particle growth and kinetic profiles. *Macromol. Symp.* **2007**, *259*, 243-252.
- 11. Eric, T.; Randall, C. Monomer Sequence Distributions in Ethylene-1-Hexene Copolymers. *Macromolecuels* **1986**, *15*, 1402-1411.
- 12. Tüdös, F.; Kelen, T.; Földes-Berezhnykh, T. Evaluation of high conversion copolymerization data by a linear graphical method. *React. Kinet. Cata. Lett.* **1975**, *2*, 439-447.
- 13. Fineman, M.; Ross, S.D. Linear Method for Determining Monomer Reactivity Ratios in Copolymerization. *J. Polym. Sci.* **1950**, *5*, 259-265.
- 14. Nishii, K.; Hagihara, H.; Ikeda, T.; Akita, M.; Shiono, T. Stereospecific polymerization of propylene with group 4 ansa-fluorenylamidodimethyl complexes. *J. Organomet. Chem.* **2006**, *691*, 193-201.
- 15. Cai, Z.; Nakayama, Y.; Shiono, T. Catalytic synthesis of a monodisperse olefin block copolymer using a living polymerization system. *Macromol. Rapid Commun.* **2008**, *29*, 525-529.

Sample Availability: Samples of the compounds are available from the authors.

© 2011 by the authors; licensee MDPI, Basel, Switzerland. This article is an open access article distributed under the terms and conditions of the Creative Commons Attribution license (http://creativecommons.org/licenses/by/3.0/).

ORIGINAL PAPER

Effects of Ti oxidation state on ethylene, 1-hexene comonomer polymerization by MgCl₂-supported Ziegler–Natta catalysts

Nichapat Senso · Piyasan Praserthdam · Bunjerd Jongsomjit · Toshiaki Taniike · Minoru Terano

Received: 12 November 2010/Revised: 13 June 2011/Accepted: 13 June 2011/Published online: 31 August 2011

© Springer-Verlag 2011

Abstract In this study, the influences of the Ti oxidation state on the catalytic properties of MgCl₂-supported Ziegler–Natta catalysts in ethylene homo- and co-polymerization with 1-hexene were investigated. Three catalysts having different Ti oxidation states were synthesized by milling TiCl₄, TiCl₃, or TiCl₂ together with MgCl₂. With these catalysts having different Ti oxidation states, the polymerization conditions such as the Al concentration, temperature, and 1-hexene concentration were varied to figure out their catalytic abilities in ethylene homo- and co-polymerization. The Ti oxidation state affected the catalyst activity largely, having unique dependences on the polymerization conditions. A higher oxidation state led to a higher activity, slightly larger comonomer incorporation, and lower molecular weight as well as its narrower distribution. However, rough characteristics of copolymers were similar among the different Ti oxidation states.

Keywords Ziegler–Natta catalyst · Titanium oxidation state · Polyethylene · Ethylene/1-hexene copolymerization · Ethylene polymerization

Introduction

Current industrial production of polyethylene and polypropylene still largely depends on MgCl₂-supported heterogeneous Ziegler–Natta (ZN) catalysts [1–3]. The mechanical and rheological properties of polyethylene and polypropylene are

N. Senso · P. Praserthdam · B. Jongsomjit

Department of Chemical Engineering, Center of Excellence on Catalysis and Catalytic Reaction Engineering, Faculty of Engineering, Chulalongkorn University, Bangkok 10330, Thailand

T. Taniike · M. Terano (⊠) School of Materials Science, Japan Advanced Institute of Science and Technology, 1-1, Asahidai, Nomi, Ishikawa 923-1292, Japan e-mail: terano@jaist.ac.jp



strongly affected by molecular weight (MW) and molecular weight distributions (MWD) [4–6, 8, 9] as well as by chemical composition distribution (CCD) in the case of copolymer. Therefore, it is industrially crucial to control these parameters by catalyst and polymerization technologies.

Homogeneous catalysts represented by metallocene catalysts are generally single-site catalysts so as to give monodisperse MW and chemical composition, and are advantageous in the incorporation of bulky or polar co-monomers. On the other hand, ZN catalysts are multi-sites catalysts and generally lead to broad MWD and CCD, which have been regarded to be advantageous for some polymer properties.

To control the MWD and CCD of polymers with Ziegler-Natta catalysts, the nature of active sites is critically important in a sense that different active sites produce polymers with different MWs and CCs. Several factors are responsible for the nature of active sites such as Ti nucreality [4, 7], dispersion [10], oxidation state [11, 13–19], interaction with MgCl₂ support [7, 12], and so on. The oxidation state of Ti species has been regarded as one of the key factors to cause CCD and MWD; Ti species undergo stepwise reduction during polymerization and as a result the Ti oxidation state becomes a mixture of tetravalent (Ti⁴⁺), trivalent (Ti³⁺), and divalent (Ti²⁺) states [17]. Many researchers have investigated the relationship between Ti oxidation state and polymerization performance. Baulin et al. [13] studied the effects of the Ti oxidation state on the activity of a TiCl₄/MgO catalyst by increasing alkylaluminum concentration. A contact of a TiCl₄/MgO catalyst with A1Et₃ under conditions similar to those of polymerization (A1/Ti of 150-200 for 1 h at 70 °C), more than 90% of Ti⁴⁺ was reduced (96% to Ti³⁺ and 4% to Ti²⁺). They were not able to find any quantitative correlation between the degree of Ti reduction and catalytic activity. It was found later that the catalytic activity decreased by precontact between catalyst and alkylaluminum [14, 17]. An even stronger reduction (80% Ti²⁺ and 20% Ti³⁺) has been reported by Kashiwa et al. [17] for a TiC1₄/EB/MgC1₂ catalyst after a 2-h reaction with A1Et₃ (A1/Ti = 50) at 60 °C. They also observed that the catalyst thus obtained was only slightly active for the polymerization of ethylene and completely inactive for propylene polymerization; however, the activity was recovered by re-oxidizing Ti with a chlorinating agent such as t-BuCl. It was concluded that a direct relationship exists between the activity and Ti oxidation state. Kissin et al. [20] studied a relationship of the molecular weight and chemical composition with the Ti oxidation state by varying the polymerization time from 5 to 40 min. Based on deconvolution of molecular weight and crystallinity distributions in gel permeation chromatography (GPC) and temperature rising elution fractionation (TREF), they obtained the following conclusions: (i) Ti⁴⁺ is active for ethylene and propylene homopolymerization and for ethylene/α-olefin copolymerization, and produces polymers with low molecular weights and high comonomer contents (ii) Ti3+ is also active for the above mentioned polymerization, producing polymers with moderately high molecular weight (iii) Ti²⁺ is active only for ethylene homopolymerization, giving very high molecular weight polymers. Zakharov et al. [6] have prepared Ti^{2+} (η^6 -benzene-Ti₂Al₂Cl₈), Ti³⁺ (TiCl₃·n-dibutylether), and Ti⁴⁺ (TiCl₄) supported on MgCl₂, and investigated behaviors of different Ti oxidation states in ethylene polymerization and ethylene/1-hexene copolymerization. Their results demonstrated that Ti²⁺,



Ti³⁺, and Ti⁴⁺ were highly active in both of ethylene polymerization and ethylene/ 1-hexene copolymerization, on the contrary to the results obtained by Kissin et al. [20]. The advantage of their work for the effects of the Ti oxidation state is to have prepared the catalysts from precursors with the corresponding oxidation states. However, not only the oxidation state but also the presence of the extra ligands such as *n*-dibutylether, and η^6 -benzene and Al₂Cl₆ might affect the catalytic behavior and polymer properties. In other words, it is not sure if the nature of η^6 -benzene-Ti₂Al₂Cl₈ is similar to that of TiCl₂ formed by reaction of TiCl₄ with alkylaluminum. Another research [21] showed that a higher temperature or a larger alkylaluminum/TiCl₄ ratio increases the activity until some optimum value for the average oxidation state is achieved, while the activity starts to drop beyond the optimum value. The optimum average oxidation state was Ti^{2.2+} for ethylene polymerization. A similar relation between the catalytic activity and optimum oxidation state was also found for different types of ZN catalysts such as TiCl₂, SiO₂/MgCl₂/THF/TiCl₄, and AlCl₃/TiCl₄ [22–24]. In finding a relationship of the oxidation state with MW and MWD of polyethylene, Zakharov et al. [5] conducted a comprehensive study with systematically varying the Ti oxidation and dispersion states using the above-mentioned three precursors [5, 6]. They found that isolated Ti²⁺ and Ti³⁺ ions supported on MgCl₂ were more active than a supported TiCl₄ catalyst, which turned into a mixture of isolated and clustered Ti3+ after the interaction with alkylaluminum. Moreover, it was shown that produced polyethvlene had similar MW and MWD in spite of the sharp distinctions in the Ti oxidation and dispersion states for their catalysts. Thus, the source of MWD was not straightforwardly understood.

From the previous reports mentioned above, the effects of the Ti oxidation state are still controversy on the catalytic activity, polymer molecular weight, and comonomer response in olefin polymerization using Ziegler–Natta catalysts. The co-presence of different Ti oxidation states during polymerization is still an importance problem. In this study, $TiCl_2$, $TiCl_3$, and $TiCl_4$ were directly supported on $MgCl_2$ to get better understanding on the role of the Ti oxidation state in ethylene homopolymerization and ethylene/1-hexene copolymerization. The activity behavior was found to be sensitive to the oxidation state of the $TiCl_x$ precursors, while polymer structures such as MW and CC were basically insensitive, supporting the previously obtained results [5, 6].

Experimental

Materials

Anhydrous $MgCl_2$ and α -Ti Cl_3 (donated by Toho Titanium Co., Ltd.), $TiCl_4$ (Wako Pure Chemical Industries, Ltd.), anhydrous $TiCl_2$ (Aldrich) and $AlEt_3$ (donated by Tosoh Finechem Co.) were used without further purification. Heptane (Wako Pure Chemical Industries, Ltd.) was used after dehydration by passing through a column with molecular sieve 13X, and 1-hexene (Wako Pure Chemical Industries, Ltd.) was distilled with sodium/benzophenone.



Catalyst preparation

Three kinds of MgCl₂-supported catalysts with different Ti oxidation states were prepared as follows [10].

- (i) TiCl₂/MgCl₂: 36 g of MgCl₂ and 2.34 g of TiCl₂ were put into a 1 L stainless steel pot containing 55 stainless steel balls (25 mm diameter) and then vibration ball-milled under nitrogen for 30 h at RT.
- (ii) TiCl₃/MgCl₂: 36 g of MgCl₂ and 3.1 g of TiCl₂ were similarly milled for 30 h at RT.
- (iii) TiCl₄/MgCl₂: 108 mL of TiCl₄, 108 mL of heptane and 36 g of MgCl₂ were similarly milled for 30 h at RT, and then the ground product was treated with TiCl₄ (200 mL) at 90 °C for 2 h with stirring under nitrogen, followed by washing with heptane repeatedly.

These catalysts, TiCl₂/MgCl₂, TiCl₃/MgCl₂, and TiCl₄/MgCl₂, are designated as Ti2M, Ti3M, and Ti4M. Their titanium contents were 2.36, 2.31, and 1.38 wt%, respectively.

Polymerization

Slurry polymerization in n-heptane was performed under constant ethylene pressure of 0.5 MPa at the polymerization temperature from 50 to 70 °C for 1 h. Triethylaluminum (TEA) was used as cocatalyst, whose concentration was 2.0–30.0 mmol/L. The polymerization was initiated by the injection of the catalyst slurry. The catalyst concentration in the polymerization slurry was fixed at 3.5 mg/L. Ethylene/1-hexene copolymerization was carried out under the same polymerization condition and procedure. The 1-hexene concentration was 2.5–10 vol%.

Polymer characterization

¹³C NMR spectra of copolymers were recorded on a Varian Gemini-300 spectrometer at 120 °C using 1,2,4-trichlorobenzene as a diluent and 1,1,2,2-tetrachloroethane-*d2* as a solvent. MW and MWD of polymers were determined by gel permeation chromatography (GPC, Alliance GPC 2000, Waters), using 1,2,4 trichlorobenzene as a mobile phase.

Results and discussion

Influence of Al concentration

The alkylaluminum concentration largely affects on the polymerization kinetics through activation and deactivation of Ti species. The deactivation rate was known to be correlated with the rate of reduction of Ti species [17]. Figure 1 shows the effect of the Al concentration on the Ti2M, Ti3M, and Ti4M catalytic activities in ethylene polymerization. The ethylene polymerizations rates for the three catalysts



showed different trends with increasing the Al concentration. In the case of Ti2M, it was rather constant, consistent with the previously reported results [23, 25]. This could be explained by the fact that Ti species can not be reduced over Ti²⁺ by alkylaluminum, and the formed active sites are regarded as quite stable with negligible deactivation with alkylaluminum. This conclusion was supported by previous experimental reports [5, 12, 26]. On the other hand, the ethylene polymerization rates for Ti3M and Ti4M increased, and then became nearly constant up to 10 mmol/L of the Al concentration. This trend appeared to be in agreement with the results obtained by Bresadola et al. [25]. They found that the catalytic activity for ethylene polymerization was nearly constant in the range of 50-200 Al/Ti. They observed a slow decrease of Ti⁴⁺ and Ti³⁺ amount accompanied with a small increase of Ti²⁺. The total amount of the Ti³⁺ and Ti²⁺ species, both of which are active for ethylene polymerization, was reported to be substantially constant, giving a constant activity. The catalytic activity for Ti4M once reached the maximum, and then gradually dropped over 2.0 mmol/L of the Al concentration, which differed from the constant trends for Ti2M and Ti3M. This could be explained by the fact that TiCl₄ easily migrates on MgCl₂ in the presence of alkylaluminum to aggregate with each other in the curse of the reduction, leading to the gradual decrease of the active site concentration [10]. TiCl₂ and TiCl₃, that are originally solids, are bound much more tightly than TiCl₄ on MgCl₂, to depress the aggregation-induced deactivation. Figure 2 shows the ethylene/1-hexene copolymerization activities with varying the alkylaluminum concentration. The activity of Ti2M was enhanced with the addition of a small amount of 1-hexene, although the activities were the lowest among the three catalysts. Interestingly, copolymers produced with Ti2M had similar composition and sequence distribution to those produced with the other two catalysts, even though the 1-hexene incorporation became lower for higher Al concentrations. These results are in disagreement with the previous explanation [20] that Ti²⁺ is comonomer insensitive and produces homopolyethylene only. In the case of Ti3M and Ti4M, the polymerization rates were drastically increased with the addition of 1-hexene, while the activity variation in terms of the Al concentration obeyed a similar trend for the homopolymerization in Fig. 1. The observed rate enhancement by the addition of 1-hexene is known as a rate enhancement effect by comonomer [27–29]. In the case of ethylene copolymerization with α-olefin, physical explanations seem more plausible, such as the acceleration of monomer diffusion through less crystallizable copolymers [30], and the acceleration of the catalyst fragmentation in copolymerization [29]. The difference in the observed rate enhancements by 1-hexene for the three catalysts might arise from the difference of their incorporation efficiency of 1-hexene.

Table 1 shows sequence distribution of ethylene/1-hexene (E/H) copolymers obtained at different Al concentrations. The copolymers contained 0.37–0.61 mol% of 1-hexene, in which butyl branches existed in an isolated manner without any HHH, HEH, and EHH triad sequences. All of Ti2M, Ti3M, and Ti4M show a similar trend, even though a higher oxidation state tends to lead to larger incorporation: the 1-hexene incorporation is the highest at the lowest Al concentration, and then drops for higher concentrations.



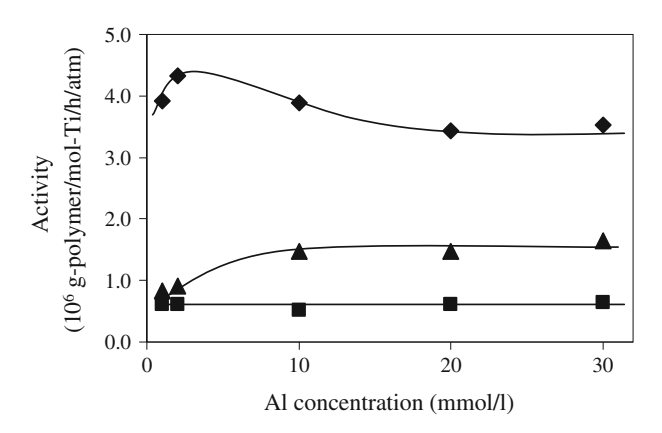


Fig. 1 Influence of the Al concentration on the ethylene homopolymerization activities. The homopolymerization was conducted at 60 °C for 1 h under 0.5 MPa of ethylene. TEA was used as cocatalyst (*filled diamond* Ti4M, *filled circle* Ti3M, and *filled square* Ti2M)

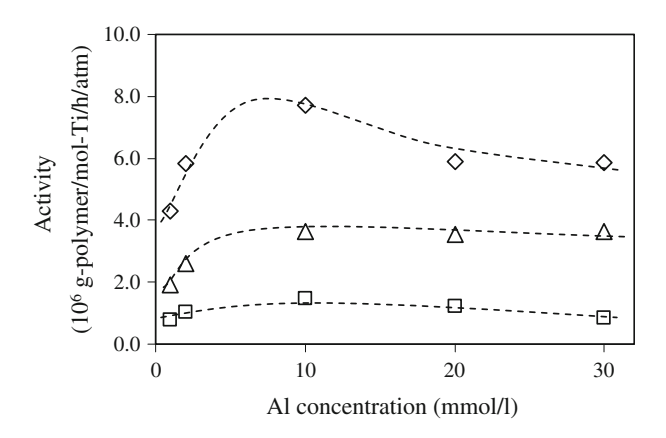


Fig. 2 Influence of the Al concentration on the ethylene copolymerization activities. The copolymerization was conducted at 60 °C for 1 h under 0.5 MPa of ethylene. 10 vol% of 1-hexene was added as the comonomer (*open diamond* Ti4M, *open circle* Ti3M, and *open square* Ti2M)

Influence of the polymerization temperature

The influence of the polymerization temperature on the activities of homo- and co-polymerization is shown in Fig. 3. The temperature was varied in the range of 50–70 °C. Higher catalyst activities for the ethylene homopolymerization were obtained by increasing the polymerization temperature. Although Ti4M was the most sensitive to the temperature change, the behavior was similar among the different Ti oxidation states. In comparison, the copolymerization activities increased more sharply than the homo-polymerization at 60 °C, but rather dropped at 70 °C, probably because the 1-hexene solubility was decreased upon increasing the reactor temperature.



Table 1 Sequence distribution of ethylene/1-hexene copolymers synthesized using $TiCl_x/MgCl_2$ catalysts (x = 2–4) at different Al concentrations

Catalyst	Al conc. (mmol/L)	ЕНЕ	ЕНН	ННН	HEH	EEH	EEE	1-hexene incorporated (mol%)
Ti2M	2.0	0.5	0.0	0.0	0.0	1.1	98.4	0.54
	10.0	0.4	0.0	0.0	0.0	0.7	98.9	0.37
	30.0	0.4	0.0	0.0	0.0	0.8	98.7	0.42
Ti3M	2.0	0.6	0.0	0.0	0.0	1.1	98.3	0.56
	10.0	0.5	0.0	0.0	0.0	1.0	98.5	0.52
	30.0	0.5	0.0	0.0	0.0	1.1	98.4	0.53
Ti4M	2.0	0.6	0.0	0.0	0.0	1.2	98.2	0.61
	10.0	0.6	0.0	0.0	0.0	1.1	98.4	0.55
	30.0	0.6	0.0	0.0	0.0	1.1	98.3	0.57

Polymerization conditions: catalyst amount = 3.5 mg/L, temperature = 60 °C, polymerization time = 1 h, ethylene pressure = 0.5 MPa, 1-hexene concentration = 10 vol%, TEA concentration = 2-30 mmol/L

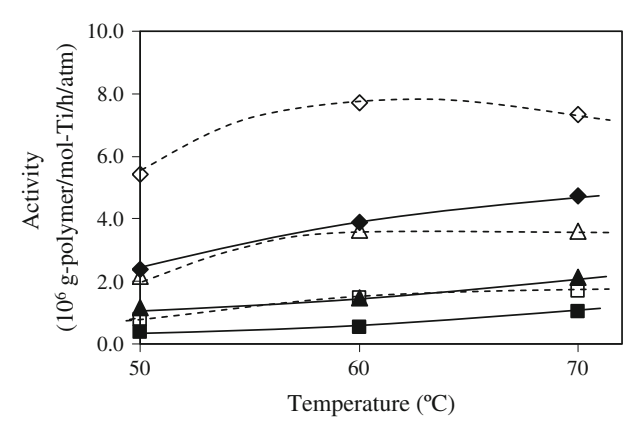


Fig. 3 Influence of the polymerization temperature on the activities of the ethylene homo- and copolymerization. The polymerization was conducted under 0.5 MPa of ethylene for 1 h. 10 mmol/L of TEA was used as cocatalyst. 10 vol% of 1-hexene was added in copolymerization

Influence of the 1-hexene concentration

The effects of the 1-hexene concentration on the polymerization rates and resulting polymer properties were investigated for the different Ti oxidation states. As shown in Fig. 4, all the catalysts activities were linearly increased for the 1-hexene concentration. The sequence distributions of copolymers prepared with the three catalysts are shown in Table 2. The produced copolymers again had similar composition and sequence distribution without sequential 1-hexene insertion. Incorporation of 1-hexene in copolymers was basically increased in correlation with the 1-hexene concentration, but not simply proportional to it. There might be a critical incorporation amount, below which the incorporation efficiency is lower for



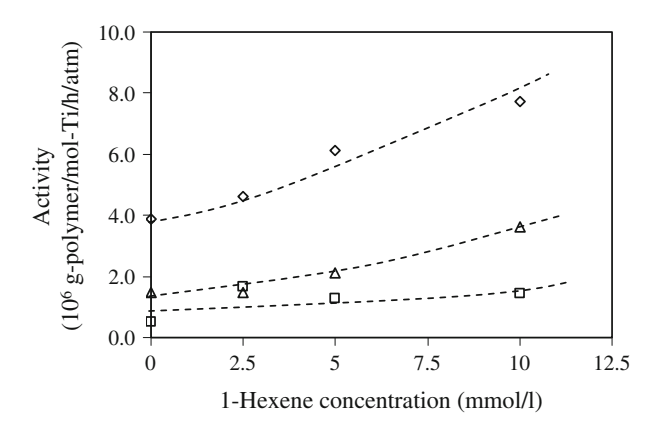


Fig. 4 Relationship between the 1-hexene concentration and catalytic activity. The copolymerization was conducted at 60 °C for 1 h under 0.5 MPa of ethylene. 10 mmol/L of TEA was used as the cocatalyst (open diamond Ti4M, open circle Ti3M, and open square Ti2M)

Table 2 Sequence distribution of ethylene/1-hexene copolymers synthesized using $TiCl_x/MgCl_2$ catalysts (x = 2–4) at different 1-hexene concentrations

Catalyst	1-Hexene injected (vol%)	ЕНЕ	ЕНН	ННН	HEH	EEH	EEE	1-Hexene incorporated (mol%)
Ti2M	2.5	0.2	0.0	0.0	0.0	0.4	99.4	0.20
	5.0	0.2	0.0	0.0	0.0	0.5	99.3	0.24
	10	0.4	0.0	0.0	0.0	0.8	98.8	0.42
Ti3M	2.5	0.3	0.0	0.0	0.0	0.6	99.1	0.32
	5.0	0.4	0.0	0.0	0.0	0.7	98.9	0.37
	10	0.5	0.0	0.0	0.0	1.0	98.5	0.52
Ti4M	2.5	0.3	0.0	0.0	0.0	0.6	99.1	0.30
	5.0	0.6	0.0	0.0	0.0	1.2	98.2	0.58
	10	0.6	0.0	0.0	0.0	1.1	98.4	0.55

Polymerization conditions: catalyst amount = 3.5 mg/L, temperature = 60 °C, polymerization time = 1 h, ethylene pressure = 0.5 MPa, 1-hexene concentration = 2.5-10 vol%, TEA concentration = 10 mmol/L

the 1-hexene concentration, and above which the incorporation efficiency discontinuously increases and then becomes stable. This might be related to some discontinuous change in the monomer diffusivity, in lowering the crystallinity by incorporation of 1-hexene. It is notable that a higher oxidation sate led to higher incorporation efficiency, even with the similar response to the 1-hexene concentration. The molecular weights and their distributions of copolymers synthesized with the three catalysts are summarized in Table 3. Ti2M produced a copolymer with the broadest MWD as compared with those obtained by Ti3M and Ti4M. The broadness of MWD for Ti2M arose mainly from the formation of a high-molecular weight tail, as indicated in the highest M_w . The lowest incorporation of 1-hexene and the highest molecular weight partly agrees with the previous proposal by Kissin



Table 3 Molecular weight and their distribution of copolymers synthesized using $TiCl_x/MgCl_2$ catalysts (x = 2-4)

Catalyst	$M_n \times 10^{-5}$	$M_w \times 10^{-5}$	M_w/M_n
Ti2M	3.6	14	4.0
Ti3M	3.2	12	3.7
Ti4M	3.7	12	3.2

Polymerization conditions: catalyst amount = 3.5 mg/L, temperature = 60 °C, polymerization time = 1 h, ethylene pressure = 0.5 MPa, 1-hexene concentration = 10 vol%, TEA concentration = 10 mmol/L

et al. [20]. However, it should be stressed that the obtained copolymers had roughly similar characteristics in CC and MW, in agreement with the results by Zakharov et al. [5, 6].

Conclusion

We have investigated the influences of the oxidation state on ethylene homo- and co-polymerization using MgCl₂-based Ziegler–Natta catalysts made directly from TiCl₄, TiCl₃, and TiCl₂ precursors. The Ti oxidation state had large effects on the catalytic activity in both of ethylene homo- and co-polymerization with 1-hexene. Especially, TiCl₂/MgCl₂ had a unique response that was very different from TiCl₄/MgCl₂ and TiCl₃/MgCl₂ upon varying the Al concentration and 1-hexene concentration. All the copolymers produced by the catalysts had similar sequence distribution, even though the increase of the oxidation state caused a slight enhancement of 1-hexene incorporation. Similarly, molecular weights and their distributions of the copolymers were not largely dependent on the Ti oxidation state. It is worth noting that these results are in accordance with those from Zakharov et al. [5,6] even through the catalyst precursors to obtain the different oxidation states of Ti were different. Thus, it was concluded that the oxidation state was not important for the copolymer characteristics, while it played a major role in the catalytic activity.

Acknowledgments The authors thank the Thailand Research Fund (TRF), Office of the Higher Education Commission (CHE), and PTT Company for the financial support of this project.

References

- Lynch DT, Jejelowo MO, Wanke SE (1991) The influence of aluminum alkyls on the polymerization of ethylene with silica/magnesium chloride-supported titanium tetrachloride catalysts. Can J Chem Eng 69:657–664
- Piotr S (1989) The role of magnesium chloride as supporter for the new generation of olefin polymerization catalysts. Polym Plast Tech Eng 28:493–510
- Chadwick JC, Miedema A, Ruisch BJ, Sudmeijer O (1992) Effects of procatalyst composition on the stereospecificity of a Ziegler–Natta catalyst system. Makromol Chem 193:1463–1468
- Echevskaya LG, Matsko MA, Mikenas TB, Nikitin VE, Zakharov VA (2006) Supported titanium-magnesium catalysts with different titanium content: kinetic peculiarities at ethylene homopoly-merization and copolymerization and molecular weight characteristics of polyethylene. J of Appl Polym Sci 102:5436–5442



- Tregubov AA, Zakharov VA, Mikenas TB (2009) Supported titanium-magnesium catalysts for ethylene polymerization: a comparative study of catalysts containing isolated and clustered titanium ions in different oxidation states. J Polym Sci Part A Polym Chem 47:6362–6372
- Mikenas TB, Tregubov AA, Zakharov VA, Echevskaya LG, Matsko MA (2008) Titanium-magnesium catalysts for olefin polymerization—effect of titanium oxidation state on catalyst performance. Polimery 53:353–357
- Potapov AG, Kriventsov VV, Kochubey DI, Bukatov GD, Zakharov VA (1997) EXAFS study of supported TiCl4/MgCl2 catalyst. Macromol Chem Phy 198:3477–3484
- Czaja K, Bialek M (2000) Effect of hydrogen on the ethylene polymerization process over Ziegler– Natta catalysts supported on MgCl2(THF)2 I studies of the chain-transfer reaction. J of Appl Polym Sci 79:356–360
- Giuliano C, Giampiero M, Anteo P (2001) Polypropene product innovation by reactor granule technology. Macromol Symp 173:195–209
- Wada T, Taniike T, Kouzai I, Takahashi S, Terano M (2009) Propylene polymerization performance of isolated and aggregated Ti species studied using a well-designed TiCl3/MgCl2 Ziegler–Natta model catalyst. Macromol Rapid Commun 30:887–891
- Mori H, Hasebe K, Terano M (1998) Variation in oxidation state of titanium species on MgCl2supported Ziegler catalyst and its correlation with kinetic behavior for propylene polymerization. Polymer 40:1389–1394
- Taniike T, Terano M (2008) Reductive formation of isospecific Ti dinuclear species on a MgCl₂ (110) surface in heterogeneous Ziegler–Natta catalysts. Macromol Rapid Commun 29:1472–1476
- Baulin AA, Novikova EI, Mal'kova GYa, Maksimov VL, Vyshinskaya LI, Ivanchev SS (1980) Correlation between the reduction of titanium in supported Ziegler catalysts and their activity in the polymerization of ethylene. Vysokomol Soed A 22:181–188
- 14. Soga K, Chen SI, Ohnishi R (1982) Correlation between the oxidation states of titanium and the polymerization activities for higher α-olefins and diene compounds. Polym Bull 8:473–478
- Soga K, Shiono T, Doi Y (1983) Titanium (IV) chloride/magnesium chloride catalytic systems. Polym Bull 10:168–174
- Soga K, Uozumi T, Park JR (1990) Effect of catalyst isospecificity on olefin copolymerization. Makromol Chem 191:2853–2864
- Kashiwa N, Yoshitake J (1984) The influence of the valence state of titanium in magnesium chloridesupported titanium catalysts on olefin polymerization. Makromol Chem 185:1133–1138
- Kashiwa N, Yoshitake J, Tsutsui T (1987) Polymerization of styrene with a highly active magnesium dichloride supported titanium tetrachloride catalyst system. Polym Commun 28:292–296
- Kojoh SI, Kioka M, Kashiwa N (1999) The influences of cocatalyst on propylene polymerization at high temperature with MgCl₂-supported TiCl₄ catalyst system. Eur Polym J 35:751–755
- Kissin YV, Mirabella FM, Meverden CC (2005) Multi-center nature of heterogeneous Ziegler–Natta catalysts: TREF confirmation. J Polym Sci Part A Polym Chem 43:4351–4362
- Ludlum DB, Anderson AW, Ashby CE (1958) Polymerization of ethylene by lower-valent compounds of titanium. J Amer Chem Soci 80:1380–1384
- Mobarakeh HS, Monfared MF, Vakili M (2006) Gas phase copolymerization of ethylene and 1-butene with prepolymerized MgCl2 supported Ziegler–Natta catalyst: effect of Al/Ti ratio. Iranian Polym J 15:569–575
- Benning CJ, Wszolek WR, Werber FX (1968) Crystalline titanium dichloride. Active catalyst in ethylene polymerization. II. Polymer structure, polymerization variables, and scope. J Polym Sci Part A-1 Polym Chem 6:755–762
- 24. Skalli MK, Markovits A, Minot C, Belmajdoub A (2001) A theoretical investigation of the role of AlR₃ as cocatalyst. Catal Lett 76:1–2
- Fregonese D, Mortara S, Bresadola S (2001) Ziegler–Natta MgCl₂-supported catalysts: relationship between titanium oxidation states distribution and activity in olefin polymerization. J Molecular Catal A Chem 172:89–95
- Ono Y, Keii T (1966) Electron spin resonance studies on Ziegler–Natta type catalyst systems.
 J Polym Sci Part A-1Polym Chem 4:2441–2446
- Ko YS, Han TK, Sadatoshi H, Woo SI (1998) Analysis of microstructure of ethylene–1-hexene copolymer prepared over thermally pretreated MgCl₂/THF/TiCl₄ bimetallic catalyst. J Polym Sci Part A Polym Chem 36:291–300



- 28. Kim I, Kim JH, Choi HK, Chung MC, Woo SI (1993) Comonomer enhancement effect of 1-hexene in ethylene copolymerization catalyzed over MgCl₂/THF/TiCl₄ catalysts. J Appl Polym Sci Part A Polym Chem 48:721–730
- Chien JCW, Nozaki T (1993) Ethylene/hexene copolymerization by heterogeneous and homogeneous Ziegler–Natta catalysts, and the comonomer effect. J Polym Sci 31:227–237
- Floyd S, Choi KY, Taylor TW, Ray WH (1986) Polymerization of olefins through heterogeneous catalysis. III. Polymer particle modelling with an analysis of intraparticle heat and mass transfer effects. J Appl Polym Sci 32:2935–2960





JOURNAL OF NATURAL GAS CHEMISTRY 天然气化学

Editors-in-Chief:

Xinhe BAO Alexis T. BELL

Vol.20 No.5 Sep. 2011

